# DIETARY PHOSPHORUS: EFFECTS ON SKELETAL DEVELOPMENT AND MINERALISATION IN ZEBRAFISH (*Danio rerio*)

SILVIA COTTI

DOCTORAL THESIS

# Dietary phosphorus: effects on skeletal development and mineralisation in zebrafish (*Danio rerio*)

Ghent University
Faculty of Sciences
Department of Biology
Evolutionary Developmental Biology Group
Ledeganckstraat 35, 9000 Gent
Belgium

University of Pavia
Faculty of Medicine
Department of Molecular Medicine
Biochemistry Unit
Via Taramelli 3B, 27100 Pavia
Italy


Academic Year 2022 – 2023

Publicly defended in Gent, Belgium, on January 30th, 2023

Co-authored one or more chapters:

Björn Busse, Claudia Di Biagio, Imke A. K. Fiedler, Antonella Forlino, Ann Huysseune, Wolfgang Koppe, Daria Larionova, Federica Marone, Martin Rücklin, P. Eckhard Witten, Eva M. Wölfel

For the citation of the published work reprinted in this thesis, please refer to the original publication (as mentioned in the beginning of each chapter).

To refer to this thesis, please cite as:

Cotti S. (2023) Dietary phosphorus: effects on skeletal development and mineralisation in zebrafish (*Danio rerio*). Ghent University and University of Pavia, 260 pp.

Cover image: Sagittal non-demineralised section of the vertebral column of wild type zebrafish (*Danio rerio*) showing the increased bone matrix production under low dietary phosphorus conditions. Von Kossa/Van Gieson staining; mineralised bone: brown; non-mineralised bone: pink. Image width: 700 ∝m. Processing and microphotography by Silvia Cotti.

Joint PhD

**PhD in Science: Biology**

**PhD in Biomedical Sciences**

# Dietary phosphorus: effects on skeletal development and mineralisation in zebrafish (*Danio rerio*)

Fosfor in de voeding: effecten op skeletontwikkeling en -mineralisatie bij zebravissen (*Danio rerio*)

by

Silvia Cotti

Supervisor: Prof. Dr. P. Eckhard Witten

*Ghent University, Belgium*

Supervisor: Prof. Dr. Antonella Forlino

*University of Pavia, Italy*

Academic Year 2022 – 2023

**Supervisors**

Prof. Dr. P. Eckhard Witten

*Department of Biology, Ghent University, Gent, Belgium*

Prof. Dr. Antonella Forlino

*Department of Molecular Medicine, University of Pavia, Pavia, Italy*

**Members of the examination committee**

Em. Prof. Dr. Ann Huysseune

*Department of Biology, Ghent University, Gent, Belgium*

*Department of Zoology, Charles University, Prague, Czech Republic*

Prof. Dr. Ing. Paul J. Coucke

*Centre for Medical Genetics, Ghent University Hospital, Gent, Belgium*

*Department of Biomolecular Medicine, Ghent University, Gent, Belgium*

Prof. Dr. Roberta Besio

*Department of Molecular Medicine, University of Pavia, Pavia, Italy*

Dr. Francesca Tonelli

*Department of Molecular Medicine, University of Pavia, Pavia, Italy*

Prof. Dr. Marc Muller

*Laboratoire d'Organogenèse et Régénération, Université de Liège, Liège, Belgium*

**Chairman**

Prof. Dr. Bart Braeckman

*Department of Biology, Ghent University, Gent, Belgium*

# Table of contents

*A chi non ha mai smesso di credere in me*

# Acknowledgments – Ringraziamenti

This journey started in December 2018. At that time, I could not have imagined how much this PhD could mean to me. Four years later, I can see how much the PhD has changed me as a researcher and a person. I obtained enormous satisfaction on the professional level, and I achieved significant personal changes. Today, I feel enriched, aware of how far my skills can bring me, and aware of my limits. Of course, it was not always easy. I spent four years far from my place of origin, from my family and my closest loved ones. But I was lucky enough to work in an exceptional environment where I could feel at home from the beginning.

I am very grateful to my supervisor Eckhard, who trusted me since the first moment I entered the lab and made me grow as a researcher. “You are the boss,” he told me during our first conversation about the PhD project. The truth is I would have been lost sometimes without his guidance.

I am thankful to Antonella, co-supervisor of this work, who introduced me to the zebrafish research in 2016 and first recognised my dedication to research. I’m grateful for recommending this PhD position and supporting the future of the current research project.

Big thanks should also go to Ann, who always positively encouraged and importantly contributed to this research project. I’m grateful for her careful remarks and advice that enormously increased the quality of this thesis’s outcomes.

Special thanks to Claudia, a great colleague and friend. Some of the present thesis's work would have been impossible without her. I’m thankful for our experiments together, for our long-lasting troubleshooting discussions, for getting along so well and for "thinking science" the same way.

I am thankful to Biomedaqu for the excellent scientific network and the opportunity to visit and work in different labs. Being part of such an inspiring, supporting and motivating community has been great.

Many thanks to Björn and Imke for their significant contribution to my research project and for welcoming and hosting me in the lab.

I would also like to thank the examination committee members for carefully reading my thesis and providing feedback, significantly increasing the quality of this work.

Thanks to my colleagues from the EvoDevo lab Lucia, Lauren and Daria, for the "insane" moments we spent together. Thanks to former members of the lab, Ana, Arianna and Mieke, who taught me a lot during my first months in Gent. I want to thank also the UZ colleagues Adelbert, Jan Willem, Lisa, Sophie, Tamara. We had a good time together, in and outside the lab. I am also grateful to Yiyen, for her kindness and sweetness. She brought the sun into the lab while this thesis was being written.

Vorrei ringraziare le mie college e amiche Francesca, Nadia e Laura, con cui ho condiviso molto sia a livello lavorativo che personale durante questi anni. Grazie a Chiara O., Elena e Chiara S. per esserci state nei momenti importanti.

Vorrei ringraziare mia mamma, mio papà, mia zia Dani e mia nonna Maria, per non avermi mai fatta sentire sola nonostante la lontananza, per avermi supportata e sopportata in ogni singolo momento e per essere la migliore famiglia che si possa desiderare.

Infine, voglio ringraziare Iacopo, il mio tutto, per non aver mai esitato nell'assecondare le mie scelte, per essere sempre stato al mio fianco e per essere una costante certezza nella mia vita.

The research presented in this thesis received funding from the European Union's Horizon 2020 Research and Innovation Programme under the Marie Skłodowska-Curie grant agreement No 766347 (Biomedaqu) and from Ghent University, Bijzonder Onderzoeksfonds grant code BOF.ITN.2021.0012.01.
Silvia Cotti received a grant for a short study visit at the research group of Prof. Dr. Björn Busse, at the University Medical Center Hamburg-Eppendorf, Hamburg, Germany, from Fonds Wetenschappelijk Onderzoek (FWO) (grant number K200621N) and from Ghent University (FCWO).

# Summary

## English summary

Phosphorus (P) is a dietary macronutrient essential for several physiological processes. It participates in cellular metabolism and cell signalling, it is a constituent of phospholipids, of nuclei acids and of highly active intracellular compounds such as ATP. In vertebrates, P together with calcium is crucial for mineralisation of the skeleton. Adequate dietary P levels are required to prevent P deficiency-related effects, i.e. growth retardation, osteomalacia and bone deformities, as well as P-excess-related consequences, i.e. soft tissue calcification and bone hypermineralisation.

The present thesis examines the effects of different dietary P levels on the skeleton using zebrafish as a model organism in skeletal research. The aims are i) to obtain insights into the mechanisms underlying osteomalacia and excess mineralisation, related both to inadequate P intake and to disease conditions, and ii) to better elucidate the processes of bone formation and mineralisation. The zebrafish skeletal elements, mainly the vertebral column, but also the dermal fin rays and the dentition, are analysed using a wide range of complementary techniques, ranging from histological procedures to different radiographic techniques, molecular analysis and mechanical testing.

The first major finding of this thesis is that bone formation and bone mineralisation are uncoupled processes. When treating zebrafish with a reduced dietary P supply, bone matrix deposition, i.e. bone formation, continues uninterrupted. New bone matrix is formed, simply this bone does not mineralise due to the lack of P. The deposition of new bone matrix is even further stimulated under low P conditions. The increased production of bone matrix does not lead to the development of skeletal malformations in zebrafish. Conversely, increased dietary P supply leads to bone hypermineralisation, increases bone stiffness and promotes fusion of vertebral bodies.

Interestingly, the large amount of non-mineralised bone matrix produced under low P conditions resumes mineralisation as soon as sufficient P is provided with the diet. These late mineralised bone structures appear normal, but the volume of the newly mineralised bone is dramatically increased. It is thus possible to increase the bone volume in zebrafish, first by stimulating bone matrix formation under low P conditions, and subsequently inducing the mineralisation of the newly formed bone by providing adequate dietary P.

The low dietary P conditions also reduce the mineral content of the bone already present in zebrafish, enhancing its biomechanical properties by increasing toughness and reducing stiffness. This approach has been applied to partially rescue the bone hypermineralisation of osteogenesis imperfecta, a rare bone disorder mainly characterised by bone fragility and severe bone deformities. In the osteogenesis imperfecta mutant zebrafish called *Chihuahua*, the data obtained from the reduced dietary P treatment suggest a reduction in the mineral content of bone, resulting in a partial improvement of the severe bone phenotype typical of the disease.

The low dietary P zebrafish model presented here allows to elucidate the effects of dietary P levels on bone development and to better understand the relationship between bone formation and bone mineralisation. Moreover, the experimental evidence linking dietary low P levels with bone quality improvement, represents a promising novel approach for the treatment of disease conditions characterised by bone hypermineralisation and bone loss. Furthermore, the alternation of low dietary P/sufficient dietary P can possibly contribute to reverse bone loss due to aging or osteoporosis conditions.

## Nederlandse samenvatting

Fosfor (P) is een macronutriënt in de voeding, essentieel voor verschillende fysiologische processen. Het neemt deel aan het cellulair metabolisme en de celsignalisatie, het is een bestanddeel van fosfolipiden, van nucleïnezuren en van zeer actieve intracellulaire verbindingen zoals ATP. Bij gewervelde dieren is P samen met calcium cruciaal voor de mineralisatie van het skelet. Adequate P-niveaus in de voeding zijn vereist, zowel om P-deficiëntie-gerelateerde effecten te voorkomen, zoals groeiachterstand, osteomalacie en botmisvormingen, als de gevolgen van excessieve P-niveaus, zoals verkalking van zacht weefsel en bothypermineralisatie.

Dit proefschrift onderzoekt de effecten van verschillende P-niveaus in de voeding op het skelet, met de zebravis als modelorganisme. De doelstellingen zijn (i) inzicht verwerven in de mechanismen die ten grondslag liggen aan osteomalacie en overmatige mineralisatie, zowel gerelateerd aan onvoldoende P-opname als aan ziektetoestanden, en (ii) de processen van botvorming en -mineralisatie beter doorgronden. De skeletelementen van de zebravis, voornamelijk de wervelkolom, maar ook de dermale vinstralen en het gebit, worden geanalyseerd met behulp van een breed scala aan complementaire technieken, gaande van histologische procedures tot verschillende radiografische technieken, moleculaire analyses en mechanische tests.

De eerste belangrijke bevinding van dit proefschrift is dat botvorming en botmineralisatie niet-gekoppelde processen zijn. Bij de behandeling van zebravissen met een verminderde P-toevoer via de voeding gaat de afzetting van botmatrix, met andere woorden de botvorming, ononderbroken door. Er wordt nieuwe botmatrix gevormd; dit bot mineraliseert echter niet door het ontbreken van P. Onder lage P-omstandigheden wordt de afzetting van nieuwe botmatrix zelfs gestimuleerd. De verhoogde productie van botmatrix leidt niet tot de ontwikkeling van skeletmisvormingen bij zebravissen. Omgekeerd leidt een verhoogde P-toevoer via de voeding tot hypermineralisatie van het bot, verhoogt het de rigiditeit (*stiffness*) van het bot en bevordert het de fusie van wervellichamen.

Interessant is dat in de grote hoeveelheid niet-gemineraliseerde botmatrix, geproduceerd onder lage P-omstandigheden, de mineralisatie hervat wordt zodra er

via het dieet voldoende P wordt toegediend. Deze laat-gemineraliseerde botstructuren lijken normaal, maar het volume van het nieuw gemineraliseerde bot is substantieel toegenomen. Het is dus mogelijk om het botvolume bij de zebravis te vergroten, eerst door de vorming van botmatrix onder lage P-omstandigheden te stimuleren en vervolgens de mineralisatie van het nieuw gevormde bot te induceren door voldoende P te verstrekken in het voedsel.

De lage P-voedingscondities verminderen ook het mineraalgehalte van het reeds aanwezige bot in de zebravis, waardoor de biomechanische eigenschappen worden verbeterd: de taaiheid (*toughness*) vergroot en de rigiditeit (*stiffness*) vermindert. Deze benadering is toegepast voor een - althans gedeeltelijke - reductie van de bothypermineralisatie in het geval van osteogenesis imperfecta, een zeldzame botaandoening die voornamelijk wordt gekenmerkt door botfragiliteit en ernstige botmisvormingen. Bij de *Chihuahua* zebravis, een mutant model voor osteogenesis imperfecta, vermindert een gereduceerd P-gehalte in het voedsel vermoedelijk het mineraalgehalte van het bot, wat resulteert in een gedeeltelijke verbetering van het ernstige botfenotype dat typisch is voor de ziekte.

Het nieuwe zebravismodel dat hier wordt gepresenteerd, maakt het mogelijk om de effecten van P-niveaus in de voeding op botontwikkeling te ontrafelen en om de relatie tussen botvorming en botmineralisatie beter te begrijpen. Bovendien vormt het experimentele bewijs dat een verlaagd P-niveau in de voeding koppelt aan een verbeterde botkwaliteit, een veelbelovende nieuwe benadering voor de behandeling van ziekten die worden gekenmerkt door bothypermineralisatie en botverlies. De afwisseling van een P-arm dieet en een dieet met voldoende P kan mogelijk botverlies als gevolg van veroudering of osteoporose ongedaan maken.

## Riassunto in italiano

Il fosforo è un macronutriente essenziale per diversi processi fisiologici e deve essere introdotto tramite l'alimentazione. È coinvolto nel metabolismo e nella segnalazione cellulare, è un costituente dei fosfolipidi di membrana, degli acidi nucleici e di molecole altamente attive come l'ATP. È inoltre fondamentale, insieme al calcio, per la mineralizzazione dello scheletro in tutti i vertebrati. È necessario assumere adeguati livelli di fosforo tramite l'alimentazione, per prevenire gli effetti correlati sia alla carenza, ovvero ritardo della crescita, ipomineralizzazione e deformità ossee, sia all'eccesso di fosforo, ovvero calcificazione dei tessuti molli e ipermineralizzazione ossea.

Lo scopo di questa tesi è analizzare che conseguenze hanno diversi apporti di fosforo sullo scheletro attraverso l'alimentazione, utilizzando lo zebrafish come organismo modello. Gli obiettivi sono i) ottenere maggiori informazioni sui meccanismi alla base dell'ipo- e dell'ipermineralizzazione ossea, dovuti sia all'assunzione inadeguata di fosforo, sia a condizioni di malattia, e ii) chiarire entrambi i processi di formazione e mineralizzazione ossea. La morfologia e la mineralizzazione di diverse strutture dello scheletro di zebrafish, in particolare la colonna vertebrale, gli elementi ossei delle pinne e i denti, sono analizzate utilizzando un'ampia gamma di tecniche complementari, che vanno da procedure istologiche a diverse tecniche radiografiche, analisi molecolari e test meccanici.

Il primo importante risultato di questa tesi è la dimostrazione che la formazione di osso e la sua mineralizzazione sono processi indipendenti. Quando zebrafish è sottoposto ad un apporto ridotto di fosforo, la deposizione di matrice ossea non subisce alcun effetto. Anzi, la formazione di nuova matrice ossea è particolarmente stimolata in queste condizioni e avviene senza la sua conseguente mineralizzazione. Tale aumento della produzione di osso non porta allo sviluppo di malformazioni scheletriche in zebrafish. Al contrario, l'aumento dell'apporto nutrizionale di fosforo causa ipermineralizzazione e aumentata rigidità ossea, favorendo la fusione delle vertebre.

È interessante notare come la grande quantità di matrice ossea non mineralizzata, prodotta in condizioni di ridotto apporto di fosforo, mineralizza non appena viene fornito fosforo in quantità sufficienti tramite l'alimentazione. Queste strutture ossee appaiono normali, ma la mineralizzazione tardiva di tali strutture ha come risultato un notevole aumento del volume osseo. Di conseguenza, si può dedurre che è possibile aumentare il volume delle ossa in zebrafish, stimolando prima la formazione di matrice ossea in condizioni di ridotto apporto di fosforo, e successivamente inducendone la mineralizzazione fornendo adeguati livelli di fosforo con l'alimentazione.

In condizioni di ridotto apporto di fosforo, le ossa di zebrafish hanno anche un ridotto contenuto di minerale, caratteristica che ne migliora le proprietà biomeccaniche, aumentandone la resistenza e riducendone la rigidità. Questo approccio ha rivelato risultati promettenti nel moderare, sebbene in modo parziale, l'eccessiva mineralizzazione delle ossa che caratterizza l'osteogenesi imperfetta, una rara malattia genetica che causa fragilità e gravi deformità ossee. Il ridotto apporto di fosforo tramite l'alimentazione nel modello zebrafish chiamato *Chihuahua*, un valido modello per lo studio dell'osteogenesi imperfetta, ha dimostrato risultati incoraggianti nel modulare parzialmente il grave fenotipo osseo della malattia.

Il nuovo modello zebrafish presentato in questa tesi è utile sia per chiarire gli effetti dei diversi apporti di fosforo sullo sviluppo osseo, sia per comprendere meglio la relazione tra formazione di matrice ossea e mineralizzazione ossea. Inoltre, l'evidenza sperimentale che lega il ridotto apporto di fosforo con la migliorata qualità dell'osso rappresenta un nuovo e promettente approccio per il trattamento di patologie caratterizzate da ipermineralizzazione ossea e/o riduzione del volume osseo. Inoltre, l'alternanza tra ridotto e aumentato apporto di fosforo può contribuire a contrastare la perdita di volume osseo dovuta all'invecchiamento o legata all'osteoporosi.

# Chapter 1

## General introduction

## Preamble

This doctoral thesis focuses on the effects of different dietary phosphorus (P) levels on bone formation and bone mineralisation. P is an essential macronutrient for several physiological processes, including bone mineralisation in vertebrates. Together with calcium, P is closely involved in the development and maintenance of the mineralised skeletal system and its adequate intake is crucial to ensure bone health.

Both dietary P insufficiency and excess are related to skeletal malformations in vertebrates. In particular, scarce dietary P results in growth retardation, deformed vertebral column, bowing of bones and osteomalacia (hypomineralised bone) in both mammals and teleosts. On the other hand, excess dietary P causes bone hypermineralisation and ectopic mineralisation of soft tissues.

A better understanding of the effects caused by scarce and excess dietary P levels on the skeleton is needed to elucidate whether dietary P supply alone is a primary cause of skeletal malformations and to expand the current knowledge on the processes of bone mineralisation and bone formation in healthy and disease conditions. To address these fundamental questions, zebrafish is employed as vertebrate model, given its popularity in the biomedical field to study bone formation and bone diseases.

Thus, in this chapter, zebrafish is first introduced as a model organism in skeletal research, together with the skeletal system and the different mineralised skeletal tissues. The introduction chapter is mainly written from the teleost (zebrafish) skeleton perspective, in comparison with the mammalian skeleton. Also, an overview of bone mineralisation and bone mineral metabolism is provided.

# Zebrafish

### *Ecology*

The zebrafish (*Danio rerio*), first described by Francis Hamilton (1822), belongs to the order Cypriniformes, family Cyprinidae (Spence et al., 2008). It is distributed throughout South and South-East Asia, but its natural range is centred around the Ganges and Brahmaputra river basins in North-Eastern India, Bangladesh and Nepal (Spence et al., 2008; Parichy, 2015). Zebrafish is omnivorous, its natural diet mostly consists of zooplankton and insects, although it may feed also on plant and algae material, fish scales and invertebrates eggs (Spence et al., 2008).

The zebrafish takes its name from the typical blue and silver stripes running the length of its body (**Figure 1.1 A**). When adult, zebrafish rarely exceeds 40 mm standard length (from the tip of the snout to the origin of the caudal fin, according to Parichy et al., 2009). Males and females are of similar colouration, although males are generally slender and tend to have larger anal fins with more yellow colouration (Laale, 1977).

In the natural environment, reproduction is more seasonal, although there is evidence that spawning may not be cued by season, but may instead be dependent on food availability (Spence et al., 2006). A single female zebrafish can produce hundreds of eggs in a single spawning. Fertilisation is external, eggs are large relative to the eggs of other fishes (0.7 mm in diameter after fertilisation) and optically transparent. Development is rapid (**Figure 1.1 B**), with precursors to all major organs developing within 36 hours and a complete embryogenesis around 72 hours post-fertilisation (Kimmel et al., 1995). Post-embryonic development is subjected to a high variation rate and developmental progress is mostly driven by size rather than age (Parichy et al., 2009). Sexual maturity is reached at about 25 mm standard length (about 75 days post-fertilisation when zebrafish are reared at 25.5°C) (Spence et al., 2008), allowing a short generation time.

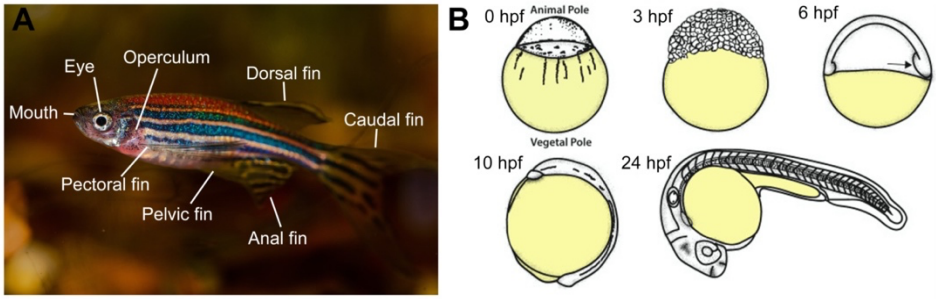


**Figure 1.1.** The zebrafish, *Danio rerio*. **A:** Photograph of an adult zebrafish. The main anatomical features are indicated. **B:** Illustrative overview of zebrafish embryonic development during the first 24 hours post-fertilisation (hpf). The single-cell embryo at fertilisation (0 hpf) presents the animal and vegetal poles. The blastula stage (3 hpf) is characterised by several blastomeres accumulating upon the yolk. The early gastrula embryo (6 hpf) has formed along one side of the embryo. At 10 hpf, gastrulation ends, the future head and tail are distinct at the animal and vegetal poles which are in the same orientation as shown in the drawing of 0 hpf. At 24 hpf, the embryo has a distinct body plan with a head, trunk, and tail somites, and developing organs (modified from Smith and Kimelman, 2020).

### *Zebrafish as a vertebrate model organism*

The first studies about zebrafish embryos appeared in the 1950s (Eisen, 2020), but zebrafish was only established as a vertebrate model organism in the early 1980s thanks to the work of George Streisinger, who pioneered its use to apply molecular genetics to the study of vertebrate embryology (Streisinger et al., 1981), and Charles B. Kimmel, who published detailed descriptions of cell differentiation and nervous system organisation (Kimmel and Warga, 1988; Kimmel, 1989). Since then, the zebrafish has become an established model for uncovering many aspects of development, differentiation, physiology, regeneration and evolution.

Zebrafish has become a popular vertebrate model due to a number of attributes that make it particularly tractable to experimental manipulation. It is a small, robust fish, so large numbers can be kept easily and cheaply in the laboratory, where it breeds all year round. Females can spawn every two/three days and a single clutch may contain several hundred eggs. Generation time is relatively short, typically three/four months, making it suitable for experiments (Spence et al., 2008). Embryos and early developmental stages are nearly transparent and suitable for microscopic observations of morphogenetic and cellular processes *in vivo* (Kimmel et al., 1995).

In the early 2000s, the zebrafish genome project at the Wellcome Sanger Institute produced the first zebrafish reference genome assembly. It revealed high conservation of orthologue genes (about 70%) and disease causing genes (about 80%) with humans. In addition, some zebrafish chromosome regions possess synteny conservation with human chromosomes, further increasing the relevance of the zebrafish in biomedical research (Howe et al., 2013). However, compared to mammals, the zebrafish ancestors underwent an additional genome duplication about 320 millions of years ago, resulting in paralogues for approximately 20% of the genes. Such paralogues might have undergone loss or retention, and they might have diverged in function, following evolutionary fates such as sub-functionalisation (the distribution of ancestral gene functions among duplicates) and neo-functionalisation (emergence of novel gene functions) (McCluskey and Braasch, 2020). Thus, these evolutionary events can complicate the translation of gene function between zebrafish and humans (Meyer and Van de Peer, 2005).

The zebrafish was the subject of the first large-scale random mutagenesis screens to be conducted in a vertebrate (Driever et al., 1996; Granato and Nüsslein-Volhard, 1996; Haffter et al., 1996). As a result, over 4000 mutations were generated and led to the identification of over 400 genes controlling vertebrate development. After, given the improved genome editing techniques, many more zebrafish mutant phenotypes have been successfully used to dissect the cellular, molecular and genetic mechanisms underlying basic developmental processes and also molecular mechanisms of human genetic disorders (Phillips and Westerfield, 2020; Rissone et al., 2020).

Understanding the molecular mechanisms underlying human genetic diseases is a prerequisite for developing new tools to diagnose and discover new drugs to treat these diseases. Zebrafish has become a widely used model for drug discovery because it is suitable for high-throughput chemical screenings, in which zebrafish embryos and/or early developmental stages are exposed to libraries containing many different molecules with pharmaceutical potential, to identify new therapeutic agents (Peterson et al., 2000; Zhang and Peterson, 2020).

Last but not least, zebrafish has also become a model used to investigate mechanisms by which environmental factors can influence developmental and physiological processes by modulating host genes and generating different phenotypes (Eisen, 2020). In this context, toxicology research exploits zebrafish to detect toxins in water samples and to investigate the mechanisms of action of environmental toxins and their related diseases (Bambino and Chu, 2017).

***Zebrafish in context of skeletal research***

Zebrafish is being studied as model for bone formation and for human skeletal diseases because basic bone cells differentiation pathways and ossification processes have been conserved across vertebrates (Witten et al., 2017). In addition, mammals and teleost fish are evolutionarily related, although there is no linear evolutionary relationship between zebrafish and humans (Metscher and Ahlberg, 1999). Extinct basal gnathostome bony fish are the common ancestors of tetrapods and ray-finned fish. Subsequently parallel lines of evolution gave rise to mammals and teleosts (Romer, 1970).

In humans, the diagnosis of skeletal diseases is based on the imaging of the skeletal phenotype, both at anatomical and cellular levels. X-ray imaging is a practical tool to diagnose skeletal abnormalities, but the routine radiological techniques used in human or veterinary medicine need to limit radiation exposure to the patient, and therefore have limited exposure settings that are not sufficient for a detailed analysis of zebrafish, due to its small skeletal structures (Bruneel and Witten, 2015). X-ray sources that have a wide range of possible X-ray output settings, e.g. the Faxitron X-ray cabinet, can instead be set to low power but long exposure time parameters, and can be used in combination with high resolution technical film to successfully image the zebrafish skeleton and diagnose malformations in 2D (Fisher et al., 2003; Tonelli et al., 2020a). Higher resolution 3D imaging of the zebrafish skeleton can be achieved by micro-computed tomography (micro-CT) or synchrotron X-ray tomographic microscopy, which allow detailed 3D reconstructions and quantitative analysis of bone samples (Witten et al., 2017; Tonelli et al., 2020a). Next to it, whole mount skeletal staining with

Alizarin red S allows high precision and high resolution analysis of the zebrafish skeleton when observed using a powerful microscope equipment (**Figure 1.2 A-D**) (Witten et al., 2017; Tonelli et al., 2020a).

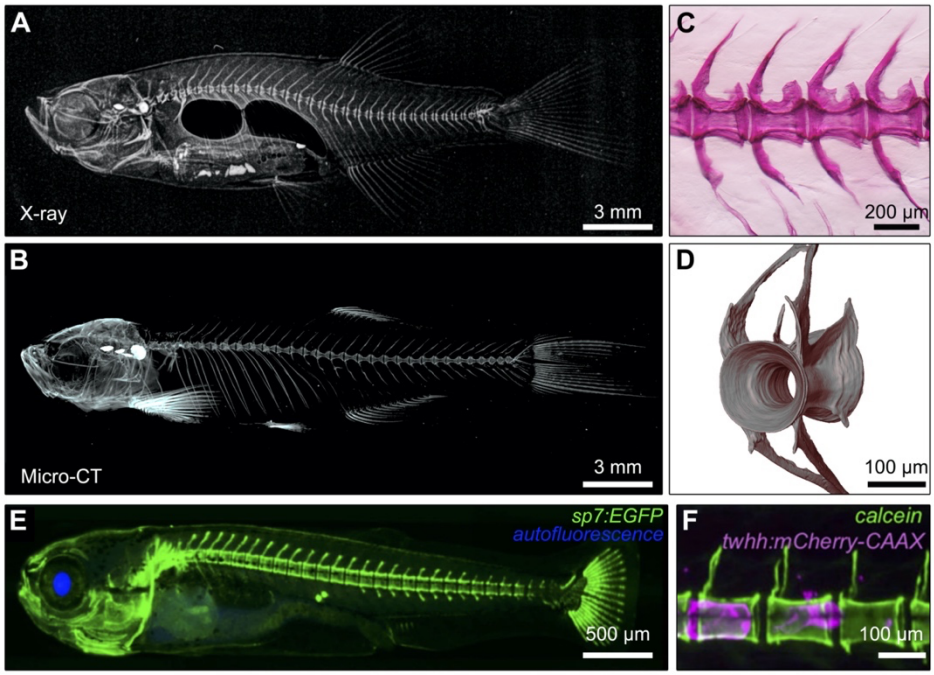


**Figure 1.2.** Imaging the zebrafish skeleton. **A:** Lateral X-ray image of an adult zebrafish acquired with a Faxitron X-ray cabinet (modified from Tonelli et al., 2020a). **B:** Lateral view of a 3D reconstructed micro-CT scanned adult zebrafish at 5 µm (modified from Tonelli et al., 2020b). **C:** Lateral image of zebrafish vertebral bodies whole mount-stained with Alizarin red S (modified from Cotti et al., 2022). **D:** Synchrotron X-ray tomographic microscopy reconstruction of a zebrafish vertebral body scanned at 0.65 µm (modified from Cotti et al., 2020). **E:** Transgenic zebrafish expressing EGFP under the promoter of the osteoblasts marker osterix (*sp7*) (modified from Busse et al., 2020). **F:** Transgenic zebrafish expressing mCherry-CAAX under the promoter of tiggy-winkle hedgehog (*twhh*), marker of notochord cells in early development, and *in vivo* calcein labelling of the mineralised chordacentra (modified from Busse et al., 2020).

Imaging zebrafish bone structures at the cellular level can be challenging, given the small size of zebrafish cells (Hanken and Wake, 1993). High precision histological procedures based on epoxide and methacrylate resins allow visualisation of bone cells and bone matrix at very high resolution (Bruneel et al., 2015; Huysseune et

al., 2022b). Histological analysis can be complemented with *in vivo* imaging, that can be applied to zebrafish embryos and early developmental stages due to their optical transparency. A large number of transgenic zebrafish lines expressing fluorescent reporters have been generated to monitor in real-time the dynamics of bone tissues development, cell differentiation, cell-cell interactions and signalling pathways (**Figure 1.2 E-F**) (Witten et al., 2017).

A multitude of zebrafish mutants with a skeletal phenotype is available, either identified in large-scale mutagenesis screens or generated by reverse genetic approach (Tonelli et al., 2020a). Their characterisation helps in understanding the mechanisms underlying human bone disorders, or to identify novel genes important for skeletal processes and bone mineralisation (Witten et al., 2017; Tonelli et al., 2020a; Dietrich et al., 2021).

Although zebrafish is a demonstrated excellent model in fundamental and preclinical skeletal research, to translate results obtained on this small teleost fish to humans requires an appropriate evolutionary perspective considering the different physiology, anatomy, and life history or the organisms being compared (Witten et al., 2017).

## The vertebrate skeleton

The vertebrate skeleton consists of a number of dynamic skeletal systems active throughout life (Hall and Witten, 2019). The skeleton fulfils many roles: i) it provides mechanical functions (protection, locomotion, feeding); ii) it is a regulator of animal's mineral metabolism; iii) it is an important signalling centre during early development and secretes several hormones (Witten and Hall, 2015).

The idea that the skeleton is not just an invariant dry matter has been established long ago. The skeleton is, in fact, a highly plastic organ system subjected to functional adaptation. The skeleton and its cells respond to intrinsic and environmental stimuli by changing morphology, structure and patterns of gene expression (Witten and Hall, 2015). These changes also reflect evolutionary adaptations. For example, teleosts and mammals, although they have common ancestors, adapted their skeleton to different habitats (aquatic and terrestrial, respectively), to the truncation of developmental process, and to body size differences (Witten and Huysseune, 2009; Apschner et al., 2011).

The following sections describe the skeletal system from the perspective of the teleost (zebrafish) skeleton, in comparison to the mammalian skeleton.

### *Evolution of the skeleton: a brief overview*

The mineralised vertebrate skeleton consists of two major subunits that evolved to a large degree independently, namely the dermal skeleton and the endoskeleton (Smith and Hall, 1990). Early mineralised structures in the vertebrate linage were the odontodes, tooth-like structures that represented the principal units of the dermal skeleton. Odontodes were already composed from bone, dentin and a hypermineralised layer (enameloid/enamel), from which the teeth of all vertebrates evolved (Reif, 1982; Huysseune et al., 2022a). Extant chondrichthyans (sharks and rays) retain odontode-like structures in their dermal skeleton (Reif, 1982; Huysseune et al., 2022a) and serve as examples for illustrating the homology between teeth and odontodes (Hall and Witten, 2007). In addition, scales and dermal fin rays of teleosts

are odontode derivatives. However, compared to their common basal osteichthyan ancestors, the postcranial dermal skeleton has been completely lost in mammals and has been largely reduced in teleost fish (Sire and Huysseune, 2003; Sire and Akimenko, 2004). Elements of the dermal skeleton can be replaced throughout life, as teleosts and other vertebrates, but not mammals, are capable of continuous teeth replacement. Scales and fin rays regenerate lifelong (Sire and Akimenko, 2004). Dermal skeletal elements usually form via intramembranous bone formation, without the need of a cartilaginous precursor (Franz-Odendaal et al., 2006).

The mineralised endoskeleton is evolutionarily younger than the mineralised dermal skeleton (Maisey, 2000). The endoskeleton consists of cranial, axial and appendicular skeletal elements, and includes cartilages and their ossification, that usually develop in deeper parts of the body (Huysseune, 2000). Perichondral ossification is the most common mode of bone formation if a cartilaginous template is present. Perichondral ossification usually starts with the transformation of a perichondrium into a periosteum (Scott-Savage and Hall, 1980). This ossification type has been considered an advanced form of intramembranous ossification (Hall, 2015). Following the evolution of cartilage degradation processes, endochondral bone formation developed, as shown mostly by studies on shark skeletogenesis (Eames et al., 2007). Endochondral ossification involves a cartilaginous template that is replaced by or remodelled into bone. Although found in most vertebrate groups, endochondral ossification is typically studied in mammalian long bones. In small teleost fish such as zebrafish, perichondral bone formation is usually not followed by endochondral bone formation (reviewed by Witten et al., 2017). Endochondral bone formation occurs, however, in larger species such as carp (*Cyprinus carpio*), a close relative of zebrafish (Huysseune, 2000; Witten et al., 2001, 2010). A typical element of the zebrafish endoskeleton consists of a perichondral bone tube with cartilage sticking out as a condyle. Membranous apolamellae can extend from the perichondral bone (Witten and Huysseune, 2007). Inside the medullary cavity, adipose tissue has replaced cartilage, along with nerves, blood vessels, and connective tissue cells.

However, there are exceptions to the rule, given that some endoskeletal bones develop intramembranously, without any association with cartilage. This is the case of teleosts vertebral body centra that, differently from mammals, derive from segmented mineralisation of the notochord sheath followed by intramembranous bone formation (Arratia et al., 2001; Witten and Hall, 2021).

Mammals and teleosts inherited their endoskeleton from common osteichthyan ancestors (Maisey, 2000; Donoghue et al., 2006). However, it should be noted that teleost fish and mammals have evolved unique traits or have lost particular skeletal elements, as mentioned above. In addition, characters of the teleost skeleton can be more advanced or elaborate compared to mammals (Witten and Huysseune, 2009). For example, the teleost skull contains at least twice the number of skeletal elements compared to the mammalian skull (Gregory, 1933; Cubbage and Mabee, 1996).

***Skeletal tissues***

Mineralised vertebrate skeletal tissues are commonly assigned to four major categories: cartilage, bone, dentin and enamel/enameloid. Apart from dentin and enamel/enameloid, which are restricted to the dermal skeleton, all skeletal tissues and respective cells occur in both mammalian and teleost dermal and endoskeleton (Witten and Huysseune, 2009). These categories represent prominent manifestations of tissue types within a continuum of skeletal tissues (Hall and Witten, 2007; Hall, 2015). In teleosts, skeletal tissues display features that are intermediate between two or more of the above mentioned categories. Chondroid, chondroid bone, different types of cartilage with intermediate characters between fibrous connective tissue, cartilage and bone, and various types of bone and dentin with intermediate characters between the two tissue types are only few examples (Beresford, 1981; Benjamin, 1990; Hall and Witten, 2007; Witten et al., 2010; Hall, 2015). In mammals such intermediate tissues are also present, but receive less attention. Some of these tissues occur transiently during skeletal development, as temporary sexual characters (for example deer antlers) or as pathological manifestations (Beresford, 1981). In teleost fish, a full range of

intermediate skeletal tissues is recognised as part of the regular (non-pathological, non-regenerating) skeleton (Benjamin, 1990; Hall and Witten, 2007; Witten and Huysseune, 2007, 2009). For the objectives of this thesis, only the four major categories of skeletal tissues will be described.

*Cartilage*

Cartilages are resilient stiff tissues which resist to compression and that, different from bone, usually lack vascularisation (Beresford, 1993; Huysseune, 2000; Hall, 2015). According to the classical mammalian histology, there are three major types of cartilage based on the differences in the minor components of the extracellular matrix: hyaline cartilage, if the matrix is composed predominantly of glycosaminoglycans; elastic cartilage, if elastic fibres are present in the extracellular matrix; fibrocartilage, if the matrix has an enriched collagenous fibre content, including collagen type I (**Figure 1.3 A**) (Hall, 2015). This classification is incomplete when referring to teleosts, for which al least 15 types and subtypes of cartilaginous tissue have been identified (Benjamin, 1990; Benjamin and Ralphs, 1991; Benjamin et al., 1992; Witten et al., 2010).

In teleosts, the cartilaginous extracellular matrix can be a thin seam surrounding numerous cells, or abundant with few cells, or all the ranges in between (Huysseune et al., 1988; Witten et al., 2010). Next to that, teleost cartilages are characterised by variation in their extracellular matrix composition. Collagen type II, the most abundant macromolecule in mammalian cartilages, is also found in teleost hyaline cartilage, although it is often lacking in cell-rich cartilages and absent in elastic cartilage. Chondroitin sulphate is ubiquitous, but keratan sulphate can be absent (Benjamin and Ralphs, 1991). Many types of cartilages in fish skeleton persist in adults and have adapted their extracellular matrix composition to specific mechanical and physiological functions (Beresford, 1993).

The first step in the development of cartilage in teleosts is condensation of mesenchymal cells (blastema stage) that turn into closely packed pre-chondroblasts, with no evidence of cartilage matrix (Huysseune and Sire, 1992). These cells

differentiate into chondroblasts and finally become separated through the secretion of extracellular cartilage matrix (Huysseune, 2000). The shape, size and cytoplasmic characteristics of chondroblasts and chondrocytes can be extremely variable, nevertheless these cells are responsible for growth of the cartilage. In appositional growth, chondroblasts are recruited from the perichondrium at the periphery; in interstitial growth, chondrocytes divide and/or increase in size and/or secrete matrix (Huysseune, 2000).

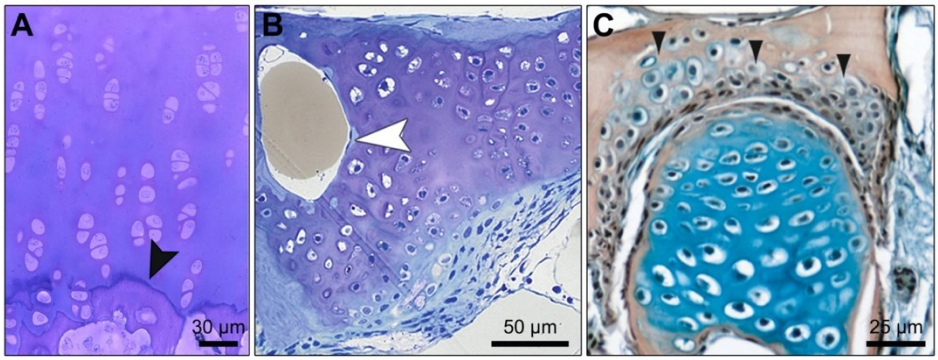


**Figure 1.3.** Histology of cartilaginous tissues. **A:** Articular cartilage derived from the medial femoral condyle of a three months old white rabbit. The mineralisation front between hyaline cartilage and calcified cartilage is visible as a blue stained line (black arrowhead) (modified from Hunziker et al., 2007). **B:** Ongoing endochondral bone formation in the braincase of an adult zebrafish. Resorption cavities filled with lipids (brown), only a very small amount of bone is deposited (white arrowhead) against the erosion front (modified from Huysseune et al., 2022b). **C:** Hyomandibular joint of an adult zebrafish with cartilage (blue) and chondroid bone (arrowheads), an intermediate tissue between cartilage and bone (modified from Weigele and Franz-Odendaal, 2016).

As in mammals, cartilage can be replaced by bone through endochondral bone formation (Huysseune, 2000) but in smaller teleost species, such as zebrafish, endochondral bone formation is rather uncommon (Witten et al., 2017). If cartilage is removed inside a bony shaft, it is typically replaced by adipose tissue (**Figure 1.3 B-C**) (Huysseune, 2000; Witten et al., 2001). Osteoblasts and adipocytes (together with chondroblasts and myocytes) differentiate from the same mesenchymal progenitors. These cells retain the plasticity to differentiate into the various cell lineages when exposed to a specific microenvironment. The differentiation is driven by upregulation

and downregulation of lineage-specific transcription factors. As an example, precursor cells from the adipogenic mesenchyme cell lineage from Atlantic salmon differentiate *in vitro* into the osteogenic lineage. This process is characterised by the reduced transcription of the adipogenic factor peroxisome proliferator activated receptor γ (*pparγ*) and by the increase of the osteogenic transcription factors RUNX family transcription factor 2 (*runx2*) and osterix (*sp7*) (Ytteborg et al., 2015).

*Bone*

Bone is a vascularised supporting skeletal tissue that consists of cells, an organic extracellular matrix mainly composed by collagen type I, that undergoes mineralisation (Hall, 2015). Thus, bone is classically the result of an ossification process, that in teleosts can be intramembranous, perichondral, or endochondral, as anticipated above. Perichondral bone is very common in fishes, given that most of the hyaline cartilages are covered at some stage during ontogeny by a layer of perichondral bone (Huysseune, 2000). Different from mammals, in miniaturised teleosts such as zebrafish, endochondral bone formation is sparse and characterises older individuals. Early life stages and juveniles that are used in experimental studies lack endochondral bone. The rarity of endochondral bone could be associated to miniaturisation of body size, occurred in many small teleost species (Hanken and Wake, 1993; Witten et al., 2017). In fact, teleost species with larger individuals, e.g. carp (*Cyprinus carpio*), a close relative of zebrafish, exhibit endochondral bone formation (Huysseune, 2000; Witten et al., 2001, 2010). Different from tetrapods, teleosts have no hematopoietic tissue inside the bone marrow space, which is filled with adipose tissue, nerves, blood vessels and other connective tissue cells. Haematopoiesis in teleosts takes place in the head kidney (Witten and Huysseune, 2009).

The major organic component of the bone matrix is fibrillar collagen type I. Other minor organic constituents are non-collagenous proteins such as glycoproteins, Gla-proteins, proteoglycans and lipids (Bonucci, 2012). Collagen type I arranges in fibrils, with a diameter between 20 and 50 nm (Chapman and Hulmes, 1984). Longitudinally, collagen type I fibrils have characteristic periodic bands of 60-70 nm

(Chapman and Hulmes, 1984). Collagen fibrils further organise into fibres and fibre bundles. Collagen is a highly tension-resistant material and the orientation and fine architecture of the fibrils/fibres/fibre bundles is very important from a functional viewpoint. Woven bone shows no preferential fibril orientation and it is usually the first bone matrix produced because it well adapts to quick embryonic development (Ricqlès et al., 1991). During ontogenetic growth, parallel-fibered bone is slowly deposited, in which collagen fibrils are parallel-oriented to the long axis of the bone (Ricqlès et al., 1991). Structurally, bone tissue in teleost fish develops first as woven bone, and subsequently, parallel-fibered and lamellar bone develops (Witten et al., 2017). Lamellar bone can also form osteons, yet not in small fish such as zebrafish (Moss, 1961; Meunier, 2011; Witten et al., 2017).

The cells secreting the non-mineralised bone matrix, named osteoid, are the osteoblasts, which derive from mesenchymal osteoprogenitors (Franz-Odendaal et al., 2006). Three types of osteoblasts are usually identified at the bone surface: preosteoblasts, active osteoblasts, and inactive/resting osteoblasts (Holtrop, 1990). Preosteoblasts are located at a distance from the bone surface, do not deposit bone matrix, and can still divide. Preosteoblasts differentiate into active bone matrix-secreting osteoblasts, which deposit organic bone matrix (Franz-Odendaal et al., 2006) (**Figure 1.4 A**).

Osteoblasts have a large eccentric nucleus, prominent rough endoplasmic reticulum (RER) and Golgi apparatus, and do not divide (Scherft and Groot, 1990). Resting osteoblasts constitute the so called bone lining cells (Hall, 2015). As bone matrix deposition continues, osteoblasts become embedded in the osteoid as osteocytes (**Figure 1.4 B**). Once embedded into the bone matrix, the osteocytes cease their matrix secretion activity and subsequently undergo a reduction in the RER and Golgi apparatus (Bonucci, 1990). Osteocytes communicate with neighbouring osteocytes and with cells on the bone surface via a network of cell processes, which are located inside canaliculi within the bone matrix (Palumbo et al., 1990). Osteocytes are mechanosensitive cells that regulate bone metabolism and control osteogenic cells on

the bone surface, through the secretion of signalling molecules (Klein-Nulend et al., 2013).

Not all vertebrates possess osteocytes, that distinguishes two categories of bone: cellular (osteocytic) and acellular (anosteocytic) bone, the latter being devoid of osteocytes (Huysseune, 2000). Similar to tetrapods, the bone of more basal teleosts, such as zebrafish, contains osteocytes. However, osteocytes are not present in all life stages and also not in all skeletal elements of teleosts. As an example, early zebrafish bone is acellular and scales and fin rays remain anosteocytic throughout life (Witten et al., 2001; Sire and Akimenko, 2004). Instead, advanced teleosts, such as medaka, have completely lost osteocytes also in the endoskeleton. Thus, alternative regulatory pathways must have evolved that compensate for the absence of osteocytes (Witten and Huysseune, 2009).

Bone, both cellular and acellular, is continuously subjected to resorption and remodelling. Usually the osteoclasts, bone resorbing cells, remove pre-existing bone and subsequently osteoblasts secrete new bone matrix. Resorption and remodelling are persistent processes that are needed i) for reshaping of the skeleton during ontogenetic growth, ii) for mechanical adaptation to certain physical conditions, iii) for physiological demands related to mineral metabolism (Ricqlès et al., 1991). In mammals, osteoclasts are multinucleated cells that originate from hematopoietic bone marrow cells and migrate to the site of bone resorption. Actively resorbing osteoclasts are anchored to the mineralised bone surface and present numerous infoldings of the plasma membrane, the so called “ruffled border”. At this location, following acidification of the extracellular environment, lysosomal acid hydrolases such as tartrate-resistant acid phosphatase (TRAP) break down bone matrix components and generate resorption lacunae (Marks and Popoff, 1990).

Typical multinucleated osteoclasts can also be found in teleosts (**Figure 1.4 C**). (Witten et al., 2000; Hall, 2015). Advanced teleosts with acellular bone usually have small, flat, mononucleated osteoclasts that resorb bone without generating resorption lacunae (Witten and Huysseune, 2009). They resemble bone lining cells rather than typical osteoclasts (**Figure 1.4 D**) (Witten, 1997; Witten et al., 2001). Thus, without

special labelling, their identification based on standard histological procedures can be challenging and these cells are often overlooked (Witten and Huysseune, 2009). Moreover, like mammals, teleosts with cellular bone can carry out bone resorption via osteocytic osteolysis (Witten et al., 2000; Wysolmerski, 2012).

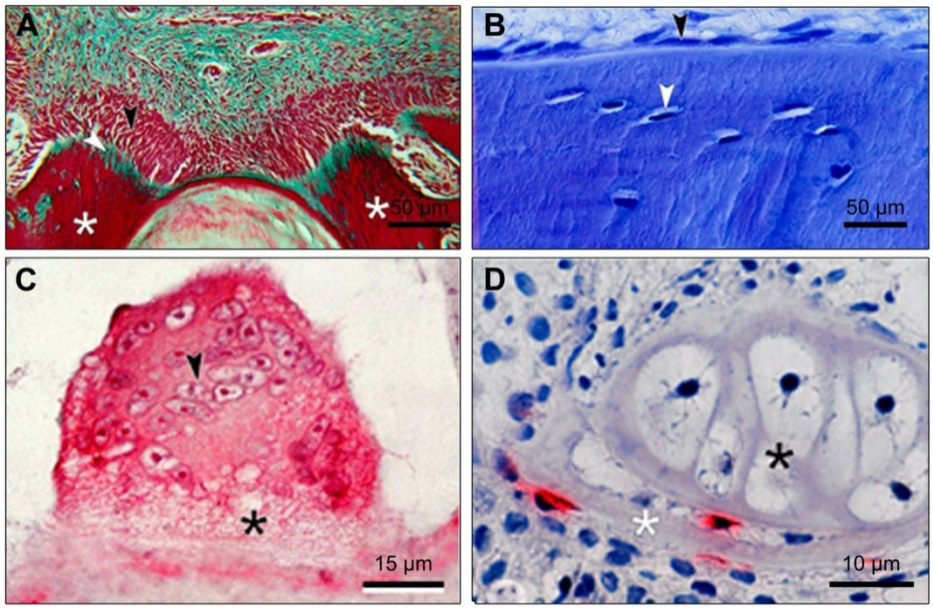


**Figure 1.4.** Histology of bone matrix and cells in teleosts. **A:** Dorsal growth zone of two opposing vertebral body endplates in salmon (*Salmo salar*). Osteoblasts (black arrowhead) secrete the non-mineralised osteoid (white arrowhead) and bone formation (white asterisks) is purely intramembranous (modified from Witten and Huysseune, 2009). **B:** Cellular bone of carp (*Cyprinus carpio*) with bone lining cells (black arrowhead) and osteocytes (white arrowhead) (modified from Witten and Huysseune, 2009). **C:** Multinucleated, tartrate-resistant acid phosphatase (TRAP) positive (red) giant osteoclast resorbing the lower jaw in salmon (*Salmo salar*). About 30 nuclei (black arrowhead) are visible. The typical ruffled border is present (black asterisk) (modified from Witten and Huysseune, 2009). **D:** Mononucleated TRAP-positive osteoclasts (red) in a 20 day old zebrafish (*Danio rerio*) along the forming dentary bone (white asterisk). Meckel's cartilage, black asterisk (modified from Witten and Huysseune, 2009).

### *Dentin*

Dentin, one of the tissues that build up vertebrate teeth, is a mineralised tissue that shares many similarities with bone. Its organic matrix is composed of largely the same major constituents as bone, mostly collagen type I, glycoproteins and lipids

(Scott and Symons, 1977). However, at least in mammals, some matrix proteins are dentin-specific, such as dentin phosphoprotein and dentin sialoprotein (Butler, 1998). Different types of dentin exist among vertebrates, and they are characterised by distinctive features at the level of collagen fibre size and orientation and/or incorporation of vascular elements or of cell bodies into the matrix (Schaeffer, 1977). Orthodentin is the only type of dentin of extant tetrapods and predominates in teleosts (Herold, 1971; Bergot, 1975).

Dentin encloses a pulp cavity where odontoblasts, the dentin-forming cells, reside together with nerves and blood vessels (Hall, 2015). Odontoblasts send cellular extensions, called odontoblasts processes, within the dentin they produce. Such cytoplasmic protrusions extend throughout the entire dentin thickness within dentinal canals, i.e. the dentinal tubules (Scott and Symons, 1977). Although dentin is highly porous due to the high density of tubules, the architecture of its collagen fibres and mineral crystals guarantees a high degree of elasticity and strength (Carlson, 1989). In addition, dentin is capped with enamel/enameloid (see below), which further ensures its integrity.

Facing the pulp cavity, the layer of dentin matrix immediately adjacent to the odontoblasts is non-mineralised and called pre-dentin. As dentin is being deposited, incremental growth lines occur along the tooth axis, as documented in both mammals and teleosts (Herold and Landino, 1970; Shellis and Berkovitz, 1976; Kerebel and Le Cabellec, 1979; Huysseune and Sire, 1998).

*Enamel/enameloid*

Enamel and enameloid are amongst the hardest biological tissues. Enameloid is present in bony fish, enamel is typical of mammals but it is also found in actinopterygian fishes (Sasagawa et al., 2009). Both enamel and enameloid cover the tooth surface and are supported by the underlying dentin. Enamel is a highly mineralised tissue, its inorganic components account for up to 97%, while its organic component (non-collagenous proteins) is less than 1% (Scott and Symons, 1977). In contrast, although still highly mineralised, the organic matrix of enameloid contains

collagen type I, sulphated glycoconjugates, and proteins homologous to those in mammalian enamel, such as amelogenins and enamelins (Sasagawa and Ferguson, 1990; Prostak et al., 1991; Ishiyama et al., 2001; Satchell et al., 2002).

Enamel is produced by the dental epithelial cells only. In contrast, enameloid is formed by the cross-talk of both odontoblasts and dental epithelial cells (Sasagawa et al., 2009). Morphological observations suggest that odontoblasts exhibit well-developed organelles such as endoplasmic reticulum and Golgi apparatus, that are related to the secretion of collagen fibrils as well as sulphated glycoconjugates and matrix vesicles during enameloid matrix formation (Sasagawa, 1988, 1995). The odontoblast processes usually continue in mature enameloid. During the later stages of enameloid formation and maturation, odontoblasts begin to make dentin beneath the enameloid, while dental epithelial cells degrade the organic matrix and supply inorganic ions for enameloid hypermineralisation (Sasagawa and Ishiyama, 2005a, 2005b; Sasagawa et al., 2006).

## The zebrafish skeleton

The zebrafish skeleton consists of a dermal skeleton and an endoskeleton. Scales, teeth, and fin rays are part of the dermal skeleton and are distinctive in their ability to regenerate (Van der heyden and Huysseune, 2000; Sire and Akimenko, 2004; Witten et al., 2010). The endoskeleton consists of cranial, axial, and appendicular skeletal elements (Bird and Mabee, 2003). The craniofacial skeleton arises mostly from the cranial neural crest cells and includes parietal bones, jaw bones, and opercles (bones covering the gills) (Kague et al., 2012). The adult zebrafish skull is composed of 74 bony elements (of which the majority are cartilage bones), and is far more complex in terms of number of bones (Hyman, 1979), diversity of skeletal types (Benjamin, 1990), and articulations, than the skulls of other model organisms including mammals (Owen, 1854; Fisher and Mabee, 2004).

The axial skeleton develops from somite-derived paraxial mesoderm (Gilbert, 2003) and comprises the vertebral column, ribs, intermuscular bones, as well as median (unpaired) dorsal, anal, and caudal fins (Bird and Mabee, 2003).

For the purpose of this thesis, the zebrafish vertebral column and dentition will be described in more detail.

### ***Vertebral column***

#### *Development*

As in other vertebrates, the vertebral column in zebrafish develops from sclerotome, a mesenchymal cell population derived from the ventral somite. Sclerotome cells, that will contribute to the vertebral column development, migrate to positions adjacent to the notochord and the neural tube (Morin-Kensicki et al., 2002). The notochord has an active function in vertebral column development. There is increasing evidence that the notochord contains patterning information that contributes to the segmentation of the vertebral column, segmentation that is yet influenced by the somites (Lleras Forero et al., 2018; Witten and Hall, 2021).

The first indication of the notochord segmentation is the establishment of mineralised centra anlagen, i.e. the chordacentra, within the notochord sheath, prior to any bone matrix deposition (Bensimon-Brito et al., 2012b; Witten and Hall, 2021). In zebrafish, the chordacentrum derives from a ring-shaped mineralisation, a feature that occurs also in other taxa (**Figure 1.5 A**) (Laerm, 1979).

The early notochord mineralisation in zebrafish is correlated to two major bone-related proteins: osteocalcin and alkaline phosphatase. Osteocalcin is the most abundant non-collagenous protein in bone of vertebrates, including teleosts (Nishimoto et al., 2003). The expression of osteocalcin (or osteocalcin1), one of the two isoforms present in teleosts (the second one is named osteocalcin-like or osteocalcin2), is detected in zebrafish prior to any osteoblast differentiation or mineralisation event. Moreover, its expression is exactly positioned in the ring where mineralisation of the chordacentrum occurs (**Figure 1.5 B-D**) (Bensimon-Brito et al., 2012b). In contrast, expression of osteocalcin2 is first detected at 7 days post-fertilisation and it is positioned at the neural and haemal arches. Therefore, it is hypothesised that osteocalcin2 is not connected to chordacentra mineralisation (Bensimon-Brito et al., 2012b). Also alkaline phosphatase activity, an enzyme essential for mineralisation, co-localises with the sites of chordacentra mineralisation prior to any bone deposition outside the notochord sheath (Grotmol et al., 2005; Bensimon-Brito et al., 2012b).

The chordacentra are laid down in a metameric manner in an anterior to posterior sequence (Du et al., 2001; Morin-Kensicki et al., 2002; Fleming et al., 2004). The chordacentra within vertebrae 3 and 4 are the first to mineralise, followed by chordacentrum 5 and two anterior chordacentra 1 and 2 (Morin-Kensicki et al., 2002; Bird and Mabee, 2003). The chordacentrum formation is followed by the differentiation of the sclerotome-derived mesenchymal cells into osteoblasts (Grotmol et al., 2003) , that lay down the first peri-notochordal bone on the chordacentrum anlagen, establishing the autocentrum (Nordvik et al., 2005). Autocentrum formation is initiated at the centre of the vertebra and proceeds anteriorly and posteriorly. At the same time the notochord, its epithelium, and the remainder of the fibrous sheath tissues become

further expanded in the intervertebral regions, giving rise to the intervertebral ligaments (**Figure 1.5 E-F**) (Laerm, 1976).

Vertebral body centra are then deposited by osteoblasts lining the outer surface of the bone through direct intramembranous ossification, without cartilaginous template (Arratia et al., 2001; Nordvik et al., 2005; Witten and Hall, 2021). Bone deposition takes place outside the elastica externa and no deposition of bone takes place on the inner surface (**Figure 1.5 E-F**) (Ekanayake and Hall, 1988; Arratia et al., 2001).

*Morphology*

The functional segmental unit of the vertebral column, the vertebra, is essentially composed of the vertebral body or autocentrum, dorsally extending neural arches and spines, ventrally extending haemal arches or attachment sites for ribs (Morin-Kensicki et al., 2002). The fully developed zebrafish vertebral column displays a mode of 33 vertebral bodies. Vertebral numbers reported in the literature range from 28 to 34 (Hall and Witten, 2019). From anterior to posterior, the vertebral column in subdivided in different regions as follows: the first four vertebrae constitute the Weberian apparatus, followed by 10 abdominal vertebrae, one or two transitional vertebrae, 15 caudal vertebrae and three to four modified caudal fin vertebrae that support the caudal fin (**Figure 1.5 G**) (Arratia et al., 2001; Bird and Mabee, 2003; Bensimon-Brito et al., 2012b).

The Weberian apparatus is very complex and it is subdivided into the Weberian ossicles (scaphium, claustrum, intercalarium, tripus), four modified vertebral centra with modified neural arches and spines and modified ribs, and supraneural bones (Bird and Mabee, 2003). The Weberian apparatus is an adaptation occurring in a large clade of teleost fishes, the otophysans, that include members of Cypriniforms such as zebrafish (Fink and Fink, 1996). It provides a route for the transmission of sound/vibration from the swim bladder to the inner ear (Weber, 1820).

The abdominal region of the vertebral column includes those vertebrae posterior to the Weberian vertebrae and anterior to the caudal vertebrae. Abdominal

vertebrae are composed of centra, neural arches and spines, parapophyses, and ribs. The caudal vertebrae do not possess ribs, but haemal arches and haemal spines (**Figure 1.5 H**). The last abdominal and/or the first caudal vertebra is frequently categorised as a "transitional" vertebra, exhibiting elongated unfused haemal arches or parapophyses, drastically shortened ribs, and absence of a haemal spine. The most posterior caudal fin vertebrae are modified to support the caudal fin (Bird and Mabee, 2003).

The vertebral centra of zebrafish, and of teleosts in general, are amphicoelous, their shape resemble biconical cylinders constricted in the centre with concave ends, called vertebral body endplates (**Figure 1.5 E,H**) (Witten and Hall, 2022). On the lateral surface of the centrum, thin longitudinal bony elements, i.e. the trabeculae, can extend along the antero-posterior axis (**Figure 1.5 E**). Likewise, the dorso-lateral and ventro-lateral surfaces of the centra exhibit longitudinal bones, i.e. the pre- and post-zygapophysis, which are a continuum of the neural and haemal arches (Laerm, 1976; Bird and Mabee, 2003).

The neural arches develop from bilaterally paired membranous bones, that extend dorsally and fuse medially to form the neural arch. Neural spines develop as single median dorsal extensions from the fused neural arches. Haemal arches and their spines are present in the caudal vertebrae only and develop as neural arches, yet ventrally oriented (Bird and Mabee, 2003). Parapophyses, found in the abdominal vertebrae, are endochondral lateral bony extensions from centra that serve as articulation points for the ribs. Ribs are intersegmental rod-shaped membranous bones serving to protect the abdominal cavity (Bird and Mabee, 2003).

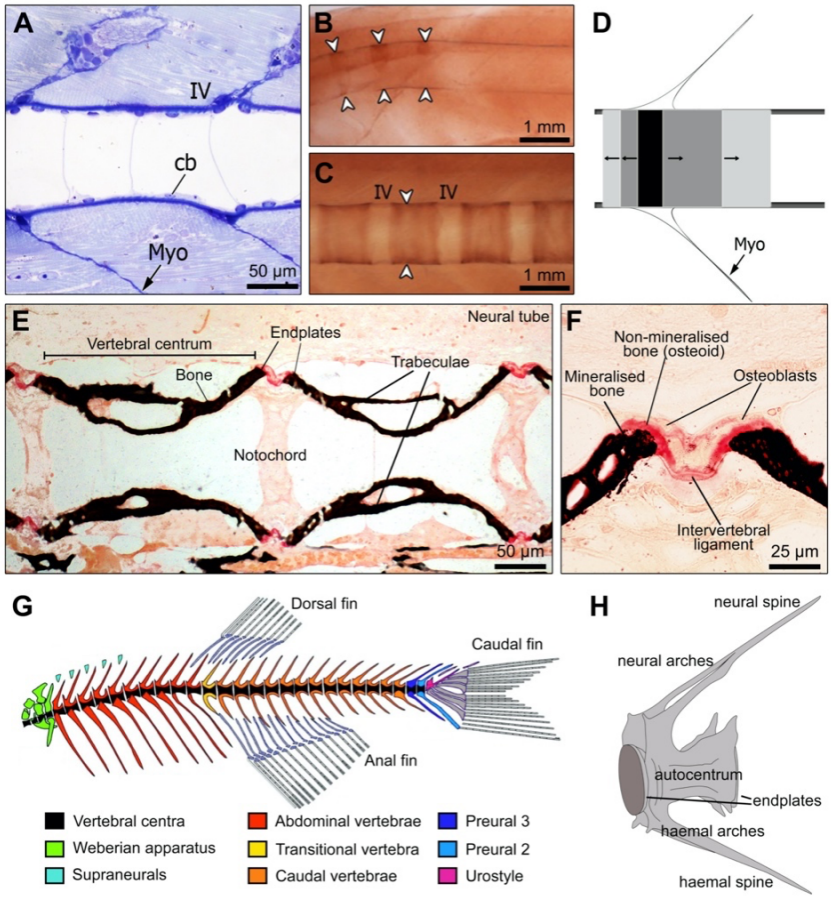


**Figure 1.5.** Vertebral column development in zebrafish. **A:** Sagittal section of a ring chordacentrum in 6 mm total length zebrafish showing the notochord (white vacuoles) and notochord cells (chordoblasts, cb) along the chordacentrum mineralisation. Myosepta (Myo) and intervertebral spaces (IV) are indicated (modified from Bensimon-Brito et al., 2012b). **B-C:** Osteocalcin immunostaining localises osteocalcin in early mineralised ring chordacentra (arrowheads in B, 4 mm total length zebrafish) and in later stages (arrowheads in C, 6 mm total length zebrafish) (modified from Bensimon-Brito et al., 2012b). **D:** Schematic representation of the mineralisation progress in a ring chordacentrum. Linear mineralisation fronts (arrows) expand along the antero-posterior axis (modified from Bensimon-Brito et al., 2012b). **E:** Sagittal section of adult zebrafish vertebral bodies showing mineralised (black) bone and trabeculae of the vertebral centra. Endplates are indicated. **F:** High magnification of vertebral body endplates, i.e. the bone growth zones, showing osteoblasts depositing non-mineralised bone matrix (the osteoid, red). Upon mineralisation, osteoid becomes mineralised bone (black). Endplates of two consecutive centra are connected by the intervertebral ligament. **G:** Scheme of the adult zebrafish axial skeleton showing vertebral centra, the different regions of the vertebral column, and the median (unpaired) fins (modified from Bird and Mabee, 2003). **H:** Schematic representation of an adult zebrafish caudal vertebral body, showing the autocentrum, the vertebral body endplates, the neural and haemal arches and spines (modified from Cotti et al., 2020).

***Dentition***

Zebrafish lack teeth in the buccal cavity. In zebrafish, teeth are associated only to the fifth ceratobranchials (the pharyngeal jaws) and are distributed along three rostro-caudal rows named ventral, mediodorsal and dorsal row, with five, four and two teeth, respectively (Van der heyden and Huysseune, 2000; Wautier et al., 2001). In total, 11 tooth positions are present on each pharyngeal jaw (**Figure 1.6 A**).

During early development, the fifth ceratobranchials develop as paired cartilaginous anlagen and further differentiate as paired rod-like elements enveloped with perichondral bone. Later, intramembranous bone formation expands dorsally these bony elements (Huysseune et al., 1998). For this reason, most of the teeth in the ventral row are formed first, followed by most of the teeth in the mediodorsal row, and finally teeth in the dorsal row (Van der heyden and Huysseune, 2000). A complete dentition is established at 26 days post-fertilisation (Van der heyden and Huysseune, 2000) but zebrafish teeth are continuously replaced throughout life. The functional lifetime of a zebrafish tooth varies between eight and 12 days in young life stages (Van der heyden and Huysseune, 2000).

During tooth formation, matrix deposition is first deposited at the tooth tip; in the meantime, the dental epithelium grows towards the basis of the developing tooth and the dentin cone is formed. Then, the newly formed tooth attaches to the pharyngeal bone by formation of an attachment bone (**Figure 1.6 B**). Once the tooth is attached and has reached its final size, eruption occurs. After a functional lifetime (approximately 8-12 days), the tooth is shed, osteoclasts resorb part of the supporting bone (jaw bone), the attachment bone, and the dentin (Huysseune et al., 1998; Van der heyden et al., 2000).

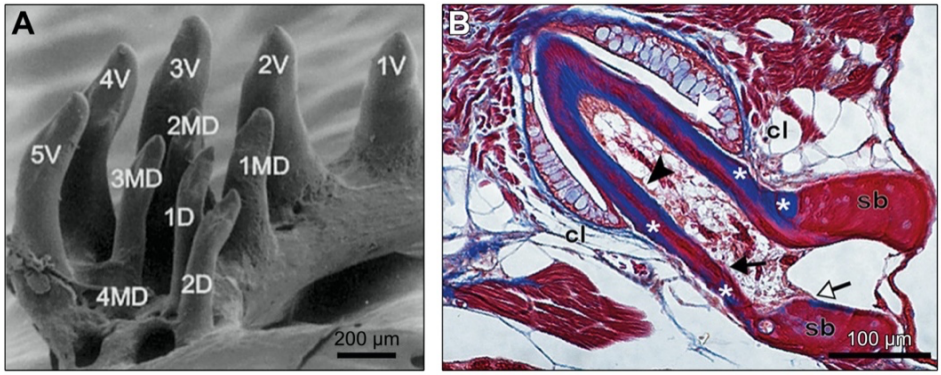


**Figure 1.6.** Zebrafish dentition. **A:** Scanning electron microscopy image of the zebrafish dentition, consisting of three tooth rows (V: ventral, MD: medio-dorsal, D: dorsal) with, respectively, five, four, and two teeth. Tooth number (1V, 2V, etc.) refers to their position in a certain row (modified from Van der heyden and Huysseune, 2000). **B:** Transverse histological section of an adult zebrafish tooth. The tooth is attached to the supporting pharyngeal bone (sb) via bone of attachment (asterisks) formed by osteoblasts-like cells (black arrow). Inside the pulp cavity, odontoblasts (black arrowhead) secrete dentin. Outside the tooth unit, ameloblasts (white arrowhead) contribute to the enameloid formation. cl, cervical loop; white arrow, osteoblasts (modified from Rosa et al., 2021).

## Bone mineralisation

Biomineralisation is the process through which living organisms produce the mineralised hard tissues of their dermal and endoskeleton. The term biomineralisation derives from the fact that tissue hardness is achieved through the deposition of various mineral ions in the context of organic extracellular matrices. When mineralised, skeletal tissues acquire certain biomechanical properties to serve specific biological functions, such as locomotion and support, feeding, protection, metabolism of calcium, phosphate and other minerals (Bonucci, 2012).

Evolutionarily, the first hard mineral fraction of mineralised tissues consisted mainly of calcium carbonate, present in the exoskeleton of marine invertebrates (Knoll, 2003; Wagner and Aspenberg, 2011). As part of the process of evolutionary adaptations, the skeletal tissues were internalised. Only two groups of invertebrates, brachiopods and conodonts, deposited calcium phosphate instead of calcium carbonate in their skeletal tissues (Hall and Witten, 2007; Turner et al., 2010). Although the exact reason that triggered this adaptation is still unclear, one hypothesis is that a calcium phosphate-based skeleton could serve as phosphorus (P) reservoir, given that P was a limiting factor in Palaeozoic aquatic ecosystems, thus providing physiological advantages to the organisms (Tarlo, 1964; Maisey, 1988; Hall and Witten, 2007; Witten and Huysseune, 2009).

The mineral composition of bone closely approximates hydroxyapatite ($Ca_{10}[PO_4]_6[OH]_2$). However, it is often modified with fluoride ($F^-$) or chloride ($Cl^-$) ions substituting the hydroxyl groups ($OH^-$), and magnesium ($Mg^{2+}$) or strontium ($Sr^{2+}$) replacing calcium ($Ca^{2+}$) (**Figure 1.7 A**) (Collins et al., 2022). The chemical structure of bone minerals implies that the extracellular levels of calcium ($Ca^{2+}$) and inorganic phosphate (Pi) are two critical determinants for bone mineralisation. Data from patients and animal models clearly demonstrate that the reduction of systemic Pi levels with or without any alteration of the $Ca^{2+}$ levels lead to osteomalacia, i.e. hypomineralised bone (Murshed, 2018; Drábiková et al., 2021).

Next to the inorganic $Ca^{2+}$ and Pi ions, of which homeostasis and metabolism will be described in the next section of this chapter, the organic part of the bone

extracellular matrix is a key determinant for mineralisation. Bone matrix is mainly composed of collagen type I. Individual collagen molecules assemble in the extracellular space to form collagen fibrils, characterised by gaps (or holes) and overlap zones that generate the typical banding pattern observed at the transmission electron microscope (Chapman and Hulmes, 1984). Early studies revealed that collagen fibrils provide a scaffold for initial nucleation of minerals, that occurs within the gap spaces, and at interfibrillar spaces between the fibrils (Sheldon and Robinson, 1957; Glimcher, 1959). In healthy conditions, the mineralisation of the non-mineralised collagen (osteoid) occurs in continuation of the existing mineralised matrix on which the newly synthesised osteoid is deposited by the osteoblasts (Murshed, 2018; Witten et al., 2019).

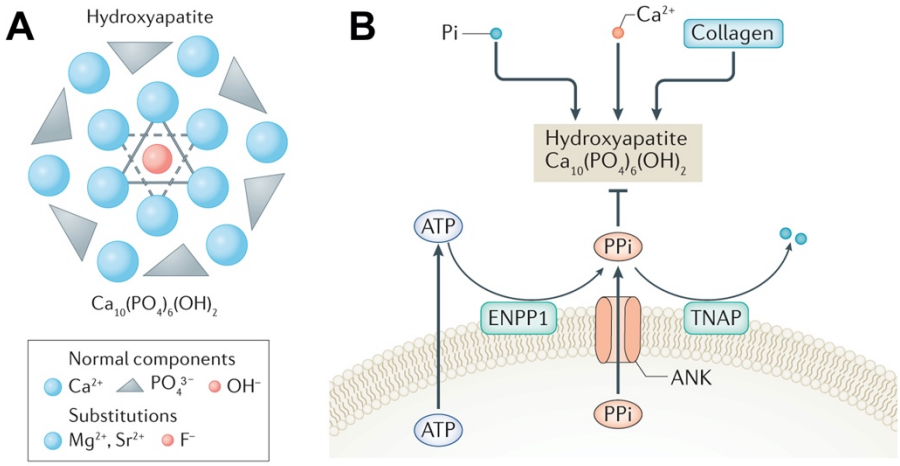


**Figure 1.7.** Bone mineralisation. **A:** Scheme of the chemical structure and composition of a generic crystal of hydroxyapatite ($Ca_{10}[PO_4]_6[OH]_2$). This structure is often modified with fluoride ($F^-$) or chloride ($Cl^-$) ions substituting the hydroxyl groups ($OH^-$), and magnesium ($Mg^{2+}$) or strontium ($Sr^{2+}$) replacing calcium ($Ca^{2+}$) (modified from Collins et al., 2022). **B:** Regulation of bone mineralisation relies on activators (inorganic phosphate (Pi or $PO_4^{3-}$), $Ca^{2+}$ and collagen) and inhibitors (pyrophosphate (PPi)). PPi is derived from nucleotide triphosphates (such as ATP) by pyrophosphatases (for example, ENPP1). Small amounts of PPi are also transported from the intracellular to the extracellular space by the transmembrane pyrophosphate channel progressive ankylosis protein homolog (ANK). Tissue non-specific alkaline phosphatase (TNAP) hydrolyses PPi (modified from Arnold et al., 2021).

***Regulation of bone mineralisation***

The process of bone mineralisation is tightly regulated by a variety of local and systemic factors. The coordinated action of these prevents hypo- and hypermineralisation of the skeleton, and prevents pathological mineralisation of soft tissues (Murshed, 2018).

The main factor preventing mineralisation is the presence of extracellular pyrophosphate (PPi), the most potent mineralisation inhibitor known for over 50 years (Fleisch and Bisaz, 1962). In soft tissues, such as blood vessels and some cartilaginous tissues, a wide distribution of PPi synthesis and/or extracellular transport machinery prevents pathological mineralisation (Murshed, 2018). The two main sources of extracellular PPi that have so far been identified are the pyrophosphate channel progressive ankylosis protein homolog (ANK) and ectonucleotide pyrophosphatase/phosphodiesterase family member 1 (ENPP1). While ANK transports intracellular PPi into the extracellular environment (Ho et al., 2000), ENPP1 exists in a secreted form as well as a membrane bound extracellular enzyme that hydrolyses extracellular ATP to AMP, releasing free PPi (**Figure 1.7 B**) (Hessle et al., 2002). Lack of ANK and ENPP1 leads to soft tissue mineralisation (Ho et al., 2000; Koshizuka et al., 2001; Apschner et al., 2014).

Interestingly, both *ANK* and *ENPP1* genes are highly expressed in the osteoblasts (Murshed et al., 2005). Although the presence of a mineralisation inhibitor in bone may appear counterintuitive, osteoblasts produce the membrane-bound enzyme tissue non-specific alkaline phosphatase (TNAP), a member of the alkaline phosphatase family of proteins that catalyse the hydrolysis of extracellular PPi (**Figure 1.7 B**) (Hessle et al., 2002). TNAP is a key player in bone mineralisation, given that patients and animal models carrying mutations in *ALPL* (the gene encoding for TNAP) suffer from hypophosphatasia associated to osteomalacia (Fedde et al., 1999; Mornet, 2000; Taillandier et al., 2001). In bone, TNAP-mediated hydrolysis of PPi results in the reduction of extracellular PPi and in the liberation of Pi ions, that enhance the formation and growth of the hydroxyapatite crystals (Hessle et al., 2002; Murshed et al., 2005). Thus, bone mineralisation can (in part) be explained by the unique co-

expression of tissue non-specific genes encoding collagen type I and TNAP. As a proof of concept, the misexpression of TNAP in other collagen-rich tissues, such as the dermis and blood vessels, causes their rapid mineralisation (Murshed et al., 2005).

However, recent studies pointed the attention to additional auxiliary mechanisms of bone mineralisation, that involve intracellular enzymes. Among those, phosphatase orphan 1 (PHOSPHO1) is an intracellular phosphatase that releases Pi from its substrates phosphoethanolamine and phosphocholine. Mice models lacking PHOSPHO1 have severe mineralisation defects (Yadav et al., 2011). How does an intracellular enzyme regulate a process that occurs outside the cells? A possible mechanism may involve matrix vesicles released by osteoblasts in mineralising tissues (Wu et al., 2002; Anderson et al., 2004; Golub, 2009). Although the exact mechanism has not been elucidated yet, it has been suggested that matrix vesicles provide an isolated microenvironment rich in $Ca^{2+}$ and Pi ions to facilitate the initial nucleation of hydroxyapatite. Mineral crystals formed inside the matrix vesicles grow progressively in size and eventually break the matrix vesicle membrane to be deposited on the collagen scaffold (Murshed, 2018).

## Bone mineral metabolism

### *Functions and sources of calcium and phosphorus*

The vertebrate skeleton represents a reservoir of calcium (Ca) and phosphorus (P) (and other minerals). Besides their role in formation and maintenance of bone, Ca and P participate in several other physiological processes.

Ca is one of the most abundant macronutrients in the body. Ca ions fulfil numerous functions that include contraction of skeletal and cardiac muscles, signal transduction, neurotransmission, and activation of several important enzymes (Lall, 2002). Different from tetrapods that rely on dietary intake only, teleosts can absorb Ca both from dietary sources as well as from the surrounding water (Vielma and Lall, 1998). The gills are an important site for Ca uptake in fish, where gas exchange provides the animals with continuous access to an unlimited Ca reservoir (Lall, 2002). However, usually Ca also occurs in adequate amounts in most fish diets (Lall, 2002).

P exists naturally as inorganic phosphate and as organic phosphate, bound in molecules such as sugars, proteins, and other components of the cell. P plays important roles as a structural component in phospholipids and nucleic acids, and as a constituent of highly active intracellular compounds, e.g. ATP. In addition, P participates in carbohydrates, lipids, and amino acids metabolism, as well as in muscle and nervous tissue metabolism (Lall, 2002). Similar to tetrapods, dietary P supplies most of the P required for growth and metabolism in teleosts (Vielma and Lall, 1998). The levels of inorganic P in water are very low (1–3 µM, according to Dean et al., 2015) and teleost fish cannot accumulate appreciable amounts of P from the environment via the gills (Vielma and Lall, 1998; Witten and Huysseune, 2009).

### *Calcium and phosphorus homeostasis*

In both mammals and teleosts, Ca plasma levels are tightly regulated and maintained within a narrow range, given that Ca level in the plasma controls cellular physiological functions (Favus et al., 2006; Guerreiro et al., 2007). Unlike the tight

control of Ca (close to 1.19 ± 0.04 mmol/L in plasma of Atlantic salmon according to Drábiková et al., 2021), P plasma levels can fluctuate widely (from 1.75 ± 0.20 to 4.76 ± 0.26 mmol/L in plasma of Atlantic salmon according to Drábiková et al., 2021) and largely depend on the efficiency of renal reabsorption. An adequate P concentration in plasma is, however, required to maintain the Ca:P ratio sufficient to support bone mineralisation and prevent mineralisation defects (low P plasma levels) as well as pathological soft tissue mineralisation (elevated P plasma levels) (Favus et al., 2006).

The hormones classically involved in mammalian P and Ca regulation play similar roles in teleost fish. These include vitamin D, fibroblast growth factor 23 (Fgf23), parathyroid hormone (Pth), stanniocalcin and calcitonin (Verri and Werner, 2019). These hormones control the absorption of Ca and P from the gastrointestinal tract, influence their deposition and resorption in bone, and influence their renal reabsorption and excretion (Lall, 2002).

The active metabolite of vitamin D, 1,25-dihydroxycholecalciferol [1,25-$(OH)_2$D], increases Ca and P levels in plasma by stimulation of Ca and P absorption in the intestine, by increase of P renal reabsorption and by stimulating bone resorption (Lall and Lewis-McCrea, 2007; Verri and Werner, 2019). In contrast, Fgf23 is a major phosphaturic hormone that decreases renal P reabsorption and the production of vitamin D in the kidney and other tissues (Hori et al., 2011).

In mammals, PTH facilitates the synthesis of active vitamin D, and increases plasma Ca levels through enhanced renal reabsorption, increased bone resorption and stimulation of intestinal Ca absorption (Favus et al., 2006). Although it was believed that teleosts lack Pth (Lall, 2002), recently the Pth-like peptide named Pth4 was discovered (Suarez-Bregua et al., 2017). Pth4 can alter Ca and P levels and affects the expression of genes involved in P homeostasis, similar to mammalian PTH. In particular, excess of Pth4 induces a significant reduction of whole body P and Ca levels, increases expression of *fgf23* and results in a significant loss of mineralised bone (Suarez-Bregua et al., 2017; Verri and Werner, 2019).

Stanniocalcin, produced by the corpuscles of Stannius in the kidney, is likely the predominant hormone in regulating P and Ca metabolism in teleosts (Lall, 2002;

Verri and Werner, 2019). This hormone has hypocalcemic effects, given that it acts in gills and intestine to reduce Ca uptake (Sundell et al., 1992; Tseng et al., 2009), and it has hyperphosphatemic effects, given that it increases P renal reabsorption (Lu et al., 1994). Although mammals lack the corpuscles of Stannius, they possess two paralogue genes encoding for stanniocalcin, namely *STC1* and *STC2*. There are evidences that STC2 inhibits P transport in the kidney through transcriptional regulation of P transporter, thus reducing renal P reabsorption (Joshi, 2020).

Calcitonin, present in both teleosts and mammals, has (acute) hypocalcemic effects and acts as a physiological antagonist of Pth and vitamin D (Lall, 2002). When the blood Ca level is high, calcitonin prevents the mobilisation of Ca into plasma, thus inhibiting the reabsorption of Ca ions in the kidney and rapidly decreasing blood Ca to normal levels (Lall, 2002). However, the effects are often only transient (Verri and Werner, 2019). Its role in P and Ca homeostasis appears far less important than other hormones, although its action may be relevant, for example, in situations of extreme Ca stress such as during reproduction in teleost fish (Suzuki, 2005; Verri and Werner, 2019).

***Mineral deficiency***

Given their important roles for several physiological functions, Ca and P deficiency can have dramatic consequences for an organism.

In the case of Ca, its plasma concentrations must be maintained within very narrow limits and mammals involve their bone to control Ca plasma levels. Thus, in mammals Ca deficiency can have severe effects for the skeleton. In contrast, Ca deficiency usually does not occur in teleosts, given that their Ca requirements can also be met by the regulation of Ca absorption from the water (Lall, 2002; Witten and Huysseune, 2009; Dean et al., 2015).

In teleosts, the attention is directed to the nutritional requirement of P. Dietary P deficiency lowers the plasma and urine P concentrations (Lall, 2002; Drábiková et al., 2021). P deficiency leads to defective skeletal mineralisation and it has implications on the intermediary energy metabolism (Lall, 2002; Lall and Lewis-McCrea,

2007). Chronic P deficiency is associated with growth retardation, impaired feed efficiency, reduced appetite, reduced bone strength, increased body fat and bone deformities (Sugiura et al., 2004).

Whether P deficiency in zebrafish is a primary cause of skeletal malformations and how it affects skeletal development will be addressed in the next chapters of this thesis.

# Chapter 2

## Objectives and thesis outline

## Objectives

Phosphorus (P) is an essential macronutrient for several physiological processes, including bone mineralisation in vertebrates. Adequate dietary P levels should be available to prevent P deficiency-related effects, i.e. growth retardation, osteomalacia and bone deformities, as well as P-excess-related consequences, i.e. both soft tissue calcification and bone hypermineralisation.

The questions of this research project are addressed using zebrafish as vertebrate model, a well-established organism for the study of bone formation and bone-related diseases (Witten et al., 2017).

The first objective of the present thesis is to provide a better understanding of the effects caused by reduced and increased dietary P supply on different skeletal tissues (bone, dentin and enamel/enameloid) in order to i) expand the current knowledge on the mechanisms underlying osteomalacia and abnormal mineralisation and ii) to provide better insights into the relationship between bone formation and bone mineralisation.

The second objective is to investigate the effects of reduced dietary P intake in diseases causing excess mineralisation, e.g. osteogenesis imperfecta, in order to understand whether a dietary treatment could improve the bone fragility phenotype typical of this pathological condition.

## Thesis outline

Apart from the general introduction (**Chapter 1**) and general discussion (**Chapter 7**), this thesis is a collection of research articles that have been published or are in preparation for submission to a scientific peer-reviewed journal. For this reason, the outline of the central chapters resembles almost exactly the published or submitted papers. Each chapter can be read as an independent unit, which leads to a partial overlap between the introduction and discussion sections of the different chapters. The referenced literature is compiled at the end of this thesis. All chapters have the PhD candidate as the first author.

**Chapter 3** examines the predominant effects of different levels of dietary P intakes on the post-cranial skeleton in zebrafish. Focusing on both endoskeletal and dermal skeletal elements, this chapter shows in detail how structure and mineralisation of different bone elements are affected by dietary P. This chapter also provides the first evidence that reduced dietary P conditions stimulate bone matrix formation in zebrafish.

**Chapter 4** addresses in more detail the increase in bone matrix formation under reduced P conditions. The non-mineralised bone formed under low dietary P retains the ability to mineralise when adequate P is supplied through the diet, resulting in an increased volume of mineralised bone. This chapter emphasises the beneficial effects of an alternation between reduced and increased dietary P intake on zebrafish bone. This approach can possibly contribute to reverse bone loss caused by age-related osteoporosis or other skeletal diseases.

**Chapter 5** provides the first evidence that a reduced dietary P intake can alleviate the bone phenotype in skeletal diseases characterised by excess mineralisation, e.g. osteogenesis imperfecta. The *Chihuahua* zebrafish mutant recapitulates the severe bone phenotype of patients, including low bone mass, bone hypermineralisation, bone fragility and skeletal malformations. This chapter describes the beneficial effects and the partial rescue of the severe bone phenotype using a reduced P dietary treatment in this zebrafish mutant.

**Chapter 6** describes the effects of dietary P levels on the zebrafish dentition, paying attention to the mineralisation of different dental tissues, i.e. enameloid, dentin, bone of attachment and pharyngeal bone. This chapter shows that dentin and bone of attachment structures are affected by dietary P and, similar to bone, their mineralisation responds to different P levels. Conversely, enameloid hypermineralisation is not influenced by dietary P. Evidence of the active mineralisation process of enameloid, based on P transport by the epithelium, is provided.

**Chapter 7** summarises the main findings of this thesis and provides a comprehensive view on the potential applications of the reduced dietary P treatment in the context of biomedical research.

# Chapter 3

## More bone with less minerals? The effects of dietary phosphorus on the post-cranial skeleton in zebrafish

This chapter is a published article:

Silvia Cotti, Ann Huysseune, Wolfgang Koppe, Martin Rücklin, Federica Marone, Eva M. Wölfel, Imke A. K. Fiedler, Björn Busse, Antonella Forlino and P. Eckhard Witten (2020) More bone with less minerals? The effects of dietary phosphorus on the post-cranial skeleton in zebrafish. *International Journal of Molecular Sciences* 21, 5429, doi:10.3390/ijms21155429.

## Introduction

Phosphorus (P) is an essential element for a wide variety of biological processes. It plays a key role in cellular metabolism, cell signalling, and the composition of phospholipid membranes and nucleic acids. For all vertebrates, P is crucial for mineralisation of the skeleton, bone, dentin, enamel/enameloid and mineralised cartilage. Naturally our ideas about bone mineral metabolism are influenced by insights that we have obtained from the mammalian (human) model. Vertebrates must control plasma calcium (Ca) within very narrow limits and mammals involve their bone to maintain plasma Ca levels.

Thus, Ca deficiency in mammals can have dramatic consequences for the skeleton. This is different for teleosts and other primary aquatic gnathostomes which are able to effectively obtain Ca from the water via the gills (reviewed by Witten and Huysseune, 2009; Dean et al., 2015). When the mineralised skeleton evolved, Palaeozoic aquatic ecosystems were rich in Ca with P as a limiting factor. Thus, it has been proposed that the early function of bone must have been the storage of P and not the storage of Ca as it is the case in mammals (Tarlo, 1964; Carroll, 1988; Hall and Witten, 2007; Witten and Huysseune, 2009).

Bone consists of an organic matrix, mainly represented by fibrillar collagen type I, and a mineral phase composed of Ca and P ions combined in apatite crystals. Osteoblasts, the bone-forming cells, secrete non-mineralised collagen matrix known as osteoid, that subsequently mineralises upon the removal of pyrophosphate by alkaline phosphatase, an enzyme produced by osteoblasts (Murshed et al., 2005). In human bone, osteoid mineralisation may start as late as 10 days after bone matrix formation (Boivin and Meunier, 2002). Bone formation and mineralisation depend on osteoblasts, whose activity in turn is regulated by osteocytes (Klein-Nulend et al., 2013).

Ca and P are closely involved in the development and maintenance of the skeletal system and their adequate intake is crucial to ensure bone health in all vertebrates. Teleost fish can obtain Ca by dietary or gill intake. Only a minimal amount of P can be obtained through the gills, thus like in tetrapods, P remains an indispensable component of the teleost diet (Vielma and Lall, 1998; Witten et al.,

2016). Similar to mammals, P homeostasis in teleosts relies on P absorption in the gut, excretion and reabsorption in the kidney and storage in the skeleton (Verri and Werner, 2019).

P deficiency can occur when dietary P supply is scarce. Dietary P deficiency in Atlantic salmon (*Salmo salar*) causes arrest of bone mineral deposition with no effects on bone matrix secretion (Witten et al., 2016, 2019). Similar effects were described for Nile tilapia (*Oreochromis niloticus*) (Takagi and Yamada, 1991). Likewise, P deprivation in murine models causes reduced mineralisation without affecting the production of the organic bone matrix (Baylink et al., 1971; Bonjour, 2011). In humans, insufficient dietary P intake is rare (Knochel, 1977) and causes hypophosphatemia, hypomineralised bones (osteomalacia) and rickets (Bonjour, 2011).

In mammals, P insufficiency is thought to be a primary cause of skeletal malformations. Early studies reported that patients suffering from hypophosphatemia are characterised by short stature, bowing of long bones and deformed vertebral column (Bishop, 1848; Anderson, 1878; Francis et al., 1995). Likewise, in teleosts under farming conditions, reduced growth, vertebral column and jaw deformities are related to dietary P deficiency (Sullivan et al., 2007; Deschamps et al., 2008; Fjelldal et al., 2012; Poirier Stewart et al., 2014; Baeverfjord et al., 2019). Interestingly, studies on Atlantic salmon under tightly controlled experimental conditions (avoidance of stress, no handling, no vaccination, control of all environmental parameters) with dietary P as a single variable do not show a direct relationship between dietary P deficiency and vertebral column malformations. Animals in their early seawater phase subjected to 10 weeks or 17 weeks of severe dietary P deficiency developed osteomalacia but none of the above mentioned malformations (Witten et al., 2016, 2019).

Excess dietary P leads to high serum P concentrations, potentially associated with toxic effects (Razzaque, 2011; Komaba and Fukagawa, 2016). For example, excess dietary P administration may induce metastatic deposition of calcium-phosphate (Knochel, 1977). Humans with normal kidney function but excess dietary P intake develop abnormal vascular calcification (Jono et al., 2000; Chen et al., 2002; Leopold, 2015). Studies on dogs that were fed a high P diet demonstrated increased soft tissue

calcification, particularly in the kidney (Saville and Krook, 1969; Krook et al., 1971; Laflamme and Jowsey, 1972; Cook et al., 1983) and increased accretion of cortical bone (Harris et al., 1976).

A better understanding of the effects caused by scarce and excess dietary P conditions on the skeleton can expand the current knowledge on the mechanisms underlying osteomalacia and abnormal mineralisation and provide better insight into the mineralisation process. *Danio rerio* (zebrafish) is an established model for the study of bone formation, given that basic bone cell differentiation pathways and ossification processes have been conserved across vertebrates (Witten et al., 2017). This study examines the post-cranial skeleton in zebrafish, given that the vertebral column is the most studied anatomical structure in biomedical research and in aquaculture (Gisbert et al., 2012; Tonelli et al., 2020b). Likewise, fin rays are popular for the study of bone regeneration and fish health (Christou et al., 2018; Phan et al., 2019). Focusing on both endoskeletal and dermal skeletal elements, this study shows in detail how structure and mineralisation of different bone structures are affected by dietary P content. With this new zebrafish model it is possible to falsify the following hypotheses: (a) under low P conditions, bone mineralisation stops but bone matrix formation increases without affecting the morphology of the bones and without causing vertebral body malformations; (b) high dietary P levels increase bone mineralisation, bone stiffness and promote vertebral body fusions; (c) bone matrix secretion and mineralisation are uncoupled processes at the cellular and subcellular level. This new zebrafish model represents a valuable tool to elucidate the primary effects of low and high dietary P levels on bone formation and mineralisation.

## Results

### *Zebrafish growth depends on dietary P*

A comparison of the standard length (SL) reveals that zebrafish treated with the low P (LP) diet are significantly smaller compared to the controls (regular P diet, RP) and high P (HP) diet treated animals after one month of treatment (**Figure 3.1 A** and **Table 3.1**). This difference becomes more evident after two months of treatment. In contrast, HP animals have significantly increased SL compared to LP at both timepoints and compared to RP after two months of treatment.

### *T0 animals display a mineralised vertebral column without any anomaly*

At the beginning of the experiment (T0), control specimens were analysed by Alizarin red S whole mount staining to establish the degree of vertebral column mineralisation and possible malformations. Bird and Mabee (2003) serve as reference for normal skeletal development in zebrafish. In addition several publications define malformations of the zebrafish axial skeleton (Ferreri et al., 2000; Martini et al., 2020; Printzi et al., 2020). The absence of any of the described malformations is regarded as normal in this study. None of the analysed samples presented malformations such as vertebral centra fusion, vertebral centra compression, curled or supernumerary arches (**Figure 3.1 B**). Histological analysis of sagittal sections further confirmed that vertebral bodies do not show malformations and that the notochord sheath, perinotochordal membrane bone and arches are properly mineralised (**Figure 3.1 C**).

**Table 3.1.** Standard length measures.

| Groups | | No. of Fish | Standard Length Mean ± SD (mm) | Pairwise *p*-Values | | |
|---|---|---|---|---|---|---|
| | | | | LP | RP | HP |
| 28 dpf | T0 | 96 | 6.02 ± 0.84 | | | |
| One Month Treatment | LP | 70 | 8.90 ± 2.47 | | $p$=0.001 | $p$=0.001 |
| | RP | 34 | 10.95 ± 3.13 | $p$=0.001 | | |
| | HP | 42 | 10.76 ± 3.03 | $p$=0.001 | | |
| Two Months Treatment | LP | 59 | 10.60 ± 2.79 | | $p$<0.001 | $p$<0.001 |
| | RP | 63 | 12.16 ± 3.15 | $p$<0.001 | | $p$<0.05 |
| | HP | 47 | 13.46 ± 3.62 | $p$<0.001 | $p$ < 0.05 | |

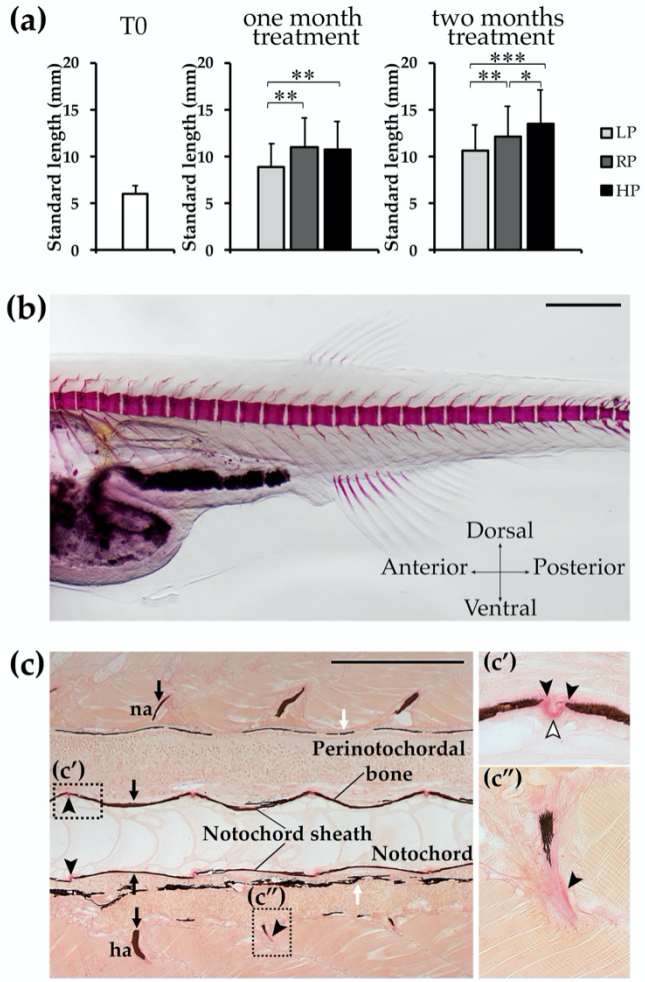


**Figure 3.1.** Zebrafish growth and T0 animals. **A**: Morphometric analysis of WT zebrafish at the beginning of the experiment (T0, 28 dpf) and after one and two months of treatment with the experimental diets. Animals treated with the low P diet (LP) are smaller than controls (RP) and high P diet (HP) treated animals, whereas HP zebrafish present a significantly increased standard length. Mann-Whitney test, *: $p<0.05$; **: $p<0.01$; ***: $p<0.001$. **B**: T0 zebrafish, prior the beginning of the experiment, stained with Alizarin red S shows normally developed vertebral column and forming vertebral bodies. No vertebral column malformations, nor vertebral body fusion or compression are present. Scale bar: 500 µm. **C**: Notochord sheath, perinotochordal membranous bone and neural (na) and haemal (ha) arches are mineralised in T0 animals, as shown by Von Kossa/Van Gieson staining on sagittal sections. Vertebral bodies are normally shaped and spaced. High magnification panels show (**C'**) vertebral endplates with osteoid (black arrowheads) and intervertebral ligament (white arrowhead, see **Figure 3.6 A** for details), (**C"**) haemal arch with non-mineralised collagen matrix (black arrowhead). Mineralised bone: brown (black arrows); pigment: black (white arrows), non-mineralised collagen matrix/osteoid: red (black arrowhead). Scale bar: 200 µm.

***Mineralisation of endoskeleton and dermal skeleton is arrested under low P conditions***

After two months of treatment, X-rays of vertebral columns from LP individuals show reduced radiodensity compared to vertebral columns of RP and HP animals (**Figure 3.2 A**). To better investigate the LP phenotype, bone mineralisation levels were evaluated on whole mount Alizarin red S stained specimens. In comparison to the control group (RP diet), LP animals display an overall low mineralised endoskeleton, including vertebral body centra and neural and haemal arches and spines. After one and two months under low P conditions, the majority of the animals have non-mineralised vertebral body endplates and largely non-mineralised neural and haemal arches. Conversely, the HP diet shows enhanced mineralisation of vertebral body endplates, neural and haemal arches. These structures are high mineralised after one and two months of dietary treatment in all the HP animals analysed (**Figure 3.2 B-E**, **Supplementary Table S3.1**). Compared to controls, LP and HP fish do not show a completely homogenous phenotype after one month of dietary treatment: a small percentage (8%, four fish out of 51) of LP animals shows fully mineralised vertebral body endplates and some HP individuals (19%, six fish out of 31) present non-mineralised endplates. However, all HP animals have fully mineralised vertebral body endplates after two months of HP diet (**Supplementary Table S3.1**). The histological analysis on non-demineralised sagittal sections of the vertebral column confirms these findings. Von Kossa staining for P allows the precise distinction between mineralised and non-mineralised bone (osteoid), comparable to the whole mount Alizarin red S staining for Ca. Both techniques show large amounts of non-mineralised collagen matrix at the rim of vertebral body endplates in LP animals. Moreover, sections stained with Von Kossa show that LP vertebral bodies are surrounded by large amounts of non-mineralised bone matrix, and vertebral centra bone trabeculae and arches present a similar phenotype (**Figure 3.2 F**). In contrast, vertebral body endplates and arches in control animals (RP diet) have narrow osteoid layers, indicative for fast mineralisation. The HP animals display an extremely thin osteoid layer at the vertebral endplates and

fully mineralised arches (**Figure 3.2 E**). The extent of bone matrix mineralisation level coincides with the dietary P content (**Supplementary Table S3.1**).

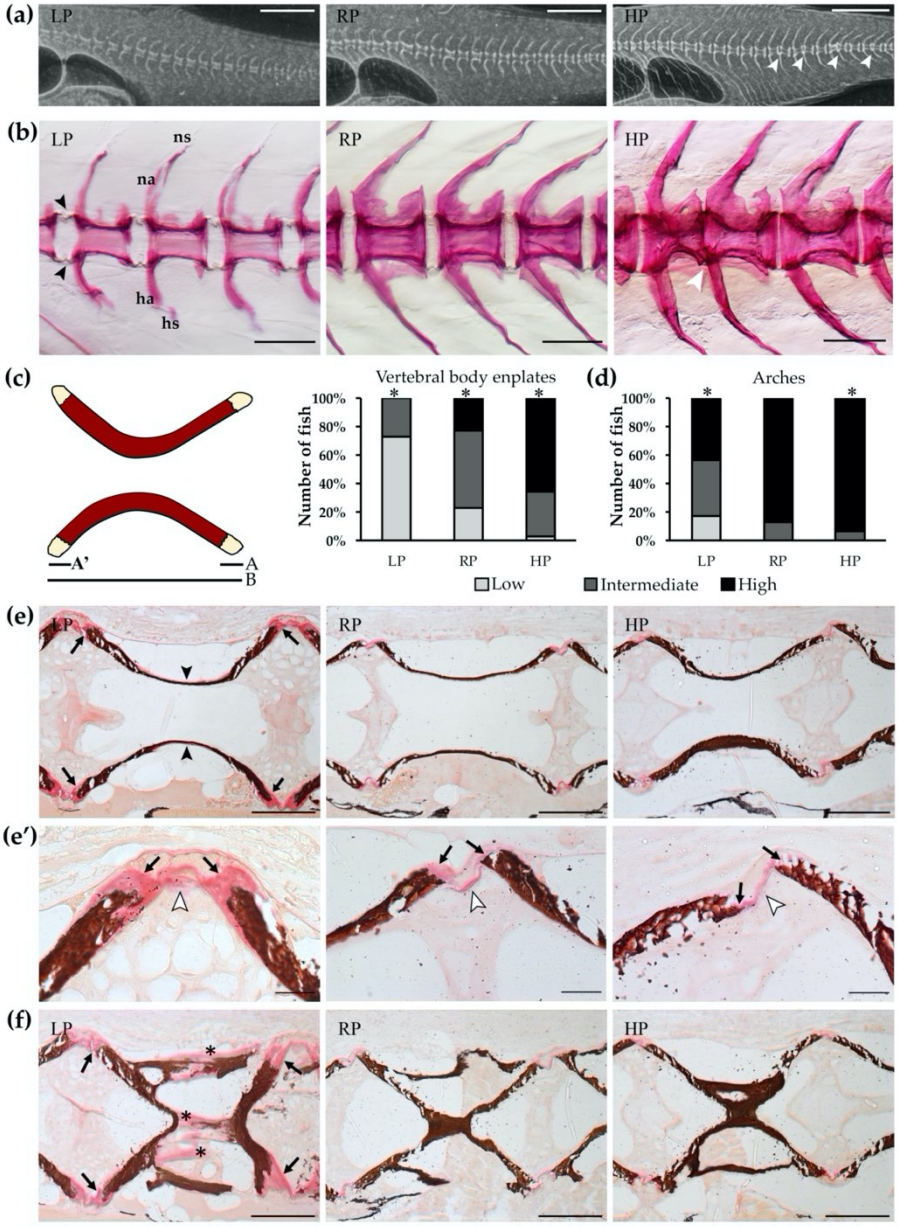


**Figure 3.2.** Mineralisation levels of vertebral column after two months of dietary treatment. **A**: Vertebral column of low P diet (LP) treated animals is characterised by reduced radiodensity compared to controls (RP) and high P diet (HP) treated animals. HP zebrafish present multiple vertebral body fusions (white arrowheads). Scale bar: 1 mm. **B**: Alizarin red S staining of vertebral

columns shows vertebral body endplates (black arrowheads) characterised by low mineralisation levels in LP animals, intermediate mineralisation in controls and high mineralisation levels in HP animals. HP zebrafish present vertebral body fusion (white arrowhead). Neural (na) and haemal arches (ha) are low mineralised and their spines (ns, hs, respectively) are deformed in LP individuals compared to RP and HP zebrafish. Scale bar: 200 µm. **C**: Quantitative analysis of vertebral body endplate mineralisation: the non-mineralised endplate is expressed as percentage of the total non-mineralised endplate length (A + A') over the total vertebral length (B), (A + A')/B. Chi-square or Fisher's exact test, pairwise comparison, *: $p<0.05$. **D**: Qualitative analysis of arch mineralisation levels. Please see Materials and Methods for further details. Chi-square or Fisher's exact test, pairwise comparison, *: $p<0.05$. **E**: Sagittal sections of vertebral bodies show large areas of non-mineralised matrix at the level of the vertebral endplates (black arrows) in LP animals compared to RP and HP animals. LP individuals present also a thin osteoid layer in the outer part of the vertebral body (black arrowheads), completely absent in RP and HP animals. Scale bar: 100 µm. (**E'**) High magnification of endplates in panel **E**. Extended non-mineralised bone matrix (black arrows) is visible in the vertebral endplates of LP animals. RP and HP zebrafish present thin endplates with reduced osteoid (black arrows). White arrowheads indicate intervertebral ligaments (see **Figure 3.6 A** for details). Scale bar: 20 µm. **F**: Mineralisation of bone trabeculae (asterisks) is also affected by low P levels in the diet. Black arrows: endplates. Von Kossa/Van Gieson staining: mineralised bone: brown; non-mineralised collagen matrix/osteoid: red. Scale bar: 100 µm.

Similar to vertebrae, mineralisation of the fin endoskeletal support elements ( pterygiophores or radials, according to Bird and Mabee, 2003) is affected after one and two months by dietary P. LP animals display a low or intermediate extent of bone matrix mineralisation, RP animals display intermediate mineralisation levels and HP animals have fully mineralised radials (**Figure 3.3** and **Supplementary Table S3.1**).

Dietary P affects also the mineralisation of the dermal skeleton as evident from the analysis of the lepidotrichia, which are paired fin ray segments that mineralise (Witten and Huysseune, 2007). Depending on dietary P content, lepidotrichia show progressively increasing mineralisation levels in the dorsal, anal, and caudal fin. After two months of treatment, the LP animals show low or intermediate lepidotrichia mineralisation. In contrast, in RP and HP animals the fin ray segments are fully mineralised (**Figure 3.3** and **Supplementary Table S3.2**).

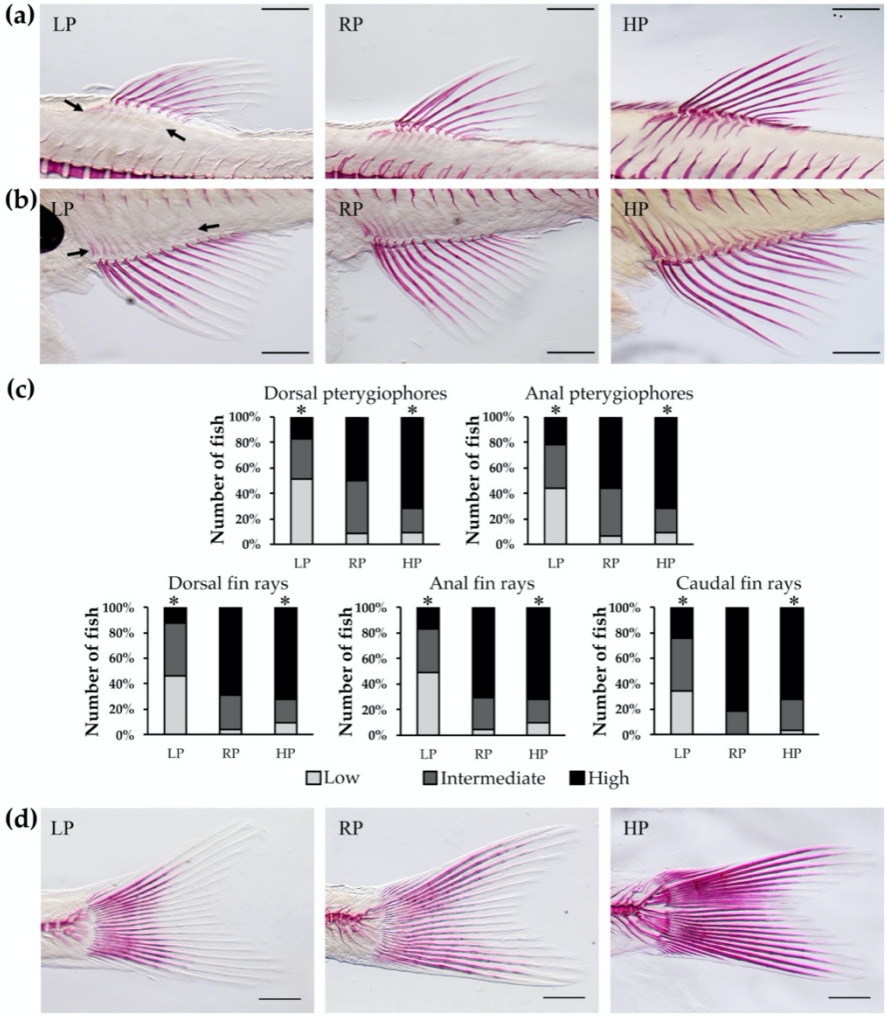


**Figure 3.3.** Mineralisation levels of median fin structures after two months of dietary treatment. Pterygiophores or radials, endoskeletal structures supporting the dorsal (**A**) and anal (**B**) fins (black arrows), present reduced mineralisation levels in low P diet (LP) treated zebrafish, in comparison with controls (RP) and high P diet (HP) fed animals. Likewise, Alizarin red S staining shows impaired mineralisation of dorsal and anal fin rays in LP animals. Scale bar: 500 µm. **C**: Analysis of pterygiophores and quantitative analysis of fin rays mineralisation levels. Pterygiophores mineralisation levels were qualitatively evaluated as low, intermediate or high depending on Alizarin red S distribution in the bone. Fin rays mineralisation levels were quantitatively analysed: low, more than two non-mineralised segments; intermediate, one or two non-mineralised segments; high: all segments mineralised. Chi-square or Fisher's exact test, pairwise comparison, *: $p<0.05$. **D**: Caudal fin rays stained with Alizarin red S display reduced mineralisation in LP animals compared to RP and HP zebrafish. Scale bar: 500 µm.

***Dietary P has no effect on vertebral morphology but HP animals have fused vertebral centra***

Detection of vertebral column abnormalities was performed on whole mount Alizarin red S stained specimens. After one or two months of treatment, none of the dietary groups display bending of the vertebral column (kyphosis, scoliosis, or lordosis). Vertebral bodies present in general a normal shape and size (but see below, vertebral fusion in HP animals). On the contrary, deformities of neural and haemal spines are present in most LP animals (**Figure 3.2 B**), suggesting that the non-mineralised collagen matrix is easily deformable by muscle contraction.

No deformities of vertebral body centra occur in LP and RP animals except a few cases of vertebral fusion and compression at both analysed timepoints (**Table 3.2**). Zebrafish treated for two months with the HP diet present an increased frequency of vertebral body fusions. More than a quarter, 28%, of the analysed specimens present at least one vertebral centra fusion. The increased occurrence of fusions in HP zebrafish is statistically significant (p=0.006). Interestingly, six out of nine animals that suffer from vertebral fusion have multiple fusions in the caudal region (Bird and Mabee, 2003) (**Table 3.2** and **Figure 3.2 A**). This suggests that high dietary P supply might promote vertebral body fusions.

**Table 3.2.** Diagnosed vertebral body malformations.

| Diets | | No. of Fish | Vertebral Body Compression | | | Vertebral Body Fusion | | |
|---|---|---|---|---|---|---|---|---|
| | | | No. of Fish with Compression | Total No. of Compression | Frequency | No. of Fish with Fusion | Total No. of Fusion | Frequency |
| One Month Treatment | LP | 51 | 5 | 6 | 10% | 4 | 4 | 8% |
| | RP | 21 | 2 | 2 | 10% | 0 | 0 | 0% |
| | HP | 31 | 4 | 4 | 13% | 1 | 1 | 3% |
| Two Months Treatment | LP | 44 | 3 | 4 | 7% | 2 | 2 | 5% |
| | RP | 49 | 2 | 2 | 4% | 7 | 10 | 14% |
| | HP | 32 | 3 | 3 | 9% | 9 * | 18 | 28% |

Vertebral centra with clear reduced anterior-posterior length were considered compressed. Statistical significance (* p=0.006) was determined by pairwise Chi-square test.

***High dietary P is associated with a higher stiffness in the vertebral endplates***

To assess if changes in dietary P influence the mechanical properties of the vertebral tissue, nanoindentation was performed (**Figure 3.4 A**). In the vertebral endplate regions, a significantly higher elastic modulus is noted in HP zebrafish with 18.48±3.18 GPa compared to LP zebrafish with 12.77±3.68 GPa (p=0.004), and a trend towards higher elastic modulus in HP compared to RP zebrafish with 15.57±4.30 GPa (p=0.073). In the central region, the elastic modulus is similar in all dietary groups with 11.44±3.05 GPa in LP, 13.47±2.01 GPa in RP, and 14.11±4.47 GPa in HP zebrafish (**Figure 3.4 B**). Endplate hardness values are different with 0.58±0.15 GPa in LP, 0.62±0.19 GPa in RP, and 0.63±0.17 GPa in HP zebrafish, but for the extremely small probes it was not possible to establish statistical significance. The same applies for hardness values in the central region, with 0.64±0.27 GPa in LP, 0.71±0.14 GPa in RP, and 0.59±0.22 GPa in HP zebrafish (**Figure 3.4 C**).

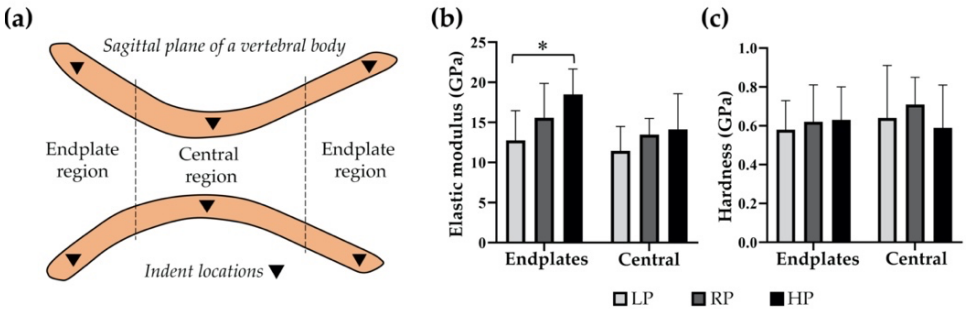


**Figure 3.4.** High dietary P is associated with higher stiffness in the bone formed after two months of treatment. **A**: Schematic representation of nanoindentation measurements in the sagittal plane of a vertebral body. **B**: In the endplates, the elastic modulus as indicator for stiffness shows significantly higher values in HP compared to LP (*: p=0.004), and a trend towards higher values in HP compared to RP (p=0.073). In the central region, all dietary groups show similar values. **C**: The hardness of the vertebrae is similar in all dietary groups in both the endplates and central regions.

***LP individuals have increased bone matrix formation and highly active osteoblasts***

Synchrotron based X-ray tomographic microscopy scans of a representative, similar-sized, specimen from each of the dietary groups reveal microstructural differences in the vertebrae of treated animals which are difficult to assess on whole mount Alizarin red S stained specimens. Although the analysed vertebral bodies in the caudal region (Bird and Mabee, 2003) of the vertebral column of LP, RP, and HP individuals have a similar length and height, the length of arches and spines varies, with a maximum value in the HP group and a minimum value in the LP group (**Figure 3.5** and **Supplementary Table S3.3**). Instead, the total vertebral body bone volume, calculated as the volume of vertebral body centra plus haemal and neural arches and haemal and neural spines, strongly differs between the representatives of the three diet groups. The total bone volume reaches a maximum in the individual from the LP group and a minimum in the HP animal. The RP individual has an intermediate bone volume. A pronounced increase in non-mineralised bone matrix is observed in the LP specimen compared to the RP and HP animals (**Figure 3.5** and **Supplementary Table S3.3**). Extensive non-mineralised bone matrix is localised at both vertebral endplates, at the neural and the haemal arches and at the neural and haemal spines in the LP animal. Volume data confirms that the volume of the newly formed bone in the LP vertebra is larger compared to the HP vertebra. In the individual from the HP group, endplates, arches and spines are completely mineralised but thinner than in RP vertebral bodies (**Figure 3.5**, and **Figure 3.2 E-F**).

Histological analysis showed that, in all dietary groups, intervertebral spaces are unaltered with normal intervertebral ligaments. The vertebral endplates are fully elongated without any malformation. Numerous osteoblasts are present in the growth zone of the vertebral body endplates (**Figure 3.6 A**). Transmission electron microscopy of representative specimens confirmed the presence of active osteoblasts in all dietary groups. All osteoblasts are characterised by a high number of endoplasmic reticulum (ER) cisternae. In the osteoblasts of the LP individual, ER cisternae are enlarged compared to the RP and HP individuals, indicative of increased cellular activity (**Figure 3.6 B**).

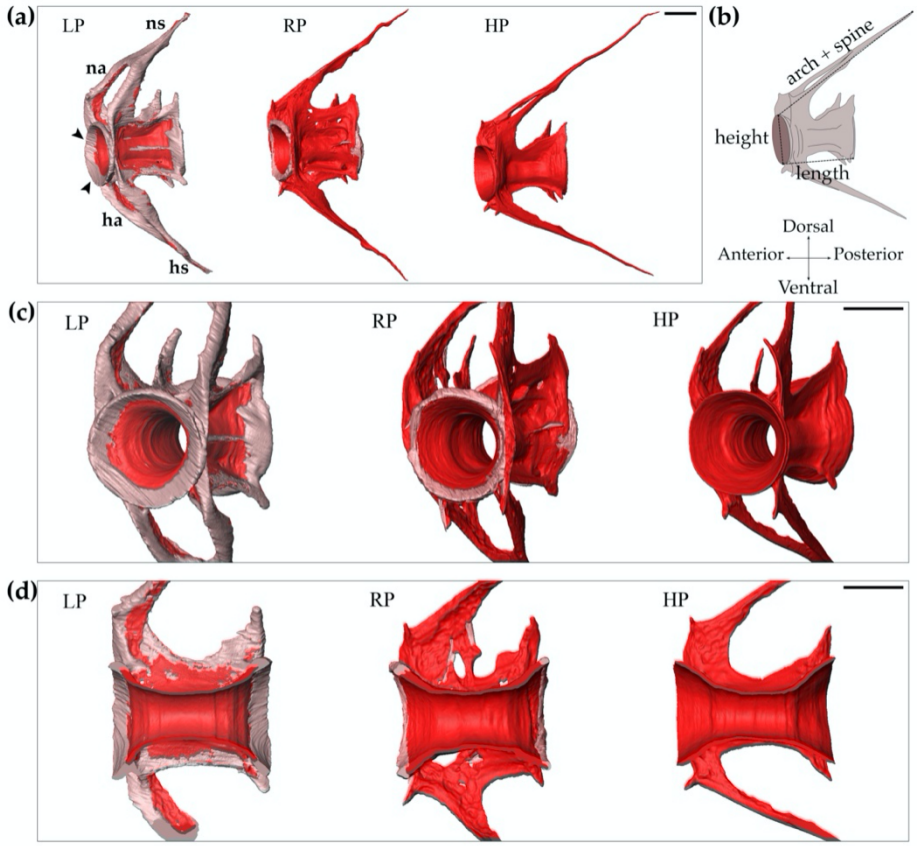


**Figure 3.5.** Increased bone formation in LP zebrafish after two months of dietary treatment. Synchrotron X-ray tomographic microscopy scans reveal an increased amount of non-mineralised matrix in the vertebral body and arches of low P diet (LP) treated animals compared to controls (RP) and high P diet (HP) treated individuals. **A**: Lateral view of the 10$^{th}$ caudal vertebral body, neural (na) and haemal (ha) arches and their spines (ns, hs, respectively). Vertebral endplates are indicated by black arrowheads. Scale bar: 100 µm. **B**: Schematic representation of the measured parameters: vertebral body length, vertebral body height, length of arch plus spine. **C**: Frontal view of vertebrae. Scale bar: 100 µm. **D**: Virtual sagittal sections of the vertebral bodies. Scale bar: 100 µm. Non-mineralised bone: pink; mineralised bone: red.

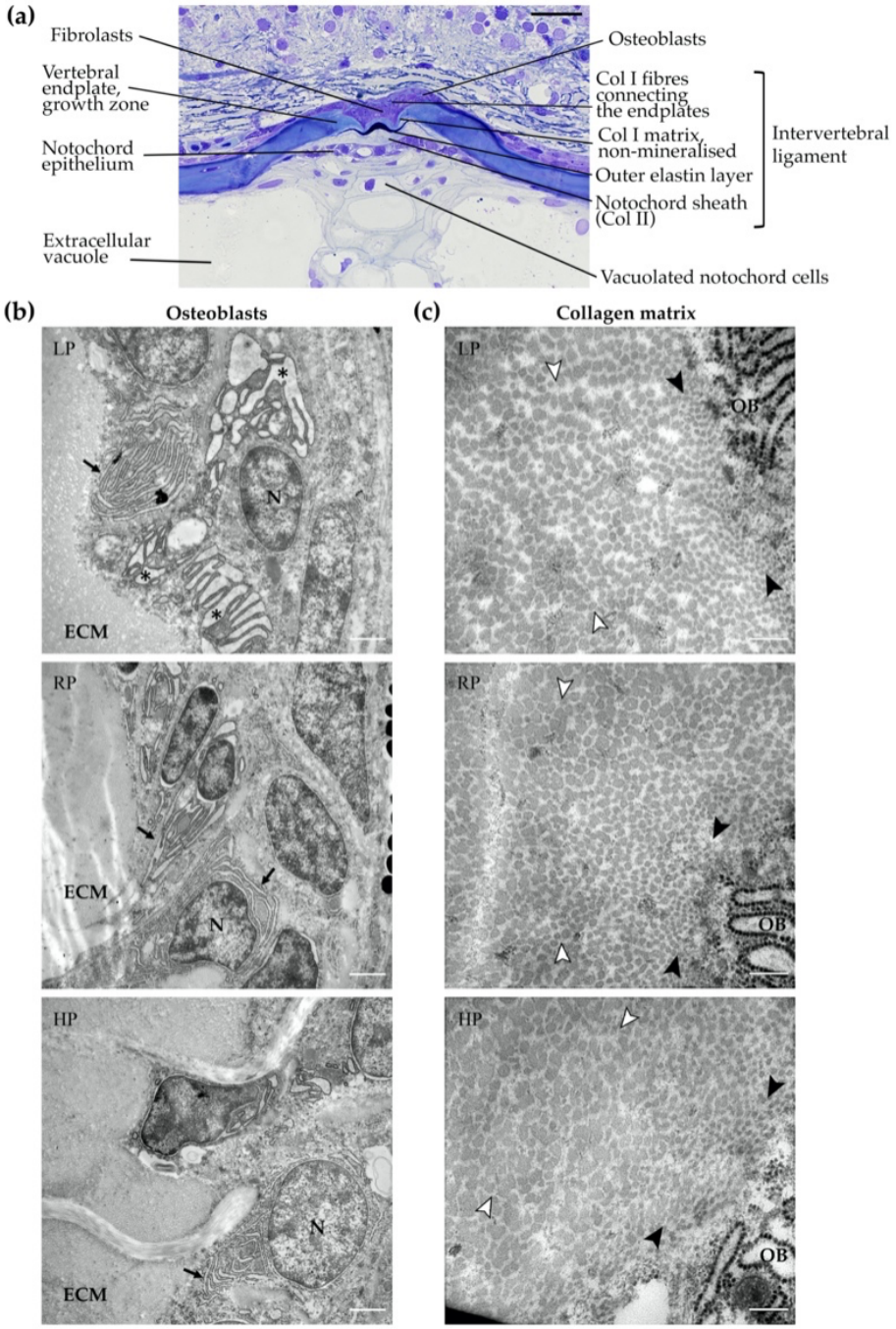


**Figure 3.6.** Osteoblasts and collagen type I in the vertebral body endplate growth zone. **A**: Representative toluidine blue stained semi-thin sagittal section showing internal structures of zebrafish vertebral centra and intervertebral ligament. Vertebral endplates are normally spaced

and fully extended in all dietary groups. The notochord sheath is composed of collagen type II (Col II) secreted by the cells of the notochord epithelium, also named chordoblasts. Vertebral bodies are interconnected by the notochord sheath and by collagen type I (Col I) fibres outside the notochord. All structures of the intervertebral ligament are unaltered. Osteoblasts in the vertebral endplate growth zone are located outside the notochord sheath between collagen type I fibres. Inside, the notochord is composed by vacuolated notochord cells and extracellular vacuoles. Scale bar: 20 µm. **B**: Transmission electron microscopy images of osteoblasts in the vertebral endplate growth zone after two months of dietary treatment. Osteoblasts are active and present a high number of endoplasmic reticulum (ER) cisternae (black arrows), which are enlarged in low P diet (LP) treated animals (asterisks) compared to controls (RP) and high P diet (HP) treated animals, indicative of increased bone matrix production. ECM: extracellular matrix, N: nucleus. Scale bar: 1 µm. **C**: Higher magnification of collagenous bone matrix located at the vertebral endplates. Collagen type I fibres in the immediate vicinity of osteoblasts (OB) have similar diameters among the three dietary groups, as well as collagen fibres located at a distance from the osteoblasts, within the extracellular matrix, indicative of unaltered fibre maturation. Black arrowheads: fibres in the vicinity of the osteoblasts with small diameters; white arrowheads: fibres at a distance from osteoblasts with large diameters. Scale bars: 200 nm.

***Collagen type I is unaltered in all dietary groups***

Electron microscopy was used to analyse collagen type I fibres in the bone growth zone of the vertebral endplates. Newly secreted collagen fibres in the close proximity of osteoblasts have similar diameters in animals of all three dietary groups (LP: 25.2±5.4 nm; RP: 26.3±7.3 nm; HP: 25.9±5.3 nm). Likewise, matured collagen fibres in the osteoid at a distance from the osteoblasts have similar diameters (LP: 49.1±11.0 nm; RP: 53.1±10.8 nm; HP: 52.6±9.4 nm) (**Figure 3.6 C**).

Given that activity of ER resident enzymes involved in collagen post-translational modification does not depend on P (Ishikawa and Bächinger, 2013), we hypothesised that normal collagen post-translational modification occurs in all dietary groups. SDS-Urea-PAGE analysis of collagen type I pepsin-extracted from bone shows similar electrophoretic migration of the α(I) chains bands in LP, RP, and HP animals, suggesting normal collagen post-translational modifications in all dietary groups (Ishikawa and Bächinger, 2013) (**Figure 3.7**).

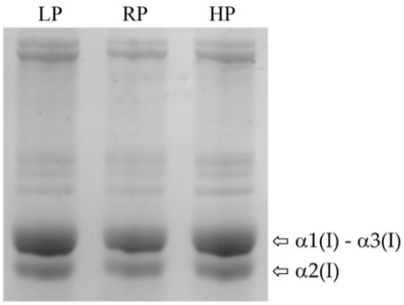


**Figure 3.7.** Electrophoretic analysis of collagen type I. Coomassie stained SDS-Urea-PAGE of collagen type I extracted from bone of low P diet (LP) treated zebrafish, controls (RP) and high P diet (HP) treated animals (pool of two samples per dietary group). Zebrafish present three collagen type I α chains [α(I)], named α1(I), α3(I) and α2(I). Collagen α(I) chains show bands with similar electrophoretic migration in all dietary groups.

## Supplementary results

**Supplementary Table S3.1.** Mineralisation levels of endoskeletal elements.

| Endoskeletal element | Diets | | No. of fish | Mineralisation level (No. of fish, %) | | | Pairwise p-values | | |
|---|---|---|---|---|---|---|---|---|---|
| | | | | Low | Intermediate | High | LP | RP | HP |
| Vertebral body endplates | one | LP | 51 | 67% | 25% | 8% | | p<0.001 | p<0.001 |
| | month | RP | 21 | 19% | 67% | 14% | p<0.001 | | p<0.05 |
| | treatment | HP | 31 | 19% | 35% | 45% | p<0.001 | p<0.05 | |
| | two | LP | 41 | 73% | 27% | 0% | | p<0.001 | p<0.001 |
| | months | RP | 48 | 23% | 54% | 23% | p<0.001 | | p<0.001 |
| | treatment | HP | 32 | 3% | 31% | 66% | p<0.001 | p<0.001 | |
| Neural and haemal arches | one | LP | 51 | 25% | 33% | 41% | | p<0.01 | p<0.01 |
| | month | RP | 21 | 0% | 24% | 76% | p<0.01 | | |
| | treatment | HP | 29 | 3% | 24% | 72% | p<0.01 | | |
| | two | LP | 41 | 17% | 39% | 44% | | p<0.001 | p<0.001 |
| | months | RP | 48 | 0% | 13% | 88% | p<0.001 | | |
| | treatment | HP | 32 | 0% | 6% | 94% | p<0.001 | | |
| Dorsal fin pterygiophores | one | LP | 51 | 38% | 31% | 29% | | | p<0.01 |
| | month | RP | 21 | 14% | 43% | 43% | | | |
| | treatment | HP | 29 | 14% | 21% | 66% | p<0.01 | | |
| | two | LP | 41 | 51% | 32% | 17% | | p<0.001 | p<0.001 |
| | months | RP | 48 | 8% | 42% | 50% | p<0.001 | | |
| | treatment | HP | 32 | 9% | 19% | 72% | p<0.001 | | |
| Anal fin pterygiophores | one | LP | 51 | 29% | 37% | 33% | | | p<0.01 |
| | month | RP | 21 | 14% | 38% | 48% | | | |
| | treatment | HP | 29 | 3% | 31% | 66% | p<0.01 | | |
| | two | LP | 41 | 44% | 34% | 22% | | p<0.001 | p<0.001 |
| | months | RP | 48 | 6% | 38% | 56% | p<0.001 | | |
| | treatment | HP | 32 | 9% | 19% | 72% | p<0.001 | | |

Statistical significance was determined by Chi-squared test or the Fisher's exact test.

**Supplementary Table S3.2.** Mineralisation levels of dermal fin rays.

| Dermal skeletal element | Diets | | No. of fish | Mineralisation level (No. of fish, %) | | | Pairwise p-values | | |
|---|---|---|---|---|---|---|---|---|---|
| | | | | Low | Intermediate | High | LP | RP | HP |
| Dorsal fin rays | one | LP | 51 | 24% | 41% | 35% | | | p<0.05 |
| | month | RP | 21 | 10% | 43% | 48% | | | |
| | treatment | HP | 31 | 7% | 28% | 66% | p<0.05 | | |
| | two | LP | 41 | 46% | 41% | 12% | | p<0.001 | p<0.001 |
| | months | RP | 48 | 4% | 27% | 69% | p<0.001 | | |
| | treatment | HP | 32 | 9% | 19% | 72% | p<0.001 | | |
| Anal fin rays | one | LP | 51 | 27% | 31% | 41% | | | p<0.05 |
| | month | RP | 21 | 10% | 29% | 62% | | | |
| | treatment | HP | 29 | 7% | 28% | 66% | p<0.05 | | |
| | two | LP | 41 | 49% | 34% | 17% | | p<0.001 | p<0.001 |
| | months | RP | 48 | 4% | 25% | 71% | p<0.001 | | |
| | treatment | HP | 32 | 9% | 19% | 72% | p<0.001 | | |
| Caudal fin rays | one | LP | 51 | 22% | 43% | 35% | | p<0.01 | p=0.01 |
| | month | RP | 21 | 10% | 14% | 76% | p<0.01 | | |
| | treatment | HP | 29 | 7% | 24% | 69% | p=0.01 | | |
| | two | LP | 41 | 34% | 41% | 24% | | p<0.001 | p<0.001 |
| | months | RP | 48 | 0% | 19% | 81% | p<0.001 | | |
| | treatment | HP | 32 | 3% | 25% | 72% | p<0.001 | | |

Statistical significance was determined by Chi-squared test or the Fisher's exact test.

**Supplementary Table S3.3.** Synchrotron X-ray tomographic microscopy data analysis.

| Diets | Vertebral body measures (∝m) | | Arches-spine length (∝m) | | Bone volume (∝m³) | | |
|---|---|---|---|---|---|---|---|
| | Length | Height | Neural arch-spine | Haemal arch-spine | Non-mineralised | Mineralised | Total |
| LP | 261.26 | 192.88 | 461.18 | 437.11 | $18.3 \times 10^5$ | $10.1 \times 10^5$ | $28.4 \times 10^5$ |
| RP | 266.82 | 191.46 | 568.44 | 521.84 | $2.2 \times 10^5$ | $18.7 \times 10^5$ | $20.9 \times 10^5$ |
| HP | 259.41 | 171.97 | 723.57 | 615.64 | 0 | $13.8 \times 10^5$ | $13.8 \times 10^5$ |

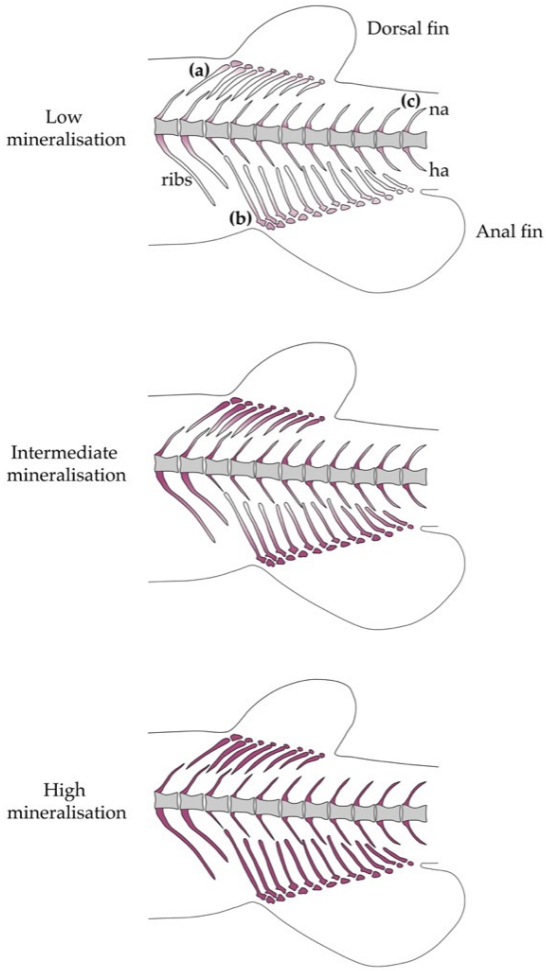


**Supplementary Figure S3.1.** Schematic representation of arches and pterygiophores mineralisation levels. Mineralisation levels of dorsal (a) and anal (b) pterygiophores and neural (na) and haemal (ha) arches (c) were qualitatively evaluated as low, intermediate or high depending on Alizarin red S distribution in bone. Red: Alizarin red S staining; grey: vertebral centra.

## Discussion

This study describes the primary effects of low and high dietary phosphorus (P) content in juvenile zebrafish. P is a critical element for several biological processes, including hard tissue mineralisation. An extended period of dietary treatment with different P levels affects growth, bone formation, bone mineralisation and bone mechanical properties. In particular, low dietary P (LP) level causes growth retardation but also increases non-mineralised bone matrix production, as indicated by histology and synchrotron X-ray tomographic microscopy. Endoplasmic reticulum cisternae of osteoblasts are enlarged, indicative for increased collagen synthesis, in line with the observed increase of bone matrix production. Conversely, high dietary P (HP) level increases growth, bone mineralisation and stiffness and promotes vertebral body fusions. Collagen post-translational modification, structure and arrangement of collagen fibres in the bone matrix are not influenced by dietary P content.

### *Skeletal mineralisation arrest under low P conditions*

The arrest of bone matrix mineralisation without the stop of bone matrix production is the primary effect of the LP diet on the skeleton of juvenile zebrafish. Structure and shape of the non-mineralised bone are normal. It can thus be defined as bone according to De Ricqlès et al. (1982): “mineralisation in bone can be missing alone or in combination with other components. Nevertheless, for reasons dealing with composition, homology, origin and function the tissue should be recognised as bone”. The LP zebrafish model recapitulates the bone phenotype typical of P deficiency that is also observed in other vertebrates. Indeed, mammals, including humans and rats, and teleost fish under dietary P deficiency, show bones with reduced radiodensity and an increased amount of osteoid at the level of epiphyseal plates (Bonjour, 2011), endosteal bone (Baylink et al., 1971), pharyngeal bone (Takagi and Yamada, 1991), and vertebral centra (Witten et al., 2016). Staining for mineral detection (whole mount Alizarin red S for Ca, Von Kossa on sections for P) reveals the lack of bone mineralisation in LP animals. Endoskeletal elements, such as vertebral body centra,

haemal and neural arches, and elements of the dermal skeleton, such as fin rays, are equally affected (**Figures 3.2** and **3.3**, **Supplementary Tables S3.1** and **S3.2**). Given that growing juvenile zebrafish were exposed for two months to low dietary P content, the presence of hypomineralised bones was expected. Still, bones are not only hypomineralised, but new bone matrix is formed and this matrix has no minerals. Our findings match previous studies that analysed the consequences of dietary P deficiency in Atlantic salmon (*Salmo salar*) (Witten et al., 2016, 2019; Baeverfjord et al., 2019) and in Nile tilapia (*Oreochromis niloticus*) (Takagi and Yamada, 1991). Moreover, the observed phenotype resembles the bone phenotype detected in murine models of heritable hypophosphatemia (Eicher et al., 1976; Tenenhouse, 1999; Wang et al., 2012), a disorder related to low P levels in the blood (Francis et al., 1995; Bacchetta and Salusky, 2012). Likewise, patients suffering from rickets present hypomineralised bones (Bonjour, 2011).

Conversely, in animals in this study that received a diet with regular P content (RP), bone mineralisation was normal and in line with previous studies that traced zebrafish skeletal mineralisation (Bird and Mabee, 2003). All bone structures analysed in the RP group present a small amount of non-mineralised bone identifiable as osteoid. Bone elements from HP fish are even further mineralised, the osteoid is extremely narrow.

This study shows that a low P diet arrests mineral deposition equally in endo- and dermal skeletal elements. The mineralised endoskeleton evolved much later than the mineralised dermal skeleton (Maisey, 2000). The latter comprises teeth, scales and fin rays (Reif, 1982; Sire and Huysseune, 2003; Witten et al., 2017). In the present study, the degree of dermal fin ray mineralisation coincides with the degree of vertebral body mineralisation (**Figures 3.2** and **3.3**, **Supplementary Tables S3.1** and **S3.2**). Likewise, a zebrafish mutant strain called nob (no bone) that completely lacks bone mineralisation presents non-mineralised dermal and endoskeletal elements to the same extent (Huitema et al., 2012). That fin rays can serve as indicators to track skeleton mineralisation has immediate applications. It will allow monitoring the mineralisation status of the overall skeleton related to dietary P content *in vivo*, using

vital mineral staining for fin rays (Bensimon-Brito et al., 2016). Such a non-invasive method avoids animal sacrifice in the context of low or high dietary P treatment or in other experiments which trace skeletal mineralisation.

***A functional and unaltered axial skeleton despite low dietary P***

In teleosts, particularly in farmed salmonids, dietary P deficiency has been linked to vertebral column malformations such as vertebral body compression and fusion (Sullivan et al., 2007; Deschamps et al., 2008; Fjelldal et al., 2012; Poirier Stewart et al., 2014; Baeverfjord et al., 2019). In this study, low dietary P content for two months does not cause vertebral centra deformities in juvenile zebrafish. Despite the lack of bone mineralisation, vertebral centra have a normal shape without alterations that would foreshadow vertebral body compression or fusion (Witten et al., 2006, 2009). Different from the unaltered centra, neural and haemal spines are twisted in LP animals. This phenotype has been described as sign of P deficiency in farmed teleost species such as Atlantic salmon, haddock (*Melanogrammus aeglefinus*), and halibut (*Hippoglossus hippoglossus*) (Baeverfjord et al., 1998; Roy and Lall, 2003; Lall and Lewis-McCrea, 2007). Similarly, low mineralised neural and haemal spines in LP zebrafish have an undulated shape (**Figure 3.2 B**), yet without signs of fracture. Indeed, the collagen-based bone matrix alone is a very tough material. The toughest known vertebrate bones are deer antlers, which can flex without damage due to their low degree of mineralisation (Currey, 1984, 2003). Notably, vertebral centra and arches and their spines are developmental modules, meaning that the control of their development is to a large degree independent (de Azevedo et al., 2012; Fleming et al., 2015; De Clercq et al., 2017). This could explain why spines are twisted but vertebral centra are not affected in LP zebrafish. In laboratory zebrafish strains, undulated spines also occur linked to conditions other than P deficiency such as increased rearing density (Martini et al., 2020) or disturbed somite formation (van Eeden et al., 1996). In addition, it has been suggested that spine deformities relate to musculature impairment (Backiel et al., 1984; Favaloro and Mazzola, 2006). The comparison of the results from this study with other studies that encountered malformed spines can,

however, be difficult. Other studies have used different species or different zebrafish strains, different rearing conditions and different diet formulations. Costa et al. (2018) tested the effect of six diets with different P levels on the zebrafish skeleton, but the diet composition was different from the one used in the present study. The diets contained poultry visceral meal and soy bean oil, whereas the diet used in this experiment contains krill meal, fish meal, and fish oil. Moreover, the inorganic P source in the present study is monoammonium phosphate (MAP), whereas dicalcium phosphate (DCP) was used by Costa et al. (2018). Solubility and digestibility, and thus the bioavailability of MAP, are considerably higher than DCP (Lall, 1991; Morales et al., 2018). This and other dietary ingredients could explain why our LP zebrafish do not develop vertebral centrum deformities, or other deformities encountered by Costa et al. (2018), such as severe bending of the vertebral column or craniofacial malformations. The phenotype of the control group (RP) in the present study, 1.0% total P based on MAP supplement, equals the phenotype obtained by Costa et al. (2018) with the diet containing 1.85% total P based on DCP supplement.

The absence of vertebral centra malformations in the LP zebrafish group is in line with what is observed in recent studies on Atlantic salmon. In two different experiments, animals in their early seawater phase received P deficient diets (50% of the total P requirement) for 10 weeks and 17 weeks. Like LP zebrafish in the current study, Atlantic salmon developed bone without minerals but no vertebral column deformities (Witten et al., 2016, 2019). It can of course not be excluded that a prolonged low P period would eventually generate skeletal malformations in growing zebrafish.

How can the absence of malformations in LP zebrafish be explained? From a functional point of view, the notochord alone in the absence of vertebral bodies can act as efficient axial skeleton. This is the case in teleost fish that hatch as embryos (Balon, 2003; Bensimon-Brito et al., 2012a) and in basal adult osteichthyans (Arratia et al., 2001). Members of several stem-ward groups, which comprise large animals such as dipnoans (lungfishes), coelacanths (crossopterygians) and sturgeons (chondrosteans, up to six meters in length), have a continuous non-constricted notochord as functional

axial skeleton and do not develop mineralised vertebral centra (Locket, 1980; Arratia et al., 2001; Leprévost et al., 2017). Also, the nob zebrafish mutant strain that completely lacks bone mineralisation, shows correctly patterned but non-mineralised vertebral body anlagen (Huitema et al., 2012). Moreover, several species of deep sea fish are characterised by extremely low mineralised skeletons and low mineralised vertebral centra (Denton and Marshall, 1958; Schnell and Johnson, 2017; Germain et al., 2019). Thus, a functional and healthy notochord that supports the axial skeleton may compensate for non-mineralised vertebral centra as it compensates for absence in other osteichthyans. Indeed, this study demonstrates that a two months period under low P conditions does not cause any morphological alteration of the vertebral centra in zebrafish, except osteomalacia. Internal vertebral centra structures appear unaltered on histological sections. Intervertebral ligaments and the notochord tissue in the intervertebral space of LP zebrafish (a region called intervertebral disk by Schaeffer, 1967) remain intact. This is an important observation because, also in teleosts, vertebral body malformations typically start with alterations of the intervertebral disk (Witten et al., 2006, 2009; Ytteborg et al., 2010). These findings strengthen the idea that P deficiency alone is not a primary cause of vertebral column abnormalities in zebrafish, and that other or additional factors trigger the development of malformations. Other factors that are currently discussed to cause vertebral column malformation in zebrafish and other teleost species are rearing temperature, excess swimming, increased rearing density or dietary vitamin A supply (Boglione et al., 2013; Fernández et al., 2018; Martini et al., 2020; Printzi et al., 2020).

***Is there a link between excess P content and vertebral fusion?***

In the present study, zebrafish from the HP group present an increased frequency of vertebral centra fusion. This suggests that high rather than low dietary P content could be a causative factor for vertebral body fusion in zebrafish. Up to now, little is known about the effects of dietary P excess on the development of skeletal malformations in teleosts (Lall and Lewis-McCrea, 2007). In mammals, however, ectopic mineralisation can be caused by excess dietary P intake. Humans with excess

dietary P ingestion develop abnormal mineralisation of the vascular tissue (Jono et al., 2000; Chen et al., 2002; Leopold, 2015). Dogs treated with high P diets developed mineralisation in the kidney (Saville and Krook, 1969; Krook et al., 1971; Laflamme and Jowsey, 1972; Cook et al., 1983) and increased accretion of cortical bone (Harris et al., 1976). Also metabolic disorders that increase plasma P levels can cause anomalous mineralisation of soft tissues, as reported in patients that suffer from chronic kidney disease (CKD) (Moe and Chen, 2008; Leopold, 2015) and in mice models of genetic diseases that cause hyperphosphatemia. Fgf23 is a hormone released by bone cells that down-regulates renal P reabsorption. Murine models with mutations of *Fgf23* or in genes encoding proteins involved in Fgf23 modifications, suffer from hypermineralisation adjacent to the growth plate in the primary spongiosa and hyperdense femur bones (Sitara et al., 2008; Ichikawa et al., 2009), similar to what observed in our HP zebrafish.

Pathological mineralisation that affects the vertebral column has been reported for zebrafish of the *enpp1* mutant strain. The lack of the ectonucleotide pyrophosphatase/phosphodiesterase-1 (Enpp1) reduces pyrophosphate, a mineralisation inhibitor generated by osteoblasts. The bones of juvenile *enpp1* mutants are hypermineralised and vertebral centra fuse (Apschner et al., 2014), a phenotype similar to vertebral fusions in HP zebrafish. Notably, the increased frequency of vertebral body fusions in HP zebrafish is only diagnosed after two months. This suggests that the prolongation of the dietary treatment is required before an effect can be observed. Further studies are required to clarify the exact mechanisms of vertebral body fusion related to high dietary P content.

Regarding the mechanical properties of the bone formed under the dietary treatment, a higher elastic modulus (increased material stiffness) was observed in the hypermineralised vertebral endplates of HP zebrafish compared to LP zebrafish. HP zebrafish also showed a tendency towards a higher elastic modulus compared to RP zebrafish. This suggests that not only a physiological increase in mineralisation, but also a dietary P-induced increase in mineralisation leads to a higher stiffness of bone (Currey, 2003; Pinheiro et al., 2009; Witten et al., 2019). It could be hypothesised that

the increased stiffness of the vertebral centra likely increased the mechanical load on the intervertebral space while swimming, causing compression and tension of the intervertebral ligaments in the caudal region (Symmons, 1979). Tension is a well-known trigger for the mineralisation of ligaments and tendons (Laerm, 1976; Weinans and Prendergast, 1996). Thus increased tension could trigger the mineralisation of the intervertebral ligaments, consequently leading to centra fusion (Witten et al., 2009).

***Less minerals but more bone production by osteoblasts***

Synchrotron X-ray tomographic microscopy allows the identification of mineralised and non-mineralised bone in the zebrafish vertebral bodies at a high resolution. The representative LP individual shows a vertebral body with an increased total bone volume in comparison to control and HP animals. The increase in bone volume is ascribed to a considerable increase of non-mineralised bone in the growth zone of the vertebral body endplates, neural and haemal arches and spines. Considering that animals of equal size were used from each group, it is intriguing to note that LP zebrafish show increased bone matrix formation. An increased production of collagen, consistent with the increased bone volume, suggests that osteoblasts are highly active at producing collagen matrix and this could explain the presence of enlarged endoplasmic reticulum cisternae in LP zebrafish (Shapiro et al., 1977; Boivin et al., 1990). The intensified matrix production does not influence collagen type I synthesis and post-translational modifications at the structural level. Collagen type I post-translational modification appears normal in LP zebrafish, as suggested by similar electrophoretic migration of α(I) chain bands in all dietary groups. Moreover, the progressive increase of collagen fibre diameter in the secreted bone matrix reflects normal fibrils maturation and aging (Jackson, 1956). Our observations agree with studies on Nile tilapia that show increased osteoid formation on pharyngeal bone in P-deprived animals (Takagi and Yamada, 1991). Likewise, hypophosphatemic rats present increased osteoid width (Baylink et al., 1971). In mammals, osteoid undergoes several chemical modifications, designated as maturation, prior to mineralisation (Baylink et al., 1970). It has been suggested that increased osteoid production in P-depleted rats

relates to a decreased rate of osteoid maturation, indicating a delay in the onset of mineralisation (Baylink et al., 1971). In Atlantic salmon, however, the non-mineralised bone formed under P deficient conditions can mineralise completely if the animals receive a P-sufficient diet (Witten et al., 2019). This, together with the normal post-translational modifications of collagen type I and the normal ultrastructure of collagen fibrils in LP zebrafish, argue in favour of normal bone matrix maturation also under low P conditions.

Maintaining bone mechanical stability could be a possible explanation for the increase of bone matrix production in LP zebrafish. As Ca and P contents in bone are always linked (Witten et al., 2016, 2019), the mechanical properties of bone change in accordance with the bones' mineral content (Currey, 2003), as also shown in this study. LP zebrafish could increase collagen secretion to compensate for the lack of minerals and reduced stiffness. Osteocytes are mechanosensitive cells that regulate bone formation and bone resorption in response to mechanical load. Upon mechanical stimuli, osteocytes are activated and produce signalling molecules that increase the activity of osteoblasts (Klein-Nulend et al., 2013). In particular, prostaglandins secreted by osteocytes stimulate bone formation in response to mechanical load *in vivo* (Smith et al., 1996; Nakashima et al., 2011). As the newly secreted matrix cannot mineralise due to insufficient P levels, stronger mechanical stimulation of osteocytes inside the soft non-mineralised bone could trigger an increased activity of the osteoblasts under LP conditions.

## Conclusions

In this experiment, a new zebrafish model for low and high dietary P levels demonstrates that low P levels in the diet have no negative effect on bone matrix formation, although new bone matrix remains non-mineralised. Moreover, no vertebral centra malformations occur, indicating that other factors may trigger the development of skeletal deformities. In contrast, high dietary P levels lead to increased bone mineralisation, increased bone stiffness and fusion of vertebral centra. Neither the lack of mineralisation, nor the high mineralisation affect collagen post-translational modifications, as expected given that ER resident enzymes do not depend on P (Ishikawa and Bächinger, 2013). Increased production of normal collagen matrix is observed in animals from the LP group: organic matrix is continuously produced and collagen fibres mature despite the arrest of mineralisation. The current findings therefore support the idea that bone matrix secretion and bone mineralisation are uncoupled processes, and explain why non-mineralised bone produced under P deficiency conditions can mineralise completely when adequate dietary P is provided (Witten et al., 2019). This new bone mineralisation zebrafish model can be used in biomedical research to obtain insights into bone mineralisation pathologies related to high and low mineralisation degree. The findings of this study may also benefit aquaculture research as a model for the effects of dietary P supply in farmed teleosts.

## Materials and methods

### *Zebrafish and ethical statement*

Wild type AB zebrafish were obtained from European Zebrafish Research Center (Eggenstein-Leopoldshafen, Germany). Zebrafish embryos were kept in petri dishes in fish water (1.2 mM $NaHCO_3$, 0.01% instant ocean, 1.4 mM $CaSO_4$, 0.0002% methylene blue) at 28°C until 7 days post-fertilisation (dpf), then housed in ZebTEC semi-closed recirculation housing systems (Techniplast, Buguggiate, Italy) at 28°C, pH 7.5 and conductivity 500 µS on a 14/10 light/dark cycle. Zebrafish from 7 to 21 dpf were fed three times a day alternating commercial dry food (ZM000, Zebrafish Management Ltd., Winchester, UK) and brine shrimp (Artemia cysts, Zebrafish Management Ltd., Winchester, UK). Fish were then fed for another week three times a day with the dry regular phosphorus (RP) diet (**Table 3.3**, see also the next section: experimental diets), until 28 dpf, to adjust them to this type of dry food. The nutrition trial started at 28 dpf: fish were randomly divided in three groups, grown in identical tanks with a density of 10 fish/L and fed three times a day with a low P (LP) diet, a regular P (RP) diet and a high P (HP) diet, respectively (**Table 3.3**). Samples were collected before the start of the experiment (T0 samples, 28 dpf) and after one and two months of dietary treatment (two and three months post-fertilisation, respectively). Fish were euthanised by tricaine (3-amino benzoic acidethylester) overdose (0.3%) and fixed for further analyses. The experiments were conducted in the centralised animal facility of the University of Pavia (Pavia, Italy). The experimental protocol was approved by the Italian Ministry of Health (Approval animal protocol No. 260/2020-PR, 26 March 2020).

### *Experimental diets*

Three experimental diets were formulated to have a total P content of 0.5%, 1.0% and 1.5%, termed LP diet, RP diet and HP diet, respectively (**Table 3.3**). P content for the control diet, RP, was based on the total dietary P requirement of 0.6 - 0.8% for

different teleost species (Rainbow trout *Oncorhynchus mykiss*, Atlantic salmon *Salmo salar*, Pacific salmon *Oncorhynchus sp*., Carp *Cyprinus carpio*, European sea bass *Dicentrachus labrax*, according to National Research Council, 2011). LP and HP diets were formulated to have, respectively, a drastic reduction and an excess of total P content. Monoammonium phosphate ($NH_4H_2PO_4$, MAP) was used as dietary inorganic P supplement. MAP has a high P bioavailability and high P retention efficiency in teleost fish (Morales et al., 2018). In order to keep all diets equal in nutrients, except for P concentration, MAP replaced the inert filler diatomaceous earth (Diamol, Imerys, Denmark). The experimental diets were formulated by SimplyFish AS (Stavanger, Norway, www.simplyfish.no) and produced by extrusion with subsequent crumbling to a suitable particle size by the Danish Technological Institute (Taastrup, Denmark, https://www.dti.dk). The P content of the product was verified at the University of Hohenheim (Stuttgart, Germany, https://www.uni-hohenheim.de) and determined with 5.04 g/kg diet, 9.84 g/kg diet and 14.64 g/kg diet for the LP, RP, and HP diet, respectively.

**Table 3.3.** Ingredients and chemical composition of the three experimental diets for zebrafish.

| Ingredients (%) | Diets | | |
|---|---|---|---|
| | LP | RP | HP |
| Rapeseed lecitin (Bergathin) | 2.00 | 2.00 | 2.00 |
| Krill meal | 3.00 | 3.00 | 3.00 |
| Wheat starch | 18.77 | 18.77 | 18.77 |
| Corn gluten meal | 8.0 | 8.0 | 8.0 |
| Wheat gluten meal | 19.01 | 19.01 | 19.01 |
| Soy protein concentrate | 31.00 | 31.00 | 31.00 |
| Capelin fish meal | 5.00 | 5.00 | 5.00 |
| Rapeseed oil | 1.58 | 1.58 | 1.58 |
| Peruvian fishoil | 2.60 | 2.60 | 2.60 |
| DL-Methionine | 0.60 | 0.60 | 0.60 |
| Biolys 54.6% | 2.00 | 2.00 | 2.00 |
| Lutavit C Aquastab 35% | 0.10 | 0.10 | 0.10 |
| Vitamin mix | 0.50 | 0.50 | 0.50 |
| Choline chloride 50% | 1.50 | 1.50 | 1.50 |
| Trace mineral mix (P free) | 0.30 | 0.30 | 0.30 |
| Monoammonium phosphate 26% | 0.00 | 1.95 | 3.90 |
| Diamol (diatomaceous earth) | 4.00 | 2.05 | 0.10 |
| Astaxanthin 10% | 0.07 | 0.07 | 0.07 |
| Total | 100.00 | 100.00 | 100.00 |
| **Chemical composition (g/kg)** | | | |
| Crude protein | 497 | 508 | 520 |
| Crude lipids | 97 | 97 | 96 |
| Crude ash | 84 | 73 | 71 |
| Calcium | 4.84 | 4.79 | 4.65 |
| Magnesium | 1.96 | 1.98 | 1.99 |
| Phosphorus | 5.04 | 9.84 | 14.64 |

***Morphometric analysis***

Fish were euthanised by tricaine overdose and lateral images were acquired with a M165FC stereomicroscope (Leica, Wetzlar, Germany) connected to a DFC425C digital camera (Leica, Wetzlar, Germany). The standard length (SL), described as the distance from the most anterior tip of the upper jaw to the most posterior region of the body where caudal fin rays insert (according to Parichy et al., 2009), was measured using the ImageJ software (NIH, Bethesda, MD, USA) (T0 n=96; one month treatment: LP n=70, RP n=34, HP n=42; two months treatment: LP n=59, RP n=63, HP n=47).

***Whole mount staining with Alizarin red S***

Zebrafish of 28 dpf (n=8), one month treated (LP n=51, RP n=21, HP n=31) and two month treated (LP n=41, RP n=48, HP n=32) fish were euthanised by tricaine overdose, fixed for 24 h in 4% paraformaldehyde (PFA) in 1× phosphate-buffered saline (PBS) at 4°C and were stained according to the following protocol: 1.5% $H_2O_2$ in 0.25% KOH (2 h); distilled $H_2O$ ($dH_2O$) (5 min); 0.01% Alizarin red S in 0.5% KOH (12 h); 1% KOH (2 h); 25% glycerol in 0.75% KOH (2 h); 50% glycerol in 0.5% KOH (2 h); 75% glycerol in 0.25% KOH (2 h); 100% glycerol (modified from Taylor and Van Dyke, 1985). Fish were analysed and imaged using an Axio Zoom V16 stereomicroscope (Carl Zeiss, Oberkochen, Germany) with oblique illumination equipped with a 5MP CCD camera. Lateral images of stained fish were used to quantitatively analyse mineralisation levels of vertebral endplates. The vertebral body in the transition region, described as the first caudal vertebra possessing elongated unfused haemal arches, drastically shortened ribs and absence of haemal spine (according to Bird and Mabee, 2003), was considered for measuring the total vertebral length and the non-mineralised endplate length. Endplates represent the growth zone of vertebral centra, where the newly formed bone is deposited. Thus, endplates provide a valuable location to characterise bone formed during the dietary treatment. The non-mineralised endplate was expressed as a percentage of the total non-mineralised endplate length (A + A') over the total vertebral length (B): (A + A')/B (**Figure 3.2**). Vertebral endplates with a non-mineralised percentage value greater than 10% were classified as low mineralised,

between 3% and 10% as intermediate mineralised, and less than 3% were considered fully mineralised. Fin rays were classified as low mineralised if more than two segments were non-mineralised, intermediate mineralised if one or two segments were non-mineralised and fully mineralised if all segments were mineralised. Mineralisation levels of neural and haemal arches and dorsal and anal pterygiophores were qualitatively evaluated as low, intermediate or high depending on Alizarin red S distribution in the bone (**Supplementary Figure S3.1**).

***Histological analysis***

Specimens for histological analysis were euthanised by tricaine overdose and fixed for 24 h in 2.5% PFA, 1.5% glutaraldehyde, 0.1 M sodium cacodylate buffer (pH 7.4) and 0.001% $CaCl_2$ at 4°C. Bone mineral detection was carried out on histological sections obtained from non-decalcified samples embedded in glycol methacrylate, according to Witten et al. (2001). Briefly, specimens were dehydrated in a graded series of acetone (30%, 50%, 70%, 90%, 100%) for 30 min each step. Samples were then impregnated with glycol methacrylate monomer solution (80 mL (2-hydroxyethyl)-methacrylate, 12 mL ethylene glycol monobuthyl ether, 270 mg benzoyl peroxide) for 60 min. For the second step of impregnation a fresh monomer solution was used for 24 h. For embedding 2% catalyst (1 mL *N*,*N*-dimethylaniline, 10 mL poly-ethylenglycole-200) was added to the monomer solution. Specimens were then embedded in polyethylene jars. Polymerisation took place at 4°C for 48 h and was completed within another 24 h at room temperature. 3 µm sections were cut on a Microm HM 360 (Marshall Scientific, Hampton, NH, USA) automated microtome and were stained following the Von Kossa/Van Gieson staining protocol: 1% $AgNO_3$ (45 min under UV light); $dH_2O$ (10 min, twice); 3% $Na_2S_2O_3$ (5 min); $dH_2O$ (10 min, twice); Van Gieson counterstain (5 min); $dH_2O$; air-drying and DPX mounting (Humason et al., 1997). Images were acquired using an Axio Imager-Z1 microscope (Carl Zeiss, Oberkochen, Germany) equipped with an Axiocam 503 colour camera (Carl Zeiss, Oberkochen, Germany).

***Transmission electron microscopy***

Specimens treated for two months (n=1 fish per dietary group) were euthanised by tricaine overdose and fixed for 24 h in 2.5% PFA, 1.5% glutaraldehyde, 0.1 M sodium cacodylate buffer (pH 7.4) and 0.001% $CaCl_2$ at 4°C. Fixed fish were decalcified in 0.1 M EDTA for 14 days. The decalcification solution was changed every three days. Specimens were subsequently rinsed in 0.1 M sodium cacodylate buffer with 10% saccharose and then post-fixed for 2 h in 1% $OsO_4$ solution in 0.1 M cacodylate buffer containing 3% saccharose. After rinsing in buffer, samples were dehydrated in a series of graded ethanol solutions and embedded in epon epoxide medium (Spurr, 1969). Semi-thin 1 µm sections were cut on a Microm HM360 microtome (Marshall Scientific, Hampton, NH, USA), stained with toluidine blue at pH 9 for 2 min (0.5% toluidine blue, 1% $Na_2B_4O_7$ in $dH_2O$), rinsed with $dH_2O$ and mounted with DPX. For transmission electron microscopy (TEM) analysis, ultrathin sections (about 70 nm) of the region of interest were prepared on an UltracutE ultramicrotome (Reichert-Jung, Buffalo, NY, USA), contrasted with uranyl acetate and lead citrate (Witten, 1997) and analysed with a Jeol JEM 1010 transmission electron microscope (Jeol Ltd., Tokyo, Japan) operating at 60 kV. Microphotographs were taken with a Veleta camera (Emsis, Muenster, Germany). TEM images were used to measure the diameter of collagen type I fibres in proximity of the osteoblasts (n=300 per dietary group) and in the extracellular matrix (n=300 per dietary group). Diameters were measured on fully transversely sectioned fibres using ImageJ software (NIH, Bethesda, MD, USA). Analysis of collagen fibres was based on previously established protocol (Tonelli et al., 2020b), the number of fibres analysed exceeds the established one.

***X-rays***

X-rays of euthanised one month (LP n=13, RP n=8, HP n=8) and two months (LP n=16, RP n=28, HP n=22) treated zebrafish were acquired with a Faxitron Mx-20 (Faxitron, Tucson, AZ, USA) using 25 kV for 10 sec (Tonelli et al., 2020b). The Kodak DirectView Elite CR System and k-Pacs software (Kodak, Rochester, NY, USA) were used for image digitalisation.

***Synchrotron X-ray tomographic microscopy***

Fish treated with the experimental diets for two months (n=1 fish per dietary group) were euthanised by tricaine overdose, fixed for 24h in 2.5% PFA, 1.5% glutaraldehyde, 0.1 M sodium cacodylate buffer (pH 7.4) and 0.001% $CaCl_2$ at 4°C and were dehydrated in a graded series of ethanol. Representative specimens of the dietary groups with similar size were selected by whole mount Alizarin red S staining of the abdominal region of the vertebral column. Synchrotron X-ray tomographic microscopy of the caudal region of the vertebral column (Bird and Mabee, 2003) was performed at the TOMCAT beamline (X02DA) (Swiss Light Source (SLS), Paul Scherrer Institut (PSI), Villigen, Switzerland, www.psi.ch/sls). Scans were acquired with 1501 projections over 180° at 16 keV with an exposure time of 150 ms using a 10× objective resulting in an effective voxel size of 0.65 µm (Doeland et al., 2019). Radiographs were phase-retrieved using the Paganin algorithm, tomographically reconstructed and subsequently analysed using Amira 3.1.1 software (TermoFisher, Waltham, MA, USA). The mineralised parts of the vertebrae were identified applying a constant greyscale-threshold to all samples, the non-mineralised parts were manually selected on each projection. The resulting segmentations and virtual sections of the $10^{th}$ caudal vertebral body (Bird and Mabee, 2003) in LP, RP and HP fish were used to visualise the mineralised and non-mineralised parts of the vertebra, neural and haemal arches. Segmentations were also used to measure vertebral body parameters (length, height), arch and spine length, and the volumes of mineralised and non-mineralised parts of the vertebrae (**Figure 3.5 B**).

***Nanoindentation***

Mechanical properties were assessed in the first four caudal vertebrae of one fish per dietary group according to previously established protocols (Fiedler et al., 2018). Briefly, fish were embedded in PMMA, ground coplanar until the sagittal plane was exposed, and polished with 3 µm and 1 µm diamond suspension followed by final polishing with 0.05 µm aluminium-oxide suspension. Indentations were performed in depth-sensing continuous stiffness mode with a final depth of 300 nm. Indentations

were placed in the proximal and distal vertebral body endplates and the central region of vertebrae (**Figure 3.4 A**). The nanoindenter (Nano Indenter G200 equipped with a Berkovich diamond tip, Keysight Technologies, Santa Rosa, CA, USA) was calibrated on fused silica before and after each measurement. Based on the Oliver and Pharr method (Oliver and Pharr, 1992) and by applying a Poisson's ratio of 0.3, the mechanical properties elastic modulus (E) and hardness (H) in the different vertebral regions were determined using in-house software (NanoSuite, Keysight Technologies, Santa Rosa, CA, USA).

***Collagen extraction from bone***

Bones were dissected following sacrifice from animals fed with the experimental P diets for two months (n=2 fish per dietary group). Bones were defatted for 6 h in 0.1 N NaOH at 4°C and then decalcified for 48 h in 0.5 M EDTA (pH 7.4) at 4°C. The pepsin-soluble collagen fraction (PSC) was obtained by digesting tissues with 0.1 mg/mL pepsin in 0.5 M acetic acid at 4°C for 48 h. The PSC was precipitated by 0.9 M NaCl in 0.5 M acetic acid overnight at 4°C (Gistelinck et al., 2016) and quantified using Sircol Soluble Collagen assay (Biocolor, Carrickfergus, UK). Equal amounts of collagen from each sample were loaded on 6% SDS-Urea-PAGE in non-reducing condition. Gels were stained overnight with 0.08 M picric acid, 0.04% Coomassie Brilliant Blue R250, rinsed in water and recorded with Versadoc3000 (Bio-Rad, Hercules, CA, USA).

***Statistical analysis***

Quantitative variables are expressed as mean ± standard deviation, categories are expressed as percentages. Statistical comparison of the standard length values was based on the non-parametric Mann-Whitney test. Differences in the occurrence of skeletal malformations and in bone mineralisation levels were evaluated by means of Chi-squared test or the Fisher's exact test. Statistical analysis was performed using Past 4.01 software (Hammer et al., 2001). Comparisons of mechanical properties was performed using ANOVA followed by a Bonferroni post hoc test. A p-value less than 0.05 was considered significant.

# Chapter 4

## The “super-bone” zebrafish model: a novel approach to stimulate bone formation by alternating dietary phosphorus levels

This chapter is a manuscript in preparation:

Silvia Cotti, Claudia Di Biagio, Ann Huysseune, Wolfgang Koppe, Antonella Forlino and P. Eckhard Witten. The “super-bone” zebrafish model: a novel approach to stimulate bone formation by alternating dietary phosphorus levels. *In preparation to submission to Nature Communications*

## Introduction

Age-related bone loss due to osteoporosis/osteopenia or by other syndromes that cause skeletal fragility represents a major health problem for humans (Greco et al., 2019). The ability of bone to withstand mechanical load depends on its structural characters, to a large extent determined by the microarchitecture of trabecular bone that is formed in response to loading conditions. Bone fragility syndromes are characterised by reduced trabecular density and poor trabeculae connectivity (Myers and Wilson, 1997; Seeman, 2003). Not only long bone fractures, but also the vertebral body fractures are of major concern in this context. Bending and lifting activities of daily life generate heavy loads that can exceed the load bearing capacity of vertebrae with low trabecular volume and connectivity. Vertebral fractures have an enormous negative impact on the quality of life (Myers and Wilson, 1997; Greco et al., 2019).

An imbalance between bone formation and bone resorption, in favour of the latter, contributes to trabecular thinning and increased porosity of plate-like trabecular structures, typical for osteoporotic conditions (Seeman, 2003). Although bone loss already occurs in young adults due to a reduction in the volume of newly formed bone, the rate of loss is initially low and only increases with the age-related increase of bone resorption (Riggs et al., 1998; Seeman, 2003). Antiresorptive drugs can help to reduce the severity of bone resorption-related loss of trabeculae, but they do not stimulate bone formation to restore the lost bone volume (Seeman, 2003). Conversely, antiresorptive drugs reduce bone turnover with the consequence that remaining bone structures undergo a more complete secondary mineralisation. This results in hypermineralised bone that has lost its elastic character and thus becomes more fragile (Currey, 1984; Seeman, 2003). Increasing the formation of new, less mineralised, bone appears to be a more promising approach to reduce bone loss and to reverse bone fragility. Moreover, the newly formed non-mineralised bone, or osteoid, protects bone surfaces from resorption (Chambers et al., 1984; Nordahl et al., 2000; Lassen et al., 2017). Osteoanabolic agents, e.g. parathyroid hormone receptor agonists and anti-sclerostin antibodies, have been recently introduced as alternatives to anti-resorption compounds in the treatment of osteoporosis (Seeman, 2003; McClung, 2021).

Besides drugs, it is well known that multiple environmental factors, including a balanced nutrition, exercise and avoidance of adverse substances (smoking, excessive alcohol and drugs) positively impact bone quality (Anderson et al., 1996). Concerning nutrition, numerous macro- and micronutrients are important for bone development and maintenance (Anderson et al., 1996). Among macronutrients, calcium and phosphorus (P) are the main inorganic components of bone and their levels are regulated to ensure optimal skeletal conditions (Verri and Werner, 2019; Peacock, 2021). In the study of bone health and mechanisms underlying skeletal diseases, the zebrafish *Danio rerio* has become an important model organism thanks to conserved basic processes of skeletal formation across gnathostomes (Witten et al., 2017; Dietrich et al., 2021). Given that teleosts, like tetrapods, depend on dietary P, they represent good models to explore the role of dietary P for the bone mineralisation (Hall and Witten, 2007; Witten and Huysseune, 2009). It is known that excess dietary P intake can reduce bone formation in humans (Kemi et al., 2006; Dermience et al., 2015). Furthermore, it has been shown that excess dietary P intake in rats promotes bone hypermineralisation which leads to increased bone stiffness and ultimately to a reduction of bone strength (maximal load) (Huttunen et al., 2007). Conversely, recent studies on zebrafish and other teleost fish (Atlantic salmon) have drawn the attention to the importance of reduced dietary P levels for bone formation and bone quality (Witten et al., 2016, 2019; Cotti et al., 2020, 2022; Drábiková et al., 2021). A decrease of dietary P intake by 50% reduces the total bone mineral content but results in increased formation of non-mineralised bone matrix. The reduced dietary P intake was shown to improve the biomechanical properties by enhancing toughness and reducing stiffness (Witten et al., 2019; Cotti et al., 2020; Drábiková et al., 2021), leading to a decreased fracture risk (Currey, 2003; Witten et al., 2019; Cotti et al., 2020; Drábiková et al., 2021). Of notice, in zebrafish and salmon, the low dietary P intake does not generate vertebral body malformations. On the contrary it was shown that low P intake can even partially rescue the severe skeletal defects that relate to hypermineralisation in the *Chihuahua* zebrafish model for osteogenesis imperfecta (Cotti et al., 2022).

Here, a detailed analysis is presented of the increase of bone volume through the formation of non-mineralised bone under P-deficient conditions. It is explored if non-mineralised zebrafish bone retains the capacity to mineralise when the dietary P supply is increased. For this purpose, the zebrafish vertebral column is analysed using several histological techniques, quantitative real-time PCR (qPCR) and micro computed tomography (micro-CT). The response to low P intake is a dramatic increase in non-mineralised bone volume along the zebrafish vertebral column. Osteoblasts respond by upregulating genes important for bone formation and mineralisation, that is resumed when adequate dietary P is administered, thus resulting in a substantial increased volume of mineralised bone.

This zebrafish model shows that disconnecting bone formation and mineralisation increases the volume of mineralised bone by alternating low and high dietary P intake. This approach will contribute to treat osteoporosis and age-related bone loss by increasing bone volume.

## Results

### *Low dietary P intake: increase of bone matrix formation and stop of mineralisation*

The teleost vertebral body consists of an hourglass-shaped double cone that forms around the mineralised notochord sheath and bone trabeculae that connect the cones. The distal parts of the cones are also designated as vertebral body endplates (Witten and Hall, 2022). After two months of dietary treatment, midline sagittal sections of the vertebral column from LP, RP (controls) and HP animals were used to measure the bone thickness of autocentra at the vertebral body endplates and in the central region of the autocentrum (**Figure 4.1 A,B**). Histomorphometry shows statistically significant increased bone thickness in LP zebrafish compared to RP and HP both at the vertebral body endplates and in the central region (**Figure 4.1 B, Table 4.1**). Conversely, HP zebrafish have thinner autocentrum bone structures compared to LP and control (RP) animals (**Figure 4.1 B, Table 4.1**).

**Table 4.1.** Bone histomorphometry.

| | | Thickness Mean ± SD (∝m) | Pairwise p-values | |
|---|---|---|---|---|
| Vertebral body endplates | LP | 19.04 ± 2.72 | LP - RP | $2.21 \times 10^{-5}$ |
| | RP | 16.39 ± 2.27 | LP - HP | $2.30 \times 10^{-20}$ |
| | HP | 13.88 ± 1.52 | RP - HP | $3.66 \times 10^{-8}$ |
| Vertebral body central region | LP | 6.78 ± 2.87 | LP - RP | $1.45 \times 10^{-3}$ |
| | RP | 4.95 ± 1.19 | LP - HP | $7.88 \times 10^{-5}$ |
| | HP | 4.76 ± 1.61 | RP - HP | ns |

Statistical analysis is based on Student's t-test followed by Bonferroni correction; ns: non-significant.

Histology shows that trabecular bone is also considerably thicker in LP animals compared to controls and HP animals (**Figure 4.1 C**). This observation coupled with the histomorphometry data clearly demonstrates increased bone formation under LP conditions. The increased bone is non-mineralised, as demonstrated by Von Kossa/Van Gieson staining, and forms at regular sites of bone apposition, i.e. the growth zone of the vertebral body endplates and the trabeculae. Some LP individuals present enlarged

and bent bone trabeculae characterised by the presence of chondroid bone (**Figure 4.1 C**), that is also largely non-mineralised (**Figure 4.1 D**). Vertebral body endplates and bone trabeculae of RP animals are mineralised and are covered by a regular non-mineralised osteoid layer. The osteoid layer is not detectable in HP animals (**Figure 4.1 D**).

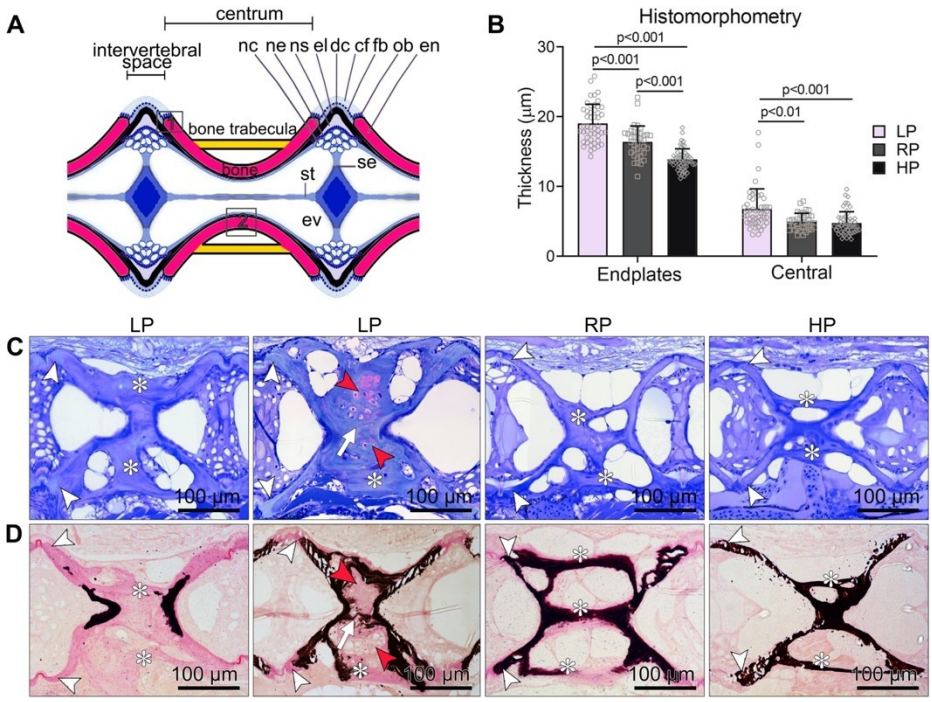


**Figure 4.1.** Bone formation increases and bone mineralisation stops under LP conditions. **A:** Scheme of the midline sagittal plane of an adult zebrafish vertebral body centrum and two intervertebral spaces. The hourglass-shaped bone that forms around the mineralised notochord sheath is designated as autocentrum. Numbers in boxes indicate regions of the autocentrum, the vertebral body endplates (1) that oppose the intervertebral space and central region of the autocentrum (2). Plate-like bone trabeculae that form in response to mechanical load (like bone trabeculae in human long bones) connect the vertebral body endplates (yellow bars). Osteoblasts (ob) deposit new bone matrix in the bone growth zones, i.e. the distal rim of the vertebral body endplates (en), that are connected by intervertebral ligaments. The ligaments consist of, from inside to outside, the notochord sheath (ns, a collagen type II layer secreted by the cells of the notochord epithelium, ne), the outer elastin layer (el) and dense collagen type I fibre bundles (dc) produced by fibroblasts (fb). The collagen type I fibre bundles (cf) continue in the bone of the vertebral body endplates (en) as Sharpey fibres. Inside the intervertebral space, the notochord is composed of vacuolated notochord cells (nc) and extracellular vacuoles (ev). Condensed notochord cells constitute the notochord septum (se) and the notochord strand (st). Boxes show locations where the bone thickness was measured, i.e. endplates (1) and central region of the

autocentrum (2). **B:** Histomorphometry measurements of bone thickness at vertebral endplates and central region of the autocentrum from LP (n=5), RP (n=4) and HP (n=5) animals after two months of dietary treatment. Compared to RP and HP animals, LP zebrafish have thicker vertebral endplates and central region of the vertebrae. Opposite, HP fish have thinner vertebral endplates compared to controls and LP (see also **Table 4.1**). Individual data points are shown. Student's t-test followed by Bonferroni correction, p-values are indicated. **C:** Toluidine blue stained sagittal sections of vertebral bodies from LP, RP and HP show that vertebral endplates (white arrowheads) and trabecular bone (asterisks) are considerably thicker in LP animals in comparison with controls and HP fish. **D:** Von Kossa/Van Gieson stained non-demineralised sections show a similar sectional plane as in **C**. The additional bone formed under the LP diet conditions is mostly non-mineralised at vertebral endplates (white arrowheads) and trabecular bone (asterisks) compared to RP and HP. Non-mineralised bone: pink; mineralised bone: black. Some vertebral bodies from LP individuals present enlarged (asterisks) and bent (white arrows) bone trabeculae characterised by the presence of chondroid bone (red arrowheads), that is largely non-mineralised as demonstrated by Von Kossa/Van Gieson staining.

### *Osteocalcin and collagen type I expression are upregulated under low dietary P intake*

Expression of osteocalcin, a well known marker of osteoblasts, was first evaluated using an *osc*:GFP transgenic zebrafish line fed different dietary P. In animals from all three dietary groups, osteocalcin is expressed in osteoblasts, bone lining cells, osteocytes and in the osteocyte canalicular network (**Figure 4.2 A-C**). In the growth zone of the vertebral body endplates, osteoblasts strongly express osteocalcin, as do bone lining cells, osteoblasts and osteocytes located in the central region of the autocentrum (**Figure 4.2 B**), the arches (**Figure 4.2 C**) and the bone trabeculae that connect the vertebral body endplates (**Figure 4.2 A**). The osteocyte canalicular network is also clearly *osc*:GFP positive and both osteocyte-osteocyte and osteoblast-osteocyte connections are visible (**Figure 4.2 C**). In contrast, fibroblasts in the intervertebral ligament are negative for osteocalcin in all dietary groups (**Figure 4.2 D**). A quantification of the *osc*:GFP-positive area occupied by osteoblasts at the vertebral body endplates (**Figure 4.2 E**), yielded a significantly increased value in LP zebrafish compared to RP ($p=0.006$) and to HP ($p=0.002$) zebrafish, suggesting upregulation of osteocalcin transcription under LP conditions (**Figure 4.2 F**).

Next, the expression osteocalcin (*bglap*) and other late osteoblast markers, i.e. the main bone extracellular component collagen type I (*col1a1a*), osteonectin (*sparc*) that is secreted by osteoblasts during bone formation, osteopontin (*spp1*) that is

produced by mature osteoblasts, as well as the expression of the early osteoblast marker collagen type X (*col10a1a*) were evaluated (**Figure 4.3 A**). *bglap* and *col1a1a* are upregulated in LP individuals compared to controls, matching the histomorphometry data about increased bone matrix apposition. In HP zebrafish, *col1a1a* expression shows a trend towards downregulation compared to RP (p=0.084). All the other markers do not show differential expression between the three dietary groups (**Figure 4.3 A**).

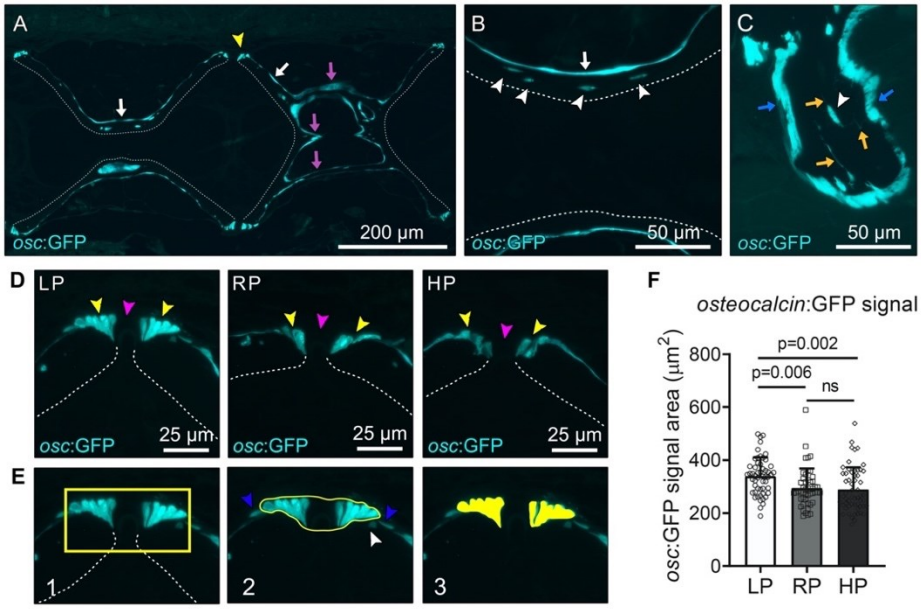


**Figure 4.2.** Expression of osteocalcin in the vertebral column assessed in a transgenic *osc:*GFP zebrafish line fed LP, RP, HP for two months. **A-C:** independent from dietary P intake, in the vertebral column osteocalcin is expressed by osteoblasts at vertebral body endplates (yellow arrowhead, **A**) and by bone lining cells at the surface of the autocentrum (white arrows, **A, B**), the trabecular bone (magenta arrows, **A**) and arches (blue arrows, **C**). Dashed lines indicate the inner bone surface in contact with the notochord sheath. Osteocytes (white arrowheads), present in the central region of the autocentrum (**B**) and in the arches (**C**) are *osc:*GFP positive. The osteocyte canalicular network is also labelled (yellow arrows, **C**). **D:** High magnification of vertebral body endplates from LP, RP and HP show that osteoblasts (yellow arrowheads) are *osc:*GFP positive, but fibroblasts (magenta arrowheads) are *osc:*GFP negative. **E-F:** Quantification of the *osc:*GFP-positive area at vertebral body endplates of LP (n=3), RP (n=3) and HP (n=3) individuals was performed as represented in panel **E**, considering only osteoblasts and excluding osteocytes and bone lining cells in 20 vertebral growth zones per specimen (see Materials and Methods for details). **F:** LP zebrafish have a significantly increased *osc:*GFP signal area at vertebral endplates compared to RP and HP. Individual data points are shown. Student’s t-test followed by Bonferroni correction, p-values are indicated, ns: non-significant.

***Markers of bone mineralisation and P regulation are upregulated under the low P diet***

To characterise the cellular response associated to the arrest of mineralisation under LP conditions, the expression of the mineralisation-related genes was evaluated. These genes encode for the ectonucleotide pyrophosphatase phosphodiesterase 1 (*enpp1*) that produces the main mineralisation inhibitor pyrophosphate (PPi), and for two key enzymes that hydrolyse extracellular PPi, namely ectonucleoside triphosphate/diphospho-hydrolase 5 (*entpd5*) and tissue non-specific alkaline phosphatase (*alpl*). Under LP conditions, *enpp1*, *entpd5* and *alpl* show statistically significant increased expression compared to controls. No differential expression is detected between RP and HP (**Figure 4.3 B**).

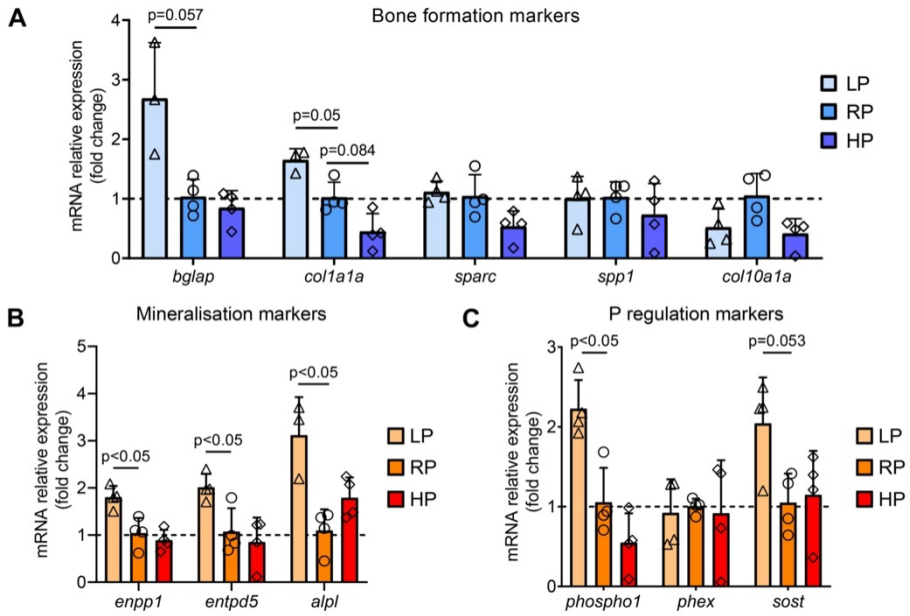


**Figure 4.3.** qPCR analysis performed on RNA extracted from the vertebral column of LP, RP and HP after two months of dietary treatment. **A:** Expression of the bone formation markers osteocalcin (*bglap*) and collagen type I (*col1a1a*) is upregulated in LP animals compared to controls. In HP zebrafish, *col1a1a* expression shows a trend towards downregulation compared to RP. Other markers of bone formation, i.e. osteonectin (*sparc*), osteopontin (*spp1*) and collagen type X (*col10a1a*), do not show differential expression between the three dietary groups. **B:** Expression of the bone mineralisation markers ectonucleotide pyrophosphatase phosphodiesterase 1 (*enpp1*), ectonucleoside triphosphate/diphospho-hydrolase 5 (*entpd5*) and tissue non-specific alkaline phosphatase (*alpl*) is significantly upregulated in LP zebrafish

compared to controls. **C:** Expression of the P regulation markers phosphatase orphan 1 (*phospho1*) and sclerostin (*sost*, that, apart from regulating osteoblastic bone formation, regulates also calcium and P homeostasis) is upregulated in LP zebrafish compared to controls. Phosphate-regulating gene with homologies to endopeptidases on the X chromosome (*phex*) is not differentially expressed. Individual data points are shown. Statistical analysis is based on Student’s t-test followed by Bonferroni correction, only LP vs. RP and HP vs. RP p-values are indicated when significant.

Low dietary P intake affects the expression of phosphatase orphan 1 (*phospho1*), an intracellular phosphatase that releases P from phosphorylated substrates, and sclerostin (*sost*) that regulates not only osteoblastic bone formation, but also calcium and P homeostasis (Hansen et al., 2019). Both *phospho1* and *sost* are upregulated in LP compared to RP. No differences are present between RP and HP (**Figure 4.3 C**). No differential expression among the three dietary groups is detected for phosphate regulating gene with homologies to endopeptidases on the X chromosome (*phex*) (**Figure 4.3 C**).

To confirm the increased expression of *alpl* in LP animals found with qPCR, enzyme histochemistry was performed on non-demineralised sections. In all dietary groups, alkaline phosphatase (ALP) activity is detected in the vertebral body endplates in specific cell types, i.e. osteoblasts, fibroblasts and cells of the notochord epithelium (**Figure 4.4 A-A”**). Interestingly, ALP activity is found in bone lining cells along the trabecular bone (**Figure 4.4 B**) and on the surface of the vertebral centrum (**Figure 4.4 C**) in LP animals only. In addition, ALP activity labels distinctively the cartilage-like cells of the chondroid bone found in LP vertebral bodies with bent trabeculae (see above) (**Figure 4.4 D,D’**).

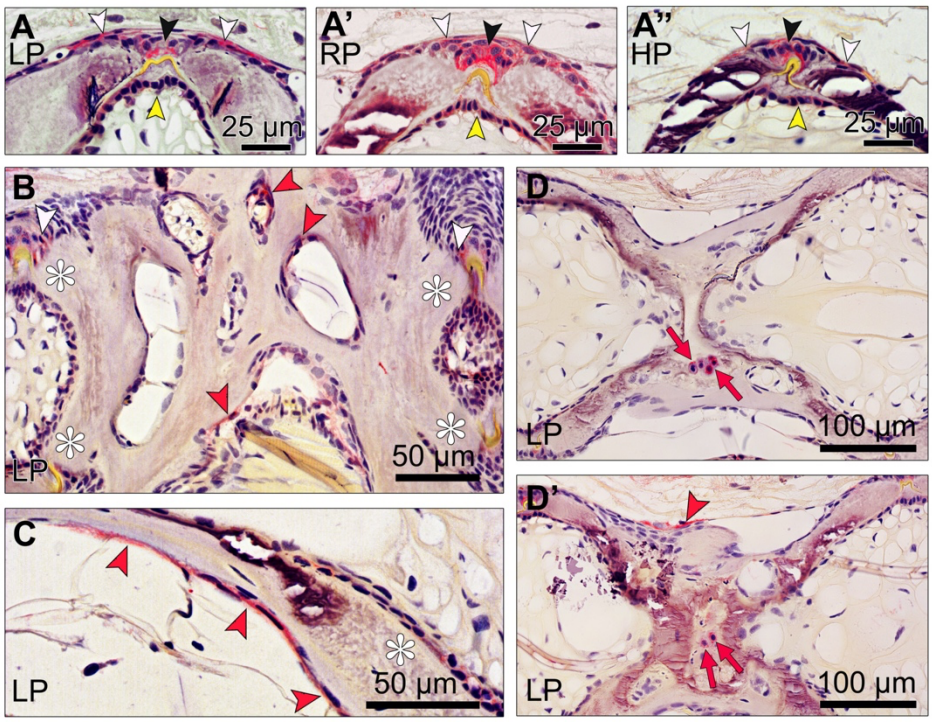


**Figure 4.4.** Demonstration of alkaline phosphatase (ALP) activity in the vertebral column of LP, RP and HP zebrafish after two months of dietary treatment. **A-A":** In all dietary groups, ALP activity (red staining) is detected in the vertebral body endplates in specific cell types, i.e. osteoblasts (white arrowheads), fibroblasts (black arrowheads) and cells of the notochord epithelium (yellow arrowheads). **B-C:** In LP animals, ALP activity (red arrowheads) is also found in the trabecular bone (**B**) and on the outer surface of the vertebral centrum (**C**). Asterisks indicate vertebral body endplates, white arrowheads indicate ALP-positive osteoblasts. **D-D':** ALP activity is detected in the cartilage-like cells (red arrows) located in LP vertebral bodies that show bent trabeculae.

***Low P conditions decrease bone mineral density but increase bone volume which retains the ability to mineralise***

Following two months of LP dietary treatment, LP zebrafish were divided in three groups and fed LP (LP-LP), RP (LP-RP) or HP (LP-HP) diets for 1.5 months up to the age of 4.5 months. A control group was fed RP diet (RP-RP) throughout the duration of the experiment. The first three caudal vertebral bodies from three individuals per dietary group were analysed by Alizarin red S, micro-CT and 3D reconstructions (**Figure 4.5**). Whole mount staining shows an increased mineralised and non-mineralised bone around the autocentra and at neural and haemal arches in all fish with LP dietary

history compared to controls (**Figure 4.5 A**). Newly formed bone in LP-LP partly mineralises. However at sites of bone apposition, the rim of LP-LP bone structures is non-mineralised. These include the vertebral body endplates, neural and haemal arches, bone trabeculae and pre- and post-zygapophysis. LP-RP and LP-HP present mineralisation of these bone elements (**Figure 4.5 A**). The increase in mineralised bone is proportional to the dietary P intake, as observed on virtual cross sections obtained from micro-CT 3D reconstructions (**Figure 4.5 B**). All vertebral bodies show the phenotype in a consistent manner throughout the vertebral column.

Micro-CT 3D analysis was applied to obtain quantitative data on the mineralised vertebral centrum only, excluding arches and zygapophysis (**Figure 4.5 C**). Bone mineral density (BMD, defined as $g/cm^3$ of calcium hydroxyapatite, calibrated against the density scales of the attenuation coefficient) is significantly reduced in LP-LP, LP-RP and LP-HP compared to controls (RP-RP), as expected given the extended period of LP dietary treatment. However, BMD shows a trend towards increased values in LP-RP compared to LP-LP, and BMD is significantly higher in LP-HP compared to LP-LP ($p<0.001$). Although the difference in BMD between controls and LP-HP is significant ($p<0.001$), BMD values in LP-HP show a tendency towards increased values. This suggests that BMD values can resume control values when sufficient dietary P is provided. Quantification of bone volume and bone surface related to the mineralised vertebral centrum show no differences between controls and LP-LP (**Figure 4.5 C**). This is not surprising considering the low BMD in LP-LP animals and the large amount on non-mineralised endplates shown in the 3D reconstructions. Similar values for mineralised bone volume and surface between LP-LP and controls are likely due to the thickened vertebral centrum in LP-LP fish. LP-RP and LP-HP animals show increased mineralised bone volume and surface compared to both controls and LP-LP in a dietary P-dependent manner (**Figure 4.5 C**).

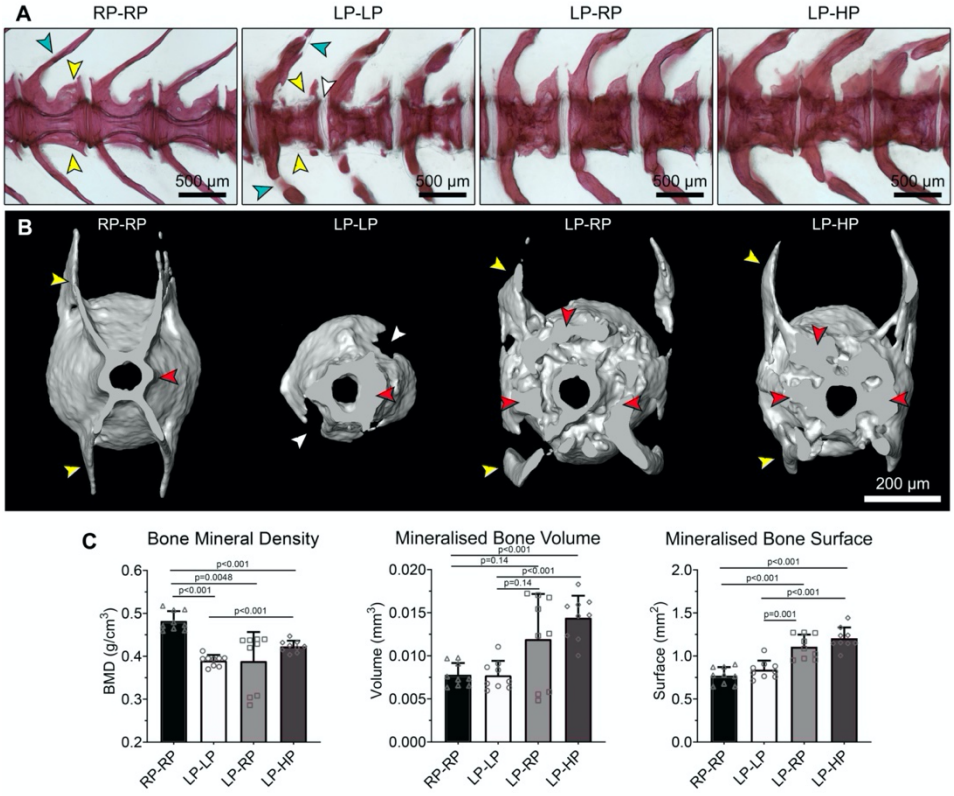


**Figure 4.5.** Alizarin red S and micro-CT analysis. After two months of LP dietary treatment, zebrafish were divided in three groups and fed LP (LP-LP), RP (LP-RP) or HP (LP-HP) diets. A control group was fed RP diet (RP-RP) throughout. **A:** Whole mount Alizarin red S staining of the first three caudal vertebral bodies from controls, LP-LP, LP-RP and LP-HP. LP-LP present several non-mineralised (translucent, negative for the staining) bone structures compared to controls, i.e. parts of the vertebral body endplates (white arrowheads), neural and haemal arches (turquoise arrowheads) and pre- and post-zygapophysis (yellow arrowheads), as also visible in virtual cross sections from micro-CT reconstructions (**B**). These structures retain the ability to mineralise when sufficient dietary P is provided, as shown in LP-RP and LP-HP. Alizarin red S shows the increased amount of bone deposited around the autocentra in all animals with LP dietary history compared to controls. **B:** Virtual cross sections of vertebral bodies show increased bone volume (red arrowheads) around the vertebral centrum in LP-LP, LP-RP and LP-HP compared to controls. **C:** Micro-CT analysis performed on the mineralised vertebral centrum only shows reduced bone mineral density (BMD) in LP-LP, LP-RP and LP-HP compared to controls, and a dietary P-dependent increase in the mineralised bone volume and bone surface in LP-RP and LP-HP compared to controls and LP-LP. Statistical analysis is based on Student's t-test followed by Bonferroni correction, p-values are indicated.

To verify that LP conditions increase bone volume (mineralised and non-mineralised) in zebrafish regardless the diet received after the low P period, sagittal

non-demineralised sections stained with Von Kossa/Van Gieson from controls (RP-RP), LP-LP, LP-RP and LP-HP were used (**Figure 4.6**). The increase in the amount of bone is evident in LP-LP, LP-RP and LP-HP compared to controls, both at the vertebral body endplates and central region of the vertebral centrum (**Figure 4.6 A**). In LP-LP animals, the amount of non-mineralised bone matrix at both areas is larger compared to LP-RP and LP-HP animals (**Figure 4.6 A**), as also shown at higher magnification in the vertebral endplates (**Figure 4.6 B**, see also below). At vertebral body endplates locations, midline sagittal sections of the vertebral column were used to quantify the total bone area normalised to vertebral length (**Figure 4.6 C**) (see Materials and Methods section for details on the analysis). The total normalised bone area is significantly increased by 1.5 folds in LP-LP, LP-RP and LP-HP compared to controls. Interestingly, there is no difference in the total (mineralised and non-mineralised) normalised bone area among LP-LP, LP-RP and LP-HP, confirming that the low P period common to the three groups caused the increase in bone volume. Concerning the mineralisation extent in LP-LP, LP-RP and LP-HP compared to controls, the mineralised bone area over the total bone area was measured at vertebral endplates locations (**Figure 4.6 D**) (see Materials and Methods section for details on the analysis). LP-LP animals have drastically reduced mineralisation ratio (less than 50%) compared to controls ($p<0.001$). LP-RP vertebrae show an increase in the mineralisation extent compared to the control values, whereas the LP-HP group has a higher mineralisation extent with respect to the controls. These data further confirm the micro-CT analysis results and suggest that non-mineralised bone retains the ability to mineralise, reaching a mineralisation extent similar to controls when sufficient dietary P is provided.

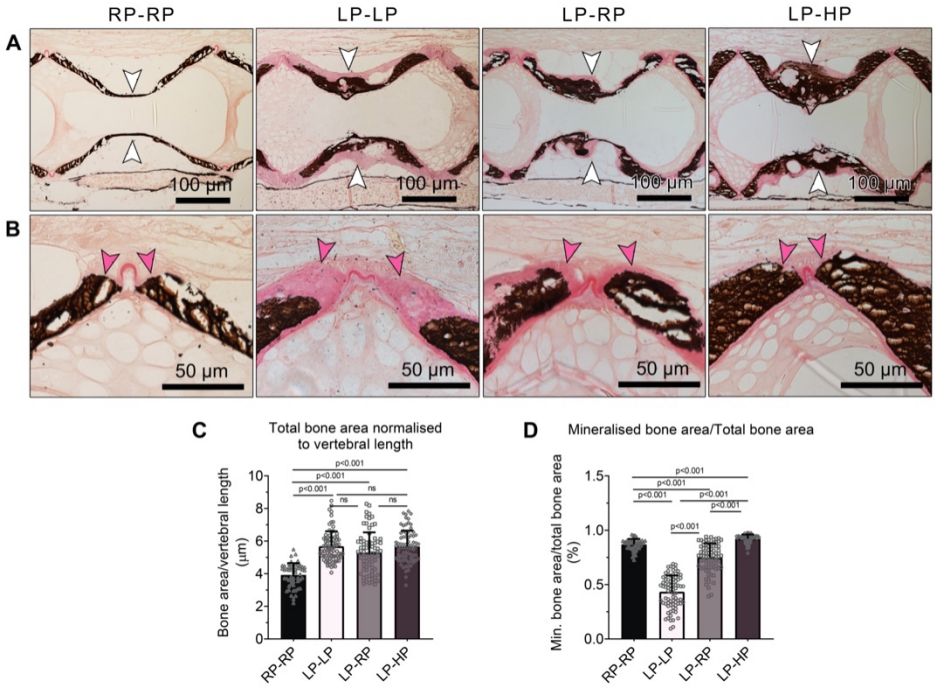


**Figure 4.6.** Low P conditions increase bone volume and subsequently the amount of mineralised bone in zebrafish. **A-B:** Sagittal non-demineralised histological sections of the vertebral column from controls (RP-RP), LP-LP, LP-RP and LP-HP stained with Von Kossa/Van Gieson. Compared to controls, LP-LP, LP-RP and LP-HP show an increase in bone volume in the central region of the vertebral centrum (white arrowheads, **A**) and at the vertebral body endplates (pink arrowheads, **B**). In LP-LP animals, the non-mineralised bone matrix (pink) at vertebral body endplates and central region is larger compared to LP-RP and LP-HP animals, in which the bone structures are mineralised (black). **C:** Quantitative analysis performed at vertebral body endplates shows that the total bone area normalised to vertebral body length is significantly increased by 1.5 folds in LP-LP, LP-RP and LP-HP compared to controls. **D:** At vertebral body endplates, the mineralised bone area divided by total bone area indicates that bone mineralisation depends on dietary P, and non-mineralised bone generated during the LP period can resume a mineralisation extent similar to controls when sufficient P is provided with the diet. Statistical analysis is based on Student's t-test followed by Bonferroni correction, p-values are indicated.

### *Characteristics of the bone formed under low P conditions*

The same vertebral bodies previously analysed by micro-CT were subsequently analysed on transverse histological sections using different staining techniques (**Figure 4.7**). As described above, the amount of extra bone formed around the autocentrum under LP conditions is striking in comparison with the control group. Bone formed under the LP diet conditions does not extend into the intervertebral spaces and thus

does not affect the mobility of the intervertebral joints. Newly formed bone matrix reduces the bone marrow space that is typically occupied by fat in teleost fish. The increase in bone volume is not only restricted to the autocentrum. Arches also appear to be enlarged (see also **Figure 4.5 A**), confirming findings of a previous study (Cotti et al., 2020). Trabecular bone, that is thin in controls, is substantially thickened under LP dietary conditions. The bone formed under LP diet is capable of mineralisation when adequate dietary P is provided, as also shown by comparing non-decalcified sections of the different treatments (**Figure 4.7 A**). Small, disjunct, patches of mineralisation are observed in LP-LP zebrafish. The extent of mineralisation increases as regular or high P are provided to the fish. Similar mineralisation patterns are evident in the arches (**Figure 4.7 A**).

On demineralised sections stained with toluidine blue (**Figure 4.7 B**), LP-LP, LP-RP and LP-HP have enlarged and bent bone trabeculae characterised by many osteocytes and by the presence of chondroid bone. Chondroid bone is largely non-mineralised (**Figure 4.7 A**) and contains actively dividing cartilage-like cells. Vertebral bodies with increased bone volume show intact intervertebral ligaments (as observed on sagittal sections, **Figure 4.6 B**) and an intact notochord in the intervertebral space.

Enlarged trabeculae are subjected to bone resorption, as assessed by the presence of tartrate-resistant acid phosphatase (TRAP) activity (**Figure 4.7 C**). In the control group, osteoclast activity is restricted to locations within the vertebral column that require resorption for allometric growth (Witten et al., 2001), i.e. the endosteal surfaces of enlarging neural and haemal arches (**Figure 4.7 C**). TRAP activity is detected at the same locations in LP-LP, LP-RP and LP-HP zebrafish, but the enzymatic activity is also detected within the enlarged trabecular bone. The comparison of serial sections, stained alternating toluidine blue and TRAP, shows that bone, but not chondroid bone is subjected to resorption at this stage of the experiment (**Figure 4.7 B,C**). This is not surprising given that the chondroid bone is largely non-mineralised (**Figure 4.7 A**). The detected TRAP activity seems in line with typical bone remodelling in teleosts, and does not appear to be extended as in disease conditions (Cotti et al., 2022).

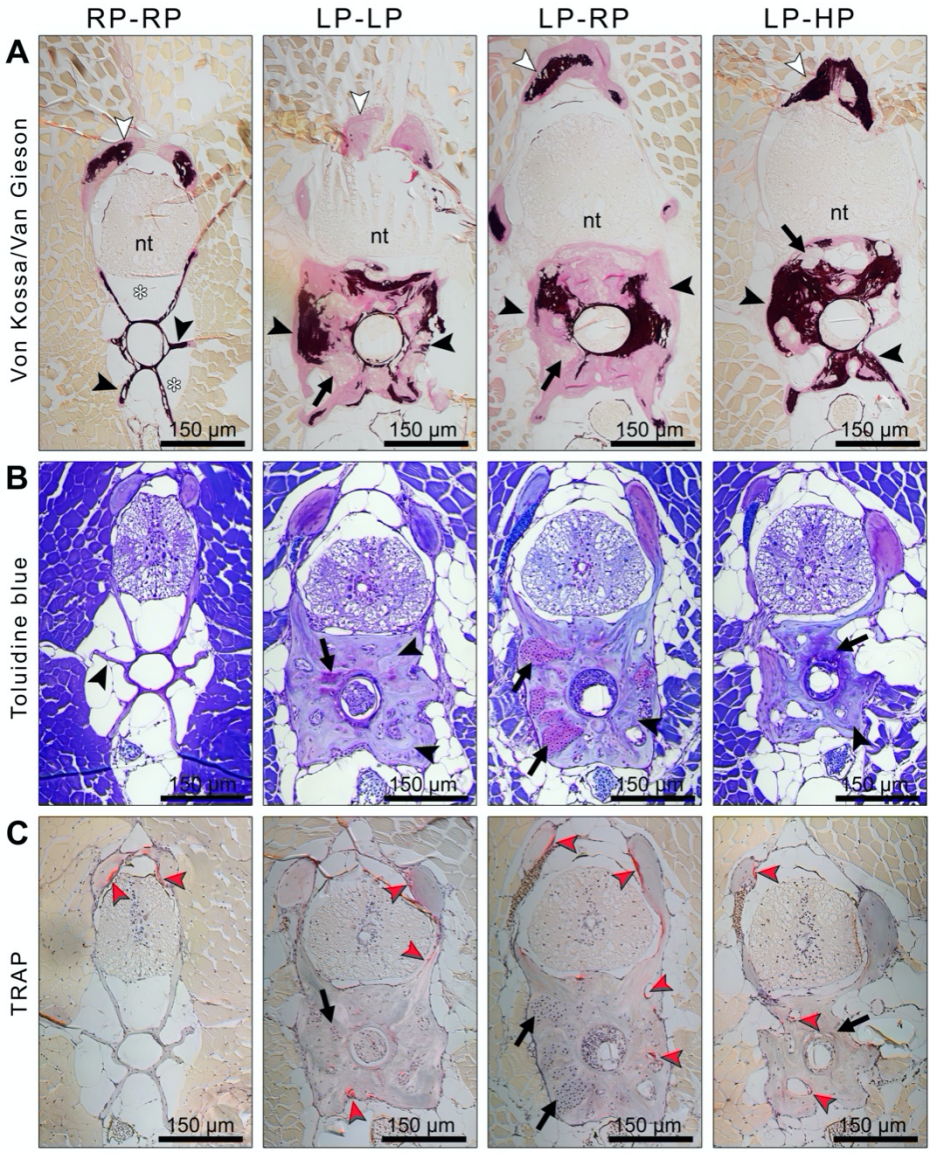


**Figure 4.7.** Histological characterisation (transverse sections) of the bone formed under low P conditions and its subsequent mineralisation. **A:** Von Kossa/Van Gieson stained non-demineralised sections show increased bone volume around the vertebral centrum in LP-LP, LP-RP and LP-HP compared to controls (RP-RP). Black arrowheads point at the trabecular bone, that is thin in controls but extremely enlarged when LP diet is provided. In LP-LP, LP-RP and LP-HP, the enlarged bone formed fills up the space that is occupied by fat in controls (asterisks). LP-LP is low mineralised, but the mineralisation extent increases with increasing dietary P. White arrowheads point at neural arches. Black: mineralised bone; pink: osteoid, non-mineralised bone. Black arrows: chondroid bone; nt: neural tube. **B:** Toluidine blue stained sections show thin trabeculae in controls (black arrowhead). LP-LP, LP-RP and LP-HP have enlarged and bent bone trabeculae

(black arrowheads) characterised by several osteocytes and by the presence of chondroid bone (black arrows). **C:** Demonstration of tartrate-resistant acid phosphatase (TRAP) activity on sections. TRAP activity (red arrowheads, red staining) is typically detected at endosteal surfaces of enlarging arches, as observed in all dietary groups. In LP-LP, LP-RP and LP-HP, TRAP activity is also detected within the bone trabeculae. Chondroid bone (black arrows) is not subjected to resorption at this stage of the experiment.

# Discussion

### *More bone with less minerals: active osteoblast response under low P conditions*

Osteoblasts, the bone-forming cells, line the outer bone surface and secrete the non-mineralised collagenous matrix known as osteoid. The osteoid mineralises upon removal of pyrophosphate (PPi) by the enzymatic activity of alkaline phosphatase (Murshed et al., 2005). However, mineralisation stops when plasma P levels are too low, yet bone matrix production continues, as demonstrated in both teleosts and mammals (Baylink et al., 1971; Takagi and Yamada, 1991; Witten et al., 2016, 2019; Cotti et al., 2020; Drábiková et al., 2021). In zebrafish, a low P dietary intake results in increased non-mineralised bone matrix formation at least on the vertebral body endplates and the periosteal surface of neural and haemal arches. The first evidence for enhanced bone matrix formation as a response to low dietary P intake in zebrafish was obtained based on laborious techniques performed on a few specimens only (Cotti et al., 2020). Here, these observations are expanded based on the study of a representative number of individuals and using cutting-edge techniques. The increase in bone matrix formation under LP conditions, demonstrated by histology and histomorphometry, is accompanied by upregulation of the bone formation markers collagen type I (*col1a1a*) and osteocalcin (*bglap*). Furthermore, histology and micro-CT analysis demonstrated that the additional bone matrix is capable of mineralisation.

Osteocalcin is the most abundant non-collagenous protein in bone. The transgenic *osc*:GFP zebrafish demonstrate that osteocalcin is not solely expressed by osteoblasts, but also by bone lining cells, by osteocytes and by odontoblasts (Chapter 6), matching reports from mammals (Bellido, 2014; Zoch et al., 2016). During early zebrafish vertebral column development, osteocalcin expression co-localises with the sites of chordacentra mineralisation (Bensimon-Brito et al., 2012b). Although osteocalcin is specific for bone and its blood level is used as indicator for bone formation, the function of osteocalcin is not fully understood. Interestingly, no human Mendelian genetic disease has yet been attributed to loss-of-function mutations in *BGLAP* (Diegel et al., 2020). However, there is evidence that genetic variants of the

*BGLAP* locus influence bone mineral density, at least in the postmenopausal women cohort examined by Raymond et al. (1999). Studies on osteocalcin in mice and rats have led to controversial results. Some studies have reported the increase of trabecular bone volume and improved biomechanical properties in osteocalcin null animals (Ducy et al., 1996; Lambert et al., 2016). Other studies did not find differences between osteocalcin-deficient animals and wild type animals (Diegel et al., 2020). While the function of this protein in bone is still uncertain, its conserved nature among species and its detection early in the process of mineralisation suggest a fundamental role for osteocalcin in attainment and maintenance of the bone mineral matrix, as well as in bone remodelling (Celeste et al., 1986; Power and Fottrell, 1991; Raymond et al., 1999). Osteocalcin has affinity for the mineral phase in bone and it is expressed at maximal levels in the subsequent stage of differentiation at the onset of mineralisation: post-proliferatively in osteoblasts, pre-osteocytes, and mature osteocytes (Zilberman et al., 2008).

Wake at al. (1983) propose the concept that, as reaction to a change of environmental conditions, dietary P in the present study, organisms remain stable and compensate until a critical point is reached. The upregulation of osteocalcin and other genes that code for enzymes with a more defined function in mineralisation shows the active response of osteoblasts that counteract the lack of mineralisation under LP conditions and thus keep the animals’ skeleton stable (Wake et al., 1983). In this study, qPCR analysis revealed increased expression of *entpd5*, encoding for the extracellular enzyme ectonucleoside triphosphate/diphospho-hydrolase 5, specifically expressed by osteoblasts. Entpd5 hydrolyses nucleotides di- and tri-phosphate to liberate inorganic P and has a crucial role for mineralisation, given that lack of *entpd5* leads to absence of bone mineralisation in zebrafish (Huitema et al., 2012). In contrast, Apschner (2014) suggests that Entpd5 possibly acts directly on PPi, not only because it is expressed at the right place and time, but also because other apyrase proteins have been shown to use PPi as a substrate (Čurdová et al., 1982). In this model, Entpd5 would bolster the PPi removal function of alkaline phosphatase. Entpd5 acts as a regulator of mineralisation, together with Enpp1 (ectonucleotide pyrophosphatase

phosphodiesterase 1), that hydrolyses ATP to produce PPi, a potent mineralisation inhibitor (Fleisch and Bisaz, 1962). In the present study, upregulation of *enpp1* under LP conditions is demonstrated, confirming the reciprocal role of Entpd5 and Enpp1 as mineralisation regulators, in line with previous studies (Huitema et al., 2012; Apschner, 2014; Apschner et al., 2014). Given the major role of PPi as mineralisation inhibitor, upregulation of *enpp1* might suggest an active inhibition of bone mineralisation under LP conditions (Collins et al., 2022). We also found upregulation of *alpl*, encoding for the membrane-bound tissue non-specific alkaline phosphatase (Tnap), that breaks down PPi to liberate P (Collins et al., 2022). Individuals with hypophosphatasia caused by mutations in *ALPL* have elevated PPi levels in plasma and abundance of PPi within bone tissue (reviewed by Millán and Whyte, 2016), which explains the osteomalacia phenotype (Millán and Whyte, 2016; Collins et al., 2022). Findings from patients indicate that increasing TNAP activity *in situ* in the skeleton is necessary to reverse the pathophysiology of hypophosphatasia (Millán and Whyte, 2016). Different treatments have been used to rescue the activity of TNAP in these patients (reviewed by Millán and Whyte, 2016), that demonstrated improvement of the osteomalacia bone phenotype (Millán and Whyte, 2016). Likewise, upregulation of *alpl* in the LP zebrafish and ALP activity (confirmed by enzyme histochemistry performed on histological sections) suggest an attempt to rescue the lack of mineralisation.

The upregulation of *phospho1*, encoding for the phosphatase orphan 1, likewise suggests increased P regulation. Phospho1 is an intracellular enzyme thought to function within matrix vesicles released from osteoblasts (Wu et al., 2002; Anderson et al., 2004; Golub, 2009). Phospho1 liberates P from its substrates phosphoethanolamine and phosphocholine (Dillon et al., 2019), indicating again an active response from the osteoblasts in case of low P levels.

In the present study, qPCR data showed also upregulation of *sost*, encoding for sclerostin. In mammals, sclerostin is specifically expressed by osteocytes (Wang et al., 2021), but in zebrafish it is primarily expressed by osteoblasts and only weakly by osteocytes (Ofer et al., 2019). Sclerostin is known as inhibitor of bone formation, given that lack of sclerostin leads to a high bone mass phenotype in patients and animal

models (Baron et al., 2006; Li et al., 2008; Wang et al., 2021). Studies, however, point at novel roles of sclerostin as regulator of bone mineralisation and P homeostasis. Sclerostin inhibits mineralisation by human primary osteoblasts *in vitro* (Atkins et al., 2011), and *Sost* mRNA was upregulated in the femur of the *HYP* mouse, model of X-linked hypophosphatemia characterised by rickets and osteomalacia/hypomineralised bone (Yuan et al., 2008; Atkins et al., 2011). Moreover, compared to controls, patients affected by X-linked hypophosphatemia presented elevated sclerostin plasma concentration, while phosphate plasma levels were reduced (Hansen et al., 2019). These data together with the upregulation of *sost* in LP zebrafish, are consistent with the hypothesis that sclerostin contributes to the reduced bone mineralisation phenotype and might have a role in regulating calcium and P homeostasis, as previously suggested (Atkins et al., 2011; Hansen et al., 2019).

Together, these data suggest that osteoblasts cope with LP conditions by providing the molecules responsible for mineralisation. These molecules should be capable to increase the availability of inorganic P via i) upregulation of *entpd5* and *phospho1* that directly provide P from their substrates; ii) upregulation of *enpp1* and *alpl*, the first providing the substrate (PPi), the second subsequently hydrolysing the mineralisation inhibitor PPi thereby providing additional P for mineralisation; and iii) upregulation of *sost,* that might have a role in regulating calcium and P homeostasis, as previously suggested (Atkins et al., 2011; Hansen et al., 2019) (**Figure 4.8**).

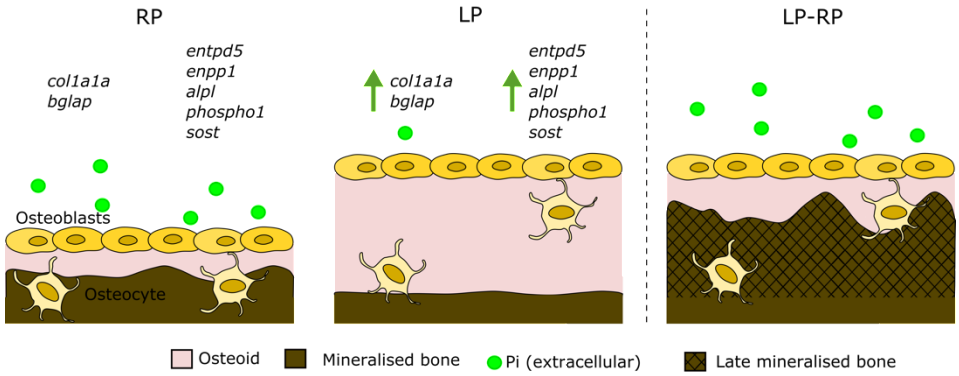


**Figure 4.8.** Schematic view of the effects of dietary P intake on bone formation and mineralisation. In presence of regular dietary P (RP), the non-mineralised bone matrix secreted by osteoblasts, named osteoid, mineralises after deposition. When low dietary P (LP) is provided, bone matrix production is stimulated, accompanied by the increased expression of the osteoblast specific markers collagen type I (*col1a1a*) and osteocalcin (*bglap*). Under LP conditions, genes important for bone mineralisation are upregulated, such as the ectonucleotide pyrophosphatase phosphodiesterase 1 (*enpp1*), the ectonucleoside triphosphate/diphospho-hydrolase 5 (*entpd5*), the tissue non-specific alkaline phosphatase (*alpl*), the phosphatase orphan 1 (*phospho1*) and sclerostin (*sost*). Thus, under LP conditions, osteoblasts increase the production of non-mineralised bone matrix and the expression of genes required for mineralisation. When sufficient dietary P is provided (LP-RP), the mineralisation of the non mineralised-matrix resumes, resulting in increased mineralised bone volume.

***The low P/sufficient P approach generates a lasting increased bone volume***

The two months of low dietary P treatment leads to a substantial increase in the formation of non-mineralised bone. Bone formation continues under a maintained low P diet, confirming earlier studies on zebrafish, salmon and mammals (Baylink et al., 1971; Witten et al., 2016; Cotti et al., 2020; Drábiková et al., 2021) that show the uncoupling of bone matrix formation and bone matrix mineralisation. The increase in bone matrix production is consistent throughout the vertebral column and is not only confined to locations of bone formation related to length increase, i.e. the vertebral body endplates, or to locations of increased mechanical loading such as the caudal part of the vertebral column. It also occurs at the periosteal surfaces of the neural and haemal arches and in the central region of the autocentra (Cotti et al., 2020). Von Kossa/Van Gieson histological staining, that distinguishes mineralised parts (detection of phosphate) of the bone matrix from non-mineralised parts, demonstrates that under LP conditions the bone matrix is largely non-mineralised after both two and 3.5 months

of dietary treatment. Consistently, micro-CT analysis shows a significant reduction in bone mineral density (BMD) in the LP-LP animals compared to controls and the LP-HP dietary group. BMD, calculated as g/cm$^3$ of calcium hydroxyapatite, is a measure of the bone mineral content (of the mineralised bone volume) and was, in this study, performed only on the mineralised parts of the autocentrum. Interestingly, LP-LP animals have reduced BMD values in the mineralised regions of the autocentra, suggesting reduced mineral content in those mineralised areas, consistent with the reduced elastic modulus and hardness demonstrated by nanoindentation assessment of LP bone mechanical properties (Cotti et al., 2020). Low BMD also typifies under-mineralised bones (osteomalacia) in humans, where it reflects the presence of large amounts of non-mineralised osteoid rather than the reduction of bone matrix volume (Bhambri et al., 2006). Irrespective of whether the disease is due to nutritional deficiencies or to genetic mutations (reviewed by Jha et al., 2019), osteomalacia is generally characterised by decreased P in the serum of patients (Bhambri et al., 2006). Since similar low P plasma levels are found in salmon fed a low P diet (Drábiková et al., 2021), it is reasonable to assume that LP zebrafish also has reduced P concentrations in plasma. Treatment of osteomalacia in humans consists of adequate calcium intake and vitamin D and phosphate oral supplementations, which promote the non-mineralised matrix to get mineralised and favour the increase of BMD values (Bhambri et al., 2006; Suzuki et al., 2009; Robinson et al., 2020). Likewise, increasing the P plasma levels by dietary means in teleosts (Witten et al., 2019; Drábiková et al., 2021), or by inactivation of excess FGF23 in X-linked hypophoshatemic patients (Carpenter et al., 2014, 2018; Imel et al., 2015; Whyte et al., 2019; Robinson et al., 2020), stimulates the mineralisation of the non-mineralised bone. In the present study, when the LP zebrafish are provided with adequate (RP diet) or increased (HP diet) dietary P, BMD value resumes control value. RP diet is sufficient to resume mineralisation of non-mineralised bone and BMD values as in the control group. The result is a dramatic increase of mineralised bone volume (**Figure 4.8**). Interestingly, massive remodelling/resorption is not observed, suggesting that the bone formed is permanent, at least within the time frame of the experiment. We provide evidence that the

alternation of low P and sufficient P dietary conditions is able to increase bone volume, first by stimulating matrix formation under LP conditions, and subsequently inducing the mineralisation of newly formed bone by providing adequate dietary P (**Figure 4.8**). The result is a “super-bone” phenotype. Importantly, the low P/sufficient P approach tested here on zebrafish can possibly contribute to design therapeutic approaches aiming to reverse osteoporosis and ageing-related bone loss.

## Materials and methods

### *Zebrafish maintenance and ethical statement*

Wild type (WT) AB zebrafish were obtained from European Zebrafish Research Center (Eggenstein-Leopoldshafen, Germany) or from the Zebrafish Facility Ghent (Ghent, Belgium). The reporter zebrafish line *osc*:GFP was a gift from Dr. A. Willaert, Ghent University Hospital, Gent, Belgium, and originally was obtained by Dr. S. Schulte-Merker, Institute for Cardiovascular Organogenesis and Regeneration, Münster, Germany (Vanoevelen et al., 2011). Zebrafish embryos were kept in petri dishes in fish water (1.2 mM $NaHCO_3$, 0.01% instant ocean, 1.4 mM $CaSO_4$, 0.0002% methylene blue) at 28°C until 7 days post-fertilisation (dpf), then grown at 28°C, pH 7.5 on a 14/10 light/dark cycle. Zebrafish from 7 to 21 dpf were fed three times a day alternating commercial dry food (ZM000, Zebrafish Management Ltd., Winchester, UK) and brine shrimp (Artemia cysts, Zebrafish Management Ltd., Winchester, UK). Fish were then fed for another week three times a day with the dry regular phosphorus (RP) diet (see also the next section), until 28 dpf, to adjust them to this type of dry food. The nutrition trial started at 28 dpf: WT and transgenic fish were randomly divided in three groups, grown in identical tanks with a density of 10 fish/L and fed three times a day with a low P (LP) diet, a regular P (RP) diet and a high P (HP) diet, respectively, for two months, as previously described (Cotti et al., 2020).

A second nutritional trial was performed. Starting from 28 dpf, WT fish were fed a LP diet for two months as described above, then were randomly divided in three groups and fed either LP (LP-LP group), RP (LP-RP group) or HP (LP-HP group) diet for 1.5 months. A control group was fed RP throughout.

Fish were euthanised by tricaine (3-amino benzoic acidethylester) overdose (0.3%) and fixed for further analyses as described below. The experiments were conducted in the centralised animal facility of the University of Pavia (Pavia, Italy) or at Ghent University, Department of Biology (Gent, Belgium). All animal studies were conducted in agreement with EU Directive 2010/63/EU for animals. The experimental

protocol was approved by the Italian Ministry of Health (Approval animal protocol No. 260/2020-PR, 26 March 2020).

***Diet composition***

Diet composition and nutritional experiment are described in detail in Cotti et al. (2020). Briefly, the diets were formulated to have a total P content of 0.5%, 1.0% and 1.5%, termed low P (LP) diet, regular P (RP) and high P (RP) diet, respectively. Monoammonium phosphate ($NH_4H_2PO_4$, MAP) was used as dietary inorganic P supplement. In order to keep all diets equal in nutrients, except for P concentration, MAP replaced the inert filler diatomaceous earth (Diamol, Imerys, Denmark). The diets were formulated by SimplyFish AS (Stavanger, Norway, www.simplyfish.no) and produced by extrusion with subsequent crumbling to a suitable particle size by the Danish Technological Institute (Taastrup, Denmark, https://www.dti.dk). The P content of the product was verified at the University of Hohenheim (Stuttgart, Germany, https://www.uni-hohenheim.de) and determined with 5.04 g/kg diet and 9.84 g/kg diet for the low P and regular P diet, respectively.

***Quantitative real-time PCR***

Following dissection of LP (n=4), RP (n=4) and HP (n=4) zebrafish, the vertebral column was cleaned from the muscles, the neural tube and the blood vessels and stored in 1 mL TRIzol reagent (Invitrogen, Waltam, MA, USA) at -80°C. The dissected vertebral column was disrupted through high speed shaking in 1.5 mL RNase-free tubes with 3 mm Tungsten Carbide beads (Qiagen, Hilden, Germany) using a TissueLyser II (Qiagen, Hilden, Germany). Total RNA was isolated following manufacturer's instructions and quantified by Nanodrop ND-1000 spectrophotometer (Thermo Fisher, Waltam, MA, USA). 1 µg of total RNA was treated with genomic DNase and retro-transcribed into cDNA using PrimeScript RT Reagent Kit (Takara Bio Inc., Kusatsu, Japan) following manufacturer's instructions. Quantitative real-time PCR (qPCR) was optimised using RNA extracted from the vertebral column of three months old WT zebrafish (not fed the P diets) and performed in a reaction volume of 10 µL containing PowerUp SYBR

Green Master Mix (Applied Biosystems, Waltam, MA, USA), validated qPCR primers (BLAST, see **Table 4.2**) and cDNA using the QuantStudio3 Real-Time PCR System (Thermo Fisher, Waltam, MA, USA). An initial 2 min step at 50°C was followed by denaturation of 2 min at 95°C and amplification (10 s at 95°C, 30 s at 58°C, 40 cycles). The melt curves of the primers were obtained by 15 s incubation at 95°C, 1 min at 58°C and 15 s at 95°C. The annealing temperature was 58°C for all the primers used. Samples were run in triplicate, *ef1a* was employed as housekeeping gene, given that it is one of the most stable genes with a low degree of variability (McCurley and Callard, 2008). The differential expression was calculated according to the $\Delta\Delta^{Ct}$ method.

**Table 4.2.** Primers used for qPCR.

| Gene acronym | NCBI gene accession number | Forward 5’-3’ | Reverse 5’-3’ |
|---|---|---|---|
| *bglap* | NM_001083857.3 | TGCTGCCTGATGACTGTGTG | GTGCAGTTCCAGCCCTCTTC |
| *col1a1a* | NM_199214.1 | CGTAATGTGCGACGAAGTGA | CTAGGTCCCTCAACACTGGG |
| *sost* | XM_001340647.5 | TACCAGAATACGCGGAGGAC | AAGTCCGTGTGTTTGCTGAC |
| *alpl* | NM_201007.2 | CAGTGGGAATCGTCACAACAA | CCACACAGTGGGCATAAGCA |
| *col10a1a* | NM_001083827.1 | CCGCAGTACCAGCCTTACTC | TTTCCAGGTGCTGAATACCC |
| *sparc* | NM_001001942.1 | CTTCTTCTTGTTCTGCCTCGCT | TCTCAGCAATAACATCCTCCAC |
| *spp1* | NM_001002308.1 | CACAGACAGCGCAGATGACACT | CCCCGGCCTGTGTTGATAATG |
| *ef1a* | NM_131263.1 | TTGAGAAGAAAATCGGTGGTGCTG | GGAACGGTGTGATTGAGGGAAATT |
| *enpp1* | NM_001030168.1 | TGTGAGCGGACCGATATTTG | TCCATTCAGGACTCCCTTGT |
| *entpd5a* | XM_679770.8 | ATATGCCTGAAAAGGGTGGA | TACTTCTTTGACCTCATTCAGCAG |
| *phex* | NM_001320330.1 | CCGTCATCACGGTATCACAA | TCTGAGCCATGGGTAAATCC |
| *phospho1* | NM_001003461.1 | TGAAAACAGGAGCAGCTGTAAA | GGGGCTGGAGATCTGCTT |

***Histology***

Specimens were fixed for 24 h in 2.5% paraformaldehyde (PFA), 1.5% glutaraldehyde, 0.1 M sodium cacodylate buffer (pH 7.4) and 0.001% $CaCl_2$ at 4°C, decalcified in 0.1 M EDTA for 14 days at 4°C and embedded in glycol methacrylate (Witten et al., 2001). Sagittal or transverse 2 µm sections were cut on a Microm HM360 (Marshall Scientific, Hampton, New Hampshire, USA) automated microtome and were stained with toluidine blue (0.5% toluidine blue, 1% $Na_2B_4O_7$ in demineralised $H_2O$

($dH_2O$), pH 9) for 15 sec, rinsed in $dH_2O$ and mounted with DPX. Images were acquired using an Axio Imager-Z1 microscope (Carl Zeiss, Oberkochen, Germany) equipped with an Axiocam 503 colour camera (Carl Zeiss, Oberkochen, Germany). Bone structure histomorphometry was analysed on images of toluidine blue stained sagittal sections of the middle plane of the vertebral column according to an established protocol (Cotti et al., 2022). Thickness of bone structures in the endplates and in the central region of five to 10 vertebral centra per specimen (LP n=5, RP n=4, HP n=5), were measured using Fiji (NIH, Bethesda, Maryland, USA) (see **Figure 4.1 A** for location). The mean values were considered for analysis.

For mineral detection on histological sections, specimens were fixed as described above and embedded in glycol methacrylate without carrying out decalcification. Sagittal or transverse sections of 2 µm were stained according to the Von Kossa/Van Gieson protocol (Humason et al., 1997). Images were acquired using an Axio Imager-Z1 microscope (Carl Zeiss, Oberkochen, Germany) equipped with a 5MP CCD camera. Sagittal sections of the middle plane of the vertebral column were used for quantification analysis of seven to 10 vertebral endplates growth zones per specimen (RP-RP control n= 3, LP-LP n=4, LP-RP n=4, LP-HP n=4). For each specimen, the region of interest corresponded to a rectangle with a defined length (one third of the total vertebral length) and height (one quarter of the total vertebral height), centred in the middle of the intervertebral ligament. Within the region of interest, the total bone area and the mineralised bone area were measured using Fiji (NIH, Bethesda, Maryland, USA) and used to calculate the following parameters: i) percentage of mineralised bone, calculated as the ratio between the mineralised bone area and the total bone area, ii) the total bone area normalised to the vertebral length. The mean values were considered for analysis.

After two months of dietary treatment, *osc*:GFP zebrafish were euthanised by tricaine overdose and kept in the dark during the following steps. To preserve and visualise GFP on sections, we followed an established protocol (Oralová et al., 2019). Briefly, *osc*:GFP zebrafish were fixed for 2 h in 4% PFA in 1× phosphate-buffered saline (PBS), pH 7.4, at RT, rinsed in tap water for 1 h and decalcified for 48 h in 10% EDTA, 4%

PFA, pH 7.4. After rinsing 1 h in tap water, samples underwent glycol methacrylate embedding (Witten et al., 2001). Sagittal sections of 3 µm were cut on a Microm HM 360 (Marshall Scientific, Hampton, NH, USA) automated microtome. Images were acquired using an Axio Imager-Z1 microscope (Carl Zeiss, Oberkochen, Germany). Sagittal sections of the middle plane of the vertebral column were used for quantification of the fluorescence-positive osteoblast area in the vertebral endplates growth zone (a total of 20 growth zones were analysed per sample, LP n=3, RP n=3, HP n=3). Osteocytes and bone lining cells were not considered in the analysis (**Figure 4.2 F**). The ZFBONE ImageJ toolset (Tarasco et al., 2020) for Fiji (NIH, Bethesda, Maryland, USA) was used for quantification. The mean of the fluorescence-positive area was considered for analysis.

***Enzyme histochemistry***

For detection of alkaline phosphatase (ALP) activity on sections, LP (n=3), RP (n=3), HP (n=3) were fixed in 4% PFA in 1× PBS, pH 7.4, for 1 h at RT. Without carrying out decalcification, specimens were embedded in glycol methacrylate as described above. Sagittal 5 µm sections were cut on a Microm HM360 (Marshall Scientific, Hampton, New Hampshire, USA) automated microtome and collected on super-frosted coated slides. Demonstration of ALP activity was adapted from published protocols (Witten et al., 2001; Grotmol et al., 2005). Briefly, sections were pre-incubated at RT for 1 h in 50 mmol Tris HCl buffer, pH 9.5. Enzymatic reaction took place at RT for 2 h in 50 mmol Tris HCl buffer, pH 9.5, containing 1 mg/mL Naphthol AS-MX phosphate, CAS Number 1596-56-1 (Sigma Aldrich, St. Louis, MO, USA) and 1 mg/mL Fast Red TR salt, CAS Number 51503-28-7 (Sigma Aldrich, St. Louis, MO, USA). Subsequently, slides were rinsed in $dH_2O$, counterstained with Meyers haematoxylin for 10 min, rinsed in running tap water for 10 min, flushed in $dH_2O$, dried at 40°C and mounted with DPX.

For demonstration of tartrate-resistant acid phosphatase (TRAP), samples (RP-RP control n=1, LP-LP n=1, LP-RP n=1, LP-HP n=1) were fixed in 4% PFA in 1× PBS, pH 7.4, for 1 h at RT and decalcified in 4% PFA, 10% EDTA, pH 7.4 for 14 days at 4°C. Specimens were embedded in glycol methacrylate (Witten et al., 2001). Transverse 5

∝m sections were cut on a Microm HM360 (Marshall Scientific, Hampton, New Hampshire, USA) automated microtome and demonstration of TRAP was performed as described in Cotti et al. (2022). Briefly, sections were pre-incubated at 37°C for 45 min in 50 mL acetate buffer (0.1 M sodium acetate, 50 mM L(+) di-sodium tartrate dehydrate, pH adjusted to 5.5 with acetic acid) to which is added 0.5 mL of enzyme substrate solution (2% Naphtol AS TR phosphate dissolved in ethylene glycol mono-butyl ether). Shortly before use, 1 mL of pararosaniline solution (4% pararosaniline chloride (CI. 42500) in 7% HCl solution) was mixed to 1 mL of fresh 5% sodium nitrite and, after hexazotiation, was added to the acetate-enzyme substrate solution. Enzymatic reaction took place in 30-60 min at 37°C. Subsequently, slides were rinsed in $dH_2O$, counterstained with Meyers haematoxylin for 10 min, rinsed in running tap water for 10 min, flushed in $dH_2O$, dried at 40°C and mounted with DPX.

***Alizarin red S***

Zebrafish (LP-LP n=3, LP-RP n=3, LP-HP n=3, RP-RP n=3) were euthanised by tricaine overdose, fixed for 24 h in 4% PFA in 1× PBS at 4°C and were stained according to the following protocol: 1.5% $H_2O_2$ in 0.25% KOH (2 h); distilled $H_2O$ ($dH_2O$) (5 min); saturated sodium tetraborate (12h); 0.01% Alizarin red S in 0.5% KOH (24 h); 1% KOH (2 h); 25% glycerol in 0.75% KOH (2 h); 50% glycerol in 0.5% KOH (2 h); 75% glycerol in 0.25% KOH (2 h); 100% glycerol (modified from Taylor and Van Dyke, 1985). The vertebral column was then dissected and imaged using an Axio Imager-Z1 microscope with DIC lens (Carl Zeiss, Oberkochen, Germany).

***Micro-computed tomography***

For micro-computed tomography (micro-CT), LP-LP (n=3), LP-RP (n=3), LP-HP (n=3), RP-RP controls (n=3) were fixed in 4% PFA in 1× PBS, pH 7.4, for 24 h at 4°C. After rising in 1× PBS, the samples were placed in a moist chamber during scanning in a SkyScan1276 (Bruker, Kontich, Belgium). Scans of the caudal region of the vertebral column were acquired at a 3.38 ∝m voxel size, with a 41 kV voltage and 72 ∝A current. A 0.25 mm aluminium filter was used. Calibration phantoms of known mineral density

(0.25 and 0.75 g/cm$^3$ hydroxyapatite) were scanned at the same time as the zebrafish samples for quantification of the density of zebrafish vertebral bodies. NRecon software (Bruker, Kontich, Belgium) was used for scans reconstruction, for which Gaussian smoothing, defect pixel masking, beam hardening correction and attenuation range were kept constant for all the samples and phantoms. Post-alignment fine tuning and ring artifact reduction were adapted to each scan. The volume of interest, including the first three caudal vertebral bodies, was first selected using DataViewer software (Bruker, Kontich, Belgium) and the analysis was performed using CTAn software (Bruker, Kontich, Belgium). The regions of interest, i.e. the vertebral centra of the first three caudal vertebral bodies, were selected applying an optimised task list of global thresholding and plug-ins like “bitwise operations”, “despeckle” and “morphological operations” to all samples. This task could only select the mineralised parts of the vertebral centra. The selected regions of interest were used to calculate bone mineral density (BMD, defined as g/cm$^3$ of calcium hydroxyapatite, calibrated against the density scales of the attenuation coefficient), the mineralised bone volume (mm$^3$) and the mineralised bone surface (mm$^2$).

For 3D visualisation of the vertebral body analysed, the volume of interest was reconstructed using Amira 3.1.1 software (TermoFisher, Waltham, MA, USA) by segmentation applying a constant greyscale-threshold to all samples, in order to visualise the mineralised parts of the vertebral bodies and arches, as previously described (Cotti et al., 2020).

***Statistical analysis***

Quantitative variables are expressed as mean ± standard deviation. Statistical analysis was performed using Past4.04 software (Hammer et al., 2001). All pairwise statistical differences were evaluated by means of Student’s t-test followed by Bonferroni correction. A p-value less than 0.05 was considered significant.

# Chapter 5

## Compression fractures and partial phenotype rescue with a low phosphorus diet in the *Chihuahua* zebrafish osteogenesis imperfecta model

This chapter is a published paper:

Silvia Cotti, Ann Huysseune, Daria Larionova, Wolfgang Koppe, Antonella Forlino and P. Eckhard Witten (2022) Compression fractures and partial phenotype rescue with a low phosphorus diet in the *Chihuahua* zebrafish osteogenesis imperfecta model. *Frontiers in Endocrinology* 13, 851879, doi:10.3389/fendo.2022.851879.

## Introduction

Osteogenesis imperfecta (OI), also known as “brittle bone disease”, is a clinically and genetically heterogeneous group of heritable disorders affecting bone and other connective tissues with collagen type I as main matrix component (Forlino and Marini, 2016). Clinical features of OI patients are short stature, skeletal deformities, low bone mass and bone fragility. Frequent fractures also in absence of trauma can occur in utero and cause death before birth (Sillence et al., 1979; Marini et al., 2017). Scoliosis and compression fractures of the vertebral bodies are the most severe complications in human patients (Benson and Newman, 1981; Zeitlin et al., 2003). Vertebral compression fractures require surgery to stabilise the vertebral column and treatment with bisphosphonates to prevent bone loss (Ben Amor et al., 2013; Wallace et al., 2017; Castelein et al., 2019).

In the majority of patients, OI is caused by autosomal dominant mutations in *COL1A1* and *COL1A2*, coding for α1 and α2 chains of the collagen type I (Marini et al., 2007). These OI forms, regarded as classical OI, were first classified in 1979 by Sillence and co-workers in four different types of OI (OI I-IV) based on clinical observations, radiographic features and the mode of inheritance (Sillence et al., 1979). The types range from mild (type I), over moderate (type IV), severe (type III) to perinatally lethal (type II). The mildest form, OI type I, is caused by quantitative deficiency of structurally unaltered collagen. Patients have a normal or slightly short stature, deformities of long bones in the legs and are susceptible to bone fractures from early on. The moderate, severe and lethal OI forms are caused instead by alterations in the collagen structure. The most common mutations causing structural alterations of collagen type I are single-nucleotide variants that substitute glycine with a bulkier or with a charged residue within the Gly-X-Y repeat, either in the α1 or α2 chains (Marini et al., 2007). This results in delayed collagen folding and excess post-translational modifications (Ishikawa and Bächinger, 2013).

Zebrafish (*Danio rerio*) has become an important model organism for the study of human skeletal disorders, due to its high reproduction rate and easy access to embryos. Moreover, basic processes of skeletal formation are conserved across

gnathostomes (Huysseune, 2000; Witten et al., 2017; Tonelli et al., 2020a; Dietrich et al., 2021). The first identified zebrafish mutant model for classical dominant OI is the *Chihuahua* (*Chi/+*). The mutant was isolated from a large N-ethyl-N-nitrosourea (ENU)-mutagenesis screen for skeletal dysplasias (Fisher et al., 2003). *Chi/+* carries a heterozygous glycine to aspartate substitution in position 736 in the α1 chain of collagen type I. Adult animals display typical OI characters, such as bending of the vertebral column, bone fragility (rib fractures), high bone mineral-to-matrix ratio and reduced bone elasticity (Gioia et al., 2017; Fiedler et al., 2018).

Next to structural alterations in collagen type I, also hypermineralisation leads to fragility and poor bone quality, both in OI patients and in zebrafish models (Fiedler et al., 2018). It is a common assumption that an increase in bone mineral content enhances the mechanical properties of bone. Proper mechanical function of bone requires, however, a balance between toughness, provided by the collagenous matrix, and stiffness, provided by the mineral phase (Currey, 2003). The antlers of deers and elks are examples for bones that withstand extreme mechanical forces. Yet, the bone mineral content of antlers is about half of that of a human femur (Veis, 2003). Excess mineralisation, on the other hand, makes bone stiff and brittle (Currey, 2003) and increases the risk of fractures (Wilton et al., 1987; Guglielmi et al., 2011). Thus, while mutations in OI patients cannot be undone, lowering the bone mineral content could possibly alleviate skeletal defects in these patients. Recent studies on teleost fish, including wild type (WT) zebrafish (Cotti et al., 2020), as well as farmed Atlantic salmon (Witten et al., 2016, 2019; Drábiková et al., 2021), have shown that periods of severely lowered dietary phosphorus (P) intake (-50%) reduce the bone mineral content and promote the formation of non-mineralised bone without causing vertebral column malformations. In contrast, but similar to OI patients and animal models, zebrafish with increased dietary P intake and animals with age-related increased bone mineral density show elevated rates of vertebral column malformations (Witten et al., 2016, 2019; Cotti et al., 2020; Drábiková et al., 2021; Kague et al., 2021).

We have used these new insights to investigate if a reduction of dietary P intake can mitigate deformities of the vertebral column in adult *Chi/+* zebrafish. To

answer this question we have characterised the *Chi/+* vertebral column phenotype at a morphological, cellular and subcellular level and assessed the effects of a low P (LP) diet on the *Chi/+* phenotype (further referred to as *Chi/+*$_{LP}$). The LP diet decreases vertebral deformities in the abdominal region and partially restores shape variation of the caudal vertebral bodies in the *Chi/+* mutant. The osteoid layer covering the bone at the endplates in WT is absent in the *Chi/+* mutants, but partially restored with the LP diet. Vertebral body fractures are observed in animals of both groups, *Chi/+* and *Chi/+*$_{LP}$. In both groups, the bone shows evidence of fracture repair and remodelling, supported by the observation of abundant osteoclast activity in *Chi/+* compared to WT fish. Finally, both *Chi/+* and *Chi/+*$_{LP}$ display osteoblasts with enlarged endoplasmic reticulum (ER) cisternae and a high protein content consistent with intracellular retention of defective collagen. The secreted collagen in *Chi/+*$_{LP}$ appears, nevertheless, better organised concerning fibre periodicity than *Chi/+*.

## Results

### *Chihuahua mutants have increased frequency of vertebral column deformities*

Starting from 28 days post-fertilisation (dpf), WT were fed a regular P diet for two months. At 28 dpf, *Chi/+* mutants were randomly divided in two groups and fed a "LP diet" (low P content, *Chi/+*$_{LP}$) or a regular P diet (*Chi/+*) for two months. Three months old *Chi/+* show severe deformities compared to WT fish on Faxitron X-ray images (**Figure 5.1 A**), confirming earlier reports (Fisher et al., 2003; Gioia et al., 2017; Fiedler et al., 2018).

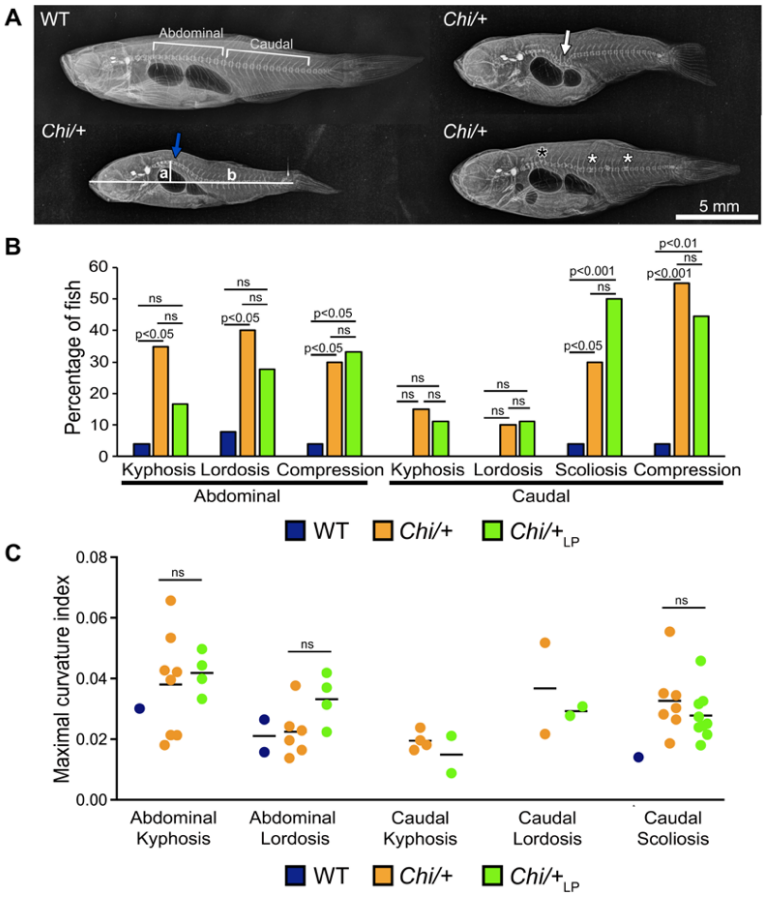


**Figure 5.1.** Vertebral column deformities in *Chi/+* and *Chi/+*$_{LP}$ mutants. **A**: Representative X-rays of three months old WT and *Chi/+* (representative also for the malformations diagnosed in

*Chi/+*$_{LP}$) zebrafish show severe vertebral column deformities in mutants, i.e. abdominal kyphosis (blue arrow), abdominal lordosis (white arrow), vertebral body compressions (white asterisks) and hemivertebra (black asterisk). **B**: Frequency of malformations. *Chi/+* mutants (n=20) show increased frequency of kyphosis, lordosis, scoliosis and vertebral body compressions in the abdominal and caudal vertebral column compared to WT animals (n=26). *Chi/+*$_{LP}$ animals (n=18) display reduced kyphosis and lordosis of the abdominal, but increased scoliosis of the caudal vertebral column. Alterations were diagnosed based on Alizarin red S whole mount-stained specimens; only the abdominal and caudal region of the vertebral column were considered for the analysis. Chi-squared test followed by Bonferroni correction; p-values are indicated; ns: non-significant. **C**: Severity assessment of the maximal curvature index diagnosed in WT, *Chi/+* and *Chi/+*$_{LP}$ related to abdominal kyphosis and lordosis, and to caudal kyphosis, lordosis and scoliosis. The graph shows individual data points and the mean value (black bar) for the maximal curvature index. The maximal kyphotic and lordotic indices were calculated in the sagittal plane of Alizarin red S stained specimens as the ratio (a/b) between the perpendicular distance from the axis (in correspondence of the maximal curvature, segment "a" in **A**) and the standard length (segment "b" in **A**). The same method but in the coronal plane was used to calculate the maximal scoliotic index. Mann-Whitney test was applied with a minimum of three values per group; ns, non-significant.

Vertebral column deformities of WT, *Chi/+* and *Chi/+*$_{LP}$ were assessed by whole mount Alizarin red S staining (details are described below). Compared to WT, *Chi/+* mutants have an increased frequency of kyphosis and lordosis in the abdominal region of the vertebral column. Kyphosis and lordosis are reduced in the abdominal region of the vertebral column in *Chi/+*$_{LP}$ fish. However, compared to *Chi/+* fish, *Chi/+*$_{LP}$ fish show increased scoliosis in the caudal vertebral column. Both *Chi/+* and *Chi/+*$_{LP}$ have a high frequency of compressed vertebral bodies; examples are shown in **Figure 5.1 A**, frequency of deformities is shown in **Figure 5.1 B**. To assess the severity of the curvature in those specimens diagnosed with kyphosis, lordosis and scoliosis, the maximal kyphotic, lordotic and scoliotic indices were measured, respectively. **Figure 5.1 C** shows the maximal curvature indices in the abdominal and caudal region of affected WT, *Chi/+* and *Chi/+*$_{LP}$ individuals. No statistical differences in the degree of curvature are detected between *Chi/+* and *Chi/+*$_{LP}$ fish at three months of age (Mann-Whitney test: non-significant).

The general metrics for the analysis of the vertebral column malformations (**Table 5.1**) show that the frequency of specimens with at least one malformation is 19% in WT, 75% in *Chi/+* and 89% in *Chi/+*$_{LP}$. The highest average malformation load is in the *Chi/+* group (3.27 malformations/deformed specimen) where a total of 49

malformations were identified. The average malformation load in the *Chi/+*$_{LP}$ group is 2.5 with a total of 40 diagnosed malformations. These data indicate a tendency towards reduced number of malformations and average malformation load in the *Chi/+*$_{LP}$ compared to untreated *Chi/+* (Chi-square test: p=0.27).

**Table 5.1.** General metrics for the analysis of vertebral column malformations in WT, *Chi/+* and *Chi/+*$_{LP}$.

| | **WT** | ***Chi/+*** | ***Chi/+*$_{LP}$** |
|---|---|---|---|
| Number of observed specimens | 26 | 20 | 18 |
| Total number of malformations | 6 | 49 | 40 |
| Frequency (%) of specimens with at least one malformation | 19 | 75 | 89 |
| Average malformation load | 1.20 | 3.27 | 2.5 |

***Partial rescue of vertebral body shape variation in Chihuahua mutants under the LP diet***

To quantify shape variation of the caudal vertebral centra in WT, *Chi/+* and *Chi/+*$_{LP}$ animals, landmark-based geometric morphometrics was applied, based on whole mount-stained specimens (**Figure 5.2 A**). The scatterplot of 2D landmarks shows differences in location of corresponding landmarks between WT, *Chi/+* and *Chi/+*$_{LP}$ animals. The scatterplot shows a high variation in the superimposition of Procrustes coordinates of *Chi/+* compared to WT. *Chi/+*$_{LP}$ display reduced variation of landmarks compared to *Chi/+* and a distribution more similar to WT (**Figure 5.2 B**). Principal component analysis (PCA) of superimposed landmarks shows the amount of variation between WT, *Chi/+* and *Chi/+*$_{LP}$. Only principal component 1 (PC1) and principal component 2 (PC2) were considered. Compared to WT, *Chi/+* show a statistically significant higher variance (*Chi/+* versus WT, PC1 0.3321, PC2 0.1795; Chi-square test: p<0.001). On the contrary, *Chi/+*$_{LP}$ animals show a non-statistically different variance compared to WT (*Chi/+*$_{LP}$ versus WT, PC1 0.2484, PC2 0.2020; Chi-square test: non-significant) (**Figure 5.2 C**).

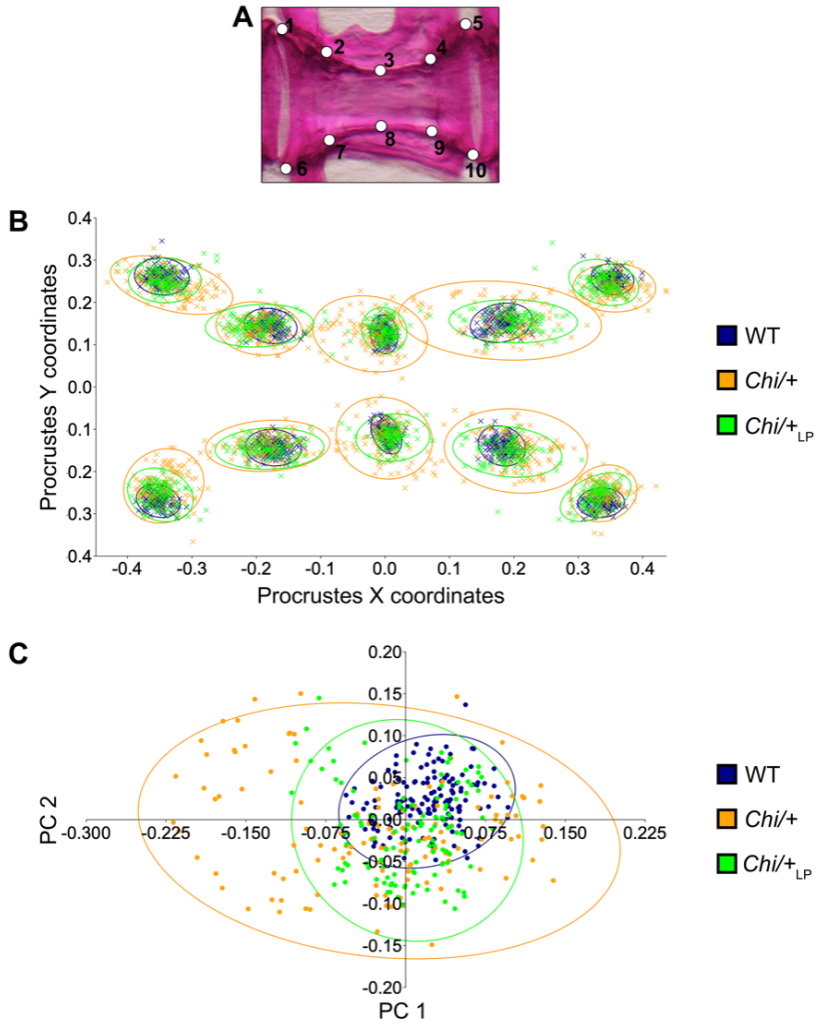


**Figure 5.2.** Vertebral body shape variation in *Chi/+* and *Chi/+*$_{LP}$ mutants. **A**: Alizarin red S stained vertebral body of a WT animal with 2D landmark positions used for quantifying the shape variation by means of geometric morphometrics, represented in **B**. **B**: The scatterplot of WT, *Chi/+* and *Chi/+*$_{LP}$ 2D landmarks shows high variation in the superimposition of X,Y Procrustes coordinates of *Chi/+* compared to WT animals. *Chi/+*$_{LP}$ animals display reduced landmark variation compared to *Chi/+* and a distribution more similar to WT indicating a partial rescue of shape variation at three months of age. The first 10 caudal vertebral centra in WT (n=15), *Chi/+* (n=13) and *Chi/+*$_{LP}$ (n=12) were analysed. The 95% confidence ellipses are shown. **C**: Principal component analysis of vertebral centra shapes. Each symbol in the plot represents a vertebral body. PC indicates Principal Component and the values in the axis labels indicate the percentage of variation accounted for by each axis. *Chi/+* animals show high variance compared to WT animals (*Chi/+* versus WT, PC1 0.3321, PC2 0.1795; Chi-square test: $p<0.001$). Variance is rescued in *Chi/+*$_{LP}$ animals (*Chi/+*$_{LP}$ versus WT, PC1 0.2484, PC2 0.2020; Chi-square test: non-significant). The 95% confidence ellipses are shown.

Histological assessment of the vertebral column in the sagittal plane confirmed the irregular shape of mutant vertebral bodies compared to WT vertebral bodies (**Figure 5.3**). Different from WT (**Figures 5.3 A,B**), in *Chi/+* animals vertebral body endplates of adjacent vertebral bodies are frequently shifted against each other along the dorsal-ventral axis (**Figure 5.3 B**). Moreover, scoliosis of the vertebral column in *Chi/+* and *Chi/+*$_{LP}$ animals, previously observed on whole mount-stained specimens is visible on histological sections as the absence of a sagittal middle plane (**Figure 5.3 B**). Histology reveals the presence of compression fractures in *Chi/+* and *Chi/+*$_{LP}$ animals (see below for details) (**Figure 5.3 B**). Vertebral centra of *Chi/+* and *Chi/+*$_{LP}$ animals display distortions of the endplates not observed in WT zebrafish (**Figure 5.3 C**). Despite these distortions, the endplates retain structurally unaltered intervertebral spaces with unaltered ligaments as in WT animals (**Figure 5.3 C**).

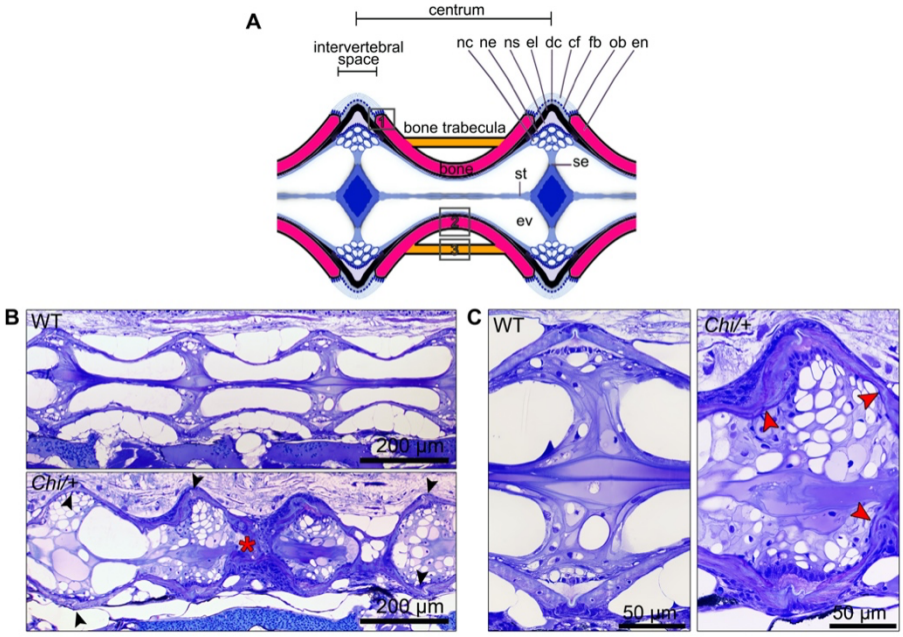


**Figure 5.3.** Histology of vertebral column of WT, *Chi/+* and *Chi/+*$_{LP}$ confirms the irregular shape of mutant vertebral bodies. **A**: Schematic representation of the medio-sagittal plane of a zebrafish vertebral body centrum and two intervertebral spaces. Vertebral centra derive from segmental mineralisation of the notochord sheath and intramembranous bone formation around the notochord. Vertebral body endplates (en) are connected by intervertebral ligaments. Ligaments consist of the enlarged notochord sheath (ns, a collagen type II layer secreted by the

cells of the notochord epithelium, ne), its outer elastin layer (el) and dense collagen type I fibre bundles (dc) produced by fibroblasts (fb) that surround the notochord. The collagen type I fibre bundles (cf) continue in the bone of the vertebral body endplates (en) as Sharpey fibres. Osteoblasts (ob) deposit new bone matrix that expands the vertebral body endplates in the bone growth zone. Inside, the notochord is composed of vacuolated notochord cells (nc) and extracellular vacuoles (ev). Condensed notochord cells constitute the notochord septum (se) and the notochord strand (st). Boxes indicate locations where the bone thickness was measured, i.e. endplates (1), central region of vertebrae (2) and trabecular bone (3). **B**: Representative three months old WT and mutant sagittal sections of the vertebral column stained with toluidine blue. Compared to WT, *Chi/+* mutants (representative also for *Chi/+*$_{LP}$) have several vertebral centra with deformed endplates that are shifted against each other along the dorsal-ventral axis (black arrowheads). *Chi/+* animals also suffer from vertebral body compression fractures (red asterisk), scoliosis, lordosis and kyphosis. Scoliosis can be appreciated from the absence of a straight sagittal midline plane as seen in the WT animal. **C**: Higher magnification of vertebral body endplates in WT and *Chi/+* (representative also for *Chi/+*$_{LP}$) animals. Toluidine blue staining shows deformed endplates of adjacent vertebral bodies (red arrowheads) in *Chi/+* mutants, yet with unaltered ligaments and unaltered intervertebral space as in WT.

### *Chihuahua vertebrae are thin, highly mineralised and lack an osteoid. LP diet restores the osteoid*

Histological sections of non-demineralised vertebrae in the sagittal plane stained with Von Kossa/Van Gieson show the absence of a detectable osteoid layer (non-mineralised new bone matrix) in the growth zone of the vertebral endplates in *Chi/+* animals (**Figure 5.4 A**). In *Chi/+*$_{LP}$ animals the non-mineralised osteoid layer is restored (**Figure 5.4 A**).

Vertebral body endplate mineralisation was assessed quantitatively based on the extent of the mineralised and non-mineralised bone matrix in whole mount specimens stained with Alizarin red S. In comparison to WT, *Chi/+* mutants show higher mineralisation of the vertebral body endplates (Chi-square test: $p<0.001$), but the LP diet is capable of partially reducing endplate mineralisation in some *Chi/+*$_{LP}$ individuals (Chi-square test: *Chi/+*$_{LP}$ versus *Chi/+*, $p<0.001$; *Chi/+*$_{LP}$ versus WT, non-significant) (**Figure 5.4 B**).

Finally, midline sections of the vertebral column were used to measure the thickness of bone structures in WT, *Chi/+* and *Chi/+*$_{LP}$. Histomorphometry reveals that *Chi/+* and *Chi/+*$_{LP}$ bone structures are significantly thinner compared to WT. This is the case for vertebral body endplates, the central region of the vertebral body and the trabecular bone (**Figure 5.4 C**, **Table 5.2**).

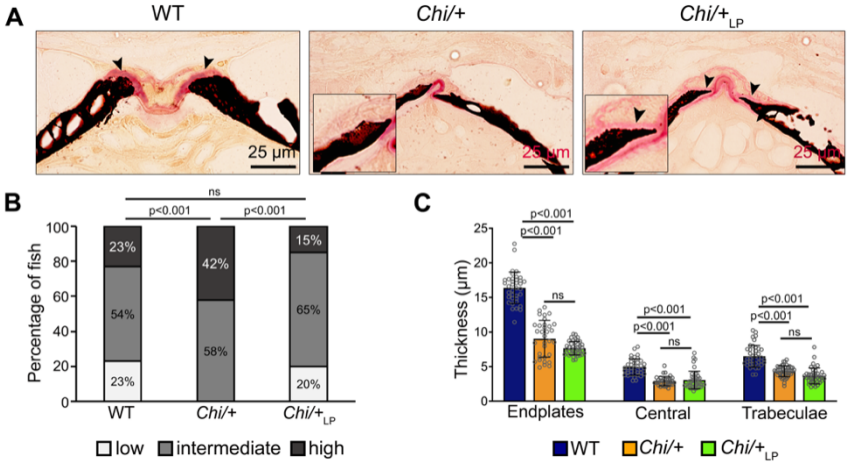


**Figure 5.4.** *Chi/+* vertebral bone structures are thin and highly mineralised. The LP diet restores the osteoid. **A**: Sagittal histological non-demineralised sections stained with Von Kossa/Van Gieson show that three months old *Chi/+* animals, compared to WT animals, have highly mineralised endplates. No osteoid layer can be identified. The osteoid (pink, black arrowheads) is restored in *Chi/+*$_{LP}$. Mineralised bone: black; dense collagen and non-mineralised bone: red. **B**: Quantitative analysis of vertebral body endplate mineralisation (scored as low, intermediate or high) based on whole mount-stained specimens shows that *Chi/+* animals exhibit a higher degree of mineralisation compared to WT animals. The LP diet reduces mineralisation of the vertebral body endplates in some *Chi/+* individuals. The first five caudal vertebral centra in WT (n=15), *Chi/+* (n=13) and *Chi/+*$_{LP}$ (n=12) were analysed. Chi-square test followed by Bonferroni correction, p-values are indicated, ns: non-significant. **C**: Measurements of bone structure thickness at three locations: (i) vertebral endplates, (ii) central region of vertebrae and (iii) trabecular bone (see **Figure 5.3 A** for locations). Compared to WT animals, *Chi/+* and *Chi/+*LP animals have thinner bone structures in all three locations (see also **Table 5.2**). Thickness of bone structures was measured on toluidine blue stained sections in five to 10 vertebral centra in WT (n=4), *Chi/+* (n=4) and *Chi/+*$_{LP}$ (n=5). Mann-Whitney test followed by Bonferroni correction, p-values are indicated, ns: non-significant.

**Table 5.2.** Bone histomorphometry.

| | | Thickness Mean ± SD (∝m) | Pairwise p-values | |
|---|---|---|---|---|
| Vertebral body endplates | WT | 16.39 ± 2.27 | WT - *Chi/+* | $4.6 \pm 10^{-12}$ |
| | *Chi/+* | 9.03 ± 2.66 | WT - *Chi/+*$_{LP}$ | $7.1 \pm 10^{-14}$ |
| | *Chi/+*$_{LP}$ | 7.63 ± 0.98 | *Chi/+* - *Chi/+*$_{LP}$ | ns |
| Vertebral body central region | WT | 4.95 ± 1.19 | WT - *Chi/+* | $3.5 \pm 10^{-10}$ |
| | *Chi/+* | 2.90 ± 0.68 | WT - *Chi/+*$_{LP}$ | $2.3 \pm 10^{-8}$ |
| | *Chi/+*$_{LP}$ | 3.10 ± 1.30 | *Chi/+* - *Chi/+*$_{LP}$ | ns |
| Trabecular bone | WT | 6.50 ± 1.58 | WT - *Chi/+* | $3.5 \pm 10^{-10}$ |
| | *Chi/+* | 4.33 ± 0.78 | WT - *Chi/+*$_{LP}$ | $2.3 \pm 10^{-8}$ |
| | *Chi/+*$_{LP}$ | 3.66 ± 1.14 | *Chi/+* - *Chi/+*$_{LP}$ | ns |

Statistical analysis is based on Mann-Whitney test followed by Bonferroni correction; ns: non-significant.

***Compression fractures and fracture repair in Chihuahua vertebral bodies***

The analysis of whole mount-stained specimens reveals that *Chi/+* and *Chi/+*$_{LP}$ animals have vertebral compression fractures that relate to the anteroposterior compression of vertebral centra (**Figure 5.5**). Compression fractures are absent in WT animals (**Figure 5.5 A**). Different severity levels of compression fractures are observed in both *Chi/+* and *Chi/+*$_{LP}$ individuals (**Figures 5.5 B–D**). Some *Chi/+*$_{LP}$ animals present compression fractures that only affect one vertebral body (**Figure 5.5 B**). Some *Chi/+*$_{LP}$ mutants show kyphosis associated with multiple compression fractures (**Figure 5.5 C**). *Chi/+* mutant fish display severely distorted vertebrae, as described above, and collapsed vertebral centra (**Figure 5.5 D**). Regardless of the inter-individual variability among the fractures, the bone of fracture repair calli appears more dense than other bone elements when visualised with fluorescent light.

Histological sections in the sagittal plane of mutant vertebral columns confirm the presence of compression fractures in *Chi/+* and *Chi/+*$_{LP}$ animals (**Figure 5.6**). A variety of fractured sites suggests that compression factures range from being in a status of repair (as evidenced by bone remodelling, see below) to fractures that do not, or not yet, display evidence of repair. Compression fractures affect the central region of the vertebral bodies. The fractured bone trabeculae become displaced into the chordocyte-filled lumen of the notochord (**Figures 5.6 A,B**). When fractures injure the notochord, the notochord strand and the notochord septum (see **Figure 5.3 A** for the anatomical terms) become condensed (keratinised in response to tissue damage according to Kague et al., 2021) (**Figures 5.6 A,B**). Analysis of serial sections from several *Chi/+* and *Chi/+*$_{LP}$ animals reveals that compression fractures display variable degrees of repair. Fractured sites show fibrocartilaginous calli at the outer surface of the compressed vertebral bodies (**Figure 5.6 C**). Repair evidently continues with replacement of fibrocartilage tissue by a bone callus (**Figure 5.6 D**). Repair at fracture locations is further confirmed by the demonstration of tartrate-resistant acid phosphatase (TRAP). TRAP is produced by osteoclasts and secreted onto the bone surface at the locations of bone resorption. TRAP activity is also linked to the resorption of fibrocartilage that is being replaced by a bone callus (**Figure 5.6 E**) (Witten

et al., 2001). Osteoclast activity is also observed at the bone trabeculae and vertebral endplates of vertebral compression fractures (**Figure 5.6 F**). No signs of fracture repair or bone resorption are detected on bone elements inside the notochord (**Figure 5.6 E**). This agrees with the fact that the notochord contains neither blood vessels, nor nerve fibres and no lymphatic vessels (Witten and Hall, 2021).

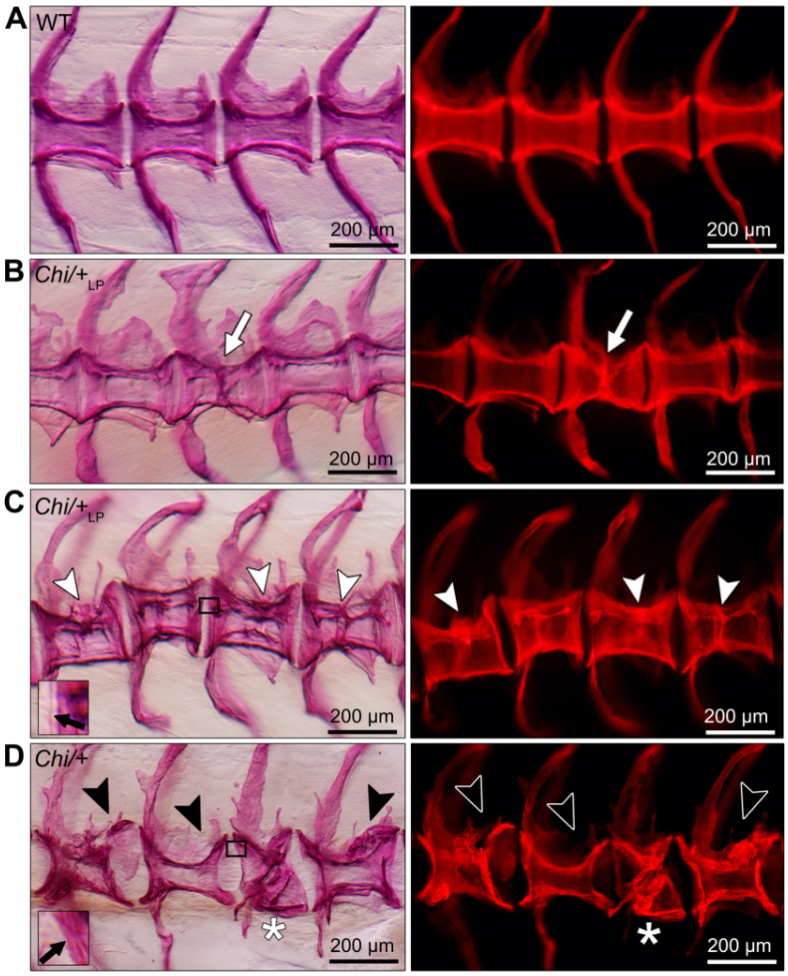


**Figure 5.5.** Different grades of *Chi/+* and *Chi/+*$_{LP}$ compression fractures. Whole mount Alizarin red S stained vertebral bodies of WT (**A**) and mutants (**B-D**) visualised in bright field (left) and with fluorescence (right). Inter-individual variability and different severity levels of compression fractures are observed in three months old mutant zebrafish. Bone calli associated to fractures appear more dense than other bone elements when visualised with fluorescent light. **B**: Example of a mutant *Chi/+*$_{LP}$ showing a compression fracture affecting only one vertebral body, bone

callus is visible (white arrow). **C**: *Chi/+*$_{LP}$ zebrafish displaying kyphosis associated with multiple compression fractures and evident bone calli (white arrowheads). **D**: Mutant *Chi/+* fish displaying severely distorted vertebrae (black arrowheads) and a collapsed vertebral body (white asterisk). The inserts in **C, D** demonstrate the identification of osteoid on whole mount-stained specimens, as identified on WT zebrafish (**A** and **Figure 3.2 B**). Black arrows indicate the presence (**C**) and absence (**D**) of osteoid in *Chi/+*$_{LP}$ and *Chi/+*, respectively.

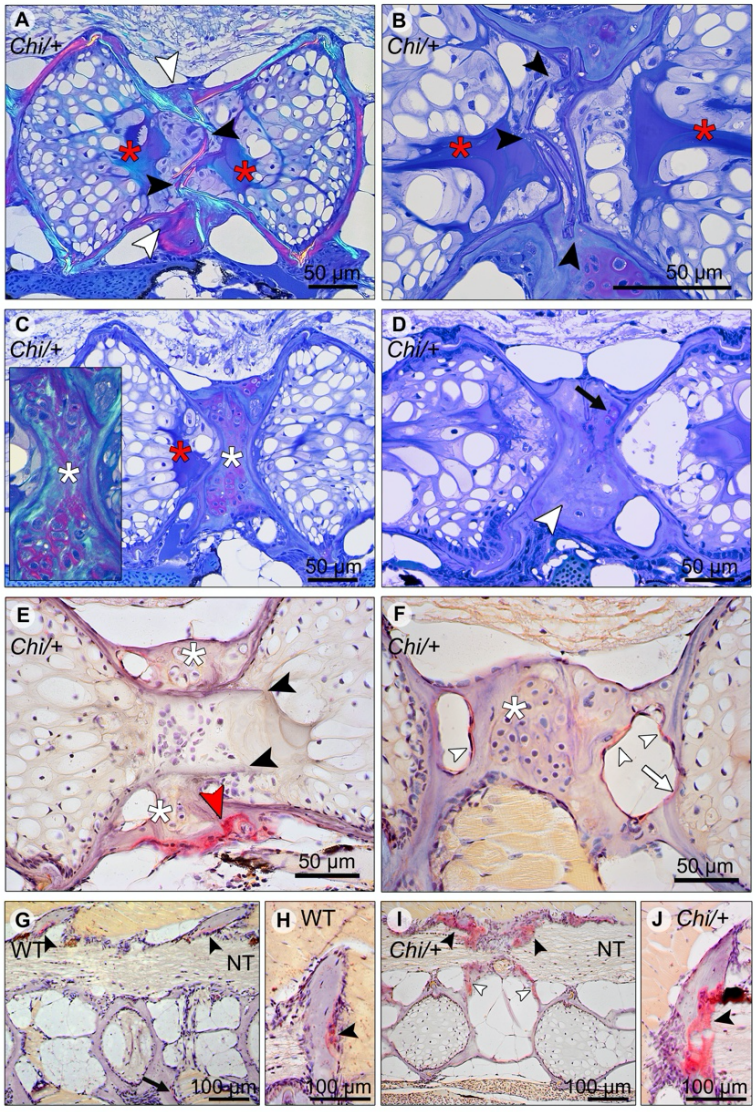


**Figure 5.6.** Compression fractures and bone resorption in *Chi/+* and *Chi/+*$_{LP}$ vertebral bodies. **A**: Toluidine blue stained medio-sagittal section of a compression fracture from three months old mutant zebrafish (representative for both *Chi/+* and *Chi/+*$_{LP}$) observed with polarised light. The

compression fracture is characterised by several fractures in the central region of the vertebral body (black arrowheads); a bone callus is present on the outside of the vertebral centrum (white arrowheads). The fracture also disrupts the notochord tissue and induces condensation of chordocytes into a fibrous tissue (a known reaction of notochord tissue to injuries) (red asterisks). **B**: High magnification of the fractured bone (black arrowheads) inside the notochord. The reaction of the notochord tissue can be seen (red asterisks). **C**: A fibrocartilaginous callus is present around the fractured central part of the vertebral body, the typical appearance for fracture callus at initial stages of repair (white asterisks). Polarised light (insert) shows collagen fibres (green) within the cartilaginous callus. Red asterisk indicates the notochord tissue condensation. **D**: Sagittal section of a healed compression fracture. Fracture repair and remodelling processes replaced the fibrocartilaginous tissue by a bone callus (white arrowhead). Remnants of the fibrocartilaginous tissue are visible (black arrow). **E**: Tartrate-resistant acid phosphatase (TRAP) staining confirms compression fracture repair. TRAP activity (red staining, red arrowhead) indicates resorption of the fibrous tissue (white asterisks) that is being replaced by a hard bone callus. The fractured bone fragments (black arrowheads) in the lumen of the notochord do not show resorption, which is consistent with the absence of blood vessels, lymphatic vessels and innervation inside the notochord. **F**: TRAP activity is detected also in the trabecular bone (white arrowheads) and vertebral endplate (white arrow) of a vertebra showing a compression fracture in mutant zebrafish (representative for both *Chi/+* and *Chi/+*$_{LP}$). White asterisk indicates the fibrocartilaginous callus. **G,H**: WT display TRAP activity (red) at sites of bone remodelling linked to bone growth, i.e. the endosteal surfaces of the neural (black arrowheads) and haemal arches (black arrow). NT, neural tube. **I,J**: *Chi/+* animals (representative also for *Chi/+*$_{LP}$) show TRAP activity at the same locations as in WT, however mutants exhibit expanded TRAP activity at all endosteal and periosteal bone surfaces, i.e. arches (black arrowheads) and bone trabeculae connecting the endplates (white arrowheads). NT, neural tube.

***Chihuahua mutants have increased bone resorption***

Osteoclasts and locations of bone resorption (other than locations of fracture repair) in growing juvenile individuals were identified by the demonstration of TRAP. In WT zebrafish, TRAP activity is typically restricted to locations within the vertebral column that require resorption for allometric growth (Witten et al., 2001), i.e. the endosteal surfaces of enlarging neural and haemal arches (**Figure 5.6 G,H**). *Chi/+* and *Chi/+*$_{LP}$ also display TRAP staining at the endosteal surfaces of the neural and haemal arches, but the enzymatic activity is increased and extends also to other bone structures such as the bone trabeculae (**Figure 5.6 I,J**).

Transmission electron microscopy (TEM) confirms the presence of osteoclasts, attached to the endosteal surfaces of arches in WT, *Chi/+* and *Chi/+*$_{LP}$ (**Figure 5.7 A**). These cells, while attached to the bone surface, reside in resorption lacunae (as shown in **Figure 5.7 A**, WT zebrafish). Actively resorbing osteoclasts exhibit a typical “ruffled border”, an electron-dense cytoplasm with abundant cytoplasmic vacuoles and

resorption vesicles in proximity of the ruffled border (as shown in **Figure 5.7 A**, *Chi/+* zebrafish).

***Chihuahua mutants show signs of ER stress and altered collagen type I***

The ultrastructure of bone cells and bone matrix in the vertebral column was analysed by TEM at the level of the medio-sagittal plane. Ultrathin sections of representative specimens show that *Chi/+* and *Chi/+*$_{LP}$ have enlarged endoplasmic reticulum (ER) cisternae in osteoblasts located in the growth zone of the vertebral body endplates (**Figure 5.7 B**, see **Figure 5.3 A** for location). Likewise, ER cisternae in osteoblasts along the neural and haemal arches are enlarged. High magnification images show that *Chi/+* ER cisternae are filled with protein (**Figure 5.7 C**). Conversely, WT osteoblasts have numerous, yet not enlarged ER cisternae, indicative for high protein synthesis activity at the growth zone of the endplates (**Figure 5.7 B**).

The collagen matrix appears altered in the *Chi/+* mutants compared to WT. In WT, newly secreted collagen fibrils in the proximity of the osteoblasts (osteoid) are dispersed prior to maturation and assemble into larger fibres at a distance from the osteoblasts. In contrast, the *Chi/+* bone matrix is characterised by densely packed collagen fibrils in the vicinity of the osteoblasts (**Figure 5.7 C**). In *Chi/+*$_{LP}$, individual collagen fibrils are partly distinguishable in close proximity of the osteoblasts, indicative for less collagen packing and a more typical osteoid (**Figure 5.7 C**).

Longitudinal sections of collagen fibres in WT zebrafish show a regular D-periodicity. The pattern is absent in *Chi/+* mutants. In *Chi/+*$_{LP}$ the collagen D-periodicity is partially visible along the fibre (**Figure 5.7 D**).

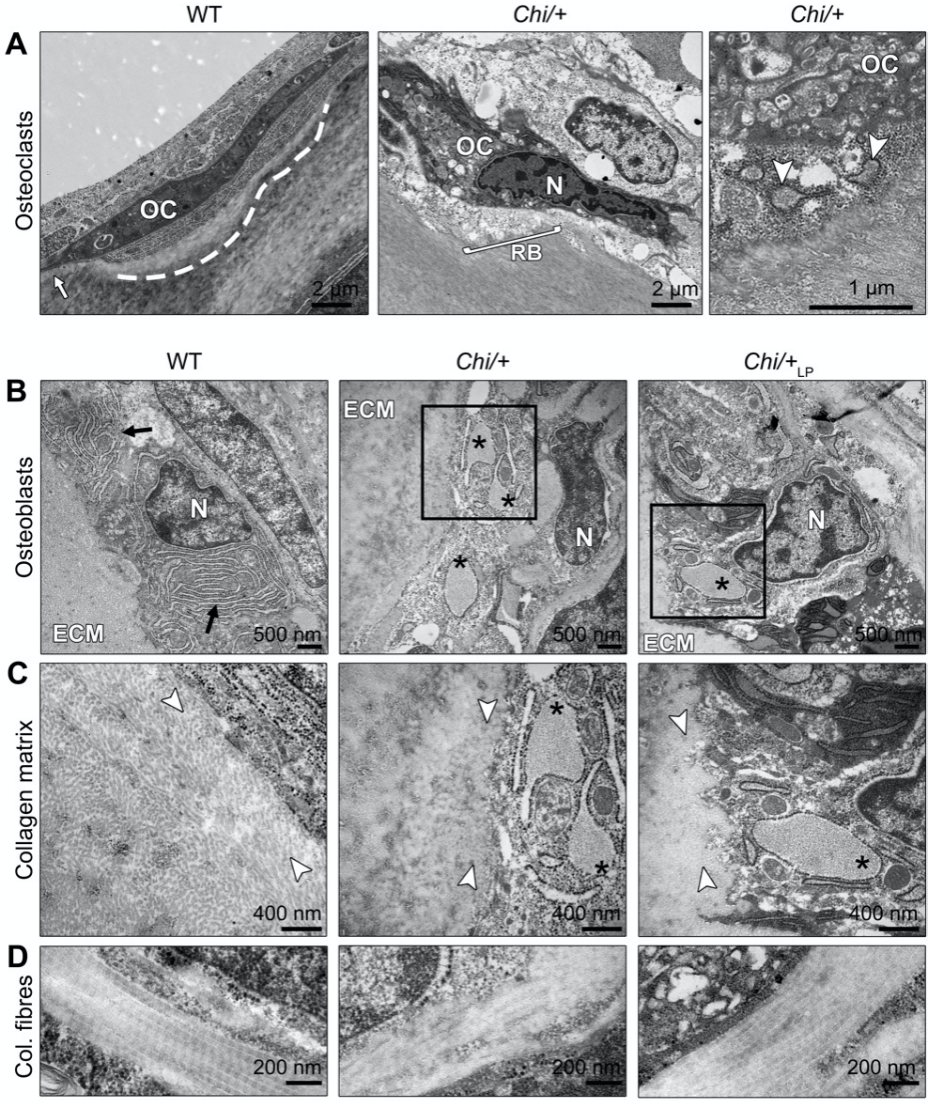


**Figure 5.7.** Ultrastructure of bone cells and bone matrix in *Chi/+* and *Chi/+*$_{LP}$ animals. **A**: Transmission electron microscopy (TEM) of osteoclasts (OC) located at the arch surface of three months old WT and *Chi/+* (representative for both *Chi/+* and *Chi/+*$_{LP}$) vertebrae. The panel WT shows a typical flat-shaped teleost osteoclast (OC) characterised by its electrodense cytoplasm. The cell resides in a shallow resorption lacuna (dashed line), yet is attached to the bone surface (white arrow). The panel *Chi/+* shows an osteoclast that resorbs the bone matrix and exhibits the typical "ruffled border" (RB), an electron-dense cytoplasm with abundant cytoplasmic vacuoles and resorption vesicles (right panel, white arrowheads) in proximity of the ruffled border. N, nucleus. **B**: TEM of WT, *Chi/+* and *Chi/+*$_{LP}$ shows mutant osteoblasts with enlarged endoplasmic reticulum (ER) cisternae (asterisks). The osteoblasts are located in the growth zone of the vertebral body endplate (see **Figure 5.3 A** for location). Higher magnification images in **C** show

that *Chi/+* osteoblast ER cisternae are filled with protein, likely mutated collagen type I. WT osteoblasts have numerous, yet not enlarged ER cisternae (arrows). ECM: extracellular matrix of the bone surface; N: nucleus. **C**: The newly secreted collagen fibrils (white arrowheads) in the proximity of the osteoblasts in WT are visibly separated prior to maturation and assemblage into collagen fibres. In contrast, the *Chi/+* animal has densely packed collagen fibrils. No space can be recognised between the fibrils. In the *Chi/+*$_{LP}$ individual collagen fibres are densely packed and space between the fibrils is distinguishable in proximity to the osteoblasts. **D**: Longitudinal sections of collagen fibres show a regular D-periodicity pattern in a WT animal, absence D-period pattern in a *Chi/+* mutant, and a less regular D-periodicity pattern a *Chi/+*$_{LP}$ specimen.

# Discussion

### *Chihuahua zebrafish suffer from vertebral column deformities, low dietary P partially rescues the bone phenotype*

Early reports on children and young patients diagnosed with OI described severe vertebral column deformities as the major complications of the disease. From very young age onwards, patients suffer from vertebral body deformities associated with progressive scoliosis, kyphosis or kyphoscoliosis (Sillence et al., 1979; Benson and Newman, 1981; Shah and Wallace, 2020). This condition is known to be age-dependent and usually worsens after the age of six (Benson et al., 1978; Benson and Newman, 1981). Likewise, *Chi/+* zebrafish display severe bending of the vertebral column, i.e. kyphosis and lordosis, at three months of age, as demonstrated by whole mount Alizarin red S staining and histological sections. Similar to human patients, such malformations progressively worsen in adult stages (Gioia et al., 2017; Fiedler et al., 2018). Vertebral body deformities, vertebral compressions and fractures represent other severe complications of young patients (Benson and Newman, 1981; Shah and Wallace, 2020). We show here for the first time that juvenile *Chi/+* zebrafish suffer from vertebral body compressions in both the abdominal and caudal region of the vertebral column. Mutant vertebral bodies are distorted and characterised by increased shape variation compared to WT, as revealed by geometric morphometrics. On top of that, *Chi/+* fish have highly mineralised vertebral body bone structures with no detectable osteoid (non-mineralised collagenous bone matrix), as confirmed by histology of non-demineralised specimens. Likewise, the osteoid thickness is reduced in the bone of human patients (Stöß et al., 1986; Iwamoto et al., 2002) and murine OI models (Kalajzic et al., 2002; Uveges et al., 2008). Moreover, hypermineralisation and bone brittleness are well documented in human patients (Sillence et al., 1979; Benson and Newman, 1981; Zeitlin et al., 2003; Shah and Wallace, 2020), OI mouse models (Enderli et al., 2016) and OI zebrafish models (Fiedler et al., 2018; Tonelli et al., 2020b). Excess bone mineralisation related to increased dietary P intake or ageing is known to increase vertebral column malformations in WT zebrafish (Cotti et al., 2020; Kague et

al., 2021). Hence, hypermineralisation alone can be considered a risk factor for bone deformities. In addition, OI bone is characterised by mutated collagen type I, which contributes to bone fragility. While mutations cannot be undone in OI patients or animal models, lowering the bone mineral content could possibly alleviate their skeletal defects. Recent findings on teleosts including WT zebrafish (Cotti et al., 2020) and Atlantic salmon (Witten et al., 2016, 2019; Drábiková et al., 2021) have shown that low dietary P administration reduces the bone mineral content and promotes the formation of non-mineralised bone without causing vertebral column malformations. To assess the effects of reduced dietary P intake on the mutant bone phenotype, *Chi/+* were fed a low P diet (LP) from one month of age. *Chi/+* zebrafish under LP conditions (*Chi/+*$_{LP}$) have reduced incidence of kyphosis and lordosis of the abdominal region of the vertebral column, and reduced shape variation of the caudal vertebral bodies. The reduced P intake restores the shape of vertebral bodies to a condition more similar to WT vertebral bodies. Moreover, the LP diet is shown to reduce the mineralisation of vertebral body endplates in some treated *Chi/+* fish and to restore the osteoid layer, that is absent in untreated mutants. It is known that the presence of an osteoid (non-mineralised matrix) has a beneficial effect on the mechanical properties of bone. The collagenous bone matrix itself is a very tough material that can withstand extreme mechanical forces and bend without fracturing. Examples for tough low mineralised bones that do not fracture are deer antlers and the bones of human infants (Currey, 2003), but also teleosts under reduced P intake show tough and deformable vertebral bodies with no signs of fractures (Witten et al., 2019; Cotti et al., 2020; Drábiková et al., 2021). In contrast, high dietary P causes excess mineralisation and higher bone stiffness in teleosts (Witten et al., 2019; Cotti et al., 2020; Drábiková et al., 2021), and results in reduced bone formation in humans (Kemi et al., 2006; Dermience et al., 2015) and reduced ultimate strength (maximal load) in rats (Huttunen et al., 2007). Our findings suggest that the mineral content of *Chi/+* bone likely was reduced by the LP diet, which could explain the reduced incidence of vertebral column deformities and the restored shape of the vertebral bodies.

***Chihuahua vertebrae have thin bone structures and are subjected to compression fractures***

One of the most severe complications in OI patients are multiple compression fractures with collapse of the vertebral bodies (Benson and Newman, 1981; Shah and Wallace, 2020). Our findings show that *Chi/+* zebrafish suffer from the same type of complications. Several compression fractures were identified on whole mount specimens and on histological sections. Which are the factors predicted to contribute to compression fractures? The first possible factor for compression fractures is the poor quality of OI bone, caused by mutated collagen production and excess mineralisation. As discussed above, overmineralised bone fractures easily; both patients and *Chi/+* zebrafish suffer from bone brittleness (Zeitlin et al., 2003; Fiedler et al., 2018). The second potential cause is reduced bone mass. Histological assessment of human biopsies showed that patients including children have thinner cortical bone and a reduced number of trabeculae in trabecular bone (Benson and Newman, 1981; Zeitlin et al., 2003). Likewise, two OI mice models (Kalajzic et al., 2002; Uveges et al., 2008) and *Chi/+* zebrafish have thinner bone elements compared to WT, thin vertebral body endplates, thin bone elements in the vertebral body central region and thin bone trabeculae. Thus, hypermineralised vertebral bodies with poor trabecular bone are at mechanical disadvantage and are easily subjected to compression fractures (Zeitlin et al., 2003). Bone with low mass and excess of minerals cannot easily withstand mechanical forces exerted along the axial skeleton. The third potential factor contributing to compression fractures is the weakness of the spinal ligaments and intervertebral discs. Early reports described that OI patients lack vertebral stability because of the laxity of the spinal ligaments (Sillence et al., 1979; Benson and Newman, 1981) and intervertebral discs (Brailsford, 1943; Watanabe et al., 2007). Similarly, the $Col1a^{Jrt}/+$ OI mouse model shows reduced cervical intervertebral space (Abdelaziz et al., 2015). Likewise, *Chi/+* zebrafish show evidence of weak intervertebral ligaments. Although on histological sections the ligaments of *Chi/+* fish display all the structural elements as in WT animals, *Chi/+* vertebral endplates are often shifted against each other along the dorsal-ventral axis. In humans weak ligaments fail to provide sufficient

support to the vertebral column and allow the progressive degeneration of the deformity into a compression fracture (Benson and Newman, 1981). It can be assumed that less severe complications appear first and subsequently progress into a severe compression fracture. To support this hypothesis, patients show microfractures of the vertebral body growth plates (McKusick, 1972; Benson and Newman, 1981). During growth in humans, vertebral growth plate microfractures can progress into complicated lesions such as compression fractures (Ishikawa et al., 1996; Shah and Wallace, 2020).

Human OI patients show evidence of fracture repair, but often fractures heal with deformities (McGreal and Bober, 2020). We show similar findings in *Chi/+* zebrafish. Compression fractures in *Chi/+* are also subjected to fracture repair but the vertebral bodies remain deformed. Analysis of histological sections from different specimens suggests the identification of fractures in different stages of repair and allows for the tentative reconstruction of the steps involved in vertebral fracture healing. Like in mammals, *Chi/+* zebrafish fractures are initially stabilised by the formation of fibrocartilaginous calli, that subsequently become ossified. Despite the observation of fractures in different stages of repair, the design of our study does not allow to generate a timeline of fracture repair. In the goldfish (*Carassius auratus*), a cyprinid species like zebrafish, a bone fracture callus takes about 35 days to replace the fibrocartilaginous template (Moss, 1962). Thus, the presence of bone calli in compressed vertebral bodies of three months old *Chi/+* indicates that mutants likely developed vertebral compression fractures before the start of the experiment. This could explain why both *Chi/+* treated with the LP diet and untreated mutants show compression fractures. Compression fractures are therefore one of the most important complications during the initial stages of the disease, both in zebrafish and children affected by OI, and are crucial in the quick progression of the OI phenotype.

***Chihuahua zebrafish have increased bone resorption and reduced bone formation, but the LP diet improves the bone matrix***

Bone from individuals with dominant OI is characterised by an increased bone turnover rate and an increased number of osteoclasts, associated to an increased eroded surface compared to controls (Baron et al., 1983; Rauch et al., 2000; Fedarko, 2014). Analogous findings derive from studies on two OI mouse models, the Oim (Kalajzic et al., 2002) and Brtl (Uveges et al., 2008) mice. Likewise, *Chi/+* zebrafish exhibit increased osteoclastic activity, as demonstrated by TRAP staining on histological sections. Resorption activity is increased at the endosteal surfaces of the neural and haemal arches compared to WT animals. TRAP activity extends also to other bone structures that are not subjected to resorption in WT zebrafish, such as the vertebral body endplates and the bone trabeculae that connect the vertebral body endplates (Witten and Huysseune, 2009). Trabecular bone surfaces display high osteoclast activity also in the Oim and Brtl mice (Kalajzic et al., 2002; Uveges et al., 2008). The bone in zebrafish can be remodelled by multinucleated osteoclasts, but different from mammals, thin bony elements are typically resorbed by mononucleated cells (Witten et al., 2001). Flat, elongated mononucleated osteoclasts occur at endosteal surfaces, for example of neural and haemal arches (Witten et al., 2001; Witten and Huysseune, 2009), as also observed in WT specimens in this study. Bone resorption in zebrafish is primarily related to the demands of allometric growth. The common type of mononucleated osteoclasts does not create deep resorption lacunae (Witten et al., 2001). TEM from *Chi/+* specimens showed osteoclasts with abundant electrondense cytoplasm characterised by several cytoplasmic vacuoles. These cells exhibit the typical ruffled border, indicative for active resorption of the bone matrix. Also osteoclasts in bone from the Oim mouse exhibited cellular changes. Oim cells have a larger diameter and exhibit three times the number of nuclei compared to osteoclasts in WT mice (Zhang et al., 2007). The abundant cytoplasmic vacuoles of osteoclasts and the larger amount of TRAP-positive bone surfaces are indicative for increased resorptive activity in OI bone, both in *Chi/+* zebrafish and mouse models (Zhang et al., 2007; Uveges et al., 2008). While endosteal bone resorption is increased in human OI patients, osteoblasts

produce less new bone, which results in a reduced osteoid thickness, as discussed above. The decrease in bone formation in human patients, reviewed by Fedarko (2014), is consistent with data from the Oim and Brtl mouse models (Kalajzic et al., 2002; Uveges et al., 2008). *In vitro* studies have shown that osteoblasts from human patients (reviewed by Fedarko, 2014) and murine models (Garibaldi et al., 2021) show decreased synthesis, processing and matrix incorporation of collagen compared to controls. The production of mutated collagen type I in OI osteoblasts results in delayed collagen folding and excess post-translational modifications, that cause intracellular retention of defective collagen and endoplasmic reticulum (ER) stress (Ishikawa and Bächinger, 2013). At an ultrastructural level, *Chi/+* zebrafish have osteoblasts in the vertebral growth zone with enlarged ER cisternae. Similar findings were previously described on osteoblasts from the caudal fin of adult *Chi/+* (Gioia et al., 2017). Here we show that ER cisternae in *Chi/+* osteoblasts are filled with protein, likely mutated collagen type I. Intracellular collagen retention leads to collagen over modification and impairs collagen secretion in *Chi/+* (Gioia et al., 2017) and in OI models (Garibaldi et al., 2021). The extracellular collagen matrix is also impaired. In close proximity of the osteoblasts, the collagen fibrils in *Chi/+* fish are densely packed and lack the typical pattern of the osteoid collagen where the fibrils have a low density and are loosely arranged (Bonucci, 2007). In contrast, in *Chi/+* the fibrils in the bone matrix have a high degree of compactness that is typical of fully mineralised bone (Bonucci, 2007). These findings correlate well with the lack of osteoid seams in *Chi/+* and OI bone in general. It is widely accepted that insufficient osteoblast performance is at the basis of the severe OI phenotype. Thus, recent studies have targeted OI osteoblasts to relieve ER stress and improve cellular functions. The treatment with 4-phenylbutyrate, a chemical chaperone already approved by the FDA for urea cycle disorders, stimulates collagen secretion in murine OI osteoblasts *in vitro* (Garibaldi et al., 2021), and improves the OI bone phenotype *in vivo* (Gioia et al., 2017). In the present study, we show that two months of reduced dietary P administration partially rescue the OI phenotype in *Chi/+*. Mutants which received the LP diet show improved extracellular matrix with less dense collagen fibrils, indicative for a more typical osteoid. This finding together with the

reduced incidence of vertebral column deformities and the rescue of the vertebral body shape, suggests that a reduced dietary P intake can alleviate the severe bone phenotype in juvenile *Chi/+* zebrafish.

## Materials and methods

### *Zebrafish maintenance and ethical statement*

Wild type (WT) AB and heterozygous *Chihuahua* (*col1a1a*$^{dc124/+}$, *Chi/+*) zebrafish were bred in-house. The mutant *Chi/+* carries a heterozygous c.2207G>A mutation in *col1a1a* causing a p.G736D (G574D) substitution in the α1 chain of collagen type I (Fisher et al., 2003). Zebrafish embryos were kept in petri dishes in fish water (1.2 mM $NaHCO_3$, 0.01% instant ocean, 1.4 mM $CaSO_4$, 0.0002% methylene blue) at 28°C until 7 days post-fertilisation (dpf), then housed in ZebTEC semi-closed recirculation housing systems (Techniplast, Buguggiate, Italy) at 28°C, pH 7.5 and conductivity 500 µS on a 14/10 light/dark cycle. Zebrafish from 7 to 21 dpf were fed three times a day alternating commercial dry food (ZM000, Zebrafish Management Ltd., Winchester, UK) and brine shrimp (Artemia cysts, Zebrafish Management Ltd., Winchester, UK). Fish were then fed for another week three times a day with a dry regular P diet (Cotti et al., 2020; see also below), until 28 dpf, to adjust them to this type of dry feed. Starting from 28 dpf, WT were fed three times a day with a regular P diet for two months. At 28 dpf, *Chi/+* were randomly divided in two groups and fed three times a day with a "LP diet" (low P content) or a regular P diet for two months (see below for details). Specimens were collected after two months of dietary treatment, euthanised by tricaine (3-amino benzoic acidethylester) overdose (0.3%) and fixed for further analyses as described below. The experiments were conducted in the centralised animal facility of the University of Pavia (Pavia, Italy). All animal studies were conducted in agreement with EU Directive 2010/63/EU for animals. The experimental protocol was approved by the Italian Ministry of Health (Approval animal protocol No. 260/2020-PR, 26 March 2020).

### *Diet composition*

Diet composition and nutritional experiment are described in detail in Cotti et al. (2020). Briefly, the diets were formulated to have a total P content of 0.5% and

1.0%, termed low P (LP) diet and regular P diet, respectively (**Table 5.3**). Monoammonium phosphate ($NH_4H_2PO_4$, MAP) was used as dietary inorganic P supplement (Morales et al., 2018). In order to keep all diets equal in nutrients, except for P concentration, MAP replaced the inert filler diatomaceous earth (Diamol, Imerys, Denmark). The diets were formulated by SimplyFish AS (Stavanger, Norway, www.simplyfish. no) and produced by extrusion with subsequent crumbling to a suitable particle size by the Danish Technological Institute (Taastrup, Denmark, https://www.dti.dk). The P content of the product was verified at the University of Hohenheim (Stuttgart, Germany, https:// www.uni-hohenheim.de) and determined with 5.04 g/kg diet and 9.84 g/kg diet for the low P and regular P diet, respectively (**Table 5.3**).

**Table 5.3.** Ingredients and chemical composition of the diets for zebrafish.

| Ingredients (%) | Low P diet | Regular P diet |
|---|---|---|
| Rapeseed lecitin (Bergathin) | 2.00 | 2.00 |
| Krill meal | 3.00 | 3.00 |
| Wheat starch | 18.77 | 18.77 |
| Corn gluten meal | 8.0 | 8.0 |
| Wheat gluten meal | 19.01 | 19.01 |
| Soy protein concentrate | 31.00 | 31.00 |
| Capelin fish meal | 5.00 | 5.00 |
| Rapeseed oil | 1.58 | 1.58 |
| Peruvian fishoil | 2.60 | 2.60 |
| DL-Methionine | 0.60 | 0.60 |
| Biolys 54.6% | 2.00 | 2.00 |
| Lutavit C Aquastab 35% | 0.10 | 0.10 |
| Vitamin mix | 0.50 | 0.50 |
| Choline chloride 50% | 1.50 | 1.50 |
| Trace mineral mix (P free) | 0.30 | 0.30 |
| Monoammonium phosphate 26% | 0.00 | 1.95 |
| Diamol (diatomaceous earth) | 4.00 | 2.05 |
| Astaxanthin 10% | 0.07 | 0.07 |
| Total | 100.00 | 100.00 |
| **Chemical composition (g/kg)** | | |
| Crude protein | 497 | 508 |
| Crude lipids | 97 | 97 |
| Crude ash | 84 | 73 |
| Calcium | 4.84 | 4.79 |
| Magnesium | 1.96 | 1.98 |
| Phosphorus | 5.04 | 9.84 |

***X-rays***

X-rays of WT, *Chi/+* and *Chi/+* under LP diet were acquired with a Faxitron Mx-20 (Faxitron, Tucson, Arizona, USA) using 25 kV for 10 sec. The Kodak DirectView Elite

CR System and k-Pacs software (Kodak, Rochester, New York, USA) were used for image digitalisation.

***Whole mount skeletal staining***

WT (n=26), *Chi/+* (n=20) and *Chi/+*$_{LP}$ (n=18) were fixed for 24 h in 4% paraformaldehyde (PFA) in 1× phosphate-buffered saline (PBS) at 4°C and were stained with Alizarin red S according to an established protocol (Taylor and Van Dyke, 1985). Fish were analysed and imaged using an Axio Zoom V16 stereomicroscope (Carl Zeiss, Oberkochen, Germany) with oblique illumination equipped with a 5MP CCD camera. Classification of the deformities was performed on whole mount-stained WT and mutants as defined by Martini et al. (2020). Only the abdominal and caudal region of the vertebral column were analysed. The maximal curvature indices related to the abdominal and the caudal region of the vertebral column were calculated according to the method described by Marie-Hardy et al. (2019). Briefly, the maximal kyphotic and lordotic indices were calculated in the sagittal plane of Alizarin red S stained specimens as the ratio (a/b) between the perpendicular distance from the axis in correspondence of the maximal curvature (segment "a" in **Figure 5.1 A**) and the standard length (described as the distance from the anterior most tip of the upper jaw to the posterior edge of the caudal peduncle where caudal fin rays insert (Parichy et al., 2009), segment "b" in **Figure 5.1 A**). The same method but in the coronal plane was used to calculate the maximal scoliotic index. Moreover, for each group, the following general metrics were calculated according to Martini et al. (2020): the frequency (%) of specimens with at least one malformation, the total number of malformations identified, the average malformation load (total number of malformations diagnosed in a group/number of malformed individuals per group).

Lateral images of stained fish were used to quantitatively analyse mineralisation levels of vertebral endplates of WT, *Chi/+* and *Chi/+*$_{LP}$ as described in Cotti et al. (2020). The first five caudal vertebral bodies (definition according to Bird and Mabee, 2003) were considered for analysis in all specimens, following the established protocol (Cotti et al., 2020). Briefly, the non- mineralised endplate was

expressed as a percentage of the total non-mineralised endplate length over the total vertebral length. Vertebral endplates with a non-mineralised percentage value greater than 10% were classified as low mineralised, between 3% and 10% as intermediate mineralised, and less than 3% were considered high mineralised.

***Geometric morphometrics of vertebral centra***

Lateral images of whole mount Alizarin red S stained specimens were used to quantify the shape variation of the first 10 caudal vertebral centra (definition according to Bird and Mabee, 2003) in WT (n=15), *Chi/+* (n=13) and *Chi/+*$_{LP}$ (n=12) by means of landmark-based geometric morphometrics. The landmarks, defined as biologically homologous anatomical loci recognisable on all specimens in the study (Webster and Sheets, 2010), were selected on the vertebral centra as represented in **Figure 5.2 A**: landmarks number 1, 5, 6 and 10 on the vertebral endplates; landmarks number 2, 4, 7 and 9 on the anterior and posterior cone of the centrum; landmarks number 3 and 8 in the central region of the centrum. A similar configuration of landmarks has been applied in a vertebral fracture assessment study in human patients (Jager et al., 2010). 2D landmarks were extracted from digital images using Fiji (NIH, Bethesda, Maryland, USA) and digitised in the same order for all vertebral centra analysed. Procrustes superimposition of digitised landmarks and visualisation of shape variations were performed using Past4.04 software (Hammer et al., 2001). Principal component analysis was performed using PCAGen8 software as described in (Webster and Sheets, 2010).

***Histology and bone histomorphometry***

WT (n=4), *Chi/+* (n=4) and *Chi/+*$_{LP}$ (n=5) were fixed for 24 h in 2.5% PFA, 1.5% glutaraldehyde, 0.1 M sodium cacodylate buffer (pH 7.4) and 0.001% $CaCl_2$ at 4°C, decalcified in 0.1 M EDTA for 14 days at 4°C and embedded in glycol methacrylate (Witten et al., 2001). Sagittal 2 µm sections were cut on a Microm HM360 (Marshall Scientific, Hampton, New Hampshire, USA) automated microtome and were stained

with toluidine blue (0.5% toluidine blue, 1% $Na_2B_4O_7$ in demineralised $H_2O$ ($dH_2O$), pH 9) for 15 sec, rinsed in $dH_2O$ and mounted with DPX. Images were acquired using an Axio Imager-Z1 microscope (Carl Zeiss, Oberkochen, Germany) equipped with an Axiocam 503 colour camera (Carl Zeiss, Oberkochen, Germany). Bone structure histomorphometry was analysed on images of toluidine blue stained sections of the middle plane of the vertebral column. Thickness of bone structures in the endplates, in the central region and in the trabeculae of five to 10 vertebral centra per specimen were measured using Fiji (NIH, Bethesda, Maryland, USA) (see **Figure 5.3 A** for location). The mean values were considered for analysis.

For mineral detection on histological sections, WT and mutant zebrafish were selected based on X-rays to be representative for the phenotype. WT (n=1), *Chi/+* (n=1) and *Chi/+*$_{LP}$ (n=1) were fixed as described above and embedded in glycol methacrylate without carrying out decalcification. Sections of 2 µm were stained according to the Von Kossa/Van Gieson protocol (Humason et al., 1997). Images were acquired using an Axio Imager-Z1 microscope (Carl Zeiss, Oberkochen, Germany) equipped with a 5MP CCD camera.

***Transmission electron microscopy***

WT (n=1), *Chi/+* (n=1) and *Chi/+*$_{LP}$ (n=1) were selected based on X-rays to be representative for the phenotype, fixed and decalcified as described above for histology, and embedded in epon epoxy medium (Spurr, 1969). Semi-thin 1 µm sagittal sections were cut on a Microm HM360 microtome (Marshall Scientific, Hampton, New Hampshire, USA), stained with toluidine blue at pH 9 for 2 min, rinsed with $dH_2O$ and mounted with DPX. For TEM analysis, ultrathin sections (about 70 nm) of the middle plane of the vertebral column were prepared on an UltracutE ultramicrotome (Reichert-Jung, Buffalo, New York, USA), contrasted with uranyl acetate and lead citrate and analysed with a Jeol JEM 1010 transmission electron microscope (Jeol Ltd., Tokyo, Japan) operating at 60 kV. Microphotographs were taken with a Veleta camera (Emsis, Muenster, Germany).

***Enzyme histochemistry***

WT (n=2), *Chi/+* (n=2) and *Chi/+*$_{LP}$ (n=2) were fixed in 4% PFA in 1× PBS, pH 7.4, for 1 h at RT and decalcified in 4% PFA, 10% EDTA, pH 7.4 for 14 days at 4°C. Specimens were embedded in glycol methacrylate (Witten et al., 2001). Sagittal 5 ∝m sections were cut on a Microm HM360 (Marshall Scientific, Hampton, New Hampshire, USA) automated microtome and demonstration of tartrate-resistant acid phosphatase (TRAP) was adapted from Witten et al. (2001). Briefly, sections were pre-incubated at 37°C for 45 min in 50 mL acetate buffer (0.1 M sodium acetate, 50 mM L(+) di-sodium tartrate dehydrate, pH adjusted to 5.5 with acetic acid) to which is added 0.5 mL of enzyme substrate solution (2% Naphtol AS TR phosphate dissolved in ethylene glycol mono-butyl ether). Shortly before use, 1 mL of pararosaniline solution (4% pararosaniline chloride (CI. 42500) in 7% HCl solution) was mixed to 1 mL of fresh 5% sodium nitrite and, after hexazotiation, was added to the acetate-enzyme substrate solution. Enzymatic reaction took place in 30-60 min at 37°C. Subsequently, slides were rinsed in $dH_2O$, counterstained with Meyers haematoxylin for 10 min, rinsed in running tap water for 10 min, flushed in $dH_2O$, dried at 40°C and mounted with DPX.

***Statistical analysis***

Quantitative variables are expressed as mean ± standard deviation, categories are expressed as percentages. Statistical analysis was performed using Past4.04 software (Hammer et al., 2001). Differences in the occurrence of vertebral column deformities and in bone mineralisation levels were evaluated by means of Chi-square test followed by Bonferroni correction. Comparison of the maximal curvature indices was based on the non-parametric Mann- Whitney test. Differences in the thickness of bone structures were evaluated by means of Mann-Whitney non-parametric test followed by Bonferroni correction. For principal component analysis of geometric morphometrics data, significant differences in principal component 1 and principal component 2 were obtained using PCAGen8 software as described in (Webster and

Sheets, 2010) using Chi-square test (paired tests, WT-*Chi/+* and WT-*Chi/+*$_{LP}$). A p-value less than 0.05 was considered significant.

# Chapter 6

## Different responses to a low phosphorus diet reveal fundamental differences in zebrafish dental tissues

This chapter is a manuscript in preparation:

Silvia Cotti, Ann Huysseune, Claudia Di Biagio, Daria Larionova, Wolfgang Koppe, Imke A. K. Fiedler, Björn Busse, Martin Rücklin, Federica Marone, Antonella Forlino and P. Eckhard Witten. Different responses to a low phosphorus diet reveal fundamental differences in zebrafish dental tissues. *In preparation to submission to Journal of Dental Research*

## Introduction

As in all gnathostomes, teleost teeth are composed of a dentin cone, covered by a hypermineralised cap and akylosed to the underlying bone (Peyer, 1968; Berkovitz and Shellis, 2016). Two types of hypermineralised, eventually protein free, caps that cover teeth are distinguished. In most tetrapods, the hypermineralised cap is designated as enamel. Enamel initially contains non-collagenous proteins that are secreted by the ameloblasts. Ameloblasts form the enamel organ which is part of the inner dental epithelium. In teleosts, the hypermineralised layer is designated as enameloid (Diekwisch et al., 2002). Enameloid distinguishes itself from enamel in that initial stages also contain collagen type I. Collagen type I is traditionally viewed to be produced by the odontoblasts (Sasagawa et al., 2006, 2009), but it has ben shown in the ameloblasts of Atlantic salmon (Huysseune et al., 2008). Enameloid is formed centripetally and completed before dentin matrix starts to be deposited. Its mineral fraction consists of calcium phosphate, in the form of apatite crystals, as in enamel (Smith, 1995). Eventually enamel and enameloid become hypermineralised through the removal of the proteins from the matrix by the ameloblasts, being collagen or non-collagenous proteins. Ameloblasts not only remove and degenerate organic matrix components from enamel and enameloid. They are also responsible for mineral transport during enamel and enameloid mineralisation and maturation (Sasagawa et al., 2006, 2009).

In addition to enameloid, teleosts show a wide diversity of dentin types that differ in architectural aspects (Ørvig, 1951, 1967). Finally, teleosts also differ widely in the way how teeth are attached to the jaw bones (Fink, 1981). Advanced teleosts have intra-medullar tooth development like mammals and teeth are ankylosed in deep bone sockets. In zebrafish, as it is typical for less advanced teleost species, teeth develop on top of the jaw bones and attach to the bone surface (Huysseune and Witten, 2006).

The evolutionary origin of the different tissues has not been completely clarified. Bone and dentin together with a hypermineralised layer were concomitantly present in the earliest elements of the dermal skeleton (Ørvig, 1951; Sire and Kawasaki, 2012; Keating et al., 2018). Dentin and bone share many characters, making the

distinction between the two tissues not always straightforward. The evolutionary origin of enameloid has been and continues to be the subject of a long-lasting controversy, whether it precedes or follows the origin of enamel (Smith, 1995; Davit-Béal et al., 2007; Kawasaki et al., 2021). According to Maisey (1988), enamel-like (i.e. epithelium-derived) substances may well have been the earliest vertebrate hard tissues.

Recent studies on Atlantic salmon (Witten et al., 2019) as well as on zebrafish (Cotti et al., 2020) have revealed the impact of a low phosphorus (P) diet on the endoskeleton. Under conditions of low dietary P intake, bone continues to grow but remains non-mineralised. Under experimental conditions, the non-mineralised bone matrix proofed to be mechanically sufficiently stable to support the animals vertebral column. Scales are also affected from dietary P deficiency. Scales grow and develop normal spaced annuli but remain non-mineralised (Witten et al., 2016). Likewise, non-mineralised bone can occur in dermal skeletal elements under natural conditions (Meunier and Huysseune, 1992). In contrast, there are no reports about non-mineralised teeth, not even from deep sea fish that can have an extremely low mineralised endoskeleton (Denton and Marshall, 1958; Schnell and Johnson, 2017; Germain et al., 2019). This raises the question if the mineralisation of teeth is regulated differently from the mineralisation of the other parts of the skeleton. If, and to what extent, a low P diet similarly affects the tooth development and the tooth mineralisation is not known at present. We have therefore engaged in a study examining the effects of dietary low P on tooth development (replacement), tooth structure and on the different dental tissues in zebrafish.

The morphology of the zebrafish dentition is well established (Huysseune et al., 1998; Van der heyden et al., 2000; Stock, 2007). Cyprinids, the group to which zebrafish belongs, have lost their oral teeth but retain pharyngeal jaws with teeth on the ceratobranchials of the posteriormost pharyngeal arch. Teeth are distributed along three rostro-caudal rows named ventral, mediodorsal and dorsal row, with five, four and two teeth, respectively (Van der heyden and Huysseune, 2000; Wautier et al., 2001). A complete dentition is established at 26 days post-fertilisation (Van der heyden and Huysseune, 2000). Zebrafish teeth are continuously replaced throughout life. It has

been reported that the functional lifetime of a tooth in juveniles is about eight days (Van der heyden et al., 2000). Moreover, the ventral teeth become larger with zebrafish growth as a result of replacement by larger teeth (Wautier et al., 2001).

The aim of the present study was to use the zebrafish dentition (i) to evaluate the effects of a P-deficient diet on the mineralisation of the pharyngeal teeth and the jaw bones, (ii) to determine whether the four mineralised tissues present, enameloid, dentin, bone of attachment and bone, respond differently to P-deficiency, and (iii) to assess potential differences between these tissues in an evolutionary perspective. From the three zebrafish tooth rows, the ventral tooth row is the most stably present across cyprinids (Pasco-Viel et al., 2010), and the most thoroughly investigated so far (Huysseune et al., 1998; Van der heyden et al., 2000; Wautier et al., 2001). Thus, this study focuses on the five, large teeth of the ventral row.

## Results and discussion

### *Dentin and bone of attachment, but not enameloid, show reduced mineralisation under low P conditions*

Comparison of the size of the five ventral teeth at the beginning and at the end of the experiment confirms that larger ventral teeth are present after one and two months of dietary treatment. Considering that a tooth replacement cycle lasts about eight days, it is safe to conclude that new replacement teeth must have been generated during the period of dietary treatment (Van der heyden and Huysseune, 2000; Wautier et al., 2001). This allows us to assess the effects of different dietary P levels on the mineralisation of enameloid, dentin and bone of attachment, i.e., the three different mineralised tissues that build up each tooth. Further, it is possible to compare the mineralisation status of the teeth with the one of the jaw bones and also with the one of the vertebral column (Cotti et al., 2020). Whole mount Alizarin red S stained pharyngeal jaws reveal that one and two months of low P (LP) dietary treatment causes mineralisation defects of the tooth-supporting (ceratobranchial) bone (**Figure 6.1 A**), in agreement with earlier findings on the vertebral column (Cotti et al., 2020). After one month of dietary treatment, the fraction of young, non-functional teeth is significantly larger in the LP group compared to controls (fed a regular P diet, RP) (LP: 27%, RP: 11%, HP: 19%; Chi-square test followed by Bonferroni correction: LP-RP $p<0.001$; LP-HP p non-significant; RP-HP p non-significant). After two months of dietary treatment, the fraction of young, non-functional teeth is significantly larger in the LP group compared to both the RP and high P (HP) dietary groups (LP: 24%, RP: 7%, HP: 8%; Chi-square test followed by Bonferroni correction: LP-RP $p<0.001$; LP-HP $p<0.001$; RP-HP p non-significant) (**Figure 6.1 B**).

In WT zebrafish, mineralisation of the attachment bone starts well before completion of predentin (Van der heyden et al., 2000). Attached and erupted teeth constitute the functional teeth (Huysseune et al., 2005). Teeth with non-mineralised bone of attachment could thus be considered as young and not yet functional. The significantly larger fraction of teeth that are considered as young and non-functional

teeth after LP treatment can at least partly be explained by a defect in attachment bone mineralisation. Indeed, within the LP group, a large fraction of the teeth analysed in all five positions is attached via non-mineralised bone of attachment (**Figure 6.1 A**). In contrast, in the control group and in the HP zebrafish, the majority of the ventral teeth is attached via fully mineralised bone of attachment after one (RP: 71%; HP: 61%) and two months (RP: 85%; HP: 87%) of dietary treatment (**Figure 6.1 A**). Statistical comparison shows that the fraction of teeth attached via non-mineralised bone of attachment is significantly larger in the LP group compared to RP and HP at both time points (one-month treatment: Chi-square test followed by Bonferroni correction: LP-RP $p<0.001$; LP-HP $p<0.001$; RP-HP p non-significant; two months treatment: Chi-square test followed by Bonferroni correction: LP-RP $p<0.001$; LP-HP $p<0.001$; RP-HP p non-significant) (**Figure 6.1 B**). Atlantic salmon has many erupted and functional teeth with non-mineralised bone of attachment. The teeth are replaced before the basis becomes fully mineralised. This example shows that teeth with non-mineralised attachment bone can be functional (Witten et al., 2005; Huysseune et al., 2007).

All dietary groups present a similar thickness of the dentin wall for those ventral teeth analysed (1V, 2V and 3V) (**Table 6.1**). However, teeth in LP zebrafish present a peculiar pattern of dentin mineralisation at different stages of maturation (defined according to Huysseune, 2006). This pattern is evidenced both by non-demineralised sections stained with Von Kossa (**Figure 6.1 C-C'**) and synchrotron X-ray tomographic microscopy (**Figure 6.1 D**). In contrast to normal dentinogenesis in zebrafish, whereby unmineralised predentin becomes rapidly mineralised after its initial deposition (Huysseune et al., 1998; Van der heyden et al., 2000), young, yet erupted and thus functional teeth under LP conditions present large amounts of non-mineralised dentin (**Figure 6.1 C**, right side). At a later stage, the peripheral dentin matrix, in contact with the inner dental epithelium, is mineralised but a broad zone of circumpulpal dentin remains non-mineralised (**Figure 6.1 D**). Finally, an old and fully mature LP tooth (as evidenced by characteristics of the pulp and by the presence of a developing replacement tooth in **Figure 6.1 C**, left side) shows completely mineralised dentin. This suggests that mineralisation proceeds during the functional lifetime of the

tooth. In contrast, RP and HP teeth show mineralised dentin (**Figure 6.1 C**) with only a thin layer of non-mineralised circumpulpal dentin, opposite the odontoblasts, and only detectable by synchrotron X-ray tomographic microscopy (**Figure 6.1 D**), as is the case in normal dentinogenesis (Huysseune et al., 1998; Van der heyden et al., 2000). In all dietary groups, darker staining lines within the dentin run parallel to the long axis of the tooth (**Figure 6.1 C'**). Possibly, these represent traces of intermittent mineral deposition, related to the incremental growth lines discussed in Huysseune and Sire (1998) and Berkovitz and Shellis (2017). In remarkable contrast to the findings related to the dentin, the enameloid in all three dietary groups presents as a hypermineralised cap, independent of the diet and the mineralisation stage of dentin and bone of attachment (**Figure 6.1 C-D**). This highlights a very important difference in the nature of enameloid versus dentin mineralisation, reflecting a different structural composition and developmental trajectory. This supports a distinctive evolutionary origin of both tissues (Maisey, 1988; Kawasaki et al., 2021). John Maisey provides a number of arguments in favour of the early evolution of enamel/enameloid prior to and independent from the evolution of bone and dentin. "Enamels" are primitively restricted to superficial epithelial ectomesenchymal tissues. Lower vertebrate enameloids typically form prior to dentin or bone. Calcium phosphate deposition is exclusively ectodermal in invertebrates, with no mesodermal interaction, arguably a primitive condition. Ameloblastic hypermineralisation provides a mechanism for rapid hydroxyapatite assimilation and P storage, that would be advantageous to an organism whose hormonal regulation (e.g. by calcitonin) and ability to form a collagenous matrix were perhaps not well developed (Maisey, 1988).

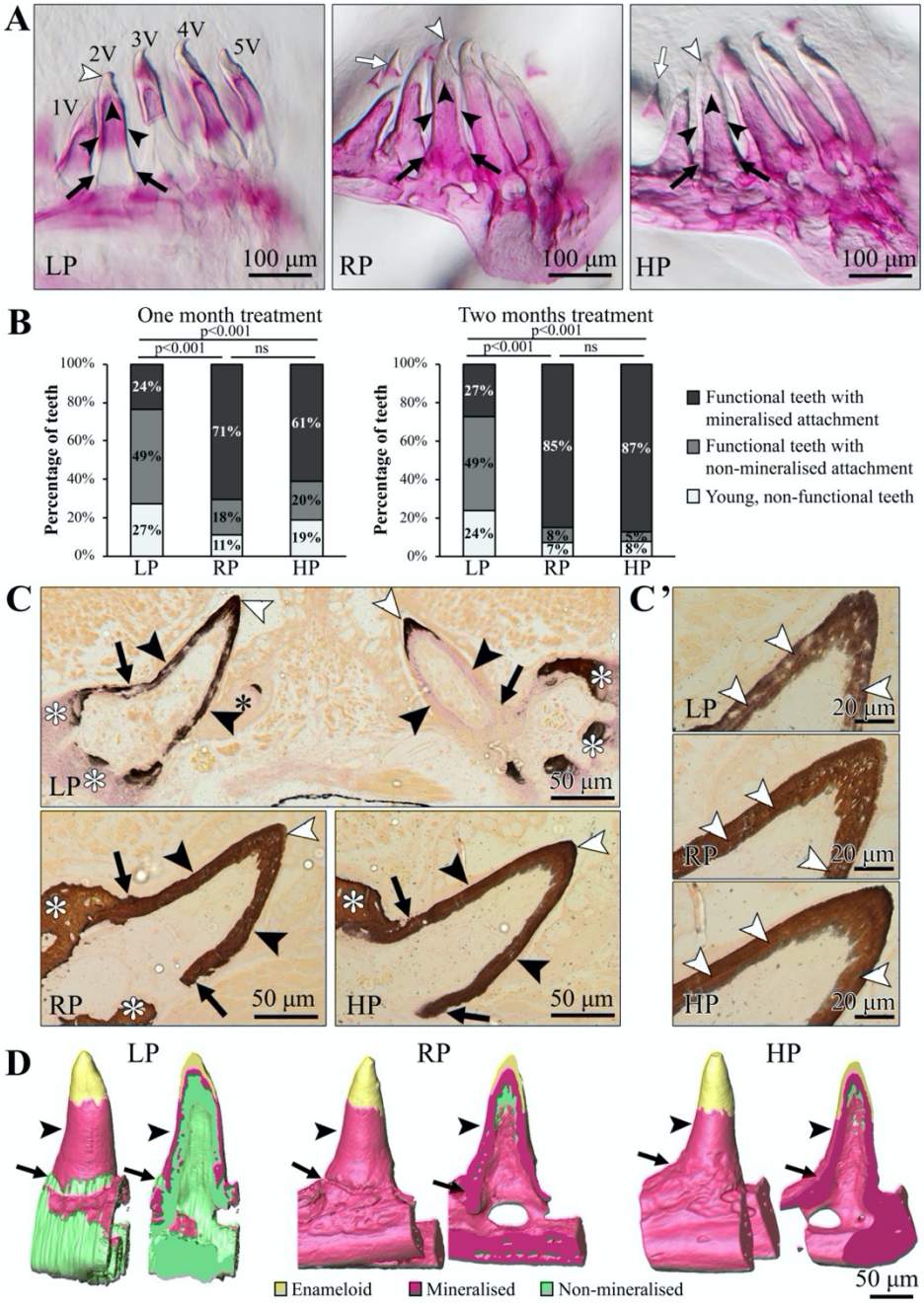


**Figure 6.1.** Mineralisation of zebrafish ventral teeth under different dietary P conditions. **A**: Whole mount Alizarin red S stained pharyngeal jaws showing the five ventral teeth (1V-5V) in LP, control (RP) and HP after two months of dietary treatment. LP teeth commonly show non-mineralised bone of attachment (black arrows) but mineralised dentin (black arrowheads) and mineralised enameloid (white arrowheads). Mature enameloid appears negatively stained as it is

an hypermineralised tissue, this is not a staining artifact. RP and HP teeth are attached to the pharyngeal bone via fully mineralised bone of attachment. Developing replacement teeth are also present (white arrows). **B**: Fraction of the ventral teeth (10 teeth per specimen analysed) presenting either as young (non-functional) teeth, or as functional teeth with non-mineralised or with mineralised attachment, after one and two months of dietary treatment. The fraction of teeth attached via non-mineralised bone of attachment is significantly larger in the LP group compared to RP and HP after one and two months of dietary treatment. Number of teeth analysed after one month of treatment: LP n=180, RP n=160, HP n=180; number of teeth analysed after two month of treatment: LP n=200, RP n=200, HP n=200. Chi-squared test followed by Bonferroni correction, p-values relative to the mineralisation of the bone of attachment are indicated, ns: non-significant. **C**: Von Kossa/Van Gieson stained non-demineralised sections of ventral tooth 1V in LP, RP and HP. Brown staining indicates mineralised tissues, pink indicates non-mineralised tissues. In the LP specimen, tooth 1V is in a different developmental stage on the two pharyngeal jaws. The LP tooth on the right side of the image is young, yet erupted (confirmed at another sectional level) and functional, and presents a large amount of non-mineralised dentin (black arrowheads). Bone of attachment (black arrows) is non-mineralised, whereas enameloid (white arrowhead) is fully mineralised. The LP tooth on the left side of the image is an old, mature tooth, as evidenced by the characteristics of the pulp and by the presence of a developing replacement tooth (black asterisks). The dentin (black arrowheads) and bone of attachment (black arrow) are mineralised throughout. The supporting bone of the LP pharyngeal jaws (white asterisks) shows large areas of non-mineralised matrix (pink). Control (RP) and HP zebrafish show functional 1V with all dental tissues as well as supporting bone (white asterisks) mineralised. **C'**: High magnification details of non-demineralised Von Kossa/Van Gieson stained sections LP, RP and HP tooth 1V showing darker staining lines (white arrowheads) parallel to the long axis of the tooth within the dentin. **D**: synchrotron X-ray tomographic microscopy 3D reconstructions and virtual sections of tooth 1V in LP, RP and HP zebrafish showing hypermineralised enameloid (yellow), dentin (arrowheads) and bone of attachment (arrows) under the different dietary treatments. The outer surface of the dentin in LP is mineralised, but a broad zone of circumpulpal dentin remains non-mineralised. RP and HP show mineralised dentin with only a thin layer of non-mineralised circumpulpal dentin, opposite the odontoblasts.

**Table 6.1.** Dentin thickness measurements of teeth 1V, 2V and 3V in LP, RP and HP zebrafish.

| Tooth | Diet | Dentin thickness/tooth height (mean ± SD) | Pairwise p-values | |
|---|---|---|---|---|
| 1V | LP | 0.047 ± 0.0079 | LP - RP | ns |
| | RP | 0.052 ± 0.0095 | LP - HP | ns |
| | HP | 0.049 ± 0.0102 | RP - HP | ns |
| 2V | LP | 0.039 ± 0.0097 | LP - RP | ns |
| | RP | 0.044 ± 0.0065 | LP - HP | ns |
| | HP | 0.043 ± 0.0077 | RP - HP | ns |
| 3V | LP | 0.037 ± 0.0054 | LP - RP | ns |
| | RP | 0.040 ± 0.0079 | LP - HP | ns |
| | HP | 0.041 ± 0.0077 | RP - HP | ns |

Dentin thickness measured at half of the total tooth height was normalised to the total tooth height. Statistical comparison is based on the non-parametric Mann-Whitney test followed by Bonferroni correction; ns: non-significant.

***Dentin, bone of attachment and supporting bone respond differently in low mineralisation conditions***

The low level of mineralisation of the dentin and bone of attachment in LP functional teeth allows us to obtain more details on the organic matrix of both tissues, which have traditionally been difficult to distinguish, and have elicited a lot of controversy. According to some authors, bone of attachment in teleosts is dentin (e.g. Hughes et al., 1994), while others consider it true bone (e.g. Clemen et al., 1997). Possibly, the nature of the bone of attachment is also species-dependent. Rosa et al. (2021) recently discussed the issue in the light of their findings in zebrafish. They concluded that anatomically, the term "pedicel" can be used, but that structurally the term 'bone of attachment' is misleading as the tissue has both dentinous and bony characters. They proposed the term "dentinous bone".

Specimens imaged with synchrotron X-ray tomographic microscopy underwent further analysis, allowing to compare the same tooth between the 3D reconstructions based on synchrotron images (i.e., prior to decalcification, **Figure 6.1 D**) and structural details obtained at the histological and ultrastructural level (i.e., after decalcification, **Figure 6.2**). On toluidine blue stained sections of tooth 1V from the same LP specimen (and same tooth) previously analysed by synchrotron X-ray tomographic microscopy, the dentin shows a smooth surface where it is in contact with the inner dental epithelium (**Figure 6.2 A**). Beyond the cervical loop (i.e. where the inner dental epithelium does not cover the tooth matrix), the dentin base appears to be an inverted cone enveloped by bone of attachment both at the outside of the tooth and at the pulpal side (**Figure 6.2 A,B**). The bone of attachment has a scalloped surface at the outside and is covered by cells that closely follow the outline of the matrix. At the pulpal side, osteoblasts (cf. Rosa et al., 2021) form a pseudo-epithelial layer that flattens down at the transition to the supporting bone (**Figure 6.2 A**). The matrix of the bone of attachment shows parallel oriented collagen fibrils under polarised light (**Figure 6.2 B**). Further down towards the supporting bone of the ceratobranchial, the boundary of the bone of attachment can be recognised by (i) the change in morphology of the pseudo-epithelium at the pulpal side, (ii) the corresponding transition from a

scalloped to a smooth matrix surface at the outside, (iii) the appearance of osteocytes that are sparsely distributed in the supporting bone and (iv) resorption lacunae where osteoclasts have removed bone matrix and osteoblasts secrete new collagen matrix (**Figure 6.2 A**). These findings are in agreement with the characterisation of this tissue as dentinous bone by Rosa et al. (2021).

***Odontoblasts show distinctive features under different dietary P conditions***

The comparison of one single tooth, prior to demineralisation (synchrotron data) and after demineralisation (histology and ultrastructure), allows to precisely identify formerly mineralised versus non-mineralised matrix under LP and RP conditions. In transmission electron microscopy (TEM) micrographs, the dentin of tooth 1V, both under LP and RP conditions, shows a smooth surface in contact with the inner dental epithelium. The dentin matrix is composed of collagen with zones that differ in electron-density. A thin layer of loosely organised collagen fibrils, representing the initial phase of predentin formation, faces the pulp cavity (**Figure 6.2 C,D**). The dentin matrix is comparable in LP and RP specimens, regardless of the differences in mineralisation (see **Figure 6.1 D**). However, LP odontoblasts show enlarged endoplasmic reticulum (ER) cisternae compared to RP (**Figure 6.2 E,F**). In contrast, the osteoblasts at the pulpal side do not present an ER phenotype in any dietary group (**Figure 6.2 G,H**). Likewise, in both LP and control specimens, osteoblasts lining the supporting bone of the pharyngeal jaw show extensive ER without enlarged cisternae, indicative of a high secretory activity (**Figure 6.2 I,J**). Osteoblasts are known to be responsible for the secretion of the immature non-mineralised collagen matrix, i.e. the osteoid, visible as a poorly electron-dense layer in contact with the cells. The supporting bone in LP specimens is mostly non-mineralised (see **Figure 6.1 D**), yet the collagen matrix does not show differences in TEM compared to the matrix of the supporting bone in RP specimens, that was fully mineralised prior to processing (**Figure 6.2 I,J**).

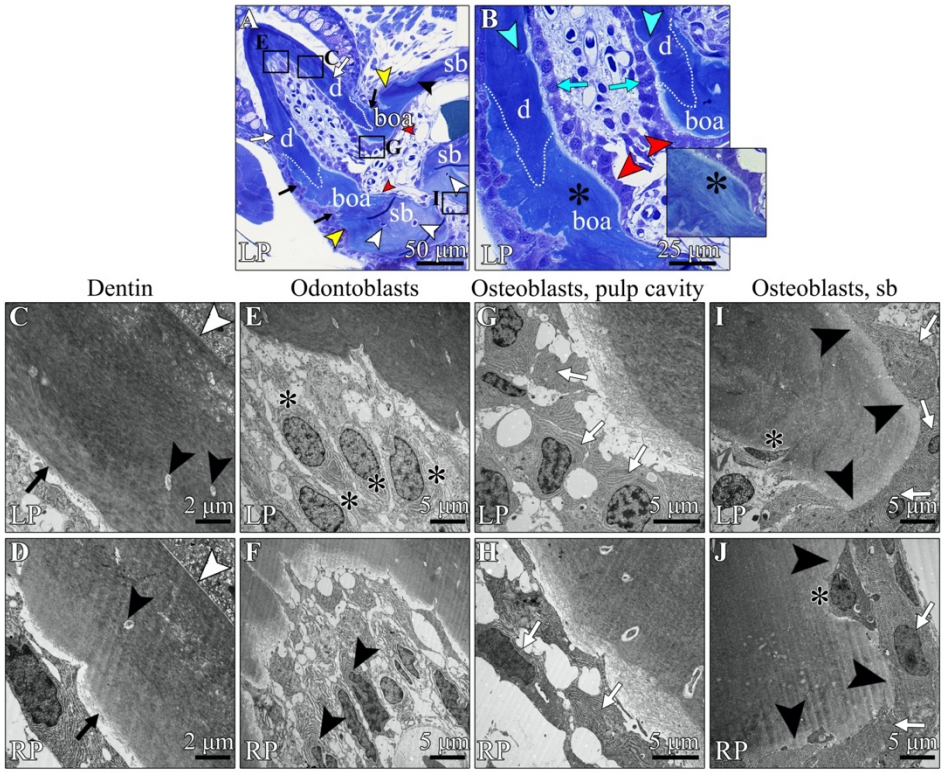


**Figure 6.2.** Dentin, bone of attachment and supporting bone in low mineralisation conditions. **A,B**: Toluidine blue stained semithin sections of LP 1V tooth, previously analysed with synchrotron X-ray tomographic microscopy, following decalcification. **A**: 1V tooth overview showing dentin (d) characterised by a smooth border (white arrows) with the inner dental epithelium. The dentin base appears like an inverted cone (white segmented line) enveloped by bone of attachment (boa), that is delimited by a scalloped outer surface (black arrows) and an osteoblasts' pseudo-epithelium (red arrowheads) at the pulpal cavity. Beyond the bone of attachment, the supporting jaw bone (sb) is characterised by a smooth outer surface (yellow arrowheads), by resorption lacunae (black arrowhead) and by the presence of osteocytes (white arrowheads). **B**: Enlargement of panel **A** showing the region between dentin (d) and bone of attachment (boa). Dentin deposited by odontoblasts (turquoise arrows) presents dentinal tubules (turquoise arrowheads); the dentin base is an inverted cone (white segmented line) enveloped by bone of attachment. Bone of attachment, delimited by an osteoblasts' pseudo-epithelium (red arrowheads) at the pulpal side, is characterised by parallel oriented collagen fibres (black asterisk) as shown by the polarised light (insert). **C-J**: Transmission electron microscopy (TEM) micrographs of LP and RP tooth 1V. Regions of interest are indicated as rectangles in panel **A**. **C-D**: Both LP and RP show dentin matrix presenting a smooth surface (white arrowhead) in contact with the inner dental epithelium, a collagen matrix with diverse electron-dense zones and a poorly electron-dense layer of recently secreted collagen, called predentin (black arrows), facing the pulp cavity. Odontoblasts send extensions in dentinal tubules that penetrate the dentin matrix (black arrowheads). **E-F**: LP odontoblasts present enlarged endoplasmic reticulum (ER) cisternae (white asterisks) compared to the control (black arrowheads). **G-H**: Osteoblasts (white arrows) in the pulp cavity of LP and control form a pseudo-epithelial layer. Osteoblasts show an extensive ER without enlarged cisternae. **I-J**: Osteoblasts

(white arrows) secreting the supporting jaw bone matrix present a similar phenotype, with extensive ER indicating that cells are active at producing collagen matrix in both LP and control. The immature collagen matrix, i.e. the osteoid (black arrowheads), is visible as a poorly electron-dense layer in contact with the osteoblasts. Osteoblasts becoming embedded in the bone matrix as osteocytes (white asterisks) are present in both LP and RP.

### *Osteocalcin expression is detected in odontoblasts, osteoblasts and osteocytes, irrespective of diet*

Given the clear impact of P deficiency on dentin maturation, we wished to examine in more detail whether the expression of osteocalcin in odontoblasts depends upon dietary P intake. Osteocalcin (also known as bone gamma-carboxyglutamate [Gla] protein), is a non-collagenous protein present in both teeth and bone matrix, but with higher expression levels in bone, at least in mammals (Komori, 2010). In mice, the osteocalcin gene is strongly expressed in maturated osteoblasts (Komori, 2010) and has even been used to distinguish odontoblasts from osteoblasts (Li et al., 2011).

To assess the expression of osteocalcin in the cells responsible for the deposition of the different dental tissues, an *osc*:GFP reporter line was used. Irrespective of the level of P intake, after two months of treatment, osteocalcin is expressed in the odontoblasts within the pulp cavity, in osteoblasts of the pseudo-epithelium at the pulpal side as well as osteoblasts depositing the bone of attachment and supporting bone, and in osteocytes (**Figure 6.3**). Odontoblasts express osteocalcin throughout the different developmental stages of the tooth, i.e. initiation and morphogenesis (**Figure 6.3 A**), cytodifferentiation (**Figure 6.3 B**), attachment (**Figure 6.3 C**), eruption (**Figure 6.3 D**), replacement (**Figure 6.3 E**) and resorption (**Figure 6.3 F**) (stages according to Borday-Birraux et al., 2006). Likewise, osteocalcin expression has been reported in active and mature odontoblasts as well as in the odontoblastic processes in the teleost fish *Argyrosomus regius* (Ortiz-Delgado et al., 2005). This is in stark contrast with findings in Atlantic salmon, where osteocalcin expression could only be detected in the aboral surface of the dentigerous bone (*in casu* the dentary), but not in odontoblasts at any stage, nor in the osteoblasts lining the attachment bone or the oral (dentigerous) surface of the dentary bone (Huysseune et al., 2008). Whether this difference is linked to the technical approach used (*in situ* hybridisation versus a

transgenic reporter line), to species-specific differences, to different paralogues, osteocalcin variants or if there is another explanation, still needs to be elucidated. The zebrafish *osc*:GFP reporter is linked to the expression of osteocalcin1, whereas the *in situ* hybridisation in salmon detected the zebrafish osteocalcin2 orthologue (Huysseune et al., 2008). However, and like in Atlantic salmon (Huysseune et al., 2008), no expression is detected in ameloblasts at any developmental stage (**Figure 6.3 A-F**). Of notice, osteocalcin GFP signal distinctively labels the odontoblast processes within the dentin and the osteocyte canaliculi in the pharyngeal bone (**Figure 6.3 G,H**).

In view of comparing the effect of P-deficiency on osteocalcin expression in more detail, the fluorescent GFP signal was measured within the pulp cavity of teeth in a comparable developmental stage in all dietary groups. Two positions were chosen based on characteristics of the pulp cavity (Huysseune, 2006): a replacement tooth in position 3V and a young functional tooth in position 1V. No significant difference is detected among dietary groups in the GFP signal area within the pulp cavity normalised to the pulp cavity area of the replacement tooth 3V (LP-*osc*:GFP 59.60% ± 10.19%; RP-*osc*:GFP 57.16% ± 9.84%; HP-*osc*:GFP 61.06% ± 7.15%) and of the young functional tooth 1V (LP-*osc*:GFP 62.59% ± 8.12%; RP-*osc*:GFP 61.19% ± 8.90%; HP-*osc*:GFP 59.38% ± 9.92%). The observations on odontoblast osteocalcin expression are in agreement with those on zebrafish osteoblasts, where the expression of osteocalcin relates to the amount of bone matrix production and it is independent from dietary P intake (Chapter 4).

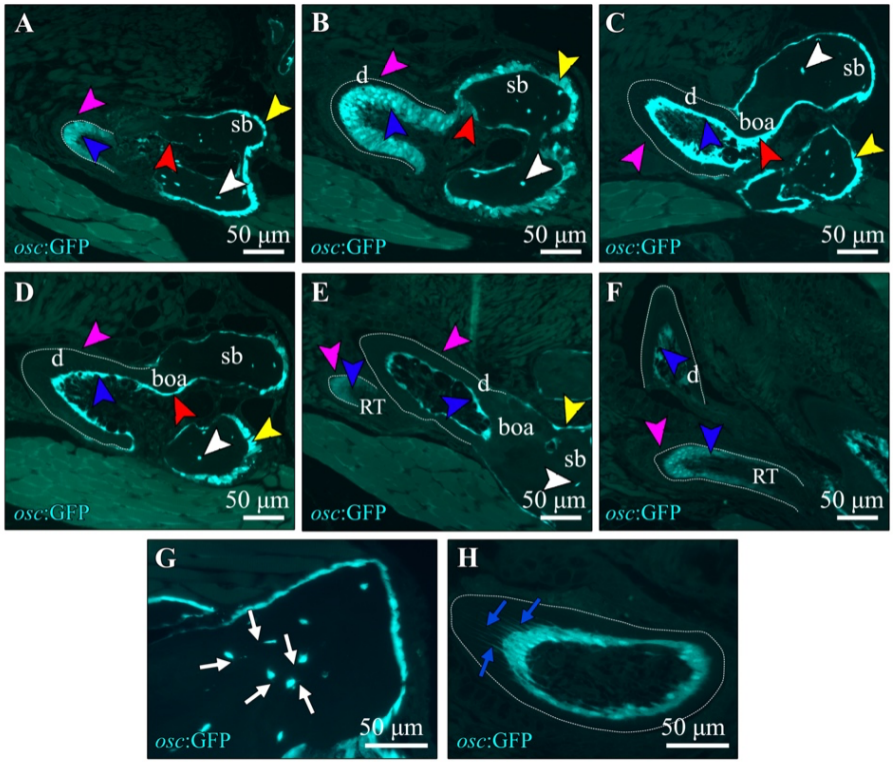


**Figure 6.3.** Expression of osteocalcin in the dental tissues forming cells. **A-F**: Representative images of tooth 1V (**A-E**) and tooth 3V (**F**) at different developmental stages from a transgenic zebrafish line expressing osteocalcin labelled with GFP (*osc*:GFP) and treated with the P diets. Irrespective of dietary P, odontoblasts (blue arrowheads) express osteocalcin during the different tooth developmental stages, i.e. initiation and morphogenesis (**A**), cytodifferentiation (**B**), attachment (**C**), eruption (**D**) replacement (**E**) and resorption (**F**). Of notice, odontoblasts are *osc*:GFP-positive also at the end of the resorption phase, as evidenced in the tooth 3V being resorbed and replaced in **F**. Osteocalcin is expressed also in osteoblasts of the pseudo-epithelium at the pulpal side (red arrowheads) as well as osteoblasts depositing the pharyngeal bone (yellow arrowheads), and in osteocytes (white asterisks). Dashed lines indicate the border of the tooth unit with the inner dental epithelium, where ameloblasts (purple arrowheads) do not express osteocalcin. Boa: bone of attachment; d: dentin; sb: supporting bone; RT: replacement tooth. **G-H**: High magnification images show that osteocalcin GFP signal distinctively labels the osteocytes' canaliculi in the pharyngeal bone (**G**, white arrows) and the odontoblasts' processes within the dentin (**H**, blue arrows).

### *The Na-P co-transporter slc34a2b is expressed at the tooth tip*

The finding that the anlage and mineralisation of the enameloid cap of the teeth is independent from the dietary P intake raised the question about mineralisation mechanisms that are distinct from bone and dentin. To understand whether enameloid

mineralisation in zebrafish might depend on an active transport of P from serum to the mineralisation sites, the expression of the Na-P co-transporter *slc34a2b* was assessed by *in situ* hybridisation. This specific gene was chosen based on its conservation across vertebrates (Schultz et al., 2014) and based on the specific expression of the Na-P co-transporter *Slc34a2* in ameloblasts from mice (Merametdjian et al., 2017). Analysis of whole mount *in situ* hybridisation and subsequent histological sections from zebrafish teeth from all dietary groups revealed that *slc34a2b* is specifically expressed at the tooth tip, that in zebrafish is covered by the inner dental epithelium (**Figure 6.4**). The signal is specific and well distinguishable from the background. *slc34a2b* is not expressed in other cell types, nor odontoblasts, osteoblasts or osteocytes (**Figure 6.4 C**).

The zebrafish Slc34a2b transporter has high-affinity and low-capacity for sodium and P (Graham et al., 2003). Similar to other Slc34 family of transporters, Slc34a2b can both secrete and reabsorb P in the kidney from fish (Gupta and Renfro, 1989), a tissue where these transporters have been extensively characterised (Verri and Werner, 2019). The characterisation of Slc34a2 transporters in dental tissues from mice suggests that the activity of P transporters is required for enamel mineralisation (Onishi et al., 2007; Merametdjian et al., 2017), as do the results from zebrafish in this study. These data well correlate with results from the no bone zebrafish mutant with mutations in *entpd5* (Huitema et al., 2012). This mutant lacks bone mineralisation, but the tip of teeth properly mineralises (Huitema et al., 2012), thus supporting the idea that enameloid mineralisation is driven by an active transport of P.

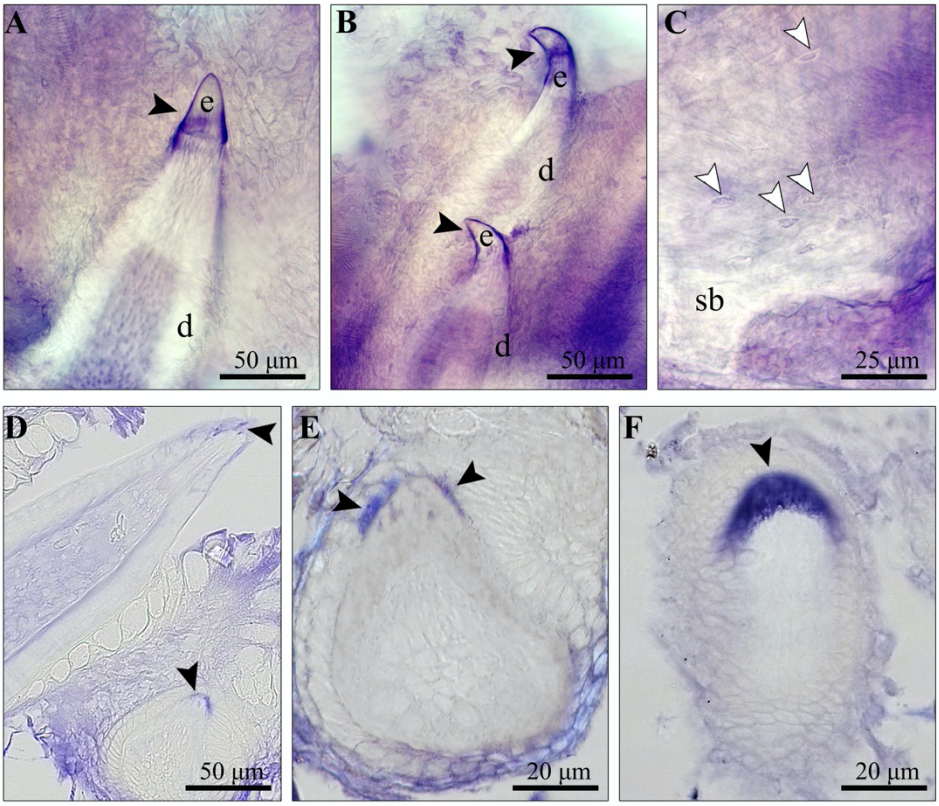


**Figure 6.4.** *In situ* hybridisation of the Na-P co-transporter *slc34a2b*. **A-B:** Expression of *slc34a2b* is specifically localised at the tooth tip, that in zebrafish is covered by the inner dental epithelium. The signal (blue staining, black arrowheads) is well distinguishable from the background. d: dentin, e: enameloid. **C:** Osteocytes (white arrowheads) in the supporting bone (sb) do not express *slc34a2b*. **D-F**: Histological sections obtained from the pharyngeal jaws show the cellular location of *slc34a2b* expression. *slc34a2b* is expressed in the cells of the inner dental epithelium of an erupted tooth (black arrowhead in **D**, upper part of the panel) and in early developmental stages teeth (black arrowhead in **D**, lower part of the panel, in **E** and **F**). Images derive from dissected pharyngeal jaws of LP zebrafish and are representative also for the other dietary groups.

## Conclusions

This study shows that the mineralisation of enameloid in zebrafish is, within the experimental parameters tested, independent from dietary P intake. Half the amount of required dietary P had a strong impact on the pharyngeal jaw bone and dentin mineralisation, but had no impact on the mineralisation of enameloid. Similar to bone matrix formation, that continued and it was further stimulated under LP conditions, tooth formation and replacement continued uninterrupted. Teeth with a clear delay in dentin and bone of attachment mineralisation had a regular shape and size. The dietary P independent mineralisation of the enameloid may relate to functional requirements, but it also suggests a mineralisation mechanism that is different from bone, bone of attachment and dentin. Functionally, as known from previous experimental studies (Witten et al., 2016, 2019; Cotti et al., 2020), from deep sea fishes (Denton and Marshall, 1958; Schnell and Johnson, 2017; Germain et al., 2019) and zebrafish mutants (Huitema et al., 2012), low mineralised bone can be a fully functional skeletal support. This is arguably not possible for teeth. A functional tooth must at least have a hard, mineralised, tooth tip and a mineralised outer shell. This is what is observed in zebrafish under low dietary P conditions. Most intriguing is the observation of the P intake independent mineralisation of the enameloid. Ameloblasts, epithelial cells of the inner dental epithelium, are indeed very different in their function and structure from osteoblasts and odontoblasts. Different from mesenchymal cells, epithelial cells are designed for active ion transport (Evans, 2002). Mammalian ameloblasts actively transport minerals for enamel mineralisation and the cells actively remove the proteins from the enamel matrix (Onishi et al., 2007; Bartlett, 2013; Merametdjian et al., 2017). Both functions have been assigned to the ameloblasts of teleosts (Prostak and Skobe, 1986; Sasagawa, 1998), but it is here demonstrated for the first time that the inner dental epithelium of a teleost fish expresses the Na-P co-transporter *slc34a2b*. Thus, enameloid mineralisation is ensured, on the one hand, by the Slc34a2b-mediated high-affinity and low-capacity transport of P (Graham et al., 2003), and, on the other hand, by the active transport of calcium across epithelia (Witten and Huysseune, 2009).

Another interesting aspect is the independence of tooth and bone formation, which also suggests the presence of two, physiologically and evolutionary, different mineralisation mechanisms. This can also be seen in several zebrafish mutants. Mutations in *eda* (ectodysplasin) or *edar* (ectodysplasin receptor) in zebrafish affect the teeth, the scales and the dermal fin rays (Harris et al., 2008). The elements of the dermal skeleton are affected but not the endoskeleton (Harris et al., 2008). Heterozygous mutations of *RUNX2* in humans cause a reduced bone phenotype, and simultaneously the development of large numbers of extra numerary teeth (Ma et al., 2018). Moreover, zebrafish osterix (*sp7*) mutants show reduced bone and dentin formation, but the enameloid caps mineralise (Kague et al., 2018). Another zebrafish model with mutations in the ectonucleoside triphosphate/diphosphohydrolase 5 (*entpd5*), an enzyme responsible for the removal of the mineralisation inhibitor pyrophosphate, have no mineralised bone (Huitema et al., 2012). Still, and like the LP zebrafish, the tooth tips are mineralised (Huitema et al., 2012).

The above cited studies and the results from this study clearly show that enameloid mineralisation follows a pathway different from bone and dentin formation. Although in the earliest vertebrates enameloid, dentin and cellular bone appear together in the fossil record, our results support the hypothesis that enamel and enameloid, as epithelial cell derived skeletal tissues, evolved independently from and likely earlier than bone (Maisey, 1988).

## Materials and methods

### *Zebrafish maintenance and ethical statement*

Wild type (WT) AB zebrafish were obtained from European Zebrafish Research Center (Eggenstein-Leopoldshafen, Germany). The reporter zebrafish line *osc*:GFP was a gift from Dr. A. Willaert, Ghent University Hospital, Gent, Belgium, and originally was obtained by Dr. S. Schulte-Merker, Institute for Cardiovascular Organogenesis and Regeneration, Münster, Germany (Vanoevelen et al., 2011). WT and transgenic zebrafish embryos were kept in petri dishes in fish water (1.2 mM $NaHCO_3$, 0.01% instant ocean, 1.4 mM $CaSO_4$, 0.0002% methylene blue) at 28°C until 7 days post-fertilisation (dpf), then grown at 28°C, pH 7.5 on a 14/10 light/dark cycle. Zebrafish from 7 to 21 dpf were fed three times a day alternating commercial dry food (ZM000, Zebrafish Management Ltd., Winchester, UK) and brine shrimp (Artemia cysts, Zebrafish Management Ltd., Winchester, UK). Fish were then fed for another week three times a day with the dry regular phosphorus (RP) diet (Cotti et al., 2020) until 28 dpf, to adjust them to this type of dry feed. The nutrition trial started at 28 dpf: fish were randomly divided in three groups, grown in identical tanks with a density of 10 fish/L and fed three times a day with a low phosphorus (P) (LP) diet, a regular P (RP) diet and a high P (HP) diet, respectively (Cotti et al., 2020) (see below for details). Samples were collected before the start of the experiment (T0 samples, 28 dpf) and after one and two months of dietary treatment (two and three months post-fertilisation, respectively) as described below. The experiments on WT zebrafish were conducted in the centralised animal facility of the University of Pavia (Pavia, Italy). The experiments on *osc*:GFP zebrafish were conducted at Ghent University (Gent, Belgium). Animal care, experimentation and euthanasia complied with EU Directive 2010/63/EU. The experimental protocol was approved by the Italian Ministry of Health (Approval animal protocol No. 260/2020-PR, 26 March 2020).

***Diet composition***

Diet composition and nutritional experiment are described in detail in Cotti et al. (2020). Briefly, the diets were formulated to have a total P content of 0.5%, 1.0% and 1.5%, termed low P (LP) diet, regular P (RP) diet and high P (HP) diet, respectively. Monoammonium phosphate ($NH_4H_2PO_4$, MAP) was used as dietary inorganic P supplement (Morales et al., 2018). In order to keep all diets equal in nutrients, except for P concentration, MAP replaced the inert filler diatomaceous earth (Diamol, Imerys, Denmark). The diets were formulated by SimplyFish AS (Stavanger, Norway, www.simplyfish.no) and produced by extrusion with subsequent crumbling to a suitable particle size by the Danish Technological Institute (Taastrup, Denmark, https://www.dti.dk). The P content of the product was verified at the University of Hohenheim (Stuttgart, Germany, https://www.uni-hohenheim.de) and determined with 5.04 g/kg diet and 9.84 g/kg diet for the low P and regular P diet, respectively.

***Whole mount staining with Alizarin red S***

WT zebrafish of 28 dpf (n=8), one month treated (LP n=18, RP n=16, HP n=18) and two months treated (LP n=20, RP n=20, HP n=20) fish were euthanised by an overdose (0.3%) of tricaine (3-amino benzoic acidethylester), and fixed for 24 h in 4% paraformaldehyde (PFA) in 1× phosphate-buffered saline (PBS) at 4°C. They were next whole mount-stained with Alizarin red S according to a previously described protocol (Taylor and Van Dyke, 1985). Following dissection of the pharyngeal jaws, the pharyngeal dentition was analysed and imaged using an Axio Zoom V16 stereomicroscope (Carl Zeiss, Oberkochen, Germany) with oblique illumination equipped with a 5MP CCD camera. Depending on Alizarin red S distribution, the bone of attachment of the ventral teeth (10 teeth per specimen analysed in total) (Wautier et al., 2001) was qualitatively evaluated as mineralised (positively stained) or non-mineralised (unstained). Replacement teeth not attached to the pharyngeal bone were considered young, yet non-functional teeth. Mature enameloid appeared negatively stained as it is an hypermineralised tissue, thus it was not a staining artifact (Bruneel et al., 2015). Ventral images of the ventral teeth 1V, 2V and 3V were used to measure

dentin thickness at half of the total tooth height, from the tip to the base, using ImageJ software (NIH, Bethesda, MD, USA). Dentin thickness was normalised to the total tooth height. The ventral strongly recurved teeth 4V and 5V (Wautier et al., 2001) were not considered in this analysis.

***Histological analysis***

WT specimens for histological analysis were euthanised by tricaine overdose and fixed for 24 h in 2.5% PFA, 1.5% glutaraldehyde, 0.1 M sodium cacodylate buffer (pH 7.4) and 0.001% $CaCl_2$ at 4°C. Bone mineral detection was carried out on histological sections obtained from non-mineralised samples embedded in glycol methacrylate (according to Witten et al., 2001). Cross sections of 3 µm were cut on a Microm HM 360 (Marshall Scientific, Hampton, NH, USA) automated microtome and were stained following the Von Kossa/Van Gieson staining protocol (Humason et al., 1997). Images were acquired using an Axio Imager-Z1 microscope (Carl Zeiss, Oberkochen, Germany) equipped with an Axiocam 503 colour camera (Carl Zeiss, Oberkochen, Germany).

After two months of dietary treatment, *osc*:GFP zebrafish (LP n=3, RP n=3, HP n=3) were euthanised by tricaine overdose and kept in the dark during the following steps. To preserve and visualise GFP on sections, we followed an established protocol (Oralová et al., 2019). Briefly, *osc*:GFP zebrafish were fixed for 2 h in 4% PFA in 1× PBS, pH 7.4, at RT, rinsed in tap water for 1 h and decalcified for 48 h in 10% EDTA, 4% PFA, pH 7.4. After rinsing 1 h in tap water, samples underwent glycol methacrylate embedding (according to Witten et al., 2001). Cross sections of 3 µm were cut on a Microm HM 360 (Marshall Scientific, Hampton, NH, USA) automated microtome. Images were acquired using an Axio Imager-Z1 microscope (Carl Zeiss, Oberkochen, Germany). To measure the fluorescent signal within the tooth pulp cavity, a replacement tooth and a young functional tooth in the same position of the ventral row were selected based on characteristics of the pulp in all dietary groups (according to Huysseune, 2006). Images of the complete sectional series of the selected teeth were used to quantify the fluorescence signal within the tooth pulp cavity using the

ZFBONE ImageJ toolset (Tarasco et al., 2020). The signal area was normalised to the pulp cavity area in all the sections, to estimate the fluorescent signal within the volume of the tooth.

***Synchrotron X-ray tomographic microscopy***

WT fish treated with the experimental diets for two months (n=1 fish per dietary group) were euthanised by tricaine overdose, fixed for 24h in 2.5% PFA, 1.5% glutaraldehyde, 0.1 M sodium cacodylate buffer (pH 7.4) and 0.001% $CaCl_2$ at 4°C and were dehydrated in a graded series of ethanol. Synchrotron X-ray tomographic microscopy of the pharyngeal jaws was performed at the TOMCAT beamline (X02DA) (Swiss Light Source (SLS), Paul Scherrer Institut (PSI), Villigen, Switzerland). Scans were acquired with 1501 projections over 180° at 16 keV with an exposure time of 150 ms using a 10× objective resulting in an effective voxel size of 0.65 µm (Cotti et al., 2020). Radiographs were phase-retrieved using the Paganin algorithm, tomographically reconstructed and subsequently analysed using Amira 3.1.1 software (TermoFisher, Waltham, MA, USA). The hypermineralised enameloid, the mineralised dentin and bone of attachment of the ventral tooth 1V, as well as the mineralised parts of the supporting pharyngeal bone, were identified applying constant greyscale-thresholds to all samples. Any non-mineralised matrix was manually identified and selected on each projection. The resulting segmentations and virtual sections of the ventral tooth 1V in LP, RP and HP fish were used to visualise the mineralised and non-mineralised dentin, bone of attachment and pharyngeal bone.

***Transmission electron microscopy***

Following synchrotron X-ray tomographic microscopy, the same specimens were further processed for transmission electron microscopy (TEM). Briefly, samples were decalcified in 0.1 M EDTA, postfixed in 1% $OsO_4$ and embedded in epon epoxide medium. Semi-thin 1 µm cross sections were cut on a Microm HM360 microtome (Marshall Scientific, Hampton, NH, USA) and stained with toluidine blue (0.5% toluidine blue, 1% $Na_2B_4O_7$ in demineralised water ($dH_2O$), pH 9) for 2 min. For TEM analysis,

ultrathin sections (about 70 nm) of tooth 1V were prepared on an UltracutE ultramicrotome (Reichert-Jung, Buffalo, NY, USA), contrasted with uranyl acetate and lead citrate and analysed with a Jeol JEM 1010 transmission electron microscope (Jeol Ltd., Tokyo, Japan) operating at 60 kV. Microphotographs were taken with a Veleta camera (Emsis, Muenster, Germany).

***In situ hybridisation***

WT two months treated zebrafish (n=2 per dietary group) were fixed for 2h at RT in 4% PFA in 1× PBS in DEPC-$dH_2O$, washed with 1× PBS in DEPC-$dH_2O$, dehydrated through a 1× PBS in DEPC-$dH_2O$/methanol gradient and stored in 100% methanol at -20°C. Prior to *in situ* hybridisation, pharyngeal jaws were dissected from each specimen. For *in situ* hybridisation, a 311 bp amplicon from the zebrafish *slc34a2b* mRNA (NM_182877.2) was amplified from zebrafish cDNA (primer sequences: forward 5'-GAATCGCAAACTGCACTCCG-3'; reverse 5'-GAGGATGGCCAGGTATCCTG-3') using Taq polymerase Kit (Invitrogen, Waltam, MA, USA). The obtained PCR product was cloned into pCR4-TOPO vector using the TOPO TA Cloning Kit for Sequencing (Invitrogen, Waltam, MA, USA). The sequence of the cloned PCR product was confirmed by sequencing. Sense and antisense RNA probes were generated from 1 µg of linearised vector using MAXIscript™ T7/T3 Kit (Invitrogen, Waltam, MA, USA) and labelled with digoxigenin-dUTP of the DIG RNA labeling kit (Roche Diagnostics, Mannheim, Germany). RNA probes were treated with RNase-free DNase, recovered by ethanol precipitation according to manufacture's instructions and stored at -80°C. Whole mount *in situ* hybridisation was performed following the protocol described in Verstraeten et al. (2012) and imaged using Axio Imager-Z1 microscope (Carl Zeiss, Oberkochen, Germany) equipped with an Axiocam 503 colour camera (Carl Zeiss, Oberkochen, Germany). Following whole mount *in situ* hybridisation, the dissected pharyngeal jaws were embedded in glycol methacrylate (Witten et al., 2001). Cross sections of 3 µm were cut on a Microm HM 360 (Marshall Scientific, Hampton, NH, USA) automated microtome. Images were acquired using an Axio Imager-Z1

microscope (Carl Zeiss, Oberkochen, Germany) equipped with an Axiocam 503 colour camera (Carl Zeiss, Oberkochen, Germany).

***Statistical Analysis***

Quantitative variables are expressed as mean ± standard deviation, categories are expressed as percentages. Statistical analysis was performed using Past4.04 software (Hammer et al., 2001). Differences in the amount of young non-functional teeth and in the bone of attachment mineralisation were evaluated by means of a Chi-squared test followed by Bonferroni correction. Comparison of dentin thickness in ventral teeth was based on the non-parametric Mann-Whitney test followed by Bonferroni correction. Differences in the *osc*:GFP fluorescence signal were based on the Student's t-test followed by Bonferroni correction. A p-value less than 0.05 was considered significant.

# Chapter 7

## General discussion, future perspectives and concluding remarks

## General discussion

The research of the present thesis describes the effects of low (LP) and high (HP) dietary phosphorus (P) levels compared to a regular P (RP) diet in the zebrafish skeleton, at the tissue, cellular and molecular levels. The aim is to address questions related to the mechanisms of bone formation and bone mineralisation. The goal is to obtain insights into the relationship between bone matrix formation and bone mineralisation and to better understand human bone pathologies such as osteomalacia and hypermineralisation.

### *Uncoupling bone formation and bone mineralisation with low dietary P levels*

The LP zebrafish model recapitulates the bone phenotype that is typical for reduced P intake. This phenotype is also observed in other vertebrates, including mammals and other teleosts. Low dietary P levels cause an arrest of bone mineral deposition with no negative effects on bone matrix secretion. Similar observations have been reported from other teleosts, such as Atlantic salmon and Nile tilapia (Takagi and Yamada, 1991; Witten et al., 2016, 2019; Drábiková et al., 2021). Also mice and humans subjected to dietary P deprivation display a similar phenotype (Baylink et al., 1971; Bhambri et al., 2006; Bonjour, 2011). The results of hypophosphatemia are hypomineralised bones (osteomalacia) and rickets (Bhambri et al., 2006; Bonjour, 2011). The low mineralisation of LP zebrafish bone is extensively demonstrated using various imaging techniques, including whole mount staining of the skeleton with Alizarin red S, histology of non-demineralised samples, synchrotron X-ray tomographic microscopy reconstructions and micro-CT analysis. Of notice, micro-CT analysis performed only on the mineralised regions of the vertebral centra, shows a significant reduction in bone mineral density (BMD) in the autocentra of LP animals, that corresponds to reduced mineral content in those mineralised areas. Low BMD is typical of under-mineralised bones also in humans, where it reflects the presence of large amounts of non-mineralised osteoid rather than the reduction of bone matrix volume (Bhambri et al., 2006).

Still, bones are not only hypomineralised, but new bone matrix is formed and this matrix has no minerals. In zebrafish, the low P dietary intake results in an increased non-mineralised bone matrix formation consistent throughout the vertebral column. Locations of new bone matrix production are sites of bone growth, i.e. the vertebral body endplates and the periosteal surface of neural and haemal arches, but also the central region of the autocentra. Likewise, the increased amount of non-mineralised collagenous matrix is found in other teleosts and mammals, including humans and rats (Baylink et al., 1971; Takagi and Yamada, 1991; Bonjour, 2011; Witten et al., 2016, 2019; Drábiková et al., 2021).

Osteoblasts, the bone-forming cells, are responsible for the secretion of the non-mineralised osteoid. Osteoid formation continues uninterrupted under LP conditions, as discussed above. An increased osteoblast activity seems to be a logical explanation for the increased bone matrix production. Evidence for the increase of the osteoblast activity under LP conditions was first obtained at the cellular level by transmission electron microscopy (TEM) observations, that revealed enlarged endoplasmic reticulum cisternae in the osteoblasts from LP zebrafish, compared to controls and HP animals. This suggests that LP osteoblasts actively produce collagen matrix (Shapiro et al., 1977; Boivin et al., 1990), yet the increase synthesis has no effects on collagen quality and post-translational modifications at the structural level. Next, gene expression analysis confirmed the upregulation of collagen type I (*col1a1a*) under LP conditions, together with the upregulation of osteocalcin (*bglap*) demonstrated both at the molecular level and *in vivo*, indicating an increased osteoblast response under LP dietary conditions. The upregulation of genes coding for bone extracellular proteins and the intensified production of bone matrix indicate increased osteoblasts activity. This is further strengthen by the upregulation of other genes important for bone mineralisation (Chapter 4, see also below).

Contrary to LP conditions, excess dietary P intake can reduce bone formation in humans (Kemi et al., 2006; Dermience et al., 2015). Likewise, the results of this thesis suggest reduced bone formation in HP zebrafish, that is characterised by thinner, fully mineralised bone elements with an extremely narrow or absent osteoid layer

compared to LP and controls (RP diet). The other consequences of HP dietary intake are further discussed below.

The current findings support the idea that bone matrix secretion and bone mineralisation are uncoupled processes. The concept of uncoupling bone formation and bone mineralisation has been already proposed by Witten et al. (2016). This idea is based on the fact the osteoblasts produce the non-mineralised bone matrix (the osteoid) first, and mineralisation only occurs later. How late does mineralisation occur? In humans, osteoid mineralisation may start as late as 10 days after bone matrix formation (Boivin and Meunier, 2002). Mineralisation of bone matrix implies two successive steps: a rapid initial mineralisation on the calcification front followed by a slow process of delayed mineralisation, progressively adding about one-half of the mineral content on bone matrix (Boivin and Meunier, 2002). In this thesis, it is shown that mineralisation can be arrested in case of reduced mineral availability, but it is restored when enough minerals are provided. Thus, the formation of bone matrix that is capable of mineralisation occurs first, but the collagenous bone matrix mineralises only when the provided minerals are available in adequate concentrations (Witten et al., 2019; Drábiková et al., 2022).

***What is the trigger of increased bone formation?***

It is likely that the non-mineralised bone under LP conditions is subjected to more intense mechanical stimuli than the mineralised bone (Cotti et al., 2020), given that soft, non-mineralised, bone can easily bend and thus withstands compression without fracture (Currey, 1979; Witten et al., 2019; Drábiková et al., 2021). Thus, under LP conditions, higher mechanical stimulus might have triggered the osteoblasts to increase bone formation. It might also have triggered osteogenic cells to undergo metaplastic differentiation and to produce cartilage-like tissue instead of bone, resulting in chondroid bone type I formation (Beresford, 1981; Witten and Hall, 2015), a phenomenon well documented for teleosts, also in animals that are subjected to low dietary P intake (Helland et al., 2006; Witten and Hall, 2015; Hall and Witten, 2019; Drábiková et al., 2022). According to Beresford (1981), chondroid bone type I develops

from osteogenic cells, generally accompanies new bone and has an intermediate nature between bone and cartilage. There is evidence that chondroid bone/cartilage-like tissue develop in response to compression is transitional in teleosts. In salmon under LP conditions, and similar to the LP zebrafish, compression due to swimming generates chondroid bone/cartilage-like formation within the soft, non-mineralised, trabecular bone of the vertebral bodies (Drábiková et al., 2022). The complete recovery and resorption of the cartilage-like tissue was observed in salmon after eight months of sufficient P diet treatment (Drábiková et al., 2022). This suggests that late mineralisation prompts resorption and replacement of the chondroid bone with regular trabecular bone, given that non-mineralised matrix is protected from resorption (Chambers et al., 1984; Nordahl et al., 2000; Lassen et al., 2017). Also in zebrafish, mineralisation of the non-mineralised bone and partly of the chondroid bone occurs when adequate dietary P is provided, but probably the experiment did not last enough to observe a complete remodelling and mineralisation of the chondroid bone into mature bone.

How is the increased mechanical load translated into more bone? Osteocytes are mechanosensitive cells that secrete signalling molecules in response to mechanical stimuli. They regulate the activity of osteoblasts and osteoclasts (Franz-Odendaal et al., 2006; Klein-Nulend et al., 2013). Over 95% of human bone cells are osteocytes. Each human osteocyte has an average of 89 dendritic process, and each cubic millimetre bone contains 20.000-30.000 cells. There can be little doubt that bone formation and remodelling in response to mechanical load is regulated by osteocytes in mammals (Bonucci, 2009; Buenzli and Sims, 2015; Moharrer and Boerckel, 2021).

In teleosts, however, a different situation persists, given that the higher orders of teleost fish have bone without osteocytes (Moss, 1961; Witten et al., 2017). In zebrafish, bone is generally osteocytic, although osteocytes are not present in the developing vertebral column, and fin rays and scales remain anosteocytic throughout life (Witten et al., 2017). In adult zebrafish, vertebral bodies possess osteocytes although less abundant compared to mammalian bone (Kague et al., 2021). Moreover, osteocytic lacunae are smaller and with less numerous canaliculi compared to mice and

humans (Fiedler et al., 2018; Suniaga et al., 2018; Busse et al., 2020). However, despite the low osteocyte connectivity, bone formation in response to mechanical load occurs in zebrafish (Suniaga et al., 2018), but likewise, also acellular bone of advanced teleosts shows a typical response to mechanical load (Huysseune et al., 1994; Ofer et al., 2019). In the presence of scarce or absent osteocyte connectivity, as in zebrafish or in anosteocytic bone of advanced teleosts, bone formation might be achieved differently. It is hypothesised that osteoblasts and bone lining cells could function as alternative receptors for mechanical load (Witten and Hall, 2015; Suniaga et al., 2018). In contrast, the increased bone matrix production is not observed in zebrafish fed regular (RP) dietary P, and animals that received high (HP) dietary P have even thinner bone structures compared to controls. Also, the mineralisation degree in RP and HP bone is higher than under the LP diet. It could be assumed that mineralised bone better tolerate mechanical load, preventing the intensified stimulus that is, instead, perceived by the mechanosensitive receptors under LP conditions. In other words, it could be suggested that mineralisation itself contributes to scale down the signalling pathways leading to increased bone matrix production.

***Comparison of different animal models with increased bone***

Zebrafish is widely used as a model in studies of bone and bone diseases, but often studies do not distinguish between bone formation and bone mineralisation. Instead, mineralisation is equated with bone formation. Micro-CT is one of the most used techniques to image the zebrafish skeleton, but without contrasting agents only mineralised tissues are recorded. Moreover, the resolution of standard micro-CT units is sufficient to visualize mouse bone structures but insufficient to visualize bone structures of zebrafish, resulting in a loss of information on aspects such as cells and non-mineralised tissues (Bruneel and Witten, 2015; Witten et al., 2017; Tonelli et al., 2020a). As an alternative, the much older technique of Alizarin red S whole mount staining shows the mineralised parts of the bone and by using oblique illumination it can also show non-mineralised bone structures (Bruneel and Witten, 2015; Witten et al., 2017; Tonelli et al., 2020a).

Similar to the findings of our study, but different in the way bone formation is stimulated, two recent studies show that exercise triggers bone formation in zebrafish and medaka, with substantial increase in osteoblast number and bone volume (Suniaga et al., 2018; Ofer et al., 2019). However, most studies on zebrafish models show enhanced bone mineralisation but not improvements in bone formation. For example, the *stocksteif* zebrafish is characterised by early hypermineralisation of the notochord, resulting in fused vertebral bodies and impaired intervertebral ligaments (Spoorendonk et al., 2008). Similarly, *enpp1* mutants exhibit pathological mineralisation and fused vertebrae due to the lack of Enpp1, that generates the mineralisation inhibitor PPi, as discussed above (Apschner et al., 2014). Also, the *abcc6* zebrafish mutant, model for ectopic mineralisation diseases such as pseudoxanthoma elasticum (PXE) and generalised arterial calcification of infancy (GACI), present increased mineralisation of the vertebral column, especially in the intervertebral regions (Mackay et al., 2015). Moreover, other mutants present an osteopetrosis phenotype, with an increased bone mass of poor quality caused by decreased bone resorption by osteoclasts. This is the case of the *panther* zebrafish, characterised by a decreased number of osteoclasts and malformations in neural and haemal arches (Chatani et al., 2011), and the *cathepsin k* transgenic medaka, in which reduced osteoclast activity results in excess bone accumulation at vertebral bodies and arches locations (To et al., 2012, 2015). Osteopetrosis is also being studied in mouse models, carrying recessive or dominant mutations in genes associated to osteopetrosis in humans. Although with some phenotypic variability, osteopetrotic mice suffer from increased bone mass with poor quality in both long bones and vertebrae, increased BMD, increased osteoclasts number with reduced resorbing activity (Kornak et al., 2001; Van Wesenbeeck and Van Hul, 2005; Del Fattore et al., 2008; Alam et al., 2014).

In contrast to these and other models (reviewed by Lleras-Forero et al., 2020), in our zebrafish with LP dietary history the entire vertebral column is fully functional. Neural and haemal arches show signs of allometric growth with normal osteoclast activity, as expected based on the literature (Witten et al., 2001; Witten and Huysseune, 2009). Autocentra have an increased bone volume but show intact

intervertebral ligaments and an intact notochord tissue in the intervertebral space. Thus, the uniqueness of the LP zebrafish model relies on promoting healthy bone formation during a long-term experiment (from juvenile stages till adulthood) by dietary means only, without impairing of the function of the vertebral column (see also below).

***Relationship between dietary P levels, bone mineralisation and bone mechanical properties***

Under low dietary P conditions, the arrest of bone mineralisation is the predominant effect observed on the zebrafish skeleton. Conversely, in zebrafish that received the RP (control) diet, bone mineralisation is in line with previous studies that traced zebrafish skeletal mineralisation (Bird and Mabee, 2003). All bone structures analysed in the RP group show a small amount of non-mineralised bone, identifiable as osteoid, at sites of bone growth. In the HP group, instead, bone elements are further mineralised, with very narrow or absent osteoid.

It is well documented that bone mineralisation is linked to plasma P levels. Osteomalacia/hypomineralised bones in patients are generally characterised by decreased P in the plasma (Bhambri et al., 2006). Similarly, low P plasma levels are found in salmon fed a low P diet (Drábiková et al., 2021). Conversely, high dietary P increases plasma P levels in salmon, that exhibit a bone mineralisation extent similar to HP zebrafish (Drábiková et al., 2021). Moreover, excess dietary P leads to high plasma P concentrations in mammals, leading to abnormal vascular calcification in humans (Jono et al., 2000; Chen et al., 2002; Leopold, 2015) and kidney calcification in dogs (Saville and Krook, 1969; Krook et al., 1971; Laflamme and Jowsey, 1972; Cook et al., 1983).

An increase of dietary P induces late mineralisation of previously non-mineralised LP bone matrix, as demonstrated in freshwater and early seawater stages of Atlantic salmon (Witten et al., 2019; Drábiková et al., 2021). Bone mineralisation is resumed, as shown by histology and by increased BMD values. The observation that mineralisation resumes similar BMD values, yet slightly lower values than controls, likely relates to the duration of the feeding phase with RP and HP diets, respectively.

Bone biomechanical properties depend on the bones' mineral content as one important factor (Currey, 2003). Proper mechanical function of bone relies on a balance between toughness, provided by the collagenous matrix, and stiffness, provided by the mineral phase (Currey, 2003). Fast growing bones with reduced mineral content (about 50% compared to mammalian long bones), such as the antlers of deers and elks, represent extremely though mammalian bone materials that can flex and resist enormous compression forces without fracture (Currey, 2003; Veis, 2003). Likewise, LP zebrafish bone presents lowered elastic modulus and hardness, indicating increased bone toughness. Excess mineralisation, on the other hand, makes bone stiff and brittle and increases the risk of fractures (Wilton et al., 1987; Currey, 2003; Guglielmi et al., 2011). This is the case in rats, where excess dietary P intake promotes bone hypermineralisation which leads to a reduction of bone strength (Huttunen et al., 2007). Similarly, the HP zebrafish bone is characterised by a higher elastic modulus. This suggests that increased dietary P intake induces bone hypermineralisation, leading to a higher bone stiffness (Currey, 2003; Pinheiro et al., 2009; Witten et al., 2019). Conversely, the reduced dietary P intake improved the bone biomechanical properties by enhancing toughness and reducing stiffness (Witten et al., 2019; Drábiková et al., 2021), thus resulting in a decreased fracture risk (Currey, 2003; Witten et al., 2019; Cotti et al., 2020; Drábiková et al., 2021).

***Link between dietary P levels and skeletal malformations***

In mammals and teleosts, P insufficiency is thought to be a primary cause of skeletal malformations. Patients with hypophosphatemia present short stature, bowing of long bones and deformed vertebral column (Bishop, 1848; Anderson, 1878; Francis et al., 1995). Teleosts under farming conditions can display reduced growth, vertebral column and jaw deformities related to dietary P deficiency (Sullivan et al., 2007; Deschamps et al., 2008; Fjelldal et al., 2012; Poirier Stewart et al., 2014; Baeverfjord et al., 2019). However, studies on Atlantic salmon under tightly controlled experimental conditions (avoidance of stress, no handling, no vaccination, control of all environmental parameters) with dietary P as a single variable do not show a direct

relationship between low dietary P intake and vertebral column malformations (Witten et al., 2016, 2019; Drábiková et al., 2021). Likewise, despite the arrest of mineralisation, the non-mineralised bone in LP zebrafish does not present signs that would foreshadow skeletal malformations. Yet, the LP vertebral bodies show increased trabecular bone volume characterised by patches of chondroid bone. Similarly, salmon under LP conditions developed chondroid bone/cartilage-like tissues within the soft non-mineralised trabecular bone, which is interpreted as a response to compression due to swimming (Drábiková et al., 2022). However, like human bone trabeculae, also trabecular structures in salmon are formed in response to the trajectories of mechanical load. Consequently, in salmon, complete recovery and resorption of the cartilage-like tissue and the re-establishment of a regular trabecular pattern occur after eight months of sufficient P diet treatment. This indicates that, evidently, the chondroid bone/cartilage-like formation is transitional in this teleost species (Drábiková et al., 2022). Teleost vertebral centra indeed undergo adaptive modelling and shape changes in response to mechanical stress during locomotion (Laerm, 1976). It is likely that also in zebrafish, mineralisation of the chondroid bone under prolonged adequate dietary P could occur, given the results based on the salmon study.

Besides the likely transitional chondroid bone formation, the structure of the non-mineralised bone in zebrafish is normal. Bone formation is stimulated outside the notochord. Autocentra with increased bone volume present intact intervertebral ligaments and an intact notochord in the intervertebral space. Thus, the findings of the present thesis strengthen the idea that, in zebrafish, reduced dietary P alone is not a primary cause of vertebral column malformations, of which the development might be triggered by other or additional factors, such as different diet composition and rearing density (Costa et al., 2018; Martini et al., 2020).

Different from the LP diet that failed to generate skeletal malformations in zebrafish, the HP diet promotes vertebral centra fusion. Likewise, factors that increase the bone mineralisation in other zebrafish mutants favour the development of vertebral column malformations. For example, the lack of ectonucleotide pyrophosphatase/phosphodiesterase 1 (*enpp1*) in zebrafish reduces pyrophosphate

(PPi), a mineralisation inhibitor, and results in hypermineralised bone and fused vertebral centra (Apschner et al., 2014). Also, the *stocksteif* zebrafish is characterised by early hypermineralisation of the notochord, that results in fused vertebral bodies and impaired intervertebral ligaments (Spoorendonk et al., 2008). Based on these evidences, excess bone mineralisation related to increased dietary P intake, disease conditions or ageing (Kague et al., 2021), is known to increase vertebral column malformations in zebrafish. Hence, hypermineralisation alone can be considered a risk factor for skeletal malformations and excess dietary P intake should be avoided.

***Mineralisation: an active or passive process?***

The low dietary P intake highlighted the uncoupling of bone formation and bone mineralisation. Both bone formation and bone mineralisation depend on osteoblasts (Klein-Nulend et al., 2013), but mineralisation per se seems to be a passive process. In bone, regular mineralisation is mainly driven by the absence of the mineralisation inhibitor PPi. In soft tissues, ectopic mineralisation is mainly driven by the absence of the mineralisation inhibitor matrix Gla protein (MGP) (Roy and Nishimoto, 2002; Sweatt et al., 2003). The removal of PPi in animal models lacking the progressive ankylosis protein homolog (ANK) or the ectonucleotide pyrophosphatase/phosphodiesterase 1 (ENPP1) is sufficient for ectopic mineralisation to occur (Ho et al., 2000; Koshizuka et al., 2001; Apschner et al., 2014). An imbalance between the PPi/P ratio, in favour of P concentration, can also trigger ectopic mineralisation of soft tissues (Murshed, 2018). Also, high P plasma concentrations result in blood vessels and kidney calcification in mammals, including humans (Saville and Krook, 1969; Cook et al., 1983; Jono et al., 2000; Leopold, 2015).

In bone, osteoblasts produce the membrane-bound tissue non-specific alkaline phosphatase (TNAP) that also hydrolyses PPi and promotes mineralisation (Hessle et al., 2002). Under normal, non-pathological conditions, upon removal of PPi, the collagen-based bone matrix undergoes mineralisation (Murshed et al., 2005). Under LP conditions, mineralisation does not occur due the lack of sufficient P. Still, in zebrafish, osteoblasts actively respond to counteract the lack of minerals, by upregulating genes

fundamental for mineralisation, e.g. the tissue non-specific alkaline phosphatase (*alpl*). Also, other genes involved in mineralisation and phosphate metabolism are upregulated under low dietary P conditions, suggesting that osteoblasts play an active role in providing the proteins that regulate mineralisation. Yet, bone mineralisation does not occur until sufficient dietary P is provided (Chapter 4; Witten et al., 2019). Interestingly, when enough dietary P is available, bone mineralisation resumes deep inside the bone and continuously with the last mineralised part of the bone, as evidenced by zebrafish and salmon (Chapter 4; Witten et al., 2019). Given that mineralisation resumes far away from the bone surface and from the osteoblasts, likely these cells are not the only player in the mineralisation, given that mineralisation occurs even in cell-free conditions, as long as calcium and P are supplied in the medium (Hamlin and Price, 2004; Witten et al., 2019). *In vitro* it is possible to induce spontaneous mineralisation by adding purified collagen type I to a metastable solution of calcium phosphate (Fleisch, 1982).

In contrast, studies on dental tissues point to an active mineralisation process of the enamel in mammals (Merametdjian et al., 2017) and of the enameloid in zebrafish. The zebrafish experiment shows that dentin and bone of attachment structures are affected by dietary P deficiency. Similar to bone, their mineralisation responds to different P levels, but different from bone, dentin continues to increase mineralisation slowly. Opposite, enameloid reaches its hypermineralised status regardless of dietary P intake. There is evidence of an active mineralisation process, that relies on the transport of P ions by the ameloblasts, that contribute to enameloid formation together with odontoblasts (Sasagawa et al., 2009). The Na-P co-transporter gene *Slc34a2* is expressed in mature ameloblasts in mice (Merametdjian et al., 2017). As shown here for the first time, *slc34a2b* is expressed at the tooth tip in zebrafish, where the inner dental epithelium is located. Moreover, in mice, specific antibody for Slc34a2 localises the transporter in the cellular portion of ameloblasts directly in contact with enamel (Merametdjian et al., 2017). Overall, these data indicate that the specific Na-P co-transporter Slc34a2 is responsible for the active P transport in the extracellular space. Ameloblasts, different from odontoblasts and osteoblasts, actively

contribute to the mineralisation of enamel/enameloid, given that even under LP conditions enameloid in zebrafish is hypermineralised, whereas dentin and bone display the typical low mineralisation phenotype.

***Extra-skeletal effects of low and high dietary P treatment***

Dietary P influences various aspects of intermediary metabolism, especially energy metabolism, thus affecting growth and feed conversion. That P deficiency disturbs growth in teleost fish is documented (Sugiura et al., 2004; Witten et al., 2016), similar to the findings on LP zebrafish that exhibited reduced standard length indicative of growth retardation. In contrast, high dietary P induced the fastest growth in juvenile zebrafish. This imposed an issue in the selection of samples for those analyses that required animals of similar size. To do so, LP zebrafish selected were among the largest animals in their group, whereas the HP fish were among the smallest. However, animals under the LP diet demonstrated continuous growth during the treatment period. Eventually, LP fish could reach a similar size as the control fish during a prolonged feeding trial (personal observation).

Importantly, P requirements are not influenced only by the feeding duration, but also on the feed efficiency and on the availability of P in the diet. The P diets used for the experiments contained monoammonium phosphate (MAP) as source of P, which was demonstrated to have high P bioavailability and high P retention efficiency in teleosts (Morales et al., 2018). Thus, the LP zebrafish model presented here does not represent an extreme dietary P deficiency condition. Is it likely that the LP zebrafish could efficiently use the available dietary P by adjusting hormonal regulation, in order to promote renal P reabsorption and to enhance intestinal P absorption (Takeda et al., 2012). An efficient use of dietary P could sustain the main physiological processes, although growth delay was observed. In contrast, high dietary P could lead to severe consequences, such as kidney stones and calcification of soft tissues (Razzaque, 2011; Komaba and Fukagawa, 2016). These side effects were not observed in the HP zebrafish. It could be speculated that zebrafish under HP conditions increased renal P

excretion to lower P plasma levels, as observed in other teleosts fed HP diets (Sugiura et al., 2000; Drábiková et al., 2021).

Reduced dietary P intake is known to influence the P levels in plasma and in tissues, such as muscles (reviewed by Sugiura et al., 2004). Experiments on P deprivation in rainbow trout markedly reduced P levels in muscles, but the levels of ATP, glucose-6-phosphate and creatinine phosphate remained stable (Sugiura et al., 2000), indicating no negative effects on muscle performance. Likewise, LP zebrafish did not show altered swimming behaviour nor altered muscle contraction, although the above mentioned parameters have not been measured. An additional observation derives from training experiments of LP zebrafish, performed using a swim tunnel equipment. During the training, LP fish could swim against the laminar flow with no signs that would foreshadow issues on muscle performance (Di Biagio, 2022).

P is required also during gametes maturation (Sugiura et al., 2004). However, P content in the ovary is much less than in the whole body, as demonstrated in rainbow trout (Shearer, 1984). Fish may not require high dietary P to increase ovary weight, as many species reduce their feed intake or even starve during sexual maturation (Sugiura et al., 2004). Moreover, red seabream (*Chrysophrys major*) fed increased P diet had lower fecundity, and produced eggs of much lower hatchability and higher abnormality than those fed a regular diet (Watanabe et al., 1984b, 1984a). Similar observations derive from the LP zebrafish, that produced several hundred eggs, even during the training experiment mentioned above (personal observation; Di Biagio, 2022). Besides the high fecundity of LP female zebrafish, no phenotypic differences associated to dietary P levels could be observed between male and female animals.

# Future perspectives

### *Low dietary P as a possible treatment for hypermineralised bone diseases*

Excess bone mineralisation due to increased P intake, aging or diseases, makes bone stiff and brittle and more prone to fracture and to develop malformations (as discussed above and in Wilton et al., 1987; Currey, 2003; Guglielmi et al., 2011). Hypermineralisation characterises also the "brittle bone disease" osteogenesis imperfecta (OI), a group of heritable disorders affecting bone and other connective tissues with collagen type I as main matrix component (Forlino and Marini, 2016). Major clinical features of OI patients are skeletal deformities, scoliosis, vertebral compression fractures and fractures of long bones (Sillence et al., 1979; Benson and Newman, 1981; Zeitlin et al., 2003; Marini et al., 2017). A comparable bone phenotype characterises murine and, as shown here particularly for fractures, zebrafish OI models (Kalajzic et al., 2002; Fisher et al., 2003; Uveges et al., 2008; Enderli et al., 2016; Gioia et al., 2017; Fiedler et al., 2018).

The severe bone phenotype of dominant forms of OI is caused by structural alterations in collagen type I, that lead to impaired secretion of aberrant collagen by osteoblasts, resulting in low bone mass and bone fragility in both patients and animal models (Kalajzic et al., 2002; Marini et al., 2007; Uveges et al., 2008; Ishikawa and Bächinger, 2013; Gioia et al., 2017; Fiedler et al., 2018). Eventually, hypermineralisation of the defective bone matrix leads to bone fragility, impaired bone biomechanical properties and poor bone quality, both in OI patients and in zebrafish models (Zeitlin et al., 2003; Fiedler et al., 2018).

Hypermineralisation is typical of OI and it is independent of the mutation type (Nijhuis et al., 2019). The size of mineral crystals size does not differ between OI type I and normal bone, but OI bone is characterised by a larger number of crystals in the same matrix volume compared to healthy bone (Fratzl-Zelman et al., 2014). The OI bone matrix contains collagen fibrils with a smaller diameter, and the individual collagen molecules within the fibril are more widely spaced, likely due to the steric hindrance caused by over-modification of collagen type I (Notbohm et al., 1999; Nijhuis

et al., 2019). Because of this increase in space, more crystals can be accommodated between the collagen molecules, resulting in the abnormally high bone matrix mineralisation (Nijhuis et al., 2019). Thus, lowering the bone mineral content could possibly alleviate skeletal defects related to bone hypermineralisation. In this thesis and in the literature, there is evidence that a reduction of dietary P intake reduces the total bone mineral content, increases formation of non-mineralised bone matrix, and overall improves the bone biomechanical properties by enhancing toughness and reducing stiffness (Witten et al., 2019; Cotti et al., 2020; Drábiková et al., 2021).

The reduced dietary P treatment performed on the *Chihuahua* (*Chi/+*) zebrafish, model of dominant OI, was able to partially rescue the severe bone phenotype of this animal model. Under LP conditions, *Chi/+*$_{LP}$ zebrafish present a reduced incidence of vertebral column deformities compared to untreated *Chi/+*, and the shape of the *Chi/+*$_{LP}$ vertebral centra better resembles the one of WT zebrafish, while untreated *Chi/+* have severely distorted vertebral bodies. Moreover, the LP treatment restores the non-mineralised osteoid at vertebral centra growth zones in *Chi/+*$_{LP}$, that was undetectable in untreated *Chi/+*, as also found in patients and murine OI models (Stöß et al., 1986; Iwamoto et al., 2002; Kalajzic et al., 2002; Uveges et al., 2008). The absent or reduced osteoid thickness in OI is a sign of reduced bone formation by osteoblasts (Kalajzic et al., 2002; Uveges et al., 2008; Fedarko, 2014), caused by intracellular retention of mutated collagen and endoplasmic reticulum (ER) stress (Ishikawa and Bächinger, 2013), evident in both *Chi/+*$_{LP}$ and *Chi/+* mutants. However, mutant zebrafish that received the LP diet show improved extracellular bone matrix with less dense collagen fibrils, indicative for a more typical osteoid. How this result could be explained, given that the mutation in *col1a1a* cannot be corrected? In the present thesis, an increased osteoblast activity is shown under LP conditions in WT zebrafish. It is reasonable to assume that also *Chi/+*$_{LP}$ osteoblast could be subjected to increased cellular activity and, possibly, increased production of collagen type I (both normal and mutated) within the ER. In patients and in the Brtl IV mouse, model of dominant OI, it was demonstrated that collagen molecules containing mutated $\alpha$(I) chains are partially retained and subsequently degraded inside the cells (Raghunath et

al., 1994; Forlino et al., 2007). In the *Chi/+* zebrafish, the selective intracellular degradation of aberrant collagen might favour the secretion of normal collagen molecules especially in the *Chi/+*$_{LP}$, where osteoblast activity could be increased. This would explain the improved collagen matrix observed at the ultrastructure level in the *Chi/+* zebrafish under LP conditions. Taken together, these findings suggest that a reduced dietary P intake can alleviate the severe bone phenotype in *Chi/+* zebrafish, likely due to a reduction of the bone mineral content and to a selective intracellular degradation of mutated collagen. Thus, the LP dietary treatment has the potential to alleviate skeletal defects related to bone hypermineralisation.

***Alternating dietary P levels to reverse bone loss due to aging or disease conditions***

Age-related bone loss due to osteoporosis/osteopenia or by other syndromes that cause skeletal fragility represents a major health problem for humans (Greco et al., 2019). The reduced trabecular density and poor trabecular connectivity of bone in such conditions cause bone fragility, that has an enormous negative impact on the quality of life (Myers and Wilson, 1997; Seeman, 2003). Bone loss is usually accompanied by an imbalance between bone formation and bone resorption. Increased bone resorption together with little formation of new bone, leads to trabecular thinning typical of osteoporotic conditions (Seeman, 2003). Thus, increasing formation of new, less mineralised, bone appears to be a more promising approach to reduce bone loss and to reverse bone fragility.

The LP dietary treatment stimulates formation of new, non-mineralised bone, characterised by increased toughness and reduced stiffness (Currey, 2003; Witten et al., 2019; Drábiková et al., 2021). The enormous amount of non-mineralised bone formed under LP conditions can mineralise when adequate P is provided, as shown in zebrafish and salmon (Witten et al., 2019; Drábiková et al., 2022). In zebrafish, when the non-mineralised bone (formed under LP treatment) mineralises, the result is a dramatic increase in mineralised bone volume, that appears to be permanent in zebrafish, at least within the time frame of the experiment. Yet, this newly mineralised bone shows slightly lowered BMD values compared to controls. This suggests that,

before a complete mineralisation is reached, the newly mineralised bone likely has improved mechanical properties, given the lower mineral content in comparison to controls.

Although it has been suggested that reducing P in human diet could be difficult (Masuyama et al., 2001), the approach tested here in zebrafish can possibly contribute to design new therapeutic approaches. Additional studies on mammalian models are required to determine the optimal periods of reduced and sufficient P intake. Based on a previous study, treatment of WT mice with a low P diet for 4 weeks, starting from weaning (3 weeks of age), did not affect BMD and breaking force of the femur, but slightly reduced its mineral content (Masuyama et al., 2001). This could represent a starting point for future investigations, with the aim to ultimately translate the reduced/sufficient dietary P approach for treatment of patients. Furthermore, osteoanabolic agents, e.g. parathyroid hormone receptor agonists and anti-sclerostin antibodies, could be used in combination with a reduced dietary P intake to further stimulate bone matrix production in the treatment of bone loss in humans.

In conclusion, a fine-tuned approach of alternating low and sufficient dietary P intake, and possibly the combination with osteoanabolic compounds, has the potential to reverse bone loss, by generating more non-mineralised bone that can subsequently mineralise. Still, if the complete mineralisation is not reached by switching back to a low dietary P intake, the bone formed will likely have a reduced mineral content and thus will be more resistant to fractures (Currey, 2003; Witten et al., 2019; Drábiková et al., 2021).

## Concluding remarks

In the present thesis, the experiments performed on zebrafish helped to elucidate the effects of reduced and increased dietary P supply on the skeleton, to better understand the relationship between bone formation and mineralisation, and the mechanisms underlying osteomalacia and excess mineralisation.

First, the low dietary P conditions showed that bone formation and bone mineralisation are uncoupled processes. Bone formation occurs independent from mineralisation, that happens later when sufficient P is available. In addition, LP condition alone is not a primary cause of skeletal malformations in zebrafish.

Second, the low dietary P treatment stimulates formation of an enormous amount of non-mineralised bone, thus characterised by a reduced BMD and increased toughness. Also, in bone hypermineralisation conditions such as in OI, the LP treatment partially improves the bone phenotype in the *Chi/+* zebrafish, likely by reducing the bone mineral content. Translated to biomedical problems, the LP approach has the potential to mitigate skeletal defects related to bone hypermineralisation in fragility syndromes.

Third, the large amount of bone formed under LP conditions is able to mineralise as soon as sufficient P is provided. The alternation of low P and high P dietary conditions is able to increase bone volume in zebrafish, first by stimulating matrix formation under LP conditions, and subsequently inducing the mineralisation of newly formed bone by providing adequate dietary P. Thus, in the biomedical context, the low P/high P approach can possibly contribute to reverse osteoporosis and ageing-related bone loss.

# References


Abdelaziz, D. M., Abdullah, S., Magnussen, C., Ribeiro-da-Silva, A., Komarova, S. V, Rauch, F., and Stone, L. S. (2015). Behavioral signs of pain and functional impairment in a mouse model of osteogenesis imperfecta. *Bone* 81, 400–406. doi: 10.1016/j.bone.2015.08.001.

Alam, I., Gray, A. K., Chu, K., Ichikawa, S., Mohammad, K. S., Capannolo, M., Capulli, M., Maurizi, A., Muraca, M., Teti, A., Econs, M. J., and Del Fattore, A. (2014). Generation of the first autosomal dominant osteopetrosis type II (ADO2) disease models. *Bone* 59, 66–75. doi: 10.1016/j.bone.2013.10.021.

Anderson, H. C., Sipe, J. B., Hessle, L., Dhanyamraju, R., Atti, E., Camacho, N. P., Millán, J. L., and Dhamyamraju, R. (2004). Impaired calcification around matrix vesicles of growth plate and bone in alkaline phosphatase-deficient mice. *Am. J. Pathol.* 164, 841–847. doi: 10.1016/s0002-9440(10)63172-0.

Anderson, J. J. B., Rondano, P., and Holmes, A. (1996). Roles of Diet and Physical Activity in the Prevention of Osteoporosis. *Scand. J. Rheumatol.* 25, 65–74. doi: 10.3109/03009749609103752.

Anderson, M. F. (1878). Phosphates in nutrition, and the mineral theory of consumption and allied diseases. *Edinb. Med. J.* 24, 449–453.

Apschner, A. (2014). *Putting crystals in place - the regulation of biomineralization in zebrafish (PhD thesis)*. Utrecht, The Netherlands: Utrecht University.

Apschner, A., Huitema, L. F., Ponsioen, B., Peterson-Maduro, J., and Schulte-Merker, S. (2014). Zebrafish *enpp1* mutants exhibit pathological mineralization, mimicking features of generalized arterial calcification of infancy (GACI) and pseudoxanthoma elasticum (PXE). *Dis. Model Mech.* 7, 811–822. doi: 10.1242/dmm.015693.

Apschner, A., Schulte-Merker, S., and Witten, P. E. (2011). Not all bones are created equal - using zebrafish and other teleost species in osteogenesis research. *Methods Cell. Biol.* 105, 239–255. doi: 10.1016/B978-0-12-381320-6.00010-2.

Arnold, A., Dennison, E., Kovacs, C. S., Mannstadt, M., Rizzoli, R., Brandi, M. L., Clarke, B., and Thakker, R. V (2021). Hormonal regulation of biomineralization. *Nat. Rev. Endocrinol.* 17, 261–275. doi: 10.1038/s41574-021-00477-2.

Arratia, G., Schultze, H. P., and Casciotta, J. (2001). Vertebral column and associated elements in dipnoans and comparison with other fishes: development and homology. *J. Morphol.* 250, 101–172. doi: 10.1002/jmor.1062.

Atkins, G. J., Rowe, P. S., Lim, H. P., Welldon, K. J., Ormsby, R., Wijenayaka, A. R., Zelenchuk, L., Evdokiou, A., and Findlay, D. M. (2011). Sclerostin is a locally acting regulator of late-osteoblast/preosteocyte differentiation and regulates mineralization through a MEPE-ASARM-dependent mechanism. *J. Bone Miner. Res.* 26, 1425–1436. doi: 10.1002/jbmr.345.

Bacchetta, J., and Salusky, I. B. (2012). Evaluation of hypophosphatemia: lessons from patients with genetic disorders. *Am. J. Kidney. Dis.* 59, 152–159. doi: 10.1053/j.ajkd.2011.08.035.

Backiel, T., Kokurewicz, B., and Ogorzałek, A. (1984). High incidence of skeletal anomalies in carp, *Cyprinus carpio*, reared in cages in flowing water. *Aquaculture* 43, 369–380. doi: 10.1016/0044-8486(84)90245-X.

Baeverfjord, G., Antony Jesu Prabhu, P., Fjelldal, P. G., Albrektsen, S., Hatlen, B., Denstadli, V., Ytteborg, E., Takle, H., Lock, E. -J., Berntssen, M. H., Lundebye, A. -K., Åsgård, T., and Waagbø, R. (2019). Mineral nutrition and bone health in salmonids. *Rev. Aquacult.* 11, 740–765. doi: 10.1111/raq.12255.

Baeverfjord, G., Åsgård, T., and Shearer, K. D. (1998). Development and detection of phosphorous deficiency in Atlantic salmon, *Salmo salar* L., parr and post-smolts. *Aquacult. Nutr.* 4, 1–11. doi: 10.1046/j.1365-2095.1998.00095.x.

Balon, E. K. (2003). “Alternative ontogenies and evolution: a farewell to gradualism,” in *Environment, development, and evolution. Toward a synthesis*, eds. B. K. Hall, R. D. Pearson, and G. B. Müller (Cambridge, UK: The MIT Press), 37–66. doi: 10.7551/mitpress/2775.003.0006.

Bambino, K., and Chu, J. (2017). “Zebrafish in toxicology and environmental health,” in *Zebrafish at the interface of development and disease research*, ed. K. Sadler (Academic Press), 331–367. doi: 10.1016/bs.ctdb.2016.10.007.

Baron, R., Gertner, J. M., Lang, R., and Vignery, A. (1983). Increased bone turnover with decreased bone formation by osteoblasts in children with osteogenesis imperfecta tarda. *Pediatr. Res.* 17, 204–207. doi: 10.1203/00006450-198303000-00007.

Baron, R., Rawadi, G., and Roman-Roman, S. B. T. (2006). Wnt signaling: a key regulator of bone mass. *Curr. Top. Dev. Biol.* 76, 103–127. doi: 10.1016/S0070-2153(06)76004-5.

Bartlett, J. D. (2013). Dental enamel development: proteinases and their enamel matrix substrates. *Int. Sch. Res. Not. - Dent.* 2013, 684607. doi: 10.1155/2013/684607.

Baylink, D., Stauffer, M., Wergedal, J., and Rich, C. (1970). Formation, mineralization, and resorption of bone in vitamin D-deficient rats. *J. Clin. Invest.* 49, 1122–1134. doi: 10.1172/JCI106328.

Baylink, D., Wergedal, J., and Stauffer, M. (1971). Formation, mineralization, and resorption of bone in hypophosphatemic rats. *J. Clin. Invest.* 50, 2519–2530. doi: 10.1172/JCI106752.

Bellido, T. (2014). Osteocyte-driven bone remodeling. *Calcif. Tissue Int.* 94, 25–34. doi: 10.1007/s00223-013-9774-y.

Ben Amor, I. M., Roughley, P., Glorieux, F. H., and Rauch, F. (2013). Skeletal clinical characteristics of osteogenesis imperfecta caused by haploinsufficiency mutations in *COL1A1*. *J Bone Min. Res* 28, 2001–2007. doi: 10.1002/jbmr.1942.

Benjamin, M. (1990). The cranial cartilages of teleosts and their classification. *J. Anat.* 169, 153–172.

Benjamin, M., and Ralphs, J. R. (1991). Extracellular matrix of connective tissues in the heads of teleosts. *J. Anat.* 179, 137–148.

Benjamin, M., Ralphs, J. R., and Eberewariye, O. S. (1992). Cartilage and related tissues in the trunk and fins of teleosts. *J. Anat.* 181, 113–118.

Bensimon-Brito, A., Cancela, M. L., Huysseune, A., and Witten, P. E. (2012a). Vestiges, rudiments and fusion events: the zebrafish caudal fin endoskeleton in an evo-devo perspective. *Evol. Dev.* 14, 116–127. doi: 10.1111/j.1525-142X.2011.00526.x.

Bensimon-Brito, A., Cardeira, J., Cancela, M. L., Huysseune, A., and Witten, P. E.

(2012b). Distinct patterns of notochord mineralization in zebrafish coincide with the localization of osteocalcin isoform 1 during early vertebral centra formation. *BMC Dev. Biol.* 12, 28. doi: 10.1186/1471-213X-12-28.

Bensimon-Brito, A., Cardeira, J., Dionísio, G., Huysseune, A., Cancela, M. L., and Witten, P. E. (2016). Revisiting in vivo staining with alizarin red S - a valuable approach to analyse zebrafish skeletal mineralization during development and regeneration. *BMC Dev. Biol.* 16, 2. doi: 10.1186/s12861-016-0102-4.

Benson, D. R., Donaldson, D. H., and Millar, E. A. (1978). The spine in osteogenesis imperfecta. *J. Bone Joint Surg. Am.* 60, 925–929. doi: 10.2106/00004623-197860070-00009.

Benson, D. R., and Newman, D. C. (1981). The spine and surgical treatment in osteogenesis imperfecta. *Clin. Orthop. Relat. Res.* 159, 147–153.

Beresford, W. A. (1981). *Chondroid bone, secondary cartilage and metaplasia*. München, Germany: Urban & Schwarzenberg.

Beresford, W. A. (1993). "Cranial skeletal sissues: diversity and evolutionary trends," in *The skull, Volume 2. Patterns of structural and systematic diversity*, eds. J. Hanken and B. K. Hall (Chiacago: The University of Chicago Press), 69–130.

Bergot, C. (1975). Mise en évidence d'un type particulier de dentine chez la truite (*Salmo* sp., Salmonidés, Téléostéens). *Bull. Soc. Zool. Fr.* 100, 587–594.

Berkovitz, B. K. B., and Shellis, R. P. (2016). *The teeth of non-mammalian vertebrates*. Amsterdam: Elsevier Academic Press doi: 10.1016/C2014-0-02210-1.

Bhambri, R., Naik, V., Malhotra, N., Taneja, S., Rastogi, S., Ravishanker, U., and Mithal, A. (2006). Changes in bone mineral density following treatment of osteomalacia. *J. Clin. Densitom.* 9, 120–127. doi: 10.1016/j.jocd.2005.11.001.

Bird, N. C., and Mabee, P. M. (2003). Developmental morphology of the axial skeleton of the zebrafish, *Danio rerio* (Ostariophysi: Cyprinidae). *Dev. Dyn.* 228, 337–357. doi: 10.1002/dvdy.10387.

Bishop, J. (1848). On the causes, pathology, and treatment of deformities in the human body (with cases and engravings). *Lancet* 52, 7–10. doi: 10.1016/S0140-6736(02)65222-5.

Boglione, C., Gisbert, E., Gavaia, P., Witten, P. E., Moren, M., Fontagné, S.,

Koumoundouros, and G (2013). Skeletal anomalies in reared European fish larvae and juveniles. Part 2: main typologies, occurrences and causative factors. *Rev. Aquacult.* 5, S121–S167. doi: 10.1111/raq.12016.

Boivin, G., Anthoine-Terrier, C., and Obrant, K. J. (1990). Transmission electron microscopy of bone tissue: a review. *Acta Orthop. Scand.* 61, 170–180. doi: 10.3109/17453679009006514.

Boivin, G., and Meunier, P. J. (2002). The degree of mineralization of bone tissue measured by computerized quantitative contact microradiography. *Calcif Tissue Int* 70, 503–511. doi: 10.1007/s00223-001-2048-0.

Bonjour, J. P. (2011). Calcium and phosphate: a duet of ions playing for bone health. *J. Am. Coll. Nutr.* 30, 438S–48S. doi: 10.1080/07315724.2011.10719988.

Bonucci, E. (1990). "The ultrastructure of the osteocyte," in *Ultrastructure of skeletal tissues*, eds. E. Bonucci and P. Motta (Boston, MA: Kluwer Academic Publishers).

Bonucci, E. (2007). *Biological calcification. Normal and pathological processes in the early stages*. Berlin, Germany: Springer-Verlag.

Bonucci, E. (2009). The osteocyte: the underestimated conductor of the bone orchestra. *Rend. Lincei* 20, 237–254. doi: 10.1007/s12210-009-0051-y.

Bonucci, E. (2012). Bone mineralization. *Front. Biosci.* 17, 100–128. doi: 10.2741/3918.

Borday-Birraux, V., Van der Heyden, C., Debiais-Thibaud, M., Verreijdt, L., Stock, D. W., Huysseune, A., and Sire, J.-Y. (2006). Expression of Dlx genes during the development of the zebrafish pharyngeal dentition: evolutionary implications. *Evol. Dev.* 8, 130–141. doi: 10.1111/j.1525-142X.2006.00084.x.

Brailsford, J. F. (1943). Osteogenesis imperfecta. *Br. J. Radiol.* 16, 129–136. doi: 10.1259/0007-1285-16-185-129.

Bruneel, B., Mathä, M., Paesen, R., Ameloot, M., Weninger, W. J., and Huysseune, A. (2015). Imaging the zebrafish dentition: from traditional approaches to emerging technologies. *Zebrafish* 12, 1–10. doi: 10.1089/zeb.2014.0980.

Bruneel, B., and Witten, P. E. (2015). Power and challenges of using zebrafish as a model for skeletal tissue imaging. *Connect. Tissue Res.* 56, 161–173. doi: 10.3109/03008207.2015.1013193.

Buenzli, P. R., and Sims, N. A. (2015). Quantifying the osteocyte network in the human

skeleton. *Bone* 75, 144–150. doi: 10.1016/j.bone.2015.02.016.

Busse, B., Galloway, J. L., Gray, R. S., Harris, M. P., and Kwon, R. Y. (2020). Zebrafish: an emerging model for orthopedic research. *J. Orthop. Res.* 38, 925–936. doi: 10.1002/jor.24539.

Butler, W. T. (1998). Dentin matrix proteins. *Eur. J. Oral Sci.* 106 Suppl, 204–210. doi: 10.1111/j.1600-0722.1998.tb02177.x.

Carlson, S. J. (1989). "Vertebrate dental tissues," in *Skeletal biomineralisation: patterns, processes and evolutionary trends*, ed. J. G. Carter (American Geophysical Union), 235–260.

Carpenter, T. O., Imel, E. A., Ruppe, M. D., Weber, T. J., Klausner, M. A., Wooddell, M. M., Kawakami, T., Ito, T., Zhang, X., Humphrey, J., Insogna, K. L., and Peacock, M. (2014). Randomized trial of the anti-FGF23 antibody KRN23 in X-linked hypophosphatemia. *J. Clin. Invest.* 124, 1587–1597. doi: 10.1172/JCI72829.

Carpenter, T. O., Whyte, M. P., Imel, E. A., Boot, A. M., Högler, W., Linglart, A., Padidela, R., van't Hoff, W., Mao, M., Chen, C.-Y., Skrinar, A., Kakkis, E., San Martin, J., and Portale, A. A. (2018). Burosumab therapy in children with X-linked hypophosphatemia. *N. Engl. J. Med.* 378, 1987–1998. doi: 10.1056/NEJMoa1714641.

Carroll, R. L. (1988). *Vertebrate paleontology and evolution*. New York, NY, USA: W. H. Freeman and Company.

Castelein, R. M., Hasler, C., Helenius, I., Ovadia, D., Yazici, M., and Group, E. S. S. (2019). Complex spine deformities in young patients with severe osteogenesis imperfecta: current concepts review. *J. Child Orthop.* 13, 22–32. doi: 10.1302/1863-2548.13.180185.

Celeste, A. J., Rosen, V., Buecker, J. L., Kriz, R., Wang, E. A., and Wozney, J. M. (1986). Isolation of the human gene for bone gla protein utilizing mouse and rat cDNA clones. *EMBO J.* 5, 1885–1890. doi: 10.1002/j.1460-2075.1986.tb04440.x.

Chambers, T. J., Thomson, B. M., and Fuller, K. (1984). Effect of substrate composition on bone resorption by rabbit osteoclasts. *J. Cell Sci.* 70, 61–71. doi: 10.1242/jcs.70.1.61.

Chapman, J. A., and Hulmes, D. J. (1984). "Electron microscopy of the collagen fibril," in

*Ultrastructure of the connective tissue matrix*, eds. A. Ruggeri and P. M. Motta (Boston: Martinus Nijhoff Publishers).

Chatani, M., Takano, Y., and Kudo, A. (2011). Osteoclasts in bone modeling, as revealed by in vivo imaging, are essential for organogenesis in fish. *Dev Biol* 360, 96–109. doi: 10.1016/j.ydbio.2011.09.013.

Chen, N. X., O'Neill, K. D., Duan, D., and Moe, S. M. (2002). Phosphorus and uremic serum up-regulate osteopontin expression in vascular smooth muscle cells. *Kidney Int.* 62, 1724–1731. doi: 10.1046/j.1523-1755.2002.00625.x.

Christou, M., Iliopoulou, M., Witten, P. E., and Koumoundouros, G. (2018). Segmentation pattern of zebrafish caudal fin is affected by developmental temperature and defined by multiple fusions between segments. *J. Exp. Zool. B. Mol. Dev. Evol.* 330, 330–340. doi: 10.1002/jez.b.22825.

Clemen, G., Wanninger, A.-C., and Greven, H. (1997). The development of the dentigerous bones and teeth in the hemiramphid fish *Dermogenys pusillus* (Atheriniformes, Teleostei). *Ann. Anat. - Anat. Anzeiger* 179, 165–174. doi: 10.1016/S0940-9602(97)80099-4.

Collins, M. T., Marcucci, G., Anders, H.-J., Beltrami, G., Cauley, J. A., Ebeling, P. R., Kumar, R., Linglart, A., Sangiorgi, L., Towler, D. A., Weston, R., Whyte, M. P., Brandi, M. L., Clarke, B., and Thakker, R. V (2022). Skeletal and extraskeletal disorders of biomineralization. *Nat. Rev. Endocrinol.* 18, 473–489. doi: 10.1038/s41574-022-00682-7.

Cook, S. D., Skinner, H. B., and Haddad, R. J. (1983). A quantitative histologic study of osteoporosis produced by nutritional secondary hyperparathyroidism in dogs. *Clin. Orthop. Relat. Res.*, 105–120. doi: 10.1097/00003086-198305000-00016.

Costa, J. M., Sartori, M. M. P., Nascimento, N. F. D., Kadri, S. M., Ribolla, P. E. M., Pinhal, D., and Pezzato, L. E. (2018). Inadequate dietary phosphorus levels cause skeletal anomalies and alter osteocalcin gene expression in zebrafish. *Int. J. Mol. Sci.* 19, 364. doi: 10.3390/ijms19020364.

Cotti, S., Huysseune, A., Koppe, W., Rücklin, M., Marone, F., Wölfel, E. M., Fiedler, I. A. K., Busse, B., Forlino, A., and Witten, P. E. (2020). More bone with less minerals? The effects of dietary phosphorus on the post-cranial skeleton in zebrafish. *Int. J.*

*Mol. Sci.* 21, 5429. doi: 10.3390/ijms21155429.

Cotti, S., Huysseune, A., Larionova, D., Koppe, W., Forlino, A., and Witten, P. E. (2022). Compression fractures and partial phenotype rescue with a low phosphorus diet in the Chihuahua zebrafish osteogenesis imperfecta model. *Front. Endocrinol. (Lausanne).* 13, 851879. doi: 10.3389/fendo.2022.851879.

Cubbage, C. C., and Mabee, P. M. (1996). Development of the cranium and paired fins in the zebrafish Danio rerio (Ostariophysi, Cyprinidae). *J. Morphol.* 229, 121–160. doi: 10.1002/(SICI)1097-4687(199608)229:2<121::AID-JMOR1>3.0.CO;2-4.

Čurdová, E., Jechová, V., and Hošťálek, Z. (1982). Properties of apyrase and inorganic pyrophosphatase in *Streptomyces aureofaciens*. *Folia Microbiol. (Praha).* 27, 159–166. doi: 10.1007/BF02877394.

Currey, J. D. (1979). Mechanical properties of bone tissues with greatly differing functions. *J. Biomech.* 12, 313–319. doi: 10.1016/0021-9290(79)90073-3.

Currey, J. D. (1984). Effects of differences in mineralization on the mechanical properties of bone. *Philos. Trans. R. Soc. Lond. B Biol. Sci.* 304, 509–518. doi: 10.1098/rstb.1984.0042.

Currey, J. D. (2003). The many adaptations of bone. *J. Biomech.* 36, 1487–1495. doi: 10.1016/S0021-9290(03)00124-6.

Davit-Béal, T., Allizard, F., and Sire, J.-Y. (2007). Enameloid/enamel transition through successive tooth replacements in *Pleurodeles waltl* (Lissamphibia, Caudata). *Cell Tissue Res.* 328, 167–183. doi: 10.1007/s00441-006-0306-1.

de Azevedo, T. P., Witten, P. E., Huysseune, A., Bensimon-Brito, A., Winkler, C., To, T. T., and Palmeirim, I. (2012). Interrelationship and modularity of notochord and somites: a comparative view on zebrafish and chicken vertebral body development. *J. Appl. Ichtyol.* 28, 316–319. doi: 10.1111/j.1439-0426.2012.01987.x.

De Clercq, A., Perrott, M. R., Davie, P. S., Preece, M. A., Wybourne, B., Ruff, N., Huysseune, A., and Witten, P. E. (2017). Vertebral column regionalisation in Chinook salmon, *Oncorhynchus tshawytscha*. *J. Anat.* 231, 500–514. doi: 10.1111/joa.12655.

De Ricqlès, A., Meunier, F. J., Castanet, J., and Francillon-Vieillot, H. (1982).

"Comparative microstructure of bone," in *Bone metabolism and mineralisation*, ed. B. K. Hall (Boca Raton, FL, USA: CRC Press), 1–19.

Dean, M. N., Ekstrom, L., Monsonego-Ornan, E., Ballantyne, J., Witten, P. E., Riley, C., Habraken, W., and Omelon, S. (2015). Mineral homeostasis and regulation of mineralization processes in the skeletons of sharks, rays and relatives (Elasmobranchii). *Semin. Cell. Dev. Biol.* 46, 51–67. doi: 10.1016/j.semcdb.2015.10.022.

Del Fattore, A., Cappariello, A., and Teti, A. (2008). Genetics, pathogenesis and complications of osteopetrosis. *Bone* 42, 19–29. doi: 10.1016/j.bone.2007.08.029.

Denton, E. J., and Marshall, N. B. (1958). The buoyancy of bathypelagic fishes without a gas-filled swimbladder. *J. Mar. Biol. Ass. UK* 37, 753–767. doi: 10.1017/S0025315400005750.

Dermience, M., Lognay, G., Mathieu, F., and Goyens, P. (2015). Effects of thirty elements on bone metabolism. *J. Trace Elem. Med. Biol.* 32, 86–106. doi: 10.1016/j.jtemb.2015.06.005.

Deschamps, M. H., Kacem, A., Ventura, R., Courty, G., Haffray, P., Meunier, F. J., and Sire, J. Y. (2008). Assessment of "discreet" vertebral abnormalities, bone mineralization and bone compactness in farmed rainbow trout. *Acquaculture* 279, 11–17. doi: 10.1016/j.aquaculture.2008.03.036.

Di Biagio, C. (2022). *Unveiling skeletal phenotypes of fish models in response to environmental factors: a multidisciplinary approach (PhD thesis)*. Roma, Italy: University of Rome Tor Vergata.

Diegel, C. R., Hann, S., Ayturk, U. M., Hu, J. C. W., Lim, K., Droscha, C. J., Madaj, Z. B., Foxa, G. E., Izaguirre, I., Transgenics Core, V. A. I. V. and, Paracha, N., Pidhaynyy, B., Dowd, T. L., Robling, A. G., Warman, M. L., and Williams, B. O. (2020). An osteocalcin-deficient mouse strain without endocrine abnormalities. *PLOS Genet.* 16, e1008361. doi: 10.1371/journal.pgen.1008361.

Diekwisch, T. G. H., Berman, B. J., Anderton, X., Gurinsky, B., Ortega, A. J., Satchell, P. G., Williams, M., Arumugham, C., Luan, X., Mcintosh, J. E., Yamane, A., Carlson, D. S., Sire, J.-Y., and Shuler, C. F. (2002). Membranes, minerals, and proteins of

developing vertebrate enamel. *Microsc. Res. Tech.* 59, 373–395. doi: 10.1002/jemt.10218.

Dietrich, K., Fiedler, I. A. K., Kurzyukova, A., López-Delgado, A. C., McGowan, L. M., Geurtzen, K., Hammond, C. L., Busse, B., and Knopf, F. (2021). Skeletal biology and disease modeling in zebrafish. *J. Bone Miner. Res.* 36, 436–458. doi: 10.1002/jbmr.4256.

Dillon, S., Staines, K. A., Millán, J. L., and Farquharson, C. (2019). How to build a bone: PHOSPHO1, biomineralization, and beyond. *J Bone Min. Res Plus* 3, e10202. doi: 10.1002/jbm4.10202.

Doeland, M., Couzens, A. M. C., Donoghue, P. C. J., and Rücklin, M. (2019). Tooth replacement in early sarcopterygians. *R. Soc. Open Sci.* 6, 191173. doi: 10.1098/rsos.191173.

Donoghue, P. C., Sansom, I. J., and Downs, J. P. (2006). Early evolution of vertebrate skeletal tissues and cellular interactions, and the canalization of skeletal development. *J. Exp. Zool.* 306B, 278–294. doi: 10.1002/jez.b.21090.

Drábiková, L., Fjelldal, P. G., De Clercq, A., Yousaf, M. N., Morken, T., McGurk, C., and Witten, P. E. (2021). Vertebral column adaptations in juvenile Atlantic salmon *Salmo salar*, L. as a response to dietary phosphorus. *Aquaculture* 541, 736776. doi: 10.1016/j.aquaculture.2021.736776.

Drábiková, L., Fjelldal, P. G., De Clercq, A., Yousaf, M. N., Morken, T., McGurk, C., and Witten, P. E. (2022). What will happen to my smolt at harvest? Individually tagged Atlantic salmon help to understand possible progression and regression of vertebral deformities. *Aquaculture* 559, 738430. doi: 10.1016/j.aquaculture.2022.738430.

Driever, W., Solnica-Krezel, L., Schier, A. F., Neuhauss, S. C., Malicki, J., Stemple, D. L., Stainier, D. Y., Zwartkruis, F., Abdelilah, S., Rangini, Z., Belak, J., and Boggs, C. (1996). A genetic screen for mutations affecting embryogenesis in zebrafish. *Development* 123, 37–46. doi: 10.1242/dev.123.1.37.

Du, S. J., Frenkel, V., Kindschi, G., and Zohar, Y. (2001). Visualizing normal and defective bone development in zebrafish embryos using the fluorescent chromophore calcein. *Dev. Biol.* 238, 239–246. doi: 10.1006/dbio.2001.0390.

Ducy, P., Desbois, C., Boyce, B., Pinero, G., Story, B., Dunstan, C., Smith, E., Bonadio, J., Goldstein, S., Gundberg, C., Bradley, A., and Karsenty, G. (1996). Increased bone formation in osteocalcin-deficient mice. *Nature* 382, 448–452. doi: 10.1038/382448a0.

Eames, B. F., Allen, N., Young, J., Kaplan, A., Helms, J. A., and Schneider, R. A. (2007). Skeletogenesis in the swell shark *Cephaloscyllium ventriosum*. *J. Anat.* 210, 542–554. doi: 10.1111/j.1469-7580.2007.00723.x.

Eicher, E. M., Southard, J. L., Scriver, C. R., and Glorieux, F. H. (1976). Hypophosphatemia: mouse model for human familial hypophosphatemic (vitamin D-resistant) rickets. *Proc. Natl. Acad. Sci. USA* 73, 4667–4671. doi: 10.1073/pnas.73.12.4667.

Eisen, J. S. (2020). "History of zebrafish research," in *The zebrafish in biomedical research*, eds. S. C. Cartner, J. S. Eisen, S. C. Farmer, K. J. Guillemin, M. L. Kent, and G. E. Sanders (Academic Press), 3–14. doi: 10.1016/B978-0-12-812431-4.00001-4.

Ekanayake, S., and Hall, B. K. (1988). Ultrastructure of the osteogenesis of acellular vertebral bone in the Japanese medaka, *Oryzias latipes* (Teleostei, Cyprinidontidae). *Am. J. Anat.* 182, 241–249. doi: 10.1002/aja.1001820305.

Enderli, T. A., Burtch, S. R., Templet, J. N., and Carriero, A. (2016). Animal models of osteogenesis imperfecta: applications in clinical research. *Orthop. Res. Rev.* 8, 41–55. doi: 10.2147/ORR.S85198.

Evans, D. H. (2002). Cell signaling and ion transport across the fish gill epithelium. *J. Exp. Zool.* 293, 336–347. doi: 10.1002/jez.10128.

Favaloro, E., and Mazzola, A. (2006). Meristic character counts and incidence of skeletal anomalies in the wild *Diplodus puntazzo* (Cetti, 1777) of an area of the south-eastern Mediterranean Sea. *Fish Physiol. Biochem* . 32, 159–166. doi: 10.1007/s10695-006-0008-3.

Favus, M. J., Bushinsky, D. A., and Lemann, J. J. (2006). "Regulation of calcium, magnesium, and phosphate metabolism," in *Primer on the metabolic bone diseases and disorders of mineral metabolism*, eds. C. J. Rosen, R. Bouillon, J. E. Compston, and V. Rosen (Wiley-Blackbell).

Fedarko, N. S. (2014). “Osteoblast/osteoclast development and function in osteogenesis imperfecta,” in *Osteogenesis imperfecta. A translational approach to brittle bone disease*, eds. J. R. Shapiro, P. H. Byers, F. H. Glorieux, and P. D. Sponseller (San Diego: Academic Press), 45–56. doi: 10.1016/B978-0-12-397165-4.00005-8.

Fedde, K. N., Blair, L., Silverstein, J., Coburn, S. P., Ryan, L. M., Weinstein, R. S., Waymire, K., Narisawa, S., Millán, J. L., MacGregor, G. R., and Whyte, M. P. (1999). Alkaline phosphatase knock-out mice recapitulate the metabolic and skeletal defects of infantile hypophosphatasia. *J. Bone Miner. Res.* 14, 2015–2026. doi: 10.1359/jbmr.1999.14.12.2015.

Fernández, I., Granadeiro, L., Darias, M. J., Gavaia, P. J., Andree, K. B., and Gisbert, E. (2018). *Solea senegalensis* skeletal ossification and gene expression patterns during metamorphosis: new clues on the onset of skeletal deformities during larval to juvenile transition. *Aquaculture* 496, 153–165. doi: 10.1016/j.aquaculture.2018.07.022.

Ferreri, F., Nicolais, C., Boglione, C., and Bmertoline, B. (2000). Skeletal characterization of wild and reared zebrafish: anomalies and meristic characters. *J. Fish Biol.* 56, 1115–1128. doi: 10.1111/j.1095-8649.2000.tb02127.x.

Fiedler, I. A. K., Schmidt, F. N., Wölfel, E. M., Plumeyer, C., Milovanovic, P., Gioia, R., Tonelli, F., Bale, H. A., Jähn, K., Besio, R., Forlino, A., and Busse, B. (2018). Severely impaired bone material quality in *Chihuahua* zebrafish resembles classical dominant human osteogenesis imperfecta. *J Bone Min. Res* 33, 1489–1499. doi: 10.1002/jbmr.3445.

Fink, S. V, and Fink, W. L. (1996). “Interrelationships of ostariophysan fishes (Teleostei),” in *Interrelationships of fishes*, eds. M. Stiassny, L. Parenti, and G. Johnson (San Diego: Academic Press), 209–249.

Fink, W. L. (1981). Ontogeny and phylogeny of tooth attachment modes in actinopterygian fishes. *J. Morphol.* 167, 167–184. doi: 10.1002/jmor.1051670203.

Fisher, S., Jagadeeswaran, P., and Halpern, M. E. (2003). Radiographic analysis of zebrafish skeletal defects. *Dev. Biol.* 264, 64–76. doi: 10.1016/s0012-1606(03)00399-3.

Fisher, S., and Mabee, P. M. (2004). "Skeletogenesis in zebrafish *Danio rerio*: evolutionary and developmental aspects," in *Fish Development and Genetics*, eds. G. Zhiyuan and V. Korzh (World Scientific), 392–423. doi: doi:10.1142/9789812565761_0011.

Fjelldal, P. G., Hansen, T., and Albrektsen, S. (2012). Inadequate phosphorus nutrition in juvenile Atlantic salmon has a negative effect on long-term bone health. *Aquaculture* 334–337, 117–123. doi: 10.1016/j.aquaculture.2011.12.043.

Fleisch, H. (1982). Mechanisms of normal mineralization in bone and cartilage. in *Biological mineralization and demineralization. Dahlem workshop reports*, ed. G. H. Nancollas (Berlin: Springer-Verlag). doi: 10.1007/978-3-642-68574-3_12.

Fleisch, H., and Bisaz, S. (1962). Mechanism of calcification: inhibitory role of pyrophosphate. *Nature* 195, 911. doi: 10.1038/195911a0.

Fleming, A., Keynes, R., and Tannahill, D. (2004). A central role for the notochord in vertebral patterning. *Development* 131, 873–880. doi: 10.1242/dev.00952.

Fleming, A., Kishida, M. G., Kimmel, C. B., and Keynes, R. J. (2015). Building the backbone: the development and evolution of vertebral patterning. *Development* 142, 1733–1744. doi: 10.1242/dev.118950.

Forlino, A., Kuznetsova, N. V, Marini, J. C., and Leikin, S. (2007). Selective retention and degradation of molecules with a single mutant α1(I) chain in the Brtl IV mouse model of OI. *Matrix Biol.* 26, 604–614. doi: 10.1016/j.matbio.2007.06.005.

Forlino, A., and Marini, J. C. (2016). Osteogenesis imperfecta. *Lancet* 387, 1657–1671. doi: 10.1016/S0140-6736(15)00728-X.

Francis, F., Hennig, S., Korn, B., Reinhardt, R., de Jong, P., Poustka, A., Lehrach, H., Rowe, P. S. N., Goulding, J. N., Summerfield, T., Mountford, R., Read, A. P., Popowska, E., Pronicka, E., Davies, K. E., O'Riordan, J. L. H., Econs, M. J., Nesbitt, T., Drezner, M. K., Oudet, C., Pannetier, S., Hanauer, A., Strom, T. M., Meindl, A., Lorenz, B., Cagnoli, B., Mohnike, K. L., Murken, J., and Meitinger, T. (1995). A gene (*PEX*) with homologies to endopeptidases is mutated in patients with X-linked hypophosphatemic rickets. *Nat. Genet.* 11, 130–136. doi: 10.1038/ng1095-130.

Franz-Odendaal, T. A., Hall, B. K., and Witten, P. E. (2006). Buried alive: how osteoblasts

become osteocytes. *Dev. Dyn.* 235, 176–190. doi: 10.1002/dvdy.20603.

Fratzl-Zelman, N., Schmidt, I., Roschger, P., Glorieux, F. H., Klaushofer, K., Fratzl, P., Rauch, F., and Wagermaier, W. (2014). Mineral particle size in children with osteogenesis imperfecta type I is not increased independently of specific collagen mutations. *Bone* 60, 122–128. doi: 10.1016/j.bone.2013.11.023.

Garibaldi, N., Contento, B. M., Babini, G., Morini, J., Siciliani, S., Biggiogera, M., Raspanti, M., Marini, J. C., Rossi, A., Forlino, A., and Besio, R. (2021). Targeting cellular stress in vitro improves osteoblast homeostasis, matrix collagen content and mineralization in two murine models of osteogenesis imperfecta. *Matrix Biol.* 98, 1–20. doi: 10.1016/j.matbio.2021.03.001.

Germain, D., Schnell, N. K., and Meunier, F. J. (2019). Histological data on bone and teeth in two dragonfishes (Stomiidae; Stomiiformes): *Borostomias panamensis* Regan & Trewavas, 1929 and *Stomias boa* Reinhardt, 1842. *Cybium* 43, 103–107. doi: 10.26028/cybium/2019-431-010.

Gilbert, S. F. (2003). *Developmental biology*. 7th ed. Sunderland, MA: Sunderland, MA.

Gioia, R., Tonelli, F., Ceppi, I., Biggiogera, M., Leikin, S., Fisher, S., Tenedini, E., Yorgan, T. A., Schinke, T., Tian, K., Schwartz, J. M., Forte, F., Wagener, R., Villani, S., Rossi, A., and Forlino, A. (2017). The chaperone activity of 4PBA ameliorates the skeletal phenotype of Chihuahua, a zebrafish model for dominant osteogenesis imperfecta. *Hum. Mol. Genet.* 26, 2897–2911. doi: 10.1093/hmg/ddx171.

Gisbert, E., Darias, M. J., and Font-i-Furnols, M. (2012). Advantages and limitations of X-ray and computed tomography systems for the study of the skeleton in meagre (*Argyrosomus regius*). *J. Appl. Ichthyol.* 28, 441–445. doi: 10.1111/j.1439-0426.2012.01981.x.

Gistelinck, C., Gioia, R., Gagliardi, A., Tonelli, F., Marchese, L., Bianchi, L., Landi, C., Bini, L., Huysseune, A., Witten, P. E., Staes, A., Gevaert, K., De Rocker, N., Menten, B., Malfait, F., Leikin, S., Carra, S., Tenni, R., Rossi, A., De Paepe, A., Coucke, P., Willaert, A., and Forlino, A. (2016). Zebrafish collagen type I: molecular and biochemical characterization of the major structural protein in bone and skin. *Sci. Rep.* 6, 21540. doi: 10.1038/srep21540.

Glimcher, M. J. (1959). Molecular biology of mineralized tissues with particular

reference to bone. *Rev. Mod. Phys.* 31, 359–393. doi: 10.1103/RevModPhys.31.359.

Golub, E. E. (2009). Role of matrix vesicles in biomineralization. *Biochim. Biophys. Acta* 1790, 1592–1598. doi: 10.1016/j.bbagen.2009.09.006.

Graham, C., Nalbant, P., Schölermann, B., Hentschel, H., Kinne, R. K. H., and Werner, A. (2003). Characterization of a type IIb sodium-phosphate cotransporter from zebrafish (Danio rerio) kidney. *Am. J. Physiol.* 284, F727–F736. doi: 10.1152/ajprenal.00356.2002.

Granato, M., and Nüsslein-Volhard, C. (1996). Fishing for genes controlling development. *Curr. Opin. Genet. Dev.* 6, 461–468. doi: 10.1016/S0959-437X(96)80068-2.

Greco, E. A., Pietschmann, P., and Migliaccio, S. (2019). Osteoporosis and Sarcopenia Increase Frailty Syndrome in the Elderly. *Front. Endocrinol. (Lausanne).* 10, 00255. doi: 10.3389/fendo.2019.00255.

Gregory, W. K. (1933). Fish skulls: a study of the evolution of natural mechanisms. *Trans. Am. Philos. Soc.* 23, 75–481.

Grotmol, S., Kryvi, H., Nordvik, K., and Totland, G. K. (2003). Notochord segmentation may lay down the pathway for the development of the vertebral bodies in the Atlantic salmon. *Anat. Embryol. (Berl).* 207, 263–272. doi: 10.1007/s00429-003-0349-y.

Grotmol, S., Nordvik, K., Kryvi, H., and Totland, G. K. (2005). A segmental pattern of alkaline phosphatase activity within the notochord coincides with the initial formation of the vertebral bodies. *J. Anat.* 206, 427–436. doi: 10.1111/j.1469-7580.2005.00408.x.

Guerreiro, P. M., Renfro, J. L., Power, D. M., and Canario, A. V. M. (2007). The parathyroid hormone family of peptides: structure, tissue distribution, regulation, and potential functional roles in calcium and phosphate balance in fish. *Am. J. Physiol.* 292, R679-96. doi: 10.1152/ajpregu.00480.2006.

Guglielmi, G., Muscarella, S., and Bazzocchi, A. (2011). Integrated imaging approach to osteoporosis: state-of-the-art review and update. *Radiographics* 31, 1343–1364. doi: 10.1148/rg.315105712.

Gupta, A., and Renfro, J. L. (1989). Control of phosphate transport in flounder renal proximal tubule primary cultures. *Am. J. Physiol.* 256, R850–R857. doi: 10.1152/ajpregu.1989.256.4.R850.

Haffter, P., Granato, M., Brand, M., Mullins, M. C., Hammerschmidt, M., Kane, D. A., Odenthal, J., van Eeden, F. J., Jiang, Y. J., Heisenberg, C. P., Kelsh, R. N., Furutani-Seiki, M., Vogelsang, E., Beuchle, D., Schach, U., Fabian, C., and Nusslein-Volhard, C. (1996). The identification of genes with unique and essential functions in the development of the zebrafish, *Danio rerio*. *Development* 123, 1–36. doi: 10.1242/dev.123.1.1.

Hall, B. K. (2015). *Bones and cartilage: developmental and evolutionary skeletal biology*. 2nd ed. London: Elsevier Academic Press doi: 10.1016/C2013-0-00143-0.

Hall, B. K., and Witten, P. E. (2007). "Plasticity of and transitions between skeletal tissues in vertebrate evolution and development," in *Major transitions in vertebrate evolution*, eds. J. S. Anderson and H. D. Sues (Bloomington, IN, USA: Indiana University Press), 13–59.

Hall, B. K., and Witten, P. E. (2019). "Plasticity and variation of skeletal cells and tissues and the evolutionary development of Actinopterygian fishes," in *Evolution and development of fishes*, eds. Z. Johanson, C. Underwood, and M. Richter (Cambridge: Cambridge University Press).

Hamilton, F. (1822). *An account of the fishes found in the river Ganges and its branches*. Edinburgh: Archibald Constable and Company.

Hamlin, N. J., and Price, P. A. (2004). Mineralization of decalcified bone occurs under cell culture conditions and requires bovine serum but not cells. *Calcif. Tissue Int.* 75, 231–242. doi: 10.1007/s00223-004-0190-1.

Hammer, Ø., Harper, D. A. T., and Ryan, P. D. (2001). Past: paleontological statistics software package for education and data analysis. *Palaeontol. Electron.* 4, 1–9.

Hanken, J., and Wake, D. B. (1993). Miniaturization of body size: organismal consequences and evolutionary significance. *Annu. Rev. Ecol. Syst.* 24, 501–519. doi: 10.1146/annurev.es.24.110193.002441.

Hansen, S., Shanbhogue, V. V, Jørgensen, N. R., and Beck-Nielsen, S. S. (2019). Elevated bone remodeling markers of CTX and P1NP in addition to sclerostin in patients

with X-linked hypophosphatemia: a cross-sectional controlled study. *Calcif. Tissue Int.* 104, 591–598. doi: 10.1007/s00223-019-00526-z.

Harris, M. P., Rohner, N., Schwarz, H., Perathoner, S., Konstantinidis, P., and Nüsslein-Volhard, C. (2008). Zebrafish *eda* and *edar* mutants reveal conserved and ancestral roles of ectodysplasin signaling in vertebrates. *PLOS Genet.* 4, e1000206. doi: 10.1371/journal.pgen.1000206.

Harris, W. H., Heaney, R. P., Davis, L. A., Weinberg, E. H., Coutts, R. D., and Schiller, A. L. (1976). Stimulation of bone formation *in vivo* by phosphate supplementation. *Calcif. Tissue Res.* 22, 85–98. doi: 10.1007/bf02010349.

Helland, S., Denstadli, V., Witten, P. E., Hjelde, K., Storebakken, T., Skrede, A., Åsgård, T., and Baeverfjord, G. (2006). Hyper dense vertebrae and mineral content in Atlantic salmon (Salmo salar L.) fed diets with graded levels of phytic acid. *Aquaculture* 261, 603–614. doi: 10.1016/j.aquaculture.2006.08.027.

Herold, R. C. (1971). The development and mature structure of dentine in the pike, *Esox lucius*, analysed by microradiography. *Arch. Oral Biol.* 16, 29–41. doi: 10.1016/0003-9969(71)90134-8.

Herold, R. C., and Landino, L. (1970). The development and mature structure of dentine in the pike, *Esox lucius*, analyzed by bright field, phase and polarization microscopy. *Arch. Oral Biol.* 15, 747-IN7. doi: 10.1016/0003-9969(70)90038-5.

Hessle, L., Johnson, K. A., Anderson, H. C., Narisawa, S., Sali, A., Goding, J. W., Terkeltaub, R., and Millan, J. L. (2002). Tissue-nonspecific alkaline phosphatase and plasma cell membrane glycoprotein-1 are central antagonistic regulators of bone mineralization. *Proc. Natl. Acad. Sci. USA* 99, 9445–9449. doi: 10.1073/pnas.142063399.

Ho, A. M., Johnson, M. D., and Kingsley, D. M. (2000). Role of the mouse *ank* gene in control of tissue calcification and arthritis. *Science* 289, 265–270. doi: 10.1126/science.289.5477.265.

Holtrop, M. (1990). “Light and electron microscopical structure of bone forming cells,” in *Bone, Vol. 1: the osteoblast and osteocyte.*, ed. K. B. Hall (Caldwell, NJ: The Telford Press).

Hori, M., Shimizu, Y., and Fukumoto, S. (2011). Minireview: fibroblast growth factor 23

in phosphate homeostasis and bone metabolism. *Endocrinology* 152, 4–10. doi: 10.1210/en.2010-0800.

Howe, K., Clark, M. D., Torroja, C. F., Torrance, J., Berthelot, C., Muffato, M., M., Collins, J. E., Humphray, S., McLaren, K., Matthews, L., McLaren, S., Sealy, I., Caccamo, M., Churcher, C., Scott, C., Barrett, J. C., Koch, R., Rauch, G-J., White, S., Chow, W., Kilian, B., Quintais, L. T., Guerra-Assunção, J. A., Zhou, Y., Gu, Y., Yen, J., Vogel, J-H., Eyre, T., Banerjee, R., Chi, J., Fu, B., Langley, E., Maguire, S. F., Laird, G., Lloyd, D., Kenyon, E., Donaldson, S., Sehra, H., Almeida-King, J., Loveland, J., Trevanion, S., Jones, M., Quail, M., Willey, D., Hunt, A., Burton, J., Sims, S., McLay, K., Plumb, B., Davis, J., Clee, C., Oliver, K., Clark, R., Riddle, C., Elliott, D., Threadgold, G., Harden, G., Ware, D., Begum, S., Mortimore, B., Kerry, G., Heath, P., Phillimore, B., Tracey, A., Corby, N., Dunn, M., Johnson, C., Wood, J., Clark, S., Pelan, S., Griffiths, G., Smith, M., Glithero, R., Howden, P., Barker, N., Lloyd, C., Stevens, C., Harley, J., Holt, K., Panagiotidis, G., Lovell, J., Beasley, H., Henderson, C., Gordon, D., Auger, K., Wright, D., Collins, J., Raisen, C., Dyer, L., Leung, K., Robertson, L., Ambridge, K., Leongamornlert, D., McGuire, S., Gilderthorp, R., Griffiths, C., Manthravadi, D., Nichol, S., Barker, G., Whitehead, S., Kay, M., Brown, J., Murnane, C., Gray, E., Humphries, M., Sycamore, N., Barker, D., Saunders, D., Wallis, J., Babbage, A., Hammond, S., Mashreghi-Mohammadi, M., Barr, L., Martin, S., Wray, P., Ellington, A., Matthews, N., Ellwood, M., Woodmansey, R., Clark, G., Cooper, J. D., Tromans, A., Grafham, D., Skuce, C., Pandian, R., Andrews, R., Harrison, E., Kimberley, A., Garnett, J., Fosker, N., Hall, R., Garner, P., Kelly, D., Bird, C., Palmer, S., Gehring, I., Berger, A., Dooley, C., Ersan-Ürün, Z., Eser, C., Geiger, H., Geisler, M., Karotki, L., Kirn, A., Konantz, J., Konantz, M., Oberländer, M., Rudolph-Geiger, S., Teucke, M., Lanz, C., Raddatz, G., Osoegawa, K., Zhu, B., Rapp, A., Widaa, S., Langford, C., Yang, F., Schuster, S. C., Carter, N. P., Harrow, J., Ning, Z., Herrero, J., Searle, S. M. J., Enright, A., Geisler, R., Plasterk, R. H. A., Lee, C., Westerfield, M., de Jong, P. J., Zon, L. I., Postlethwait, J. H., Volhard, C. N., Hubbard, T. J. P., Crollius, H. Roest., Rogers, J., and Stemple, D. L. (2013). The zebrafish reference genome sequence and its relationship to the human genome. *Nature* 496, 498–503. doi:

10.1038/nature12111.

Hughes, D. R., Bassett, J. R., and Moffat, L. A. (1994). Structure and origin of the tooth pedicel (the so-called bone of attachment) and dental-ridge bone in the mandibles of the sea breams *Acanthopagrus australis*, *Pagrus auratus* and *Rhabdosargus sarba* (Sparidae, Perciformes, Teleostei). *Anat. Embryol. (Berl).* 189, 51–69. doi: 10.1007/BF00193129.

Huitema, L. F., Apschner, A., Logister, I., Spoorendonk, K. M., Bussmann, J., Hammond, C. L., and Schulte-Merker, S. (2012). *Entpd5* is essential for skeletal mineralization and regulates phosphate homeostasis in zebrafish. *Proc. Natl. Acad. Sci. USA* 109, 21372–21377. doi: 10.1073/pnas.1214231110.

Humason, G. L., Presnell, J. K., and Schreibman, M. P. (1997). *Humason's animal tissue techniques*. Baltimore, MD, USA: Johns Hopkins University Press.

Hunziker, E. B., Kapfinger, E., and Geiss, J. (2007). The structural architecture of adult mammalian articular cartilage evolves by a synchronized process of tissue resorption and neoformation during postnatal development. *Osteoarthr. Cartil.* 15, 403–413. doi: 10.1016/j.joca.2006.09.010.

Huttunen, M. M., Tillman, I., Viljakainen, H. T., Tuukkanen, J., Peng, Z., Pekkinen, M., and Lamberg-Allardt, C. J. E. (2007). High dietary phosphate intake reduces bone strength in the growing rat skeleton. *J. Bone Miner. Res.* 22, 83–92. doi: 10.1359/jbmr.061009.

Huysseune, A. (2000). "Skeletal system," in *The laboratory fish. Part 4. Microscopic functional anatomy*, ed. G. K. Ostrander (San Diego: Academic Press), 307–317.

Huysseune, A. (2006). Formation of a successional dental lamina in the zebrafish (*Danio rerio*): support for a local control of replacement tooth initiation. *Int. J. Dev. Biol.* 50, 637–643. doi: 10.1387/ijdb.052098ah.

Huysseune, A., Cerny, R., and Witten, P. E. (2022a). The conundrum of pharyngeal teeth origin: the role of germ layers, pouches, and gill slits. *Biol. Rev.* 97, 414–447. doi: 10.1111/brv.12805.

Huysseune, A., Delgado, S., and Witten, P. E. (2005). How to replace a tooth: fish(ing) for answers. *Oral Biosci. Med.* 2, 75–81.

Huysseune, A., Hall, B. K., and Witten, P. E. (2007). Establishment, maintenance and

modifications of the lower jaw dentition of wild Atlantic salmon (*Salmo salar* L.) throughout its life cycle. *J. Anat.* 211, 471–484. doi: 10.1111/j.1469-7580.2007.00788.x.

Huysseune, A., Sire, J.-Y., and Meunier, F. J. (1994). Comparative study of lower pharyngeal jaw structure in two phenotypes of *Astatoreochromis alluaudi* (teleostei: Cichlidae). *J. Morphol.* 221, 25–43. doi: 10.1002/jmor.1052210103.

Huysseune, A., and Sire, J. Y. (1992). Development of cartilage and bone tissues of the anterior part of the mandible in cichlid fish: a light and TEM study. *Anat Rec* 233, 357–375. doi: 10.1002/ar.1092330304.

Huysseune, A., and Sire, J. Y. (1998). Evolution of patterns and processes in teeth and tooth-related tissues in non-mammalian vertebrates. *Eur. J. Oral Sci.* 106 Suppl, 437–481. doi: 10.1111/j.1600-0722.1998.tb02211.x.

Huysseune, A., Soenens, M., Sire, J.-Y., and Witten, P. E. (2022b). "High-resolution histology for craniofacial studies on zebrafish and other teleost models," in *Craniofacial development*, ed. S. Dworkin (New York, NY: Springer US), 249–262. doi: 10.1007/978-1-0716-1847-9_17.

Huysseune, A., Takle, H., Soenens, M., Taerwe, K., and Witten, P. E. (2008). Unique and shared gene expression patterns in Atlantic salmon (*Salmo salar*) tooth development. *Dev. Genes Evol.* 218, 427–437. doi: 10.1007/s00427-008-0237-9.

Huysseune, A., Van der heyden, C., and Sire, J.-Y. (1998). Early development of the zebrafish (*Danio rerio*) pharyngeal dentition (Teleostei, Cyprinidae). *Anat. Embryol. (Berl).* 198, 289–305. doi: 10.1007/s004290050185.

Huysseune, A., Verraes, W., and Desender, K. (1988). Mechanisms of branchial cartilage growth in *Astatotilapia elegans* (Teleostei: Cichlidae). *J. Anat.* 158, 13–30.

Huysseune, A., and Witten, P. E. (2006). Developmental mechanisms underlying tooth patterning in continuously replacing osteichthyan dentitions. *J. Exp. Zool.* 306B, 204–215. doi: 10.1002/jez.b.21091.

Hyman, L. H. (1979). *Hyman's comparative vertebrate anatomy*. 3rd ed. , ed. M. H. Wake Chiacago: University of Chicago Press.

Ichikawa, S., Sorenson, A. H., Austin, A. M., Mackenzie, D. S., Fritz, T. A., Moh, A., Hui, S. L., and Econs, M. J. (2009). Ablation of the *Galnt3* gene leads to low-circulating

intact fibroblast growth factor 23 (Fgf23) concentrations and hyperphosphatemia despite increased *Fgf23* expression. *Endocrinology* 150, 2543–2550. doi: 10.1210/en.2008-0877.

Imel, E. A., Zhang, X., Ruppe, M. D., Weber, T. J., Klausner, M. A., Ito, T., Vergeire, M., Humphrey, J. S., Glorieux, F. H., Portale, A. A., Insogna, K., Peacock, M., and Carpenter, T. O. (2015). Prolonged correction of serum phosphorus in adults with X-linked hypophosphatemia using monthly doses of KRN23. *J. Clin. Endocrinol. Metab.* 100, 2565–2573. doi: 10.1210/jc.2015-1551.

Ishikawa, S., Kumar, S. J., Takahashi, H. E., and Homma, M. (1996). Vertebral body shape as a predictor of spinal deformity in osteogenesis imperfecta. *J. Bone Joint Surg. Am.* 78, 212–219. doi: 10.2106/00004623-199602000-00007.

Ishikawa, Y., and Bächinger, H. P. (2013). A molecular ensemble in the rER for procollagen maturation. *Biochim. Biophys. Acta* 1833, 2479–2491. doi: 10.1016/j.bbamcr.2013.04.008.

Ishiyama, M., Inage, T., and Shimokawa, H. (2001). Abortive secretion of an enamel matrix in the inner enamel epithelial cells during an enameloid formation in the Gar-Pike, *Lepisosteus oculatus* (Holostei, Actinopterygii). *Arch. Histol. Cytol.* 64, 99–107. doi: 10.1679/aohc.64.99.

Iwamoto, J., Takeda, T., and Ichimura, S. (2002). Increased bone resorption with decreased activity and increased recruitment of osteoblasts in osteogenesis imperfecta type I. *J. Bone Miner. Metab.* 20, 174–179. doi: 10.1007/s007740200025.

Jackson, S. F. (1956). The fine structure of developing bone in the embryonic fowl. *Proc. R. Soc. Lond. B Biol. Sci.* 146, 270–280. doi: 10.1098/rspb.1957.0010.

Jager, P. L., Slart, R. H., Webber, C. L., Adachi, J. D., Papaioannou, A. L., and Gulenchyn, K. Y. (2010). Combined vertebral fracture assessment and bone mineral density measurement: a patient-friendly new tool with an important impact on the Canadian Risk Fracture Classification. *Can. Assoc. Radiol. J.* 61, 194–200. doi: 10.1016/j.carj.2009.12.012.

Jha, S., Chapman, M., and Roszko, K. (2019). When low bone mineral density and fractures is not osteoporosis. *Curr. Osteoporos. Rep.* 17, 324–332. doi:

10.1007/s11914-019-00529-7.

Jono, S., McKee, M. D., Murry, C. E., Shioi, A., Nishizawa, Y., Mori, K., Morii, H., and Giachelli, C. M. (2000). Phosphate regulation of vascular smooth muscle cell calcification. *Circ. Res.* 87, E10-7. doi: 10.1161/01.res.87.7.e10.

Joshi, A. D. (2020). New insights into physiological and pathophysiological functions of stanniocalcin 2. *Front. Endocrinol. (Lausanne).* 11. doi: 10.3389/fendo.2020.00172.

Kague, E., Gallagher, M., Burke, S., Parsons, M., Franz-Odendaal, T., and Fisher, S. (2012). Skeletogenic fate of zebrafish cranial and trunk neural crest. *PLoS One* 7, e47394. doi: 10.1371/journal.pone.0047394.

Kague, E., Turci, F., Newman, E., Yang, Y., Brown, K. R., Aglan, M. S., Otaify, G. A., Temtamy, S. A., Ruiz-Perez, V. L., Cross, S., Royall, C. P., Witten, P. E., and Hammond, C. L. (2021). 3D assessment of intervertebral disc degeneration in zebrafish identifies changes in bone density that prime disc disease. *Bone Res.* 9, 39. doi: 10.1038/s41413-021-00156-y.

Kague, E., Witten, P. E., Soenens, M., Campos, C. L., Lubiana, T., Fisher, S., Hammond, C., Brown, K. R., Passos-Bueno, M. R., and Huysseune, A. (2018). Zebrafish sp7 mutants show tooth cycling independent of attachment, eruption and poor differentiation of teeth. *Dev. Biol.* 435, 176–184. doi: 10.1016/j.ydbio.2018.01.021.

Kalajzic, I., Terzic, J., Rumboldt, Z., Mack, K., Naprta, A., Ledgard, F., Gronowicz, G., Clark, S. H., and Rowe, D. W. (2002). Osteoblastic response to the defective matrix in the osteogenesis imperfecta murine (oim) mouse. *Endocrinology* 143, 1594–1601. doi: 10.1210/endo.143.5.8807.

Kawasaki, K., Keating, J. N., Nakatomi, M., Welten, M., Mikami, M., Sasagawa, I., Puttick, M. N., Donoghue, P. C. J., and Ishiyama, M. (2021). Coevolution of enamel, ganoin, enameloid, and their matrix SCPP genes in osteichthyans. *iScience* 24, 102023. doi: 10.1016/j.isci.2020.102023.

Keating, J. N., Marquart, C. L., Marone, F., and Donoghue, P. C. J. (2018). The nature of aspidin and the evolutionary origin of bone. *Nat. Ecol. Evol.* 2, 1501–1506. doi: 10.1038/s41559-018-0624-1.

Kemi, V. E., Kärkkäinen, M. U. M., and Lamberg-Allardt, C. J. E. (2006). High phosphorus intakes acutely and negatively affect Ca and bone metabolism in a dose-dependent manner in healthy young females. *Br. J. Nutr.* 96, 545–552. doi: doi:10.1079/BJN20061838.

Kerebel, L. M., and Le Cabellec, M. T. (1979). Structure and ultrastructure of dentine in the teleost fish, *Lophius*. *Arch. Oral Biol.* 24, 745–751. doi: 10.1016/0003-9969(79)90034-7.

Kimmel, C. B. (1989). Genetics and early development of zebrafish. *Trends Genet.* 5, 283–288. doi: 10.1016/0168-9525(89)90103-0.

Kimmel, C. B., Ballard, W. W., Kimmel, S. R., Ullmann, B., and Schilling, T. F. (1995). Stages of embryonic development of the zebrafish. *Dev. Dyn.* 203, 253–310. doi: 10.1002/aja.1002030302.

Kimmel, C. B., and Warga, R. M. (1988). Cell lineage and developmental potential of cells in the zebrafish embryo. *Trends Genet.* 4, 68–74. doi: 10.1016/0168-9525(88)90043-1.

Klein-Nulend, J., Bakker, A. D., Bacabac, R. G., Vatsa, A., and Weinbaum, S. (2013). Mechanosensation and transduction in osteocytes. *Bone* 54, 182–190. doi: 10.1016/j.bone.2012.10.013.

Knochel, J. P. (1977). The pathophysiology and clinical characteristics of severe hypophosphatemia. *Arch. Intern. Med.* 137, 203–220. doi: 10.1001/archinte.1977.03630140051013.

Knoll, A. H. (2003). Biomineralization and evolutionary history. *Rev. Mineral. Geochemistry* 54, 329–356. doi: 10.2113/0540329.

Komaba, H., and Fukagawa, M. (2016). Phosphate - a poison for humans? *Kidney Int.* 90, 753–763. doi: 10.1016/j.kint.2016.03.039.

Komori, T. (2010). Regulation of bone development and extracellular matrix protein genes by RUNX2. *Cell Tissue Res.* 339, 189. doi: 10.1007/s00441-009-0832-8.

Kornak, U., Kasper, D., Bösl, M. R., Kaiser, E., Schweizer, M., Schulz, A., Friedrich, W., Delling, G., and Jentsch, T. J. (2001). Loss of the ClC-7 chloride channel leads to osteopetrosis in mice and man. *Cell* 104, 205–215. doi: 10.1016/S0092-8674(01)00206-9.

Koshizuka, Y., Ikegawa, S., Sano, M., Nakamura, K., and Nakamura, Y. (2001). Isolation of novel mouse genes associated with ectopic ossification by differential display method using *ttw*, a mouse model for ectopic ossification. *Cytogenet. Cell Genet.* 94, 163–168. doi: 10.1159/000048809.

Krook, L., Lutwak, L., Henrikson, P. A., Kallfelz, F., Hirsch, C., Romanus, B., Bélanger, L. F., Marier, J. R., and Sheffy, B. E. (1971). Reversibility of nutritional osteoporosis: physicochemical data on bones from an experimental study in dogs. *J. Nutr.* 101, 233–246. doi: 10.1093/jn/101.2.233.

Laale, H. W. (1977). The biology and use of zebrafish, *Brachydanio rerio* in fisheries research. *J. Fish Biol.* 10, 121–173. doi: 10.1111/j.1095-8649.1977.tb04049.x.

Laerm, J. (1976). The development, function, and design of amphicoelous vertebrae in teleost fishes. *Zool. J. Linn. Soc.* 58, 237–254. doi: 10.1111/j.1096-3642.1976.tb00830.x.

Laerm, J. (1979). The origin and homology of the chondrostean vertebral centrum. *Can. J. Zool.* 57, 475–485. doi: 10.1139/z79-058.

Laflamme, G. H., and Jowsey, J. (1972). Bone and soft tissue changes with oral phosphate supplements. *J. Clin. Invest.* 51, 2834–2840. doi: 10.1172/JCI107106.

Lall, S. P. (1991). “Digestibility, metabolism and excretion of dietary phosphorous in fish,” in *Nutritional strategies and aquaculture wastes*, eds. C. B. Cowey and C. Y. Cho (Guelph, ON, Canada: University Guelph), 21–36.

Lall, S. P. (2002). “The minerals,” in *Fish nutrition, 3rd edition*, eds. J. E. Halver and R. W. Hardy (Dan Diego: Academic Press Inc), 259–308.

Lall, S. P., and Lewis-McCrea, L. M. (2007). Role of nutrients in skeletal metabolism and pathology in fish - An overview. *Aquaculture* 267, 3–19. doi: 10.1016/j.aquaculture.2007.02.053.

Lambert, L. J., Challa, A. K., Niu, A., Zhou, L., Tucholski, J., Johnson, M. S., Nagy, T. R., Eberhardt, A. W., Estep, P. N., Kesterson, R. A., and Grams, J. M. (2016). Increased trabecular bone and improved biomechanics in an osteocalcin-null rat model created by CRISPR/Cas9 technology. *Dis. Model. Mech.* 9, 1169–1179. doi: 10.1242/dmm.025247.

Lassen, N. E., Andersen, T. L., Pløen, G. G., Søe, K., Hauge, E. M., Harving, S., Eschen, G.

E. T., and Delaisse, J.-M. (2017). Coupling of bone resorption and formation in real time: new knowledge gained from human haversian BMUs. *J. Bone Miner. Res.* 32, 1395–1405. doi: 10.1002/jbmr.3091.

Leopold, J. A. (2015). Vascular calcification: Mechanisms of vascular smooth muscle cell calcification. *Trends Cardiovasc. Med.* 25, 267–274. doi: 10.1016/j.tcm.2014.10.021.

Leprévost, A., Azaïs, T., Trichet, M., and Sire, J. (2017). Identification of a new mineralized tissue in the notochord of reared Siberian sturgeon (*Acipenser baerii*). *J. Morphol.* 278, 1586–1597. doi: 10.1002/jmor.20734.

Li, S., Kong, H., Yao, N., Yu, Q., Wang, P., Lin, Y., Wang, J., Kuang, R., Zhao, X., Xu, J., Zhu, Q., and Ni, L. (2011). The role of runt-related transcription factor 2 (Runx2) in the late stage of odontoblast differentiation and dentin formation. *Biochem. Biophys. Res. Commun.* 410, 698–704. doi: 10.1016/j.bbrc.2011.06.065.

Li, X., Ominsky, M. S., Niu, Q.-T., Sun, N., Daugherty, B., D'Agostin, D., Kurahara, C., Gao, Y., Cao, J., Gong, J., Asuncion, F., Barrero, M., Warmington, K., Dwyer, D., Stolina, M., Morony, S., Sarosi, I., Kostenuik, P. J., Lacey, D. L., Simonet, W. S., Ke, H. Z., and Paszty, C. (2008). Targeted deletion of the sclerostin gene in mice results in increased bone formation and bone strength. *J. Bone Miner. Res.* 23, 860–869. doi: 10.1359/jbmr.080216.

Lleras-Forero, L., Winkler, C., and Schulte-Merker, S. (2020). Zebrafish and medaka as models for biomedical research of bone diseases. *Dev. Biol.* 457, 191–205. doi: 10.1016/j.ydbio.2019.07.009.

Lleras Forero, L., Narayanan, R., Huitema, L. F. A., VanBergen, M., Apschner, A., Peterson-Maduro, J., Logister, I., Valentin, G., Morelli, L. G., Oates, A. C., and Schulte-Merker, S. (2018). Segmentation of the zebrafish axial skeleton relies on notochord sheath cells and not on the segmentation clock. *Elife* 7, e33843. doi: 10.7554/eLife.33843.

Locket, N. A. (1980). Review lecture: some advances in coelacanth biology. *Proc. R. Soc. Lond. B* 208, 265–307. doi: 10.1098/rspb.1980.0052.

Lu, M., Wagner, G. F., and Renfro, J. L. (1994). Stanniocalcin stimulates phosphate reabsorption by flounder renal proximal tubule in primary culture. *Am. J. Physiol.*

267, R1356-62. doi: 10.1152/ajpregu.1994.267.5.R1356.

Ma, D., Wang, X., Guo, J., Zhang, J., and Cai, T. (2018). Identification of a novel mutation of *RUNX2* in a family with supernumerary teeth and craniofacial dysplasia by whole-exome sequencing: a case report and literature review. *Medicine (Baltimore).* 97. doi: 10.1097/MD.0000000000011328.

Mackay, E. W., Apschner, A., and Schulte-Merker, S. (2015). Vitamin K reduces hypermineralisation in zebrafish models of PXE and GACI. *Development* 142, 1095–1101. doi: 10.1242/dev.113811.

Maisey, J. G. (1988). "Phylogeny of early vertebrate skeletal induction and ossification patterns," in *Evolutionary biology*, eds. M. K. Hecht, B. Wallace, and G. T. Prance (Boston, MA: Springer US), 1–36. doi: 10.1007/978-1-4613-0931-4_1.

Maisey, J. G. (2000). *Discovering fossil fishes*. Boulder, CO, USA: Westview Press.

Marie-Hardy, L., Khalifé, M., Slimani, L., and Pascal-Moussellard, H. (2019). Computed tomography method for characterising the zebrafish spine. *Orthop. Traumatol. Surg. Res.* 105, 361–367. doi: 10.1016/j.otsr.2018.12.008.

Marini, J. C., Forlino, A., Bächinger, H. P., Bishop, N. J., Byers, P. H., Paepe, A., Fassier, F., Fratzl-Zelman, N., Kozloff, K. M., Krakow, D., Montpetit, K., and Semler, O. (2017). Osteogenesis imperfecta. *Nat Rev Dis Prim.* 3, 17052. doi: 10.1038/nrdp.2017.52.

Marini, J. C., Forlino, A., Cabral, W. A., Barnes, A. M., San Antonio, J. D., Milgrom, S., Hyland, J. C., Körkkö, J., Prockop, D. J., De Paepe, A., Coucke, P., Symoens, S., Glorieux, F. H., Roughley, P. J., Lund, A. M., Kuurila-Svahn, K., Hartikka, H., Cohn, D. H., Krakow, D., Mottes, M., Schwarze, U., Chen, D., Yang, K., Kuslich, C., Troendle, J., Dalgleish, R., and Byers, P. H. (2007). Consortium for osteogenesis imperfecta mutations in the helical domain of type I collagen: regions rich in lethal mutations align with collagen binding sites for integrins and proteoglycans. *Hum. Mutat.* 28, 209–221. doi: 10.1002/humu.20429.

Marks, S. C., and Popoff, S. (1990). "Ultrastructural biology and pathology of the osteoclast," in *Ultrastructure of skeletal tissues*, eds. E. Bonucci and P. M. Motta (Boston, MA: Kluwer Academic Publishers).

Martini, A., Huysseune, A., Witten, P. E., and Boglione, C. (2020). Plasticity of the

skeleton and skeletal deformities in zebrafish (*Danio rerio*) linked to rearing density. *J. Fish Biol.* 98, 971–986. doi: 10.1111/jfb.14272.

Masuyama, R., Nakaya, Y., Tanaka, S., Tsurukami, H., Nakamura, T., Watanabe, S., Yoshizawa, T., Kato, S., and Suzuki, K. (2001). Dietary phosphorus restriction reverses the impaired bone mineralization in vitamin D receptor knockout mice. *Endocrinology* 142, 494–497. doi: 10.1210/endo.142.1.8050.

McClung, M. R. (2021). Role of bone-forming agents in the management of osteoporosis. *Aging Clin. Exp. Res.* 33, 775–791. doi: 10.1007/s40520-020-01708-8.

McCluskey, B., and Braasch, I. (2020). "Zebrafish taxonomy and phylogeny," in *The zebrafish in biomedical research*, eds. S. C. Cartner, J. S. Eisen, S. C. Farmer, K. J. Guillemin, M. L. Kent, and G. E. Sanders (Academic Press), 15–24. doi: 10.1016/B978-0-12-812431-4.00002-6.

McCurley, A. T., and Callard, G. V (2008). Characterization of housekeeping genes in zebrafish: male-female differences and effects of tissue type, developmental stage and chemical treatment. *BMC Mol. Biol.* 9, 102. doi: 10.1186/1471-2199-9-102.

McGreal, C., and Bober, M. B. (2020). "Patient evaluation and medical treatment for osteogenesis imperfecta," in *Osteogenesis imperfecta. A case-based guide to surgical decision-making and care*, ed. R. W. Kruse (Cham, Switzerland: Springer), 11–19. doi: 10.1007/978-3-030-42527-2.

McKusick, V. A. (1972). *Heritable disorders of connective tissue*. 4th ed. , ed. C. V Mosby St Louis.

Merametdjian, L., Beck-Cormier, S., Bon, N., Couasnay, G., Sourice, S., Guicheux, J., Gaucher, C., and Beck, L. (2017). Expression of phosphate transporters during dental mineralization. *J. Dent. Res.* 97, 209–217. doi: 10.1177/0022034517729811.

Metscher, B. D., and Ahlberg, P. E. (1999). Zebrafish in context: uses of a laboratory model in comparative studies. *Dev. Biol.* 210, 1–14. doi: 10.1006/dbio.1999.9230.

Meunier, F. J. (2011). The Osteichtyes, from the Paleozoic to the extant time, through histology and palaeohistology of bony tissues. *Comptes Rendus Palevol* 10, 347–

355. doi: 10.1016/j.crpv.2011.04.005.

Meunier, F. J., and Huysseune, A. (1992). The concept of bone tissue in Osteichthyes. *Netherlands J. Zool.* 42, 445–458. doi: 10.1163/156854291X00441.

Meyer, A., and Van de Peer, Y. (2005). From 2R to 3R: evidence for a fish-specific genome duplication (FSGD). *BioEssays* 27, 937–945. doi: 10.1002/bies.20293.

Millán, J. L., and Whyte, M. P. (2016). Alkaline phosphatase and hypophosphatasia. *Calcif. Tissue Int.* 98, 398–416. doi: 10.1007/s00223-015-0079-1.

Moe, S. M., and Chen, N. X. (2008). Mechanisms of vascular calcification in chronic kidney disease. *J. Am. Soc. Nephrol.* 19, 213–216. doi: 10.1681/ASN.2007080854.

Moharrer, Y., and Boerckel, J. D. (2021). Tunnels in the rock: dynamics of osteocyte morphogenesis. *Bone* 153, 116104. doi: 10.1016/j.bone.2021.116104.

Morales, G. A., Azcuy, R. L., Casaretto, M. E., Márquez, L., Hernández, A. J., Gómez, F., Koppe, W., and Mereu, A. (2018). Effect of different inorganic phosphorus sources on growth performance, digestibility, retention efficiency and discharge of nutrients in rainbow trout (*Oncorhynchus mykiss*). *Aquaculture* 495, 568–574. doi: 10.1016/j.aquaculture.2018.06.036.

Morin-Kensicki, E. M., Melancon, E., and Eisen, J. S. (2002). Segmental relationship between somites and vertebral column in zebrafish. *Development* 129, 3851–3860. doi: 10.1242/dev.129.16.3851.

Mornet, E. (2000). Hypophosphatasia: the mutations in the tissue-nonspecific alkaline phosphatase gene. *Hum. Mutat.* 15, 309–315. doi: 10.1002/(SICI)1098-1004(200004)15:4<309::AID-HUMU2>3.0.CO;2-C.

Moss, M. L. (1961). Studies of the acelluar bone of teleost fish. I. Morphological and systematic variations. *Acta Anat. (Basel).* 46, 343–362.

Moss, M. L. (1962). Studies of the acellular bone of teleost fish. II. Response to fracture under normal and acalcemic conditions. *Acta Anat. (Basel).* 48, 46–60. doi: 10.1159/000141826.

Murshed, M. (2018). Mechanism of bone mineralization. *Cold Spring Harb. Perspect. Med.* 8. doi: 10.1101/cshperspect.a031229.

Murshed, M., Harmey, D., Millán, J. L., McKee, M. D., and Karsenty, G. (2005). Unique coexpression in osteoblasts of broadly expressed genes accounts for the spatial

restriction of ECM mineralization to bone. *Genes. Dev.* 19, 1093–1104. doi: 10.1101/gad.1276205.

Myers, E. R., and Wilson, S. E. (1997). Biomechanics of osteoporosis and vertebral fracture. *Spine (Phila. Pa. 1976).* 22, 25S-31S.

Nakashima, T., Hayashi, M., Fukunaga, T., Kurata, K., Oh-Hora, M., Feng, J. Q., Bonewald, L. F., Kodama, T., Wutz, A., Wagner, E. F., Penninger, J. M., and Takayanagi, H. (2011). Evidence for osteocyte regulation of bone homeostasis through RANKL expression. *Nat. Med.* 17, 1231–1234. doi: 10.1038/nm.2452.

National Research Council (2011). *Nutrient requirements of fish and shrimp*. Washington D. C., WA, USA: The National Academies Press doi: doi:10.17226/13039.

Nijhuis, W. H., Eastwood, D. M., Allgrove, J., Hvid, I., Weinans, H. H., Bank, R. A., and Sakkers, R. J. (2019). Current concepts in osteogenesis imperfecta: bone structure, biomechanics and medical management. *J. Child. Orthop.* 13, 1–11. doi: 10.1302/1863-2548.13.180190.

Nishimoto, S. K., Waite, J. H., Nishimoto, M., and Kriwacki, R. W. (2003). Structure, activity, and distribution of fish osteocalcin. *J. Biol. Chem.* 278, 11843–11848. doi: 10.1074/jbc.M211449200.

Nordahl, J., Hollberg, K., Mengarelli-Widholm, S., Andersson, G., and Reinholt, F. P. (2000). Morphological and functional features of clasts in low phosphate, vitamin D-deficiency rickets. *Calcif. Tissue Int.* 67, 400–407. doi: 10.1007/s002230001151.

Nordvik, K., Kryvi, H., Totland, G. K., and Grotmol, S. (2005). The salmon vertebral body develops through mineralization of two preformed tissues that are encompassed by two layers of bone. *J. Anat.* 206, 103–114. doi: 10.1111/j.1469-7580.2005.00372.x.

Notbohm, H., Nokelainen, M., Myllyharju, J., Fietzek, P. P., Müller, P. K., and Kivirikko, K. I. (1999). Recombinant human type II collagens with low and high levels of hydroxylysine and Its glycosylated forms show marked differences in fibrillogenesis *in vitro*. *J. Biol. Chem.* 274, 8988–8992. doi: 10.1074/jbc.274.13.8988.

Ofer, L., Dean, M. N., Zaslansky, P., Kult, S., Shwartz, Y., Zaretsky, J., Griess-Fishheimer,

S., Monsonego-Ornan, E., Zelzer, E., and Shahar, R. (2019). A novel nonosteocytic regulatory mechanism of bone modeling. *PLOS Biol.* 17, e3000140. doi: 10.1371/journal.pbio.3000140.

Oliver, W. C., and Pharr, G. M. (1992). An improved technique for determining hardness and elastic modulus using load and displacement sensing indentation experiments. *J. Mater. Res.* 7, 1564–1583. doi: 10.1557/JMR.1992.1564.

Onishi, T., Okawa, R., Ogawa, T., Shintani, S., and Ooshima, T. (2007). *Phex* mutation causes the reduction of *Npt2b* mRNA in teeth. *J. Dent. Res.* 86, 158–162. doi: 10.1177/154405910708600210.

Oralová, V., Rosa, J. T., Soenens, M., Bek, J. W., Willaert, A., Witten, P. E., and Huysseune, A. (2019). Beyond the whole-mount phenotype: high-resolution imaging in fluorescence-based applications on zebrafish. *Biol. Open* 8, bio042374. doi: 10.1242/bio.042374.

Ortiz-Delgado, J. B., Simes, D. C., Gavaia, P., Sarasquete, C., and Cancela, M. L. (2005). Osteocalcin and matrix GLA protein in developing teleost teeth: identification of sites of mRNA and protein accumulation at single cell resolution. *Histochem. Cell Biol.* 124, 123–130. doi: 10.1007/s00418-005-0015-y.

Ørvig, T. (1951). Histologic studies of placoderms and fossil elasmobranchs. 1. The endoskeleton, with remarks on the hard tissues of lower vertebrates in general. *Ark. för Zool.* 2, 321–454.

Ørvig, T. (1967). "Phylogeny of tooth tissues: evolution of some calcified tissues in early vertebrates," in *Structural and chemical organization of teeth*, ed. A. E. W. Miles (London: Academic Press), 45–110.

Owen, R. (1854). *The principal forms of the skeleton and the teeth as the basis for a system of natural history and comparative anatomy*. New York, NY: William Wood.

**P**arichy, D. M. (2015). Advancing biology through a deeper understanding of zebrafish ecology and evolution. *Elife* 4, e05635. doi: 10.7554/eLife.05635.

Parichy, D. M., Elizondo, M. R., Mills, M. G., Gordon, T. N., and Engeszer, R. E. (2009). Normal table of postembryonic zebrafish development: staging by externally visible anatomy of the living fish. *Dev. Dyn.* 238, 2975–3015. doi:

10.1002/dvdy.22113.

Pasco-Viel, E., Charles, C., Chevret, P., Semon, M., Tafforeau, P., Viriot, L., and Laudet, V. (2010). Evolutionary trends of the pharyngeal dentition in Cypriniformes (Actinopterygii: Ostariophysi). *PLoS One* 5, e11293. doi: 10.1371/journal.pone.0011293.

Peacock, M. (2021). Phosphate metabolism in health and disease. *Calcif. Tissue Int.* 108, 3–15. doi: 10.1007/s00223-020-00686-3.

Peterson, R. T., Link, B. A., Dowling, J. E., and Schreiber, S. L. (2000). Small molecule developmental screens reveal the logic and timing of vertebrate development. *Proc. Natl. Acad. Sci. USA* 97, 12965–12969. doi: 10.1073/pnas.97.24.12965.

Peyer, B. (1968). *Comparative odontology*. Chiacago: University of Chicago Press.

Phan, H. E., Northorp, M., Lalonde, R. L., Ngo, D., and Akimenko, M. A. (2019). Differential *actinodin1* regulation in embryonic development and adult fin regeneration in *Danio rerio*. *PLoS One* 14, e0216370. doi: 10.1371/journal.pone.0216370.

Phillips, J. B., and Westerfield, M. (2020). "Zebrafish as a model to understand human genetic diseases," in *The zebrafish in biomedical research*, eds. S. C. Cartner, J. S. Eisen, S. C. Farmer, K. J. Guillemin, M. L. Kent, and G. E. Sanders (Academic Press), 619–626. doi: 10.1016/B978-0-12-812431-4.00047-6.

Pinheiro, M. M., Schuch, N. J., Genaro, P. S., Ciconelli, R. M., Ferraz, M. B., and Martini, L. A. (2009). Nutrient intakes related to osteoporotic fractures in men and women - The Brazilian Osteoporosis Study (BRAZOS). *Nutr. J.* 8, 6. doi: 10.1186/1475-2891-8-6.

Poirier Stewart, N., Deschamps, M. H., Witten, P. E., Le Luyer, J., Proulx, E., Huysseune, A., Bureau, D. P., and Vandenberg, G. W. (2014). X-ray-based morphometrics: an approach to diagnose vertebral abnormalities in under-mineralized vertebrae of juvenile triploid all-female rainbow trout (*Oncorhynchus mykiss*) fed with a phosphorus deficient diet. *J. Appl. Ichtyol.* 30, 496–803. doi: 10.1111/jai.12520.

Power, M. J., and Fottrell, P. F. (1991). Osteocalcin: diagnostic methods and clinical applications. *Crit. Rev. Clin. Lab. Sci.* 28, 287–335. doi: 10.3109/10408369109106867.

Printzi, A., Fragkoulis, S., Dimitriadi, A., Keklikoglou, K., Arvanitidis, C., Witten, P. E., and Koumoundouros, G. (2020). Exercise-induced lordosis in zebrafish *Danio rerio* (Hamilton, 1822). *J. Fish Biol.* doi: 10.1111/jfb.14240.

Prostak, K., Seifert, P., and Skobe, Z. (1991). Tooth matrix formation and mineralization in extant fishes. in *Mechanisms and phylogeny of mineralization in biological systems*, eds. S. Suga and H. Nakahara (Tokyo: Springer Japan), 465–469.

Prostak, K., and Skobe, Z. (1986). Ultrastructure of the dental epithelium during enameloid mineralization in a teleost fish, *Cichlasoma cyanoguttatum*. *Arch. Oral Biol.* 31, 73–85. doi: https://doi.org/10.1016/0003-9969(86)90030-0.

Raghunath, M., Bruckner, P., and Steinmann, B. (1994). Delayed triple helix formation of mutant collagen from patient with Osteogenesis Imperfecta. *J. Mol. Biol.* 236, 940–949. doi: 10.1006/jmbi.1994.1199.

Rauch, F., Travers, R., Parfitt, A. M., and Glorieux, F. H. (2000). Static and dynamic bone histomorphometry in children with osteogenesis imperfecta. *Bone* 26, 581–589. doi: 10.1016/s8756-3282(00)00269-6.

Raymond, M. H., Schutte, B. C., Torner, J. C., Burns, T. L., and Willing, M. C. (1999). Osteocalcin: genetic and physical mapping of the human gene BGLAP and its potential role in postmenopausal osteoporosis. *Genomics* 60, 210–217. doi: 10.1006/geno.1999.5893.

Razzaque, M. S. (2011). Phosphate toxicity: new insights into an old problem. *Clin. Sci.* 120, 91–97. doi: 10.1042/CS20100377.

Reif, W. E. (1982). “Evolution of dermal skeleton and dentition in vertebrates. The odontode regulation theory,” in *Evolutionary biology*, eds. M. K. Hecht, B. Wallace, and G. T. Prance (New York, NY, USA: Plenum Press), 287–368. doi: 10.1007/978-1-4615-6968-8_7.

Ricqlès, A., Meunier, F., Castanet, J., and Francillon-Vieillot, H. (1991). “Bone matrix and bone specific products,” in *Bone, Vol. 3*, ed. K. B. Hall (Boca Raton: CRC Press).

Riggs, B. L., Khosla, S., and Melton III, L. J. (1998). A unitary model for involutional osteoporosis: estrogen deficiency causes both type I and type II osteoporosis in postmenopausal women and contributes to bone loss in aging men. *J. Bone Miner. Res.* 13, 763–773. doi: 10.1359/jbmr.1998.13.5.763.

Rissone, A., Ledin, J., and Burgess, S. M. (2020). “Targeted editing of zebrafish genes to understand gene function and human disease pathology,” in *The zebrafish in biomedical research*, eds. S. C. Cartner, J. S. Eisen, S. C. Farmer, K. J. Guillemin, M. L. Kent, and G. E. Sanders (Academic Press), 637–647. doi: 10.1016/B978-0-12-812431-4.00049-X.

Robinson, M.-E., AlQuorain, H., Murshed, M., and Rauch, F. (2020). Mineralized tissues in hypophosphatemic rickets. *Pediatr. Nephrol.* 35, 1843–1854. doi: 10.1007/s00467-019-04290-y.

Romer, A. S. (1970). *The vertebrate body*. Philadelphia: W.B. Saunders Company.

Rosa, J. T., Witten, P. E., and Huysseune, A. (2021). Cells at the edge: the dentin–bone interface in zebrafish teeth. *Front. Physiol.* 12, 723210. doi: 10.3389/fphys.2021.723210.

Roy, M. E., and Nishimoto, S. K. (2002). Matrix Gla protein binding to hydroxyapatite is dependent on the ionic environment: calcium enhances binding affinity but phosphate and magnesium decrease affinity. *Bone* 31, 296–302. doi: 10.1016/S8756-3282(02)00821-9.

Roy, P. K., and Lall, S. P. (2003). Dietary phosphorus requirement of juvenile haddock (*Melanogrammus aeglefinus* L.). *Aquaculture* 221, 451–468. doi: 10.1016/S0044-8486(03)00065-6.

Sasagawa, I. (1988). The appearance of matrix vesicles and mineralization during tooth development in three teleost fishes with well-developed enameloid and orthodentine. *Arch. Oral Biol.* 33, 75–86. doi: 10.1016/0003-9969(88)90049-0.

Sasagawa, I. (1995). Fine structure of tooth germs during the formation of enameloid matrix in *Tilapia nilotica*, a teleost fish. *Arch. Oral Biol.* 40, 801–814. doi: 10.1016/0003-9969(95)00050-Y.

Sasagawa, I. (1998). Mechanisms of mineralization in the enameloid of elasmobranchs and teleosts. *Connect. Tissue Res.* 39, 207–214. doi: 10.3109/03008209809023928.

Sasagawa, I., and Ferguson, M. W. J. (1990). Fine structure of the organic matrix remaining in the mature cap enameloid in *Halichoeres poecilopterus*, teleost. *Arch. Oral Biol.* 35, 765–770. doi: 10.1016/0003-9969(90)90101-F.

Sasagawa, I., and Ishiyama, M. (2005a). Fine structural and cytochemical mapping of enamel organ during the enameloid formation stages in gars, *Lepisosteus oculatus*, Actinopterygii. *Arch. Oral Biol.* 50, 373–391. doi: 10.1016/j.archoralbio.2004.07.013.

Sasagawa, I., and Ishiyama, M. (2005b). Fine structural and cytochemical observations on the dental epithelial cells during cap enameloid formation stages in *Polypterus senegalus*, a bony fish (Actinopterygii). *Connect. Tissue Res.* 46, 33–52. doi: 10.1080/03008200590935538.

Sasagawa, I., Ishiyama, M., and Akai, J. (2006). Cellular influence in the formation of enameloid during odontogenesis in bony fishes. *Mater. Sci. Eng. C* 26, 630–634. doi: 10.1016/j.msec.2005.04.010.

Sasagawa, I., Ishiyama, M., Yokosuka, H., Mikami, M., and Uchida, T. (2009). Tooth enamel and enameloid in actinopterygian fish. *Front. Mater. Sci. China* 3, 174–182. doi: 10.1007/s11706-009-0030-3.

Satchell, P. G., Anderton, X., Ryu, O. H., Luan, X., Ortega, A. J., Opamen, R., Berman, B. J., Witherspoon, D. E., Gutmann, J. L., Yamane, A., Zeichner-David, M., Simmer, J. P., Shuler, C. F., and Diekwisch, T. G. H. (2002). Conservation and variation in enamel protein distribution during vertebrate tooth development. *J. Exp. Zool.* 294, 91–106. doi: 10.1002/jez.10148.

Saville, P. D., and Krook, L. (1969). Gravimetric and isotopic studies in nutritional hyperparathyroidism in beagles. *Clin. Orthop. Relat. Res.* 62, 15–24. doi: 10.1007/BF02065206.

Schaeffer, B. (1967). Osteichthyan vertebrae. *Zool. J. Linn. Soc.* 47, 185–195. doi: 10.1111/j.1096-3642.1967.tb01402.x.

Schaeffer, B. (1977). “The dermal skeleton in fishes,” in *Problems in vertebrate evolution*, eds. S. M. Andrews, R. S. Miles, and A. D. Walker (London: Academic Press), 25–52.

Scherft, J. P., and Groot, C. G. (1990). “The electron microscopic structure of the osteoblast,” in *Ultrastructure of skeletal tissues*, eds. E. Bonucci and P. M. Motta (Boston, MA: Kluwer Academic Publishers), 209–222.

Schnell, N. K., and Johnson, G. D. (2017). Evolution of a functional head joint in deep-

sea fishes (Stomiidae). *PLoS One* 12, e0170224. doi: 10.1371/journal.pone.0170224.

Schultz, A. G., Guffey, S. C., Clifford, A. M., and Goss, G. G. (2014). Phosphate absorption across multiple epithelia in the Pacific hagfish (*Eptatretus stoutii*). *Am. J. Physiol. Integr. Comp. Physiol.* 307, R643–R652. doi: 10.1152/ajpregu.00443.2013.

Scott-Savage, P., and Hall, B. K. (1980). Differentiative ability of the tibial periosteum from the embryonic chick. *Cells Tissues Organs* 106, 129–140. doi: 10.1159/000145174.

Scott, J. M., and Symons, N. B. (1977). *Introduction to dental anatomy*. Edinburgh: Churchill Livingstone.

Seeman, E. (2003). Reduced bone formation and increased bone resorption: rational targets for the treatment of osteoporosis. *Osteoporos. Int.* 14, 2–8. doi: 10.1007/s00198-002-1340-9.

Shah, S. A., and Wallace, M. J. (2020). "Osteogenesis imperfecta in the spine," in *Osteogenesis imperfecta. A case-based guide to surgical decision-making and care*, ed. R. W. Kruse (Cham, Switzerland: Springer), 221–230. doi: 10.1007/978-3-030-42527-2.

Shapiro, F., Holtrop, M. E., and Glimcher, M. J. (1977). Organization and cellular biology of the perichondrial ossification groove of ranvier: a morphological study in rabbits. *J. Bone Jt. Surg. Am.* 59, 703–723. Available at: https://www.ncbi.nlm.nih.gov/pubmed/71299.

Shearer, K. D. (1984). Changes in elemental composition of hatchery-reared rainbow trout, *Salmo gairdneri*, sssociated with growth and reproduction. *Can. J. Fish. Aquat. Sci.* 41, 1592–1600. doi: 10.1139/f84-197.

Sheldon, H., and Robinson, R. A. (1957). Electron microscope studies of crystal-collagen relationships in bone. IV. The occurrence of crystals within collagen fibrils. *J. Biophys. Biochem. Cytol.* 3, 1011–1016. doi: 10.1083/jcb.3.6.1011.

Shellis, R. P., and Berkovitz, B. K. B. (1976). Observations on the dental anatomy of piranhas (Characidae) with special reference to tooth structure. *J. Zool.* 180, 69–84. doi: 10.1111/j.1469-7998.1976.tb04664.x.

Sillence, D. O., Senn, A., and Danks, D. M. (1979). Genetic heterogeneity in osteogenesis imperfecta. *J. Med. Genet.* 16, 101–116. doi: 10.1136/jmg.16.2.101.

Sire, J., and Kawasaki, K. (2012). "Origin and evolution of bone and dentin and of acidic secretory calcium-binding phosphoproteins," in *Phosphorylated extracellular matrix proteins of bone and dentin, Vol. 2*, ed. M. Goldberg (Bentham Science Publishers), 3–60. doi: 10.2174/978160805465711202010003.

Sire, J. Y., and Akimenko, M. A. (2004). Scale development in fish: a review, with description of sonic hedgehog (*shh*) expression in the zebrafish (*Danio rerio*). *Int. J. Dev. Biol.* 48, 233–247. doi: 10.1387/ijdb.15272389.

Sire, J. Y., and Huysseune, A. (2003). Formation of dermal skeletal and dental tissues in fish: a comparative and evolutionary approach. *Biol. Rev. Camb. Philos. Soc.* 78, 219–249. doi: 10.1017/s1464793102006073.

Sitara, D., Kim, S., Razzaque, M. S., Bergwitz, C., Taguchi, T., Schüler, C., Erben, R. G., and Lanske, B. (2008). Genetic evidence of serum phosphate-independent functions of FGF-23 on bone. *PLoS Genet.* 4, e1000154. doi: 10.1371/journal.pgen.1000154.

Smith, K. K. (1995). "Heterochrony in the evolution of enamel in vertebrates," in *Evolutionary change and heterochrony*, ed. K. J. McNamara (London: John Wiley & Sons), 125–150.

Smith, M. M., and Hall, B. K. (1990). Development and evolutionary origins of the vertebrate skeletogenic and odontogenic tissues. *Biol. Rev.* 65, 277–373. doi: 10.1111/j.1469-185X.1990.tb01427.x.

Smith, N. L., and Kimelman, D. (2020). "Establishing the body plan: the first 24 hours of zebrafish development," in *The zebrafish in biomedical research*, eds. S. C. Cartner, J. S. Eisen, S. C. Farmer, K. J. Guillemin, M. L. Kent, and G. E. Sanders (Academic Press), 81–88. doi: 10.1016/B978-0-12-812431-4.00007-5.

Smith, W. L., Garavito, R. M., and DeWitt, D. L. (1996). Prostaglandin endoperoxide H synthases (Cyclooxygenases)-1 and -2. *J. Biol. Chem.* 271, 33157–33160. doi: 10.1074/jbc.271.52.33157.

Spence, R., Fatema, M. K., Reichard, M., Huq, K. A., Wahab, M. A., Ahmed, Z. F., and Smith, C. (2006). The distribution and habitat preferences of the zebrafish in

Bangladesh. *J. Fish Biol.* 69, 1435–1448. doi: 10.1111/j.1095-8649.2006.01206.x.

Spence, R., Gerlach, G., Lawrence, C., and Smith, C. (2008). The behaviour and ecology of the zebrafish, *Danio rerio*. *Biol. Rev. Camb. Philos. Soc.* 83, 13–34. doi: 10.1111/j.1469-185X.2007.00030.x.

Spoorendonk, K. M., Peterson-Maduro, J., Renn, J., Trowe, T., Kranenbarg, S., Winkler, C., and Schulte-Merker, S. (2008). Retinoic acid and Cyp26b1 are critical regulators of osteogenesis in the axial skeleton. *Development* 135, 3765–3774. doi: 10.1242/dev.024034.

Spurr, A. R. (1969). A low-viscosity epoxy resin embedding medium for electron microscopy. *J. Ultrastruct. Res.* 26, 31–43. doi: 10.1016/S0022-5320(69)90033-1.

Stock, D. W. (2007). Zebrafish dentition in comparative context. *J. Exp. Zool. Part B Mol. Dev. Evol.* 308B, 523–549. doi: 10.1002/jez.b.21187.

Stöß, H., Pontz, B. F., Pesch, H.-J., and Ott, R. (1986). Heterogeneity of osteogenesis imperfecta. Biochemical and morphological findings in a case of type III according to Sillence. *Eur. J. Pediatr.* 145, 34–39. doi: 10.1007/BF00441849.

Streisinger, G., Walker, C., Dower, N., Knauber, D., and Singer, F. (1981). Production of clones of homozygous diploid zebrafish (*Brachydanio rerio*). *Nature* 291, 293–296. doi: 10.1038/291293a0.

Suarez-Bregua, P., Cal, L., Cañestro, C., and Rotllant, J. (2017). PTH reloaded: a new evolutionary perspective. *Front. Physiol.* 8. doi: doi.org/10.3389/fphys.2017.00776.

Sugiura, S. H., Dong, F. M., and Hardy, R. W. (2000). Primary responses of rainbow trout to dietary phosphorus concentrations. *Aquac. Nutr.* 6, 235–245. doi: 10.1046/j.1365-2095.2000.00142.x.

Sugiura, S. H., Hardy, R. W., and Roberts, R. J. (2004). The pathology of phosphorus deficiency in fish – a review. *J. Fish Dis.* 27, 255–265. doi: doi.org/10.1111/j.1365-2761.2004.00527.x.

Sullivan, M., Reid, S. W., Ternent, H., Manchester, N. J., Roberts, R. J., Stone, D. A., and Hardy, R. W. (2007). The aetiology of spinal deformity in Atlantic salmon, *Salmo salar* L.: influence of different commercial diets on the incidence and severity of the preclinical condition in salmon parr under two contrasting husbandry

regimes. *J. Fish. Dis.* 30, 759–767. doi: 10.1111/j.1365-2761.2007.00890.x.

Sundell, K., Björnsson, B. T., Itoh, H., and Kawauchi, H. (1992). Chum salmon (Oncorhynchus keta) stanniocalcin inhibitis <i>in vitro<i> intestinal calcium uptake in Atlantic cod (Gadus morhua). *J. Comp. Physiol. B* 162, 489–495. doi: 10.1007/BF00264807.

Suniaga, S., Rolvien, T., Vom Scheidt, A., Fiedler, I. A. K., Bale, H. A., Huysseune, A., Witten, P. E., Amling, M., and Busse, B. (2018). Increased mechanical loading through controlled swimming exercise induces bone formation and mineralization in adult zebrafish. *Sci. Rep.* 8, 3646. doi: 10.1038/s41598-018-21776-1.

Suzuki, E., Yamada, M., Ariyasu, D., Izawa, M., Miyamoto, J., Koto, S., and Hasegawa, Y. (2009). Patients with hypophosphatemic osteomalacia need continuous treatment during adulthood. *Clin. Pediatr. Endocrinol.* 18, 29–33. doi: 10.1297/cpe.18.29.

Suzuki, N. (2005). Physiological significance of calcitonin in fish. *Clin. Calcium* 15, 139–146.

Sweatt, A., Sane, D. C., Hutson, S. M., and Wallin, R. (2003). Matrix Gla protein (MGP) and bone morphogenetic protein-2 in aortic calcified lesions of aging rats. *J. Thromb. Haemost.* 1, 178–185. doi: 10.1046/j.1538-7836.2003.00023.x.

Symmons, S. (1979). Notochordal and elastic components of the axial skeleton of fishes and their functions in locomotion. *J. Zool.* 189, 157–206. doi: 10.1111/j.1469-7998.1979.tb03958.x.

Taillandier, A., Lia-Baldini, A. S., Mouchard, M., Robin, B., Muller, F., Simon-Bouy, B., Serre, J. L., Bera-Louville, A., Bonduelle, M., Eckhardt, J., Gaillard, D., Myhre, A. G., Körtge-Jung, S., Larget-Piet, L., Malou, E., Sillence, D., Temple, I. K., Viot, G., and Mornet, E. (2001). Twelve novel mutations in the tissue-nonspecific alkaline phosphatase gene (*ALPL*) in patients with various forms of hypophosphatasia. *Hum. Mutat.* 18, 83–84. doi: 10.1002/humu.1154.

Takagi, Y., and Yamada, J. (1991). “Effects of calcium and phosphate deficiencies on bone metabolism in a teleost, Tilapia (Oreochromis niloticus): a histomorphometric study,” in *Mechanisms and phylogeny of mineralization in*

*biological systems*, eds. S. Suga and H. Nakahara (Tokyo, Japan: Springer), 187–191. doi: 10.1007/978-4-431-68132-8_31.

Takeda, E., Yamamoto, H., Yamanaka-Okumura, H., and Taketani, Y. (2012). Dietary phosphorus in bone health and quality of life. *Nutr Rev* 70, 311–321. doi: 10.1111/j.1753-4887.2012.00473.x.

Tarasco, M., Cordelières, F. P., Cancela, M. L., and Laizé, V. (2020). ZFBONE: An ImageJ toolset for semi-automatic analysis of zebrafish bone structures. *Bone* 138, 115480. doi: https://doi.org/10.1016/j.bone.2020.115480.

Tarlo, L. B. H. (1964). "The origin of bone," in *Bone and tooth. Proceedings of the first european bone and tooth symposium*, ed. H. J. J. Blackwood (Oxford, UK: Pergamon Press), 3–15.

Taylor, W. R., and Van Dyke, G. C. (1985). Revised procedures for staining and clearing small fishes and other vertebrates for bone and cartilage study. *Cybium* 9, 107–119.

Tenenhouse, H. S. (1999). X-linked hypophosphataemia: a homologous disorder in humans and mice. *Nephrol. Dial. Transplant.* 14, 333–341. doi: 10.1093/ndt/14.2.333.

To, T. T., Witten, P. E., Huysseune, A., and Winkler, C. (2015). An adult osteopetrosis model in medaka reveals the importance of osteoclast function for bone remodeling in teleost fish. *Comp. Biochem. Physiol. Part C Toxicol. Pharmacol.* 178, 68–75. doi: 10.1016/j.cbpc.2015.08.007.

To, T. T., Witten, P. E., Renn, J., Bhattacharya, D., Huysseune, A., and Winkler, C. (2012). Rankl-induced osteoclastogenesis leads to loss of mineralization in a medaka osteoporosis model. *Development* 139, 141–150. doi: 10.1242/dev.071035.

Tonelli, F., Bek, J. W., Besio, R., De Clercq, A., Leoni, L., Salmon, P., Coucke, P. J., Willaert, A., and Forlino, A. (2020a). Zebrafish: a resourceful vertebrate model to investigate skeletal disorders. *Front. Endocrinol.* 11, 489. doi: 10.3389/fendo.2020.00489.

Tonelli, F., Cotti, S., Leoni, L., Besio, R., Gioia, R., Marchese, L., Giorgetti, S., Villani, S., Gistelinck, C., Wagener, R., Kobbe, B., Larionova, D., Fiedler, I. A. K., Busse, B., Eyre, D., Rossi, A., Witten, P. E., and Forlino, A. (2020b). *Crtap* and *p3h1* knock out

zebrafish support defective collagen chaperoning as the cause of their osteogenesis imperfecta phenotype. *Matrix Biol.* 90, 40–60. doi: 10.1016/j.matbio.2020.03.004.

Tseng, D. Y., Chou, M. Y., Tseng, Y. C., Hsiao, C. D., Huang, C. J., Kaneko, T., and Hwang, P. P. (2009). Effects of stanniocalcin 1 on calcium uptake in zebrafish (*Danio rerio*) embryo. *Am. J. Physiol.* 296, R549-57. doi: 10.1152/ajpregu.90742.2008.

Turner, S., Burrow, C. J., Schultze, H.-P., Blieck, A., Reif, W.-E., Rexroad, C. B., Bultynck, P., and Nowlan, G. S. (2010). False teeth: conodont-vertebrate phylogenetic relationships revisited. *Geodiversitas* 32, 545–594. doi: 10.5252/g2010n4a1.

Uveges, T. E., Collin-Osdoby, P., Cabral, W. A., Ledgard, F., Goldberg, L., Bergwitz, C., Forlino, A., Osdoby, P., Gronowicz, G. A., and Marini, J. C. (2008). Cellular mechanism of decreased bone in Brtl mouse model of OI: imbalance of decreased osteoblast function and increased osteoclasts and their precursors. *J. bone Miner. Res.* 23, 1983–1994. doi: 10.1359/jbmr.080804.

Van der heyden, C., and Huysseune, A. (2000). Dynamics of tooth formation and replacement in the zebrafish (*Danio rerio*) (Teleostei, Cyprinidae). *Dev. Dyn.* 219, 486–496. doi: 10.1002/1097-0177(2000)9999:9999<::AID-DVDY1069>3.0.CO;2-Z.

Van der heyden, C., Huysseune, A., and Sire, J. Y. (2000). Development and fine structure of pharyngeal replacement teeth in juvenile zebrafish (*Danio rerio*) (Teleostei, Cyprinidae). *Cell Tissue Res.* 302, 205–219. doi: 10.1007/s004410000180.

van Eeden, F. J., Granato, M., Schach, U., Brand, M., Furutani-Seiki, M., Haffter, P., Hammerschmidt, M., Heisenberg, C. P., Jiang, Y. J., Kane, D. A., Kelsh, R. N., Mullins, M. C., Odenthal, J., Warga, R. M., Allende, M. L., Weinberg, E. S., and Nüsslein-Volhard, C. (1996). Mutations affecting somite formation and patterning in the zebrafish, *Danio rerio*. *Development* 123, 153–164. doi: 10.1242/dev.123.1.153.

Van Wesenbeeck, L., and Van Hul, W. (2005). Lessons from osteopetrotic mutations in animals: impact on our current understanding of osteoclast biology. *Crit. Rev. Eukaryot. Gene Expr.* 15, 133–162. doi: 10.1615/critreveukaryotgeneexpr.v15.i2.40.

Vanoevelen, J., Janssens, A., Huitema, L. F. A., Hammond, C. L., Metz, J. R., Flik, G., Voets, T., and Schulte-Merker, S. (2011). Trpv5/6 is vital for epithelial calcium uptake and bone formation. *FASEB J.* 25, 3197–3207. doi: 10.1096/fj.11-183145.

Veis, A. (2003). "Mineralization in organic matrix frameworks," in *Biomineralization. Reviews in mineralogy and geochemistry*, eds. P. M. Dove, J. J. Yoreo, and S. W. Weiner (Chantilly, VA: Mineralogical Society of America), 249–289.

Verri, T., and Werner, A. (2019). Type II Na+ -phosphate cotransporters and phosphate balance in teleost fish. *Pflugers Arch.* 471, 193–212. doi: 10.1007/s00424-018-2239-4.

Verstraeten, B., Sanders, E., and Huysseune, A. (2012). "Whole mount immunohistochemistry and in situ hybridization of larval and adult zebrafish dental tissues," in *Odontogenesis: methods and protocols*, ed. C. Kioussi (Totowa, NJ: Humana Press), 179–191. doi: 10.1007/978-1-61779-860-3_16.

Vielma, J., and Lall, S. P. (1998). Phosphorus utilization by Atlantic salmon (*Salmo salar*) reared in freshwater is not influenced by higher dietary calcium intake. *Aquaculture* 160, 117–128. doi: 10.1016/S0044-8486(97)00300-1.

Wagner, D. O., and Aspenberg, P. (2011). Where did bone come from? *Acta Orthop.* 82, 393–398. doi: 10.3109/17453674.2011.588861.

Wake, D. B., Roth, G., and Wake, M. H. (1983). On the problem of stasis in organismal evolution. *J. Theor. Biol.* 101, 211–224. doi: 10.1016/0022-5193(83)90335-1.

Wallace, M. J., Kruse, R. W., and Shah, S. A. (2017). The spine in patients with osteogenesis imperfecta. *J. Am. Acad. Orthop. Surg.* 25, 100–109. doi: 10.5435/JAAOS-D-15-00169.

Wang, J. S., Mazur, C. M., and Wein, M. N. (2021). Sclerostin and osteocalcin: candidate bone-produced hormones. *Front. Endocrinol. (Lausanne).* 12. doi: 10.3389/fendo.2021.584147.

Wang, X., Wang, S., Li, C., Gao, T., Liu, Y., Rangiani, A., Sun, Y., Hao, J., George, A., Lu, Y., Groppe, J., Yuan, B., Feng, J. Q., and Qin, C. (2012). Inactivation of a novel FGF23 regulator, FAM20C, leads to hypophosphatemic rickets in mice. *PLoS Genet.* 8, e1002708. doi: 10.1371/journal.pgen.1002708.

Watanabe, G., Kawaguchi, S., Matsuyama, T., and Yamashita, T. (2007). Correlation of

scoliotic curvature with Z-score bone mineral density and body mass index in patients with osteogenesis imperfecta. *Spine (Phila. Pa. 1976).* 32, E488-94. doi: 10.1097/BRS.0b013e31811ec2d9.

Watanabe, T., Arakawa, T., Kitajima, C., and Fujita, S. (1984a). Effect of nutritional quality of broodstock diets on reproduction of red sea bream (*Chrysophrys major*). *Bull. Japanese Soc. Sci. Fish.* 50, 495–501.

Watanabe, T., Ohhashi, S., Itoh, A., Kitajima, C., and Fujita, S. (1984b). Effect of nutritional composition of diets on chemical components of red sea bream broodstock and eggs produced. *Bull. Japanese Soc. Sci. Fish.* 50, 503–515.

Wautier, K., der heyden, C., and Huysseune, A. (2001). A quantitative analysis of pharyngeal tooth shape in the zebrafish (*Danio rerio*, Teleostei, Cyprinidae). *Arch. Oral Biol.* 46, 67–75. doi: 10.1016/s0003-9969(00)00091-1.

Weber, E. H. (1820). *De aure et auditu hominis et animalium, Pars I. De Aure Animalium Aquatilium*. Lips.

Webster, M., and Sheets, H. (2010). "A practical introduction to landmark-based geometric morphometrics," in *The paleontological society papers*, eds. J. Alroy and G. Hunt, 163–188. doi: 10.1017/S1089332600001868.

Weigele, J., and Franz-Odendaal, T. A. (2016). Functional bone histology of zebrafish reveals two types of endochondral ossification, different types of osteoblast clusters and a new bone type. *J Anat* 229, 92–103. doi: 10.1111/joa.12480.

Weinans, H., and Prendergast, P. J. (1996). Tissue adaptation as a dynamical process far from equilibrium. *Bone* 19, 143–149. doi: 10.1016/8756-3282(96)00143-3.

Whyte, M. P., Carpenter, T. O., Gottesman, G. S., Mao, M., Skrinar, A., San Martin, J., and Imel, E. A. (2019). Efficacy and safety of burosumab in children aged 1–4 years with X-linked hypophosphataemia: a multicentre, open-label, phase 2 trial. *Lancet Diabetes Endocrinol.* 7, 189–199. doi: 10.1016/S2213-8587(18)30338-3.

Wilton, T., Hosking, D., Pawley, E., Stevens, A., and Harvey, L. (1987). Osteomalacia and femoral neck fractures in the elderly patient. *J. Bone Joint Surg. Br.* 69-B, 388–390. doi: 10.1302/0301-620X.69B3.3584190.

Witten, P. E. (1997). Enzyme histochemical characteristics of osteoblasts and mononucleated osteoclasts in a teleost fish with acellular bone (*Oreochromis*

*niloticus*, Cichlidae). *Cell Tissue Res.* 287, 591–599. doi: 10.1007/s004410050782.

Witten, P. E., Fjelldal, P. G., Huysseune, A., McGurk, C., Obach, A., and Owen, M. A. G. (2019). Bone without minerals and its secondary mineralization in Atlantic salmon. *J. Exp. Biol.* 222, jeb188763. doi: 10.1242/jeb.188763.

Witten, P. E., Gil-Martens, L., Huysseune, A., Takle, H., and Hjelde, K. (2009). Towards a classification and an understanding of developmental relationships of vertebral body malformations in Atlantic salmon (*Salmo salar* L.). *Aquaculture* 295, 6–14. doi: 10.1016/j.aquaculture.2009.06.037.

Witten, P. E., and Hall, B. K. (2021). "The Ancient, segmented, active and permanent notochord," in *Ancient fishes and their living relatives: a tribute to John G. Maisey*, eds. A. Pradel, J. S. S. Denton, and P. Janvier (München, Germany: Verlag Dr. Friedrich Pfeil), 215–224.

Witten, P. E., Hall, B. K., and Huysseune, A. (2005). Are breeding teeth in Atlantic salmon a component of the drastic alterations of the oral facial skeleton? *Arch. Oral Biol.* 50, 213–217. doi: 10.1016/j.archoralbio.2004.10.018.

Witten, P. E., and Hall, K. B. (2015). Teleost skeletal plasticity: modulation, adaptation, and remodelling. *Copeia* 103, 727–739. doi: 10.1643/CG-14-140.

Witten, P. E., and Hall, K. B. (2022). *The notochord. Development, evolution and contributions to the vertebral column*. 1st ed. Boca Raton: CRC Press, Taylor and Francis Group.

Witten, P. E., Hansen, A., and Hall, B. K. (2001). Features of mono- and multinucleated bone resorbing cells of the zebrafish *Danio rerio* and their contribution to skeletal development, remodeling, and growth. *J. Morphol.* 250, 197–207. doi: 10.1002/jmor.1065.

Witten, P. E., Harris, M. P., Huysseune, A., and Winkler, C. (2017). Small teleost fish provide new insights into human skeletal diseases. *Methods Cell. Biol.* 138, 321–346. doi: 10.1016/bs.mcb.2016.09.001.

Witten, P. E., and Huysseune, A. (2007). "Mechanisms of chondrogenesis and osteogenesis in fins," in *Fins into limbs: evolution, development, and transformation*, ed. B. K. Hall (Chicago, IL, USA: The University of Chicago Press), 79–92.

Witten, P. E., and Huysseune, A. (2009). A comparative view on mechanisms and functions of skeletal remodelling in teleost fish, with special emphasis on osteoclasts and their function. *Biol. Rev. Camb. Philos. Soc.* 84, 315–346. doi: 10.1111/j.1469-185X.2009.00077.x.

Witten, P. E., Huysseune, A., and Hall, B. K. (2010). A practical approach for the identification of the many cartilaginous tissues in teleost fish. *J. Appl. Ichthyol.* 26, 257–262. doi: 10.1111/j.1439-0426.2010.01416.x.

Witten, P. E., Obach, A., Huysseune, A., and Baeverfjord, G. (2006). Vertebrae fusion in Atlantic salmon (*Salmo salar*): development, aggravation and pathways of containment. *Aquaculture* 258, 164–172. doi: 10.1016/j.aquaculture.2006.05.005.

Witten, P. E., Owen, M. A., Fontanillas, R., Soenens, M., McGurk, C., and Obach, A. (2016). A primary phosphorus-deficient skeletal phenotype in juvenile Atlantic salmon *Salmo salar*: the uncoupling of bone formation and mineralization. *J. Fish Biol.* 88, 690–708. doi: 10.1111/jfb.12870.

Witten, P. E., Villwock, W., Peters, N., and Hall, B. K. (2000). Bone resorption and bone remodelling in juvenile carp, *Cyprinus carpio* L. *J. Appl. Ichthyol.* 16, 254–261. doi: 10.1046/j.1439-0426.2000.00233.x.

Wu, L. N. Y., Genge, B. R., Kang, M. W., Arsenault, A. L., and Wuthier, R. E. (2002). Changes in phospholipid extractability and composition accompany mineralization of chicken growth plate cartilage matrix vesicles. *J. Biol. Chem.* 277, 5126–5133. doi: 10.1074/jbc.M107899200.

Wysolmerski, J. J. (2012). Osteocytic osteolysis: time for a second look? *Bonekey Rep.* 1, 229. doi: 10.1038/bonekey.2012.229.

Yadav, M. C., Simão, A. M. S., Narisawa, S., Huesa, C., McKee, M. D., Farquharson, C., and Millán, J. L. (2011). Loss of skeletal mineralization by the simultaneous ablation of PHOSPHO1 and alkaline phosphatase function: a unified model of the mechanisms of initiation of skeletal calcification. *J. Bone Miner. Res.* 26, 286–297. doi: 10.1002/jbmr.195.

Ytteborg, E., Todorcevic, M., Krasnov, A., Takle, H., Kristiansen, I. Ø., and Ruyter, B. (2015). Precursor cells from Atlantic salmon (*Salmo salar*) visceral fat holds the

plasticity to differentiate into the osteogenic lineage. *Biol. Open* 4, 783–791. doi: 10.1242/bio.201411338.

Ytteborg, E., Torgersen, J., Baeverfjord, G., and Takle, H. (2010). Morphological and molecular characterization of developing vertebral fusions using a teleost model. *BMC Physiol.* 10, 13. doi: 10.1186/1472-6793-10-13.

Yuan, B., Takaiwa, M., Clemens, T. L., Feng, J. Q., Kumar, R., Rowe, P. S., Xie, Y., and Drezner, M. K. (2008). Aberrant Phex function in osteoblasts and osteocytes alone underlies murine X-linked hypophosphatemia. *J. Clin. Invest.* 118, 722–734. doi: 10.1172/JCI32702.

Zeitlin, L., Fassier, F., and Glorieux, F. H. (2003). Modern approach to children with osteogenesis imperfecta. *J. Pediatr. Orthop. B* 12, 77–87. doi: 10.1097/01.bpb.0000049567.52224.fa.

Zhang, H., Doty, S. B., Hughes, C., Dempster, D., and Camacho, N. P. (2007). Increased resorptive activity and accompanying morphological alterations in osteoclasts derived from the oim/oim mouse model of osteogenesis imperfecta. *J. Cell. Biochem.* 102, 1011–1020. doi: 10.1002/jcb.21337.

Zhang, T., and Peterson, R. T. (2020). "Zebrafish as a platform for drug screening," in *The zebrafish in biomedical research*, eds. S. C. Cartner, J. S. Eisen, S. C. Farmer, K. J. Guillemin, M. L. Kent, and G. E. Sanders (Academic Press), 659–675. doi: 10.1016/B978-0-12-812431-4.00051-8.

Zilberman, Y., Gafni, Y., Pelled, G., Gazit, Z., and Gazit, D. (2008). "Bioluminescent imaging in bone," in *Osteoporosis: methods and protocols*, ed. J. J. Westendorf (Totowa, NJ: Humana Press), 261–272. doi: 10.1007/978-1-59745-104-8_18.

Zoch, M. L., Clemens, T. L., and Riddle, R. C. (2016). New insights into the biology of osteocalcin. *Bone* 82, 42–49. doi: 10.1016/j.bone.2015.05.046.

# List of figures and tables

## Chapter 1



## Chapter 3

## Chapter 4

## Chapter 5



## Chapter 6

# List of symbols and abbreviations

| | |
|---|---|
| × | concentration folds |
| ± | plus or minus |
| % | percentage |
| ° | degrees |
| °C | degrees centigrade |
| + | plus |
| < | smaller than |
| = | equals to |
| 2D | two dimensions |
| 3D | three dimensions |
| *abcc6* | ATP binding cassette subfamily C member 6 (gene) |
| $AgNO_3$ | silver nitrate |
| ALP | alkaline phosphatase (activity) |
| *ALPL* or *alpl* | tissue non-specific alkaline phosphatase (gene) |
| AMP | adenosine monophosphate |
| ANK | progressive ankylosis protein homolog |
| *ANK* | progressive ankylosis protein homolog (gene) |
| ATP | adenosine triphosphate |
| BGLAP | bone Gla protein, osteocalcin |
| *BGLAP or bglap* | bone Gla protein, osteocalcin (gene) |
| BMD | bone mineral density |
| bp | base pair |
| $Ca_{10}(PO_4)_6(OH)_2$ | hydroxyapatite |
| $Ca^{2+}$ or Ca | calcium |
| $CaCl_2$ | calcium chloride |
| $CaSO_4$ | calcium sulphate |
| cDNA | complementary DNA |

| | |
|---|---|
| cf. | *confer/conferatur*, compare |
| *Chi/+* | *Chihuahua* zebrafish |
| *Chi/+*$_{LP}$ | *Chihuahua* zebrafish on the low phosphorus diet |
| CKD | chronic kidney disease |
| $Cl^-$ | chloride |
| $cm^3$ | cubic centimetres |
| *col10a1a* | collagen type X alpha 1a (gene) |
| *COL1A1* | collagen type I alpha 1 (gene) |
| *col1a1a* | collagen type I alpha 1a (gene) |
| *COL1A2* | collagen type I alpha 2 (gene) |
| D | dorsal tooth row |
| d-UTP | deoxy-uridine triphosphate |
| DCP | dicalcium phosphate |
| DEPC | diethyl pyrocarbonate |
| $dH_2O$ | distilled water |
| dpf | days post-fertilisation |
| E | elastic modulus |
| *eda* | ectodysplasin (gene) |
| *edar* | ectodysplasin receptor (gene) |
| e.g. | *exempli gratia*, for example |
| ECM | extracellular matrix |
| EDTA | ethylenedinitrilotetraacetic acid |
| *ef1a* | elongation factor 1 alpha (gene) |
| EGFP | enhanced green fluorescent protein |
| *ENPP1 or enpp1* | ectonucleotide pyrophosphatase/phosphodiesterase 1 (gene) |
| ENPP1 or Enpp1 | ectonucleotide pyrophosphatase/phosphodiesterase 1 |
| Entpd5 | ectonucleoside triphosphate/diphospho-hydrolase 5 |
| *entpd5* | ectonucleoside triphosphate/diphospho-hydrolase 5 (gene) |
| ENU | N-ethyl-N-nitrosourea |

| | |
|---|---|
| ER | endoplasmic reticulum |
| EU | European Union |
| $F^-$ | fluoride |
| FDA | U.S. Food and Drug Administration |
| FGF23 or Fgf23 | fibroblast growth factor 23 |
| *FGF23* or *fgf23* | fibroblast growth factor 23 (gene) |
| g | grams |
| GACI | generalised arterial calcification of infancy |
| GFP | green fluorescent protein |
| GPa | gigapascal |
| h | hours |
| H | hardness |
| $H_2O$ | water |
| $H_2O_2$ | hydrogen peroxide |
| ha | haemal arches |
| HCl | hydrogen chloride |
| HP | high phosphorus diet |
| hpf | hours post-fertilisation |
| hs | haemal spines |
| i.e. | *id est*, that is |
| keV | kiloelectronvolt |
| kg | kilograms |
| KOH | potassium hydroxide |
| kV | kilovolts |
| L | litres |
| LP | low phosphorus diet |
| M | molar |
| MAP | monoammonium phosphate |
| MD | mediodorsal tooth row |
| mg | milligrams |

| | |
|---|---|
| $Mg^{2+}$ | magnesium |
| MGP | matrix Gla protein |
| micro-CT | micro-computed tomography |
| min | minutes |
| mL | millilitres |
| mm | millimetres |
| mM | millimolar |
| $mm^2$ | square metres |
| $mm^3$ | cubic metres |
| mmol | millimoles |
| mRNA | messenger RNA |
| ms | milliseconds |
| N | normal |
| na | neural arches |
| $Na_2B_4O_7$ | sodium tetraborate |
| $Na_2S_2O_3$ | sodium tetraborate |
| NaCl | sodium chloride |
| $NaHCO_3$ | sodium bicarbonate |
| NaOH | sodium hydroxide |
| $NH_4H_2PO_4$ | monoammonium phosphate |
| nm | nanometres |
| No. or n | number |
| nob | no bone |
| ns | neural spines |
| OB | osteoblasts |
| OC | osteoclast |
| $OH^-$ | hydroxyl group |
| OI | osteogenesis imperfecta |
| *osc*:GFP | osteocalcin GFP reporter line |
| $OsO_4$ | osmium tetroxide |

| | |
|---|---|
| p | p-value |
| P | phosphorus |
| P-Cho | phosphocholine |
| PAGE | polyacrylamide gel electrophoresis |
| PBS | phosphate-buffered saline |
| PC | principal component |
| PCA | principal component analysis |
| PCR | polymerase chain reaction |
| PFA | paraformaldehyde |
| *phex* | phosphate-regulating endopeptidase homologue X-linked (gene) |
| *phospho1* | phosphatase orphan 1 (gene) |
| PHOSPHO1 or Phospho1 | phosphatase orphan 1 |
| Pi or $PO_4^{3-}$ | inorganic phosphate |
| PMMA | polymethyl methacrylate |
| *pparγ* | peroxisome proliferator activated receptor γ (gene) |
| PPi | pyrophosphate |
| PSC | pepsin-soluble collagen fraction |
| PSI | Paul Scherrer Institut |
| PTH or Pth | parathyroid hormone |
| Pth4 | Pth-like peptide 4 |
| PXE | pseudoxanthoma elasticum |
| qPCR | quantitative real-time PCR |
| RB | ruffled border |
| RER | rough endoplasmic reticulum |
| RNA | ribonucleic acid |
| RP | regular phosphorus diet |
| RT | room temperature |
| *RUNX2 or runx2* | RUNX family transcription factor 2 (gene) |
| Sb | supporting pharyngeal bone |

| | |
|---|---|
| SD | standard deviation |
| SDS | sodium dodecyl sulphate |
| sec or s | seconds |
| SL | standard length |
| Slc34a2 | solute carrier family 34 member 2 |
| *Slc34a2* | solute carrier family 34 member 2 (gene) |
| *slc34a2b* | solute carrier family 34 member 2b (gene) |
| SLS | Swiss Light Source |
| *Sost* or *sost* | sclerostin (gene) |
| *sp*. | species |
| *sp7* | osterix (gene) |
| *sparc* | osteonectin (gene) |
| *spp1* | osteopontin (gene) |
| $Sr^{2+}$ | strontium |
| *STC1* | stanniocalcin 1 (gene) |
| *STC2* | stanniocalcin 2 (gene) |
| STC2 | stanniocalcin 2 |
| T0 | time 0 (beginning of the experiment) |
| TEM | transmission electron microscopy |
| TNAP or Tnap | tissue non-specific alkaline phosphatase |
| TRAP | tartrate-resistant acid phosphatase |
| *twhh* | tiggy-winkle hedgehog |
| UV | ultraviolet |
| V | ventral tooth row |
| WT | wild type |
| α(I) | alpha chains of collagen type I |
| µA | microamperes |
| µL | microlitres |
| µm | micrometres |
| µS | microsiemens |

# Publication list

## Peer-reviewed articles

- Tonelli F, Leoni L, Daponte V, Gioia R, **Cotti S**, Fiedler IAK, Larionova D, Willaert A, Coucke PJ, Villani S, Busse B, Besio R, Rossi A, Witten PE, Forlino A (**2023**) Zebrafish Tric-b is required for skeletal development and bone cells differentiation. *Frontiers in Endocrinology, in press,* doi.org/10.3389/fendo.2023.1002914
- **Cotti S**, Huysseune A, Larionova D, Koppe W, Forlino A, Witten PE (**2022**) Compression fractures and partial phenotype rescue with a low phosphorus diet in the *Chihuahua* zebrafish osteogenesis imperfecta model. *Frontiers in Endocrinology, 13*, 851879, doi.org/10.3389/fendo.2022.851879
- **Cotti S**, Huysseune A, Koppe W, Rücklin M, Marone F, Wölfel EM, Fiedler IAK, Busse B, Forlino A, Witten PE (**2020**) More bone with less minerals? The effects of dietary phosphorus on the post-cranial skeleton in zebrafish. *International Journal of Molecular Sciences*, *21*, 5429, doi.org/10.3390/ijms21155429
- Tonelli F, **Cotti S**, Leoni L, Besio R, Gioia R, Marchese L, Giorgetti S, Villani S, Gistelinck C, Wagener R, Kobbe B, Larionova D, Fiedler IAK, Busse B, Eyre D, Rossi A, Witten PE, Forlino A (**2020**) *Crtap* and *p3h1* knock out zebrafish support defective collagen chaperoning as the cause of their osteogenesis imperfecta phenotype. *Matrix Biology*, *90*, 40-60, doi.org/10.1016/j.matbio.2020.03.004

## Articles in preparation

- **Cotti S**, Di Biagio C, Huysseune A, Koppe W, Forlino A, Witten PE. The "super-bone" zebrafish model: a novel approach to stimulate bone formation by alternating dietary phosphorus levels. *In preparation to submission to Nature Communications*
- **Cotti S**, Huysseune A, Di Biagio C, Larionova D, Koppe W, Fiedler IAK, Busse B, Rücklin M, Marone F, Forlino A, Witten PE. Different responses to a low phosphorus diet reveal fundamental differences in zebrafish dental tissues. *In preparation to submission to Journal of Dental Research*

## Conference contributions

- Witten PE, **Cotti S**, Drabikova L, Di Biagio C, Huysseune A (**2022**) Tough of stiff? Some mechanical aspects of mineralised skeletons. *GOA Consortium meeting 13.12.2022* (Ghent, Belgium), *Oral presentation*
- **Cotti S**, Di Biagio C, Huysseune A, Forlino A, Witten PE (**2022**) The "super-bone" zebrafish model: a novel approach to stimulate bone formation by alternating dietary phosphorus levels. *6th Interdisciplinary Approaches on Fish Skeletal Biology* (Olhão, Portugal), *Oral presentation*
- Di Biagio C, **Cotti S**, Huysseune A, Boglione C, Witten PE (**2022**) Physical exercise and dietary phosphorus levels: novel insights into bone homeostasis in response to mechanical load. *6th Interdisciplinary Approaches on Fish Skeletal Biology* (Olhão, Portugal), *Oral presentation*
- **Cotti S**, Huysseune A, Larionova D, Koppe W, Forlino A, Witten PE (**2022**) Compression fractures and partial phenotype rescue with a low phosphorus diet in the *Chihuahua* zebrafish osteogenesis imperfecta model. *6th Interdisciplinary Approaches on Fish Skeletal Biology* (Olhão, Portugal), *Poster presentation*
- Sahd L, **Cotti S**, Witten PE, Huysseune A (**2022**) The aged zebrafish skeleton: a shape and radiographical analysis. *6th Interdisciplinary Approaches on Fish Skeletal Biology* (Olhão, Portugal), *Poster presentation*
- **Cotti S**, Huysseune A, Forlino A, Witten PE (**2022**) More bone without minerals: alternating dietary phosphorus increases bone volume in zebrafish. *International Network on Ectopic calcification (INTEC) kick-off meeting* (Ghent, Belgium), *Oral presentation*
- **Cotti S**, Huysseune A, Koppe W, Forlino A, Witten PE (**2022**) More healthy bone: alternating dietary phosphorus increases bone volume in zebrafish. *Matrix Biology Europe* (Florence, Italy), *Poster presentation*
- Tonelli F, Leoni L, Daponte V, Masiero C, Gioia R, **Cotti S**, Larionova D, Fiedler IAK, Busse B, Witten PE, Forlino A (**2022**) Zebrafish tmem38b knock out unveils the *in vivo* role of Trimeric Intracellular Cation (TRIC) channel B on cell homeostasis. *Matrix Biology Europe* (Florence, Italy), *Oral presentation*
- Drábiková L, **Cotti S**, Fjelldal PG, Morken T, Owen MAG, Huysseune A, Witten PE (**2022**) Healthy salmon bone: matrix formation and mineralization can be uncoupled. *Matrix Biology Europe* (Florence, Italy), *Poster presentation*

- **Cotti S**, Huysseune A, Koppe W, Forlino A, Witten PE (**2022**) More healthy bone: alternating dietary phosphorus increases bone volume in zebrafish. *Aquaculture Europe, Special session "Aquaculture meets biomedicine: innovation in skeletal health research"* (Rimini, Italy), *Oral presentation*

- **Cotti S**, Huysseune A, Forlino A, Witten PE (**2022**) Differential effects of dietary phosphorus on dentin and enameloid mineralization. *14th Tooth Morphogenesis and Differentiation* (Prague, Czech Republic), *Oral presentation*

- **Cotti S**, Huysseune A, Koppe W, Rücklin M, Marone F, Wölfel EM, Fiedler IAK, Busse B, Forlino A, Witten PE (**2022**) More bone with less minerals. The effects of dietary phosphorus on the post-cranial skeleton in zebrafish. *49th European calcified Tissue Society* (Helsinki, Finland), doi:10.1016/j.bonr.2022.101446, *Oral and poster presentation*

- **Cotti S**, Huysseune A, Larionova D, Koppe W, Forlino A, Witten PE (**2022**) Compression fractures and partial phenotype rescue with a low phosphorus diet in the *Chihuahua* zebrafish osteogenesis imperfecta model. *49th European calcified Tissue Society* (Helsinki, Finland), doi:10.1016/j.bonr.2022.101496, *Oral and poster presentation*

- Tonelli F, Leoni L, Daponte V, Masiero C, **Cotti S**, Larionova D, Fiedler IAK, Busse B, Witten PE, Forlino A (**2022**) Zebrafish tmem38b Knock out unveils the *in vivo* role of Trimeric Intracellular Cation (TRIC) channel B on cell homeostasis. *49th European calcified Tissue Society* (Helsinki, Finland), doi:10.1016/j.bonr.2022.101280, *Oral presentation*

- Di Biagio C, **Cotti S**, Huysseune A, Boglione C, Witten PE (**2022**) Soft bone due to low dietary phosphorus intake: the response to exercise. *20th International Symposium on Fish Nutrition and Feeding* (Sorrento, Italy), *Poster presentation*

- **Cotti S**, Huysseune A, Forlino A, Witten PE (**2021**) The *Chihuahua* zebrafish model for osteogenesis imperfecta. Partial phenotype rescue with a low phosphorus diet. *GOA Consortium meeting 07.12.2021* (Ghent, Belgium), *Oral presentation*

- **Cotti S**, Huysseune A, Forlino A, Witten PE (**2021**) Variation of shape, bone structure and mineralisation of vertebral centra in young adult *chihuahua*, a zebrafish model for human classical osteogenesis imperfecta. *48th European calcified Tissue Society* (online), doi.org/10.1016/j.bonr.2021.101048, *Poster presentation*

- Leoni L, Daponte V, Tonelli F, Gioia R, **Cotti S**, Larionova D, Witten PE, Fiedler I, Busse B, Forlino A (**2021**) Knock out of tmem38b by CRISPR/Cas9 in zebrafish unveils the *in vivo* role of Trimeric intracellular cation (TRIC) channel B on cell

homeostasis. *48th European calcified Tissue Society* (online), doi.org/10.1016/j.bonr.2021.101054, *Poster presentation*

- **Cotti S**, Huysseune A, Forlino A, Witten PE (**2021**) The *Chihuahua* zebrafish model for osteogenesis imperfecta: new insights into bone structure, mineralisation and compression fractures. *GOA Consortium meeting 07.06.2021* (Ghent, Belgium), *Oral presentation*

- Tonelli F, **Cotti S**, Leoni L, Besio R, Gioia R, Marchese L, Giorgetti S, Villani S, Gistelinck C, Wagener R, Kobbe B, Fiedler IAK, Larionova D, Busse B, Eyre D, Rossi A, Witten PE, Forlino A (**2021**) *Crtap* and *p3h1* knock out zebrafish support defective collagen chaperoning as the cause of their osteogenesis imperfecta phenotype. *Yearbook of Paediatric Endocrinology*, *18*, 5.11, doi.org/10.1530/ey.18.5.11, *Oral presentation*

- **Cotti S**, Huysseune A, Forlino A, Witten PE (**2021**) The effects of dietary phosphorus on the post-cranial skeleton in zebrafish. *GOA Consortium meeting 20.01.2021* (Ghent, Belgium), *Oral presentation*

- Tonelli F, Leoni L, **Cotti S**, Giannini G, Daponte G, Gioia R, Fiedler IAK, Besio R, Rossi A, Busse B, Witten PE, Forlino A (**2019**) Altered 3 hydroxylation complex in bone homeostasis. *9th International Conference on Children's Bone Health* (Salzburg, Austria), doi.org/10.1530/boneabs.7.OC19, *Oral presentation*

- Leoni L, Tonelli F, **Cotti S**, Giannini G, Daponte V, Gioia R, Besio R, Garibaldi N, Rossi A, Forlino A (**2019**) Generation of osteogenesis imperfecta type XIV zebrafish models. *9th International Conference on Children's Bone Health* (Salzburg, Austria), doi.org/10.1530/boneabs.7.P37, *Poster presentation*

- Besio R, Tonelli F, Garibaldi N, Leoni L, **Cotti S**, Forlino A (**2019**) Endoplasmic reticulum stress in osteoblasts. *9th International Conference on Children's Bone Health* (Salzburg, Austria), doi.org/10.1530/boneabs.7.IS10*, Oral presentation*

- **Cotti S**, Forlino A, Huysseune A, Witten PE (**2019**) The effects of phosphorus deficiency and oversupply: vertebral column malformations and bone mineralization in zebrafish. *31st "A. Castellani" meeting of PhD students in Biomedical Sciences* (Brallo di Pregola, Italy), *Poster presentation*

This doctoral thesis examines the effects of different dietary phosphorus levels on the skeleton using zebrafish as a model organism. The objectives are to obtain insights into the mechanisms underlying bone hypo- and hypermineralisation, related both to inadequate phosphorus intake and to pathological conditions, and to better elucidate the processes of bone formation and mineralisation. The results show that a period of reduced phosphorus intake can increase bone volume and represents a promising novel approach for treating human pathologies characterised by bone hypermineralisation and bone loss.

This research has been promoted by Prof. Dr. P. Eckhard Witten and Prof. Dr. Antonella Forlino, and was mainly carried out at the Evolutionary Developmental Biology laboratory of Ghent University (Belgium) and at the Connective Tissue Disorders laboratory of the University of Pavia (Italy). Part of the research was conducted at the University Medical Center Hamburg-Eppendorf (Germany) and at the University of Rome Tor Vergata (Italy). The project was supported by the European Union's Horizon 2020 Research and Innovation Programme under the Marie Skłodowska-Curie grant agreement No. 766347 "Biomedaqu" and by the Special Research Fund from Ghent University (BOF.ITN.2021.0012.01).

The present doctoral thesis has been submitted to obtain the degree of Doctor of Science: Biology from Ghent University and the degree of Doctor of Biomedical Sciences from the University of Pavia.